Geothermal Paving Systems for Urban Runoff Treatment and Renewable Energy Efficiency

Effectiveness of geothermal paving systems (permeable pavements integrated with geothermal heat pumps) for urban runoff treatment, photocatalytic disinfection, renewable energy applications, and artificial neural networks for stormwater management.

Kiran Tota-Maharaj, BSc, MSc

A thesis submitted for the degree of Doctor of Philosophy
The University of Edinburgh
Scotland, U.K

November 2010.

Declaration

I hereby declare that the research documented in this Thesis is my own work, except where otherwise stated, and has not been submitted in any form for any other degree or professional qualification. Information derived from the work of others has been acknowledged and referenced.

.

Edinburgh, November 2010

Kiran Tota-Maharaj

"A more sustainable, cleaner and safer world can be created by making wiser water and energy choices. The development of timely and novel technologies such as combined permeable pavement and ground-source heat pump systems will lead to conservation of energy and water"

Prof Miklas Scholz, University of Salford, November 2010.

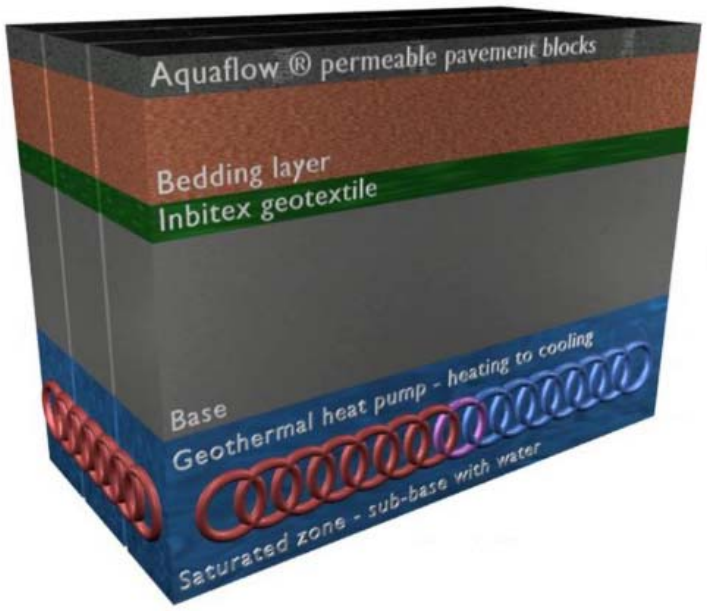

"Permeable pavements are a tried and tested solution for the attenuation of stormwater, improving the flood resilience of hard landscaped areas and raising the quality of discharge, particularly where geotextiles are deployed in the upper layers to trap and treat pollutants. Water stored in the pavement is such a valuable resource; a prime objective to be achieved was the assessment of any contamination risk before it was recommended that this water was used for secondary purposes. This would increase the market for rain water harvesting and allow commercial organizations such as Hanson Formpave to confidently state that the water was of sufficient quality for reuse. Additionally, the energy reserve present in such pavements has shown to be a viable source for taking into buildings via ground source heat pumps. The production of solid research data on the efficiency of such systems, allied to the analysis of any change in water quality produced by an integrated heat and rainwater source was of vast importance to the future of this combined technology. The research presented in this thesis represents a leap in the understanding of the properties and viability of such combined systems and assists the widespread adoption of these innovative sustainable solutions."

Dr. Stephen John Coupe (Research Manager Hanson Formpave, & Senior Lecturer at Coventry University, November 2010).

Abstract

Water and energy are two of the most precious and essential resources which are inseparably connected; vital for the survival and well-being of humanity. Sustainable water resources and energy management emphasizes the requirement for a holistic approach in meeting the needs of the present and future generations. In order to indentify the needs and obstacles relating to water reuse and renewable energy initiatives, Hanson Formpave in partnership with The University of Edinburgh implement a five-year pilot project between May 2005 and June 2010. The research project addressed the use of sustainable urban drainage systems (SUDS) such as permeable pavements systems (PPS) and integration of renewable energy tools such as geothermal heat pumps (GHPs). The research uses the novel and timely urban drainage system and focuses on water quality assessment when incorporated with GHPs. Twelve-tanked laboratory scaled experimental PPS were evaluated at The King's Building campus (The University of Edinburgh, Scotland) using different compositions. Variations in designs included the presence of geotextiles layers and geothermal heating/cooling applications. The experimental rigs were examined for a two year period (March 2008 to April 2010). Two types of urban stormwater were used in the analysis; (i) gully pot liquor and (ii) gully pot liquor spiked with *Canis lupus familiaris* (dog) faeces. This urban wastewater represented the extreme worst-case scenario from a storm event, which can occur on a permeable pavement parking lot. The pavement systems operated in batch-flow to mimic weekly storm events and reduce pumping costs. Six PPS were located indoor in a controlled environment and six corresponding PPS were placed outdoors to allow for a direct comparison of controlled and uncontrolled environmental conditions. The outdoor rig simulated natural weather conditions whilst the indoor rig operated under controlled environmental conditions such as regulated temperature, humidity and light. The project assessed the performance of these pavement rigs with the integration of ground-source heating and cooling, standalone PPS and the abilities for water quality treatment from a physical, chemical and microbiological perspective. The performance efficiency of the GHP was measured by the energy efficiency ration (EER) for steady state cooling efficiency and the coefficient of performance (COP) for the heating cycle efficiency. Findings from the combined PPS and GHP system and standalone systems were able to significantly lower levels for all physiochemical and microbial water quality parameters in the range of (70-99.99%) respectively. Outflow concentrations for all pavement systems met the European Commission Environment Urban Wastewater Treatment Directive (91/271/EEC). The presence of geotextiles resulted in a significant reduction of contaminants when compared to PPS systems without ($p < 0.05$). Photocatalytic disinfection with titanium dioxide (TIO_2) was applied to the effluent from PPS for further treatment and polishing of the stormwater. After the photocatalytic disinfection, the water met the requirements for the United States Environmental Protection Agency (US EPA) water recycling guidelines and the World Health Organisation (WHO) guidelines for potable water consumption with regards to microbial contamination. An Energy and temperature balance was developed for two PPS using a 4^{th} order Runge-Kutta numerical method to model the heat fluxes and energy balance within the pavement system. Machine learning techniques such as artificial neural networks (backpropagatioin feed-

forward neural networks) and self-organising maps (SOM) were applied and successfully predicted the effluent concentrations of nutrients, biochemical oxygen demand (BOD) and microbial pollutants. The overall outcome of this research is a significant contribution to the development of a new generable of sustainable and eco-friendly pavements. The research project proves scientifically that PPS is one of the most appropriate systems for GHP installation and does not affect its efficiency for water pollutant removal.

Awards and Publications

Awards:

First place (1st) prize for poster presentation - Permeable Pavement Engineering for Sustainable Urban Runoff Reuse Integrated with Geothermal Heat Pumps, at the Innovation Poster Presentation at The Concrete Society's Conference Concrete Innovations May, 2009 Constructing the Future. Marriott Hotel, Glasgow.

Journal papers:

Tota-Maharaj, K., Grabowiecki, P. and Scholz, M. (2009). An Energy and Temperature Performance Analysis of Geothermal (Ground Source) Heat Pumps Integrated with Permeable Pavement Systems for Urban Runoff Reuse. *International Journal for Sustainable Engineering*. 2 (3), 201-213.

Tota-Maharaj, K. and Scholz, M. (2009). Permeable (pervious) pavements ad geothermal heat pumps: addressing sustainable urban stormwater management and renewable energy. *International journal of Green Economics.* 3(3/4), 447-461.

Tota-Maharaj, K. and Scholz, M. (2010). Efficiency of permeable pavement systems for the removal of urban runoff pollutants under varying environmental conditions. *Environmental Progress and Sustainable Energy*. 29(3), 358-369.

Tota-Maharaj, K., Scholz, M., Ahmed, T., French, C. and Pagaling, E. (2010). The Synergy of Permeable Pavements and Geothermal Heat Pumps for Stormwater Treatment and Reuse, *Environmental Technology.* (in press).

Tota-Maharaj, K., Scholz, M. and Coupe, S.J. (2009). Modelling Temperature and Energy Balances within Geothermal Paving Systems. *Road Materials and Pavement Design an International Journal*. (in press)

Tota-Maharaj, K., Scholz, M. and Coupe, S.J. (2010). Utilisation of Geothermal Heat Pumps within Permeable Pavements for Sustainable Energy and Water Practices. *Journal of Energy and Power Engineering*. (in press).

Tota-Maharaj, K. and Scholz, M. (2010). Combined Permeable Pavement and Photocatalytic Titanium Dioxide Oxidation System for Urban Runoff Treatment and Disinfection. *Water and Environment Journal.* (under review)

Tota-Maharaj, K., and Scholz, M. (2010). Artificial Neural Network Simulation of Combined Permeable Pavement and Earth Energy Systems Treating Storm Water. *Journal of Environmental Engineering*. (under review)

Tota-Maharaj, K. and Scholz, M. (2010). Modelling the efficacy of permeable pavements for treatment of concentrated urban runoff using kohonen self-organizing maps (KSOM). *Civil Engineering and Environmental Systems.* (under review)

Conference papers:

Tota-Maharaj, K., Scholz M., and Coupe, S.J. (2010). "Utilisation of geothermal heat pumps within permeable pavements for sustainable energy and water practices". *Proceedings of the Renewable Energy Research Conference, June 7th-8th, 2010, Zero Emission Buildings.* (Eds): Haase, M. and Hestnes, A.G, NTNU (Norwegian University of Science and Technology), Trondheim, Norway. Renewable Energy Conference & Tapir Academic Press. pp 215-225, ISBN 978-82-519-2623-2.

Tota-Maharaj, K. and Scholz, M. (2010). "Permeable pavement engineering and geothermal (geoexchange) systems for stormwater treatment and reuse". *First European IAHR-(International Association for Hydro-Environment Engineering) Congress*, 4-6th May, 2010, Heriot Watt University, Riccarton, Edinburgh, U.K.

Tota-Maharaj, K., Scholz, M., Grabowiecki, P., Ahmed, T. and Coupe, S.J. (2009). "Molecular characterization of bacterial populations in urban runoff for combined pervious pavements and geothermal heat pumps". *Proceedings of the SUDsnet (Sustainable Urban Drainage Network) National Conference.* November 12-13, 2009, Coventry University, TechnoCentre, Coventry, U.K.

Coupe, S.J., **Tota-Maharaj, K.,** Scholz, M. and Grabowiecki, P. (2009). "Water stored within permeable paving and the effect of ground source heat pump applications on water quality". *Proceedings of the 9th International Conference on Concrete Block Paving,* "*Concrete Block Paving as a Sustainable Tool for a Comprehensive Development*", 18-21 October, 2009, Sheraton Hotel and Convention Center, Buenos Aires, Argentina.

Tota-Maharaj, K. and Scholz, M. (2009). "Permeable (pervious) pavements ad geothermal heat pumps: addressing sustainable urban stormwater management and renewable energy". (Eds) Kennet, M. and Nicholsby, D. *In: proceedings of the 4th Annual Green Economics Conference (31st July-1st August 2009)*, Oxford University, U.K: Volker Heinemann of the Green Economics Institute. pp 164-169.

Tota-Maharaj, K., Grabowiecki, P., Scholz, M., and Coupe, S.J. (2009). "Hybrid urban runoff treatment system incorporating permeable pavements and geothermal heat pumps". *Proceedings of the National Telford Institute Workshop, Sustainable Water Management. 2-3rd April, 2009.* University of Edinburgh, Institute of Infrastructure and Environment, Edinburgh, Scotland.

Grabowiecki, P., **Tota-Maharaj, K.,** Scholz, M. And Coupe, S.J.(2008). Combined permeable pavement and ground source heat pump system to treat urban runoff during storms and recycle energy. *Proceedings of the 10th British Hydrological Society National Hydrology Symposium*. Sustainable Hydrology for the 21st Century. 15th - 17th September 2008. Peter Chalk Centre, University of Exeter, Exeter, U.K.

Poster presentations, extended abstracts and seminars:

National Telford Institute Workshop, Edinburgh, Scotland. Sustainable Water Management. 2-3 April, 2009. Poster title *"Hybrid urban runoff treatment system incorporating permeable pavements and geothermal heat pumps."*

Graduate School of Engineering Poster Day Event, University of Edinburgh, 24th April, 2009. Poster title "*Permeable pavement engineering integrated with geothermal heat pumps-synergy of sustainable urban drainage and renewable energy applications*"

The Concrete Society National Conference, Concrete Innovations 2009, 'Constructing the Future' 8th May, 2009, Marriott Hotel, Glasgow, Scotland, U.K. Poster title "*Permeable pavement engineering for sustainable urban runoff reuse integrated with geothermal heat pumps*".

Edinburgh Research Partnership in Engineering and Mathematics (ERPem).Industry Evening Seminars and Postgraduate Student Poster Presentation Alexander Graham Bell Building, The King's Buildings, The University of Edinburgh. 13th October, 2009. Poster title "*Permeable pavements ad geothermal heat pumps: addressing sustainable urban stormwater management and renewable energy*".

The School of Engineering, The University of Edinburgh, Postgraduate Research Conference, 3rd May 2010. Presentation Title "*Geothermal paving systems (combined permeable pavements and ground-source heat pumps)*. Pentland Suite, John McIntyre Conference Centre, Pollock Halls, Edinburgh, Scotland U.K.

Institute of Environmental Management and Assessment (IEMA) Scotland Central Event "*Novel permeable pavement systems to control flooding and diffuse pollution*" Alexander Graham Bell Building, Institute for Infrastructure and Environment, School of Engineering, University of Edinburgh, Scotland, U.K., 12th May, 2010.

Acknowledgements

First and foremost, I would like to thank and praise Bhagawan (Almighty God) for guidance and support. I am extremely grateful to Hanson Formpave Heidelberg Cement Group for their financial support of this research project. I would specially like to express my sincere gratitude to my supervisor Professor Miklas Scholz for his endless support and for keeping me focused on the topic. Your pleasant personality, friendship and competent supervision encouraged me to further develop as a scientific researcher. I am also thankful to my industrial supervisor Dr. Stephen John Coupe from Coventry University and research manager at Hanson Formpave Heidelberg Cement Group for introducing me to the field of sustainable urban drainage, for which he is one of the pioneers. I am very thankful to Dr. Chris French, for giving me the opportunity to work in his research group at the School of Biological Science, The University of Edinburgh, and gain insightful knowledge about biology and its links and applications to urban wastewater treatment.

Several people have given me assistance with the work presented in this thesis; I would like to thank both past and present members of the Urban Water Research group, Institute for Infrastructure and Environment, The University of Edinburgh, including Dr. Atif Mustafa, Dr. Paul Eke, Dr. Sara Kazemi Yazdi, Ola Sawalha, Qinli Yang and Yu Dong. Much appreciation to you all for assistance in the laboratory, experimental trouble-shooting and fruitful discussions both professionally and socially. I would also like to thank Dr. Piotr Grabowiecki for initial assistance in the laboratory and experimental setup, as well as being a patient colleague and a good friend. I would like to extend my gratitude to Dr. Toqeer Ahmed visiting researcher from Quasi-Azad University, Pakistan, for his collaboration regarding the molecular microbiological analysis and techniques.

I am also grateful to Dr. Sanjay Bahadoorsingh for his encouragement, support and advice throughout my academic years. Appreciation is extended to my cousin Dr. Amrit Sharma, for his never-ending feedback and never loosing faith for my completion of this PhD. Deepest thanks and admiration is dedicated to my Guru (Godfather) Pundit Jeewan Maharaj for his guidance and blessings.

My heart felt gratitude goes to all my family in the U.K. (sister Vyana, brother-in-law Rishi, niece Prithivi and nephew Vivek) and my younger sister Kavita for all thier support, always being positive, joyful and a powerful source of inspiration to me. Special thanks are devoted to my parents (Dr. Vidhya Gyan Tota-Maharaj and Tawari Anand Tota-Maharaj) for your never-ending support, understanding, love, endless patience, and commitment to my education. My heart full thanks and admiration to my fiancé Sapna Roopchand, for her love and support during the years of my PhD research.

Dedication

To my brother, Arvind Tota-Maharaj (1979-1999).

.

May the memories held deep in our hearts help to soothe us, May Bhagawan's blessings always be with you as you are always in our prayers

Table of Contents

GEOTHERMAL PAVING SYSTEMS FOR URBAN RUNOFF TREATMENT AND RENEWABLE ENERGY EFFICIENCY ..... **I**

DECLARATION ..... **II**

ABSTRACT ..... **IV**

ACKNOWLEDGEMENTS ..... **IX**

DEDICATION ..... **X**

TABLE OF CONTENTS ..... **XI**

LIST OF TABLES ..... **XV**

LIST OF FIGURES ..... **XVI**

CHAPTER 1 INTRODUCTION **1**

1.1 BACKGROUND TO THE PROJECT **1**
1.2. RATIONALE, AIMS AND OBJECTIVES OF THIS RESEARCH **4**
1.3. OUTLINE OF THESIS CONTENTS **6**

CHAPTER 2 SUSTAINABLE URBAN DRAINAGE AND PERMEABLE PAVEMENTS **9**

2.1 URBAN RUNOFF **9**
2.2. SUSTAINABLE URBAN DRAINAGE SYSTEMS (SUDS) **13**
2.2.1. SUDS Techniques *14*
2.2.1.1 Green (Vegetated) roofs 14
2.2.1.2 Rainwater harvesting (water butts for runoff capture and reuse) 15
2.2.1.3 Filtration Trenches and Drains 15
2.2.1.4 Filter strips 16
2.2.1.5 Swales 16
2.2.1.6 Infiltration Basins 17
2.2.1.7 Subsurface Infiltration Bed 18
2.2.1.8 Constructed Wetlands 19
2.2.1.9 Wet Ponds (Retention Basins) 19
2.2.1.10 Dry ponds 20
2.3 PERMEABLE PAVEMENT ENGINEERING **21**
2.3.1 Permeable Pavement Structure and Design *23*
2.3.2 Porous Aggregates for Sub-base *24*
2.3.3 Geotextiles *25*
2.3.4 Types of Permeable Pavement Structures *26*
2.3.5 Pavement thickness design *28*
2.3.6 Stress Loads *28*
2.3.6.1 Corner Stresses 28
2.3.6.2 Edge loading stresses 30
2.3.6.3 Interior loading stresses 30
2.3.7 Sizing permeable (pervious) paving systems *31*
2.3.8 Hydrology and hydraulics *34*
2.3.9 Pollution Removal Processes and Water Quality *39*
2.3.10 Clogging, Maintenance and Serviceability *44*
2.3.11. Reduction of Heat Island Effect *47*
2.3.12. Comparative Costs Analysis of PPS and SUDS *49*

CHAPTER 3 GEOTHERMAL HEAT PUMPS **56**

3.1 INTRODUCTION **56**
3.2 ENERGY SOURCE: THE GROUND **57**
3.3 DESCRIPTION OF GEOTHERMAL HEAT PUMPS **59**
3.3.1 Heat Pump *60*
3.3.2 Earth connection *61*
3.3.2.1 Ground-Coupled Heat Pumps (GCHPs) 62
3.3.2.2 Groundwater Heat Pumps (GWHPs) 62

3.3.2.3 Surface Water Heat Pumps (SWHPs) 63
3.3.3 Interior heating or cooling distribution system *64*
3.4 ENERGETIC THERMODYNAMIC PERFORMANCE **64**
3.5 GREENHOUSE GAS REDUCTION, ENERGY SAVINGS AND ECONOMICS **69**
BENEFITS **69**
3.6 ENVIRONMENTAL CONCERNS **73**
3.6.1 Water Quality *73*
3.6.2 Geologic Hazards *75*

CHAPTER 4 EXPERIMENTAL DESIGN AND METHODOLOGY **77**

4.1. GEOTHERMAL (COMBINED PPS AND GHPS) PAVING EXPERIMENTS **77**
4.1.1 Design, construction and composition of experimental rigs *77*
4.1.2. Experimental design variations *82*
4.1.3 Selected pollutant loadings onto pavements *83*
4.1.4. Geothermal heating/cooling operational conditions *87*
4.2 WATER QUALITY PARAMETERS **88**
4.2.1 Physiochemical Parameters *90*
4.2.1.1 Temperature 90
4.2.2.2 pH 90
4.2.2.3 Biochemical Oxygen Demand (BOD) 91
4.2.2.4 Chemical Oxygen Demand (COD) 92
4.2.2.5 Suspended Solids 93
4.2.2.6 Turbidity 93
4.2.2.7 Dissolved Oxygen 94
4.2.2.8 Redox potential 95
4.2.2.9 Conductivity 96
4.2.2.10 Total Dissolved Solids 96
4.2.2.11 Nutrients – Nitrates (NO_3-N), Ammonia (NH_4-N) and Phosphates (PO_4-P) 97
4.2.3 Physiochemical water quality determinations *100*
4.2.3.1Temperature, pH, total dissolved solids (TDS) and conductivity 100
4.2.3.2 Dissolved oxygen (DO) and redox potential determinations 100
4.2.3.3 Suspended solids and Turbidity determinations 101
4.2.3.4 Biochemical oxygen demand (BOD) determinations 101
4.2.3.5 Chemical oxygen demand (COD) determinations 102
4.2.3.6 Nutrient determinations (PO_4, NH_4, NO_3) 102
4.3 PATHOGENIC BACTERIAL MICROORGANIMS **103**
4.3.1 Total Heterotrophic Bacteria *103*
4.3.2 Coliform bacteria and Escherichia coli 104
4.3.3 Faecal Streptococci (Enterococci sp.) 106
4.3.4 Salmonella sp *106*
4.3.5 Shigella sp *107*
4.3.6 Legionella sp. *108*
4.4 MICROBIOLOGICAL ANALYSIS **108**
4.4.1 Gram staining Analysis *110*
4.4.2 Molecular Microbiology *111*
4.5 CARBON DIOXIDE (CO_2) GAS MONITORING **114**
4.6 ENERGY EFFICIENCY ANALYSIS OF GEOTHERMAL HEATING AND COOLING **115**
4.7 HEALTH AND SAFETY RISKS ASSESSMENT /PROCEDURES **116**

CHAPTER 5 OVERALL WATER QUALITY, TREATMENT AND ENERGETIC PERFORMANCE **118**

5.1. INFLOW STORMWATER QUALITY **118**
5.2 WATER REUSE STANDARDS AND GUIDELINES. **121**
5.3 STATISTICAL ANALYSIS **122**
5.4 WATER QUALITY RESULTS **128**
5.4.1 Water Sample Temperature *128*
5.4.2 pH *130*
5.4.3 Electroconductivity *132*
5.4.4. Redox potential *135*
5.4.5 Sediments (Total dissolved solids, suspended solids and turbidity *137*

5.4.5.1 Total dissolved solids (TDS) ... 137
5.4.5.2 Suspended solids ... 140
5.4.5.3 Turbidity ... 142
5.4.6 Organic content (BOD, COD, DO) ... 146
5.4.6.1 Biochemical Oxygen Demand (BOD) ... 146
5.4.6.2 Chemical Oxygen Demand (COD) ... 149
5.4.6.3 Dissolved Oxygen (DO) ... 152
5.4.7 Carbon Dioxide (CO_2) ... 155
5.4.8 Nutrients (ammonia-nitrogen, nitrate-nitrogen and ortho-phosphate-phosphorous) ... 156
5.4.8.1 Ammonia-nitrogen (NH_4-N) ... 156
5.4.8.2 Nitrate-Nitrogen (NO_3-N) ... 159
5.4.8.3 Ortho-Phosphate-Phosphorous ... 162
5.4.9 Microbial pathogenic organisms ... 165
5.4.9.1 Escherichia Coli ... 165
5.4.9.2 Enterococci sp. ... 168
5.4.9.3 Total coliforms ... 171
5.4.9.4 Total Heterotrophic Bacteria (THB) ... 174
5.4.9.5 Salmonella sp. ... 177
5.4.9.6 Shigella sp. ... 180
5.5 MICROBIAL REMOVAL PROCESSES WITHIN PPS. ... 183
5.5.1 Molecular Microbiology Results ... 186
5.5.1.1 Gram staining results ... 186
5.5.1.2 Molecular microbiological results ... 188
5.6 ENERGETIC PERFORMANCE OF COMBINED GHPS AND PPS. ... 194
5.6.1 Geothermal heating/cooling sub-base temperatures ... 194
5.6.2 Energy Efficiency Ratio - Cooling Mode ... 196
5.6.3 Coefficient of Performance COP –Heating Mode ... 198

CHAPTER 6 PHOTOCATALYTIC OXIDATION WITH TITANIUM DIOXIDE (TIO2) FOR DECONTAMINATION AND DISINFECTION. ... 200

6.1 HETEROGENEOUS PHOTOCATALYTIC PROCESSES WITH TITANIUM DIOXIDE (TiO_2) ... 200
6.2 RESEARCH AIMS AND OBJECTIVES ... 203
6.3 PHOTOCATALYTIC REACTOR AND PHOTOCHEMICAL EXPERIMENTS ... 204
6.4 RESULTS AND DISCUSSION ... 206
6.4.1 The photocatalytic disinfection model (Chick-Watson model) ... 206
6.4.2 Total coliform photochemical deactivation ... 207
6.4.3 E.coli photochemical deactivation ... 209
6.4.4 Enterococci sp. photochemical deactivation ... 210
6.5 BACTERIAL POLLUTANTS REAPPEARANCE ANALYSIS ... 212
6.6 SUMMARY ... 213

CHAPTER 7 RUNGE-KUTTA METHODOLOGY FOR SIMULATION OF TEMPERATURE AND ENERGY BALANCES ... 215

7.1. JUSTIFICATION OF THERMOGEOLOGICAL MODEL FOR GEOTHERMAL PAVEMENT. ... 215
7.2 MODELLING METHODOLOGY ... 216
7.3 GOVERNING EQUATIONS AND PARAMETERIZATION OF ENERGY AND TEMPERATURE FLUXES ... 216
7.3.1. Solar Radiation Heat Gain q_{solar} ... 221
7.3.2. Heat Transfer through thermal radiation $q_{thermal}$ ... 221
7.3.3. Sky longwave radiation (q_{sky}) ... 222
7.3.4. Heat Transfer through Conduction q_{pps} ... 223
7.3.5. Convection Heat Fluxes q_{conv} ... 224
7.3.6. Heat Transfer due to Evaporation q_{evap} ... 226
7.3.8. Energy Associated with Movements of Water from Seepage (q_{seep}) ... 227
7.3.9. Heat Transfer from slinky coils (q_{coils}) ... 228
7.3.10. Mircobial respiration (q_{resp}) ... 229
7.4 SOLVING THE OVERALL ENERGY BALANCE EQUATION ... 229
7.5 VALIDATION OF 4TH ORDER RUNGE-KUTTA NUMERICAL ANALYSIS FOR MODELLING. ... 231
7.6. RESULTS AND DISCUSSION ... 232
7.7 SUMMARY ... 239

CHAPTER 8 APPLICATION OF BACKPROPAGATION ARTIFICIAL NEURAL NETWORK MODELS 241

8.1 INTRODUCTION 241
8.2 AIM AND OBJECTIVES 243
8.3 BACK PROPAGATION FEED-FORWARD ARTIFICIAL NEURAL NETWORK MODELS 243
8.4 ALGORITHMS 245
8.5 DATA NORMALIZATION 248
8.7 OPTIMIZATION AND MODEL PERFORMANCE EVALUATION 250
8.8 RESULTS AND DISCUSSION 252
8.9 SUMMARY 265

CHAPTER 9 APPLICATION OF KOHONEN SELF-ORGANISING MAP MODEL 267

9.1 MODELLING MICROBIAL PATHOGENIC ORGANISMS FOR STORMWATER REUSE. 267
9.2. KOHONEN SELF ORGANISING MAPS (KSOM) 267
9.3 AIMS AND OBJECTIVES 272
9.4 KSOM NUMERICAL ANALYSIS AND MODELLING 273
9.5 RESULTS AND DISCUSSION 274
9.6. SUMMARY 288

CHAPTER 10 CONCLUSIONS AND RECOMMENDATIONS 290

10.1 CONCLUSIONS 290
10.2 RECOMMENDATIONS FOR FUTURE RESEARCH 296

REFERENCES 298

List of Tables

TABLE 2-1: SUMMARY OF URBAN RUNOFF POLLUTANTS (ADAPTED FROM US EPA, 1993; CAMPBELL *ET AL., 2004*; METCALF AND EDDY, 2007)..... 12
TABLE 2-2: DISCHARGE FROM BOTTOM OF AN OPEN-JOINTED BLOCK PARKING LOT IN WHEATLEY, ENGLAND (ADAPTED FROM ABBOTT AND COMINO-MATEOS, 2003) 38
TABLE 2-3: ASSOCIATED COST OF POLLUTIONS IN SURFACE WATER OUTFLALLS (CIWEM, 2000)..... 50
TABLE 2-4: TOTAL FINANCIAL SUMMARY OF COST-BENEFIT ANALYSIS OF SUDS (ENVIRONMENT AGENCY, 2007) 53
TABLE 3-1: HEATING VALUE, EFFICIENCIES, COST AND CONSUMPTION IN TURKEY (ESEN *ET AL.,* 2006) 72
TABLE 4-1: PAVEMENT RIG COMPONENTS AND CHARACTERISTICS IN EXPERIMENTATION 79
TABLE 4-2: EXPERIMENTAL DESIGN AND VARIATIONS FOR INDOOR AND OUTDOOR RIGS. 82
TABLE 5-1: OVERALL INFLUENT CONCENTRATIONS FOR INFLOW 1 (GULLY POT LIQUOR) AND INFLOW 2 IN BRACKETS (GULLY POT LIQUOR MIXED WITH DOG FAECES) FROM MARCH 2008 TO APRIL 2010 (SAMPLE NUMBER N = 113) 120
TABLE 5-2: GUIDELINES FOR RECLAIMED WATER QUALITY AND TREATMENT REQUIREMENTS (EUROPEAN COMMISSION ENVIRONMENT, 1991, 2006; US EPA, 2004 B). 122
TABLE 5-3: ONE-SAMPLE KOLMOGOROV-SMIRNOV TEST FOR NORMALITY. FOR SIGNIFICANCE A > 0.05 SAMPLE FOLLOWS A NORMAL DISTRIBUTION (IN BOLD). 123
TABLE 5-4: ONE WAY ANOVA BETWEEN IN INDOOR (PPS 1-PPS 6) AND OUTDOOR RIG (PPS 1-PPS 6), SIGNIFICANT VALUES (P <0.05) IN BOLD. 126
TABLE 5-5: PAIRED ANOVA (INDOOR AND OUTDOOR RIGS) BETWEEN PPS STRUCTURE VARIATIONS AND TYPE OF URBAN RUNOFF TREATED, SIGNIFICANT VALUES (P <0.05) IN BOLD. 127
TABLE 5-6: PAIRED ANOVA BETWEEN HEATING AND COOLING CYCLES FOR PPS 1, 2, 4 AND 5 (INDOOR AND OUTDOOR RIGS), SIGNIFICANT VALUES (P<0.05) IN BOLD. 128
TABLE 5-7: DEOXYRIBONUCLEIC ACID SEQUENCING RESULTS FOR SAMPLES COLLECTED FROM INDOOR AND OUTDOOR RIGS 192
TABLE 5-8: MORPHOLOGY AND HEALTH SIGNIFICANCE OF WATERBORNE PATHOGENS IN THE PERMEABLE PAVEMENT SYSTEM 193
TABLE 5-9: AVERAGE COP AND EER PERFORMANCE INDEX RATIOS FOR THE GHP SYSTEM. 199
TABLE 6-1: THE PRINCIPLE PHOTOCHEMICAL REACTIONS AND MECHANISMS FOR TITANIUM DIOXIDE TiO_2 (AFTER WANG AND HONG, 1999; RINCÓN AND PULGARIN, 2003). 203
TABLE 6-2: UV LAMPS SPECIFICATIONS USED IN PHOTOCATALYTIC REACTOR (ULTRAVIOLET PRODUCTS LTD UNIT 1, TRINITY HALL FARM ESTATE, NUFFIELD ROAD, CAMBRIDGE, UK). 205
TABLE 6-3: INACTIVATION RATE CONSTANTS *K* (MIN-1) FOR TOTAL COLIFORMS, *E.COLI* AND *ENTEROCOCCI SP*. WITH UV, UV AND TITANIUM DIOXIDE IN BOTH IMMOBILISED AND SUSPENSION. 212
TABLE7-1: TYPICAL VALUES OF HYDRAULIC AND THERMAL PROPERTIES OF PERMEABLE PAVEMENT SYSTEMS (ADAPTED FROM- FREEZE AND CHERRY, 1979; LING *ET AL*., 1993; CHARBENEAU, 2000; HERMANSSON, 2001, 2004; BANKS, 2008; HERB *ET AL*., 2008.)..... 218
TABLE 7-2: THE USE OF DIFFERENT EMPIRICAL STATISTICAL EQUATIONS TO MEASURE THE ACCURACY OF THE 4^{TH} ORDER RUNGE-KUTTA METHOD IN PREDICTING THE TEMPERATURES..... 238
TABLE 8-1: RESULTS FOR THE OPTIMUM STRUCTURE OF THE BACK-PROPAGATION FEED-FORWARD NETWORK TRAINED USING VARIOUS ALGORITHMS 250
TABLE 8-2. STATISTICAL PERFORMANCE PARAMETERS OF ALGORITHMS FOR BACK-PROPAGATION FEED-FORWARD NEURAL NETWORKS..... 252
TABLE 9-1: SUMMARY OF STATISTICAL MEASUREMENTS OF KSOM MODELS FOR *ESCHERICHIA COLI*, *ENTEROCOCCI SP*. AND TOTAL COLIFORMS PREDICTIONS DURING TRAINING AND (VERIFICATION) WITH PPS 4 (PERMEABLE PAVEMENT COMBINED WITH GEOTHERMAL HEAT PUMP) AND PPS 6 (STANDALONE PERMEABLE PAVEMENT SYSTEM)..... 288

List of Figures

FIGURE 2-1: PERMEABLE PAVEMENT SURFACE WITH A STONE RESERVOIR UNDERNEATH (FROM TECECO, 2009). 21
FIGURE 2-2: SCHEMATIC LAYOUT OF A PERMEABLE PAVING PARKING BAY CONSISTING OF A SERIES OF LATTICE PLASTIC, CELLULAR UNITS, CONNECTED TOGETHER TO FORM A RAFT STRUCTURE THAT REPLACES SOME OR ALL OF THE PERMEABLE SUB-BASE, DEPENDING UPON THE ANTICIPATED TRAFFIC LOADING (INTERPAVE, 2010) 23
FIGURE 2-3: SCHEMATIC LAYOUT OF PERMEABLE (PERVIOUS) PAVEMENT SYSTEM (ADAPTED FROM INTERPAVE, 2010) 24
FIGURE 2-4: VARIOUS TYPES OF PERMEABLE PAVEMENT STRUCTURES REGARDING STORMWATER RUNOFF FOR (A) PARTIAL INFILTRATION, (B) TOTAL INFILTRATION AND (C) NO INFILTRATION (ADAPTED FROM INTERPAVE, (2010)). 27
FIGURE 2-5: STRESS LOADS ON PAVMENT BLOCK SURFACE (ADAPTED FROM DELATTE, (2008)). 31
FIGURE 2-6: HYDROLOGY AND HYDRAULIC FEATURES OF PERMEABLE PAVEMENTS (ADAPTED FROM FERGUSON, 2005). 35
FIGURE 2-7: INFILTRATION OF RAINFALL AND SERVICE LIFE OF PERMEABLE PAVEMENTS (ADAPTED FROM INTERPAVE, 2010) 45
FIGURE 2-8: UNIT WHOLE LIFE COSTS AND PAVEMENT TYPE FOR CBR OF 3 % AND 6 % (INTERPAVE/SCOTT WILSON, 2006). 55
FIGURE 3-1: DISTANCE BENEATH THE GROUND AND TEMPERATURE PROFILE IN THE U.K. DURING SUMMER (1), AUTUMN (2), WINTER 3 AND SPRING (4) (ADAPTED FROM BANKS, 2008) 58
FIGURE 3-2: DOMESTIC GEOTHERMAL HEAT PUMP COMPONENTS FOR SPACE HEATING AND COOLING (AFTER OCHSNER, (2007). 60
FIGURE 3-3: VARIOUS TYPES OF EARTH CONNECTION SYSTEMS ASSOCIATED WITH GHPS (GEOTHERMAL INTERNATIONAL, 2010) 64
FIGURE 3-4: THERMODYNAMIC CYCLE OF GEOTHERMAL HEAT PUMPS ACROSS COMPOMENTS (CENGEL AND BOLES, 2007) 65
FIGURE 3-6: COMPARISON OF CO_2 PRODUCED AND COST PER KWH FOR VARIOUS HEATING SYSTEMS (ADAPTED FROM COOL PLANET/MITSUBISHI ELECTRIC, 2009) 71
FIGURE 4-2: SCHEMATIC OF SIMULATED GEOTHERMAL HEATING AND COOLING SYSTEM SHOWING THE INTEGRATION OF PERMEABLE PAVEMENTS WITH THE WATER HEATER, WATER COOLER, AND POLYPROPYLENE TUBES PLACED IN THE LOWER SUB-BASE SATURATED WATER ZONE. 81
FIGURE 4-3: (A) INDOOR AND (B) OUTDOOR EXPERIMENTAL BINS FOR PPS AND COMBINED PPS-GHP 88
FIGURE 4-4: SCHEMATIC DIAGRAM OF THE NITROGEN CYCLE IN WATER. (ADAPTED FROM KIELY, 1997 AND CHIN, 2006) 99
FIGURE 4-5: GENERAL OVERVIEW OF KEY MOLECULAR MICROBIOLOGICAL TECHNIQUES. DNA, DEOXYRIBONUCLEIC ACID; RNA, RIBONUCLEIC ACID; PCR, POLYMERASE CHAIN REACTION; RT-PCR, REAL-TIME POLYMERASE CHAIN REACTION; DGGE, DENATURING GRADIENT GEL ELECTROPHORESIS; TGGE, TEMPERATURE GRADIENT GEL ELECTROPHORESIS. 114
FIGURE 4-6: CARBON DIOXIDE SAMPLING POINTS INSTALLED WITHIN PPS (NOT DRAWN TO SCALE) .. 115
FIGURE 5-1: EXPERIMENTAL LAYOUT OF INDOOR AND OUTDOOR RIGS WITH DESIGN VARIABLES FOR STATISTICAL ANALYSES. 119
FIGURE 5-2: WATER SAMPLE TEMPERATURES (°C) FOR INFLOW 1 (GULLY POT LIQUOR), INFLOW 2 (GULLY POT LIQUOR AND DOG FAECES) AND OUTFLOW FOR THE INDOOR AND OUTDOOR BINS. THE PLOTS REPRESENT THE 25TH PERCENTILE, MEDIAN AND THE 75TH PERCENTILE. THE WHISKERS REPRESENT THE 10TH AND 90TH PERCENTILES; SOLID CIRCLES REPRESENTS OUTLIERS (MARCH 2008 TO APRIL 2010, N = 113). 130
FIGURE 5-3: PH VALUES FOR INFLOW 1 (GULLY POT LIQUOR), INFLOW 2 (GULLY POT LIQUOR AND DOG FAECES) AND OUTFLOW FOR THE INDOOR AND OUTDOOR BINS. THE PLOTS REPRESENT THE 25TH PERCENTILE, MEDIAN AND THE 75TH PERCENTILE. THE WHISKERS REPRESENT THE 10TH AND 90TH PERCENTILES; SOLID CIRCLES REPRESENTS OUTLIERS AND STARS REPRESENTS EXTREME OUTLIERS (MARCH 2008 TO APRIL 2010, N = 113). 131
FIGURE 5-4: ELECTROCONDUCTIVITY CONCENTRATIONS FOR INFLOW 1 (GULLY POT LIQUOR) AND INFLOW 2 (GULLY POT LIQUOR AND DOG FAECES) (A) AND OUTFLOW FOR THE INDOOR AND OUTDOOR BINS (B). THE PLOTS REPRESENT THE 25TH PERCENTILE, MEDIAN AND THE 75TH

PERCENTILE. THE WHISKERS REPRESENT THE 10TH AND 90TH PERCENTILES (MARCH 2008 TO APRIL 2010, N = 113). 133
FIGURE 5-5: MEAN REMOVAL EFFICIENCIES WITH ERROR BARS FOR ELECTROCONDUCTIVITY DURING THE 1ST COOLING CYCLE (APRIL TO SEPTEMBER 2008), 1ST HEATING CYCLE (OCTOBER 2008 TO MARCH 2009), 2ND COOLING CYCLE (APRIL TO SEPTEMBER 2009) AND 2ND HEATING CYCLE (OCTOBER 2009 TO APRIL 2010) FOR INDOOR RIG (A) AND OUTDOOR RIG (B) (PPS1 TO PPS 6) RESPECTIVELY. 134
FIGURE 5-6: REDOX POTENTIAL CONCENTRATIONS FOR INFLOW 1 (GULLY POT LIQUOR) AND INFLOW 2 (GULLY POT LIQUOR AND DOG FAECES) AND OUTFLOW FOR THE INDOOR AND OUTDOOR BINS. THE PLOTS REPRESENT THE 25TH PERCENTILE, MEDIAN AND THE 75TH PERCENTILE. THE WHISKERS REPRESENT THE 10TH AND 90TH PERCENTILES (MARCH 2008 TO APRIL 2010, N = 113)..... 135
FIGURE 5-7: MEAN REMOVAL EFFICIENCIES WITH ERROR BARS FOR REDOX POTENTIAL DURING THE 1ST COOLING CYCLE (APRIL TO SEPTEMBER 2008), 1ST HEATING CYCLE (OCTOBER 2008 TO MARCH 2009), 2ND COOLING CYCLE (APRIL TO SEPTEMBER 2009) AND 2ND HEATING CYCLE (OCTOBER 2009 TO APRIL 2010) FOR INDOOR RIG (A) AND OUTDOOR RIG (B) (PPS1 TO PPS 6) RESPECTIVELY. 136
FIGURE 5-8: TOTAL DISSOLVED SOLIDS CONCENTRATIONS FOR INFLOW 1 (GULLY POT LIQUOR) AND INFLOW 2 (GULLY POT LIQUOR AND DOG FAECES) (A) AND OUTFLOW FOR THE INDOOR AND OUTDOOR BINS (B). THE PLOTS REPRESENT THE 25TH PERCENTILE, MEDIAN AND THE 75TH PERCENTILE. THE WHISKERS REPRESENT THE 10TH AND 90TH PERCENTILES; SOLID CIRCLES REPRESENTS OUTLIERS AND STARS REPRESENTS EXTREME OUTLIERS (MARCH 2008 TO APRIL 2010, N = 113). 138
FIGURE 5-9: MEAN REMOVAL EFFICIENCIES WITH ERROR BARS FOR TOTAL DISSOLVED SOLIDS DURING THE 1ST COOLING CYCLE (APRIL TO SEPTEMBER 2008), 1ST HEATING CYCLE (OCTOBER 2008 TO MARCH 2009), 2ND COOLING CYCLE (APRIL TO SEPTEMBER 2009) AND 2ND HEATING CYCLE (OCTOBER 2009 TO APRIL 2010) FOR INDOOR RIG (A) AND OUTDOOR RIG (B) (PPS1 TO PPS 6) RESPECTIVELY. 139
FIGURE 5-10: SUSPENDED SOLIDS CONCENTRATIONS FOR INFLOW 1 (GULLY POT LIQUOR) AND INFLOW 2 (GULLY POT LIQUOR AND DOG FAECES) (A) AND OUTFLOW FOR THE INDOOR AND OUTDOOR BINS (B). THE PLOTS REPRESENT THE 25TH PERCENTILE, MEDIAN AND THE 75TH PERCENTILE. THE WHISKERS REPRESENT THE 10TH AND 90TH PERCENTILES; SOLID CIRCLES REPRESENTS OUTLIERS AND STARS REPRESENTS EXTREME OUTLIERS (MARCH 2008 TO APRIL 2010, N = 113). 140
FIGURE 5-11: MEAN REMOVAL EFFICIENCIES WITH ERROR BARS FOR SUSPENDED SOLIDS DURING THE 1ST COOLING CYCLE (APRIL TO SEPTEMBER 2008), 1ST HEATING CYCLE (OCTOBER 2008 TO MARCH 2009), 2ND COOLING CYCLE (APRIL TO SEPTEMBER 2009) AND 2ND HEATING CYCLE (OCTOBER 2009 TO APRIL 2010) FOR INDOOR RIG (A) AND OUTDOOR RIG (B) (PPS1 TO PPS 6) RESPECTIVELY. 142
FIGURE 5-12: TURBIDITY CONCENTRATIONS FOR INFLOW 1 (GULLY POT LIQUOR) AND INFLOW 2 (GULLY POT LIQUOR AND DOG FAECES) (A) AND OUTFLOW FOR THE INDOOR AND OUTDOOR BINS (B). THE PLOTS REPRESENT THE 25TH PERCENTILE, MEDIAN AND THE 75TH PERCENTILE. THE WHISKERS REPRESENT THE 10TH AND 90TH PERCENTILES; SOLID CIRCLES REPRESENTS OUTLIERS AND STARS REPRESENTS EXTREME OUTLIERS (MARCH 2008 TO APRIL 2010, N = 113)..... 143
FIGURE 5-13: MEAN REMOVAL EFFICIENCIES WITH ERROR BARS FOR TURBIDITY DURING THE 1ST COOLING CYCLE (APRIL TO SEPTEMBER 2008), 1ST HEATING CYCLE (OCTOBER 2008 TO MARCH 2009), 2ND COOLING CYCLE (APRIL TO SEPTEMBER 2009) AND 2ND HEATING CYCLE (OCTOBER 2009 TO APRIL 2010) FOR INDOOR RIG (A) AND OUTDOOR RIG (B) (PPS1 TO PPS 6) RESPECTIVELY. 145
FIGURE 5-14: BIOCHEMICAL OXYGEN DEMAND CONCENTRATIONS FOR INFLOW 1 (GULLY POT LIQUOR) AND INFLOW 2 (GULLY POT LIQUOR AND DOG FAECES) (A) AND OUTFLOW FOR THE INDOOR AND OUTDOOR BINS (B). THE PLOTS REPRESENT THE 25TH PERCENTILE, MEDIAN AND THE 75TH PERCENTILE. THE WHISKERS REPRESENT THE 10TH AND 90TH PERCENTILES; SOLID CIRCLES REPRESENTS OUTLIERS AND STARS REPRESENTS EXTREME OUTLIERS (MARCH 2008 TO APRIL 2010, N = 113). 147
FIGURE 5-15: MEAN REMOVAL EFFICIENCIES WITH ERROR BARS FOR BIOCHEMICAL OXYGEN DEMAND DURING THE 1ST COOLING CYCLE (APRIL TO SEPTEMBER 2008), 1ST HEATING CYCLE (OCTOBER 2008 TO MARCH 2009), 2ND COOLING CYCLE (APRIL TO SEPTEMBER 2009) AND 2ND HEATING CYCLE (OCTOBER 2009 TO APRIL 2010) FOR INDOOR RIG (A) AND OUTDOOR RIG (B) (PPS1 TO PPS 6) RESPECTIVELY. 148

FIGURE 5-16: CHEMICAL OXYGEN DEMAND CONCENTRATIONS FOR INFLOW 1 (GULLY POT LIQUOR) AND INFLOW 2 (GULLY POT LIQUOR AND DOG FAECES) (A) AND OUTFLOW FOR THE INDOOR AND OUTDOOR BINS (B). THE PLOTS REPRESENT THE 25TH PERCENTILE, MEDIAN AND THE 75TH PERCENTILE. THE WHISKERS REPRESENT THE 10TH AND 90TH PERCENTILES; SOLID CIRCLES REPRESENTS OUTLIERS AND STARS REPRESENTS EXTREME OUTLIERS (MARCH 2008 TO APRIL 2010, N = 113). 150
FIGURE 5-17: MEAN REMOVAL EFFICIENCIES WITH ERROR BARS FOR BIOCHEMICAL OXYGEN DEMAND DURING THE 1ST COOLING CYCLE (APRIL TO SEPTEMBER 2008), 1ST HEATING CYCLE (OCTOBER 2008 TO MARCH 2009), 2ND COOLING CYCLE (APRIL TO SEPTEMBER 2009) AND 2ND HEATING CYCLE (OCTOBER 2009 TO APRIL 2010) FOR INDOOR RIG (A) AND OUTDOOR RIG (B) (PPS1 TO PPS 6) RESPECTIVELY. 151
FIGURE 5-18: DISSOLVED OXYGEN CONCENTRATIONS FOR INFLOW 1 (GULLY POT LIQUOR) AND INFLOW 2 (GULLY POT LIQUOR AND DOG FAECES) AND OUTFLOW FOR THE INDOOR AND OUTDOOR BINS. THE PLOTS REPRESENT THE 25TH PERCENTILE, MEDIAN AND THE 75TH PERCENTILE. THE WHISKERS REPRESENT THE 10TH AND 90TH PERCENTILES; SOLID CIRCLES REPRESENTS OUTLIERS (MARCH 2008 TO APRIL 2010, N = 113). 152
FIGURE 5-19: MEAN REMOVAL EFFICIENCIES WITH ERROR BARS FOR DISSOLVED OXYGEN DURING THE 1ST COOLING CYCLE (APRIL TO SEPTEMBER 2008), 1ST HEATING CYCLE (OCTOBER 2008 TO MARCH 2009), 2ND COOLING CYCLE (APRIL TO SEPTEMBER 2009) AND 2ND HEATING CYCLE (OCTOBER 2009 TO APRIL 2010) FOR INDOOR RIG (A) AND OUTDOOR RIG (B) (PPS1 TO PPS 6) RESPECTIVELY. 154
FIGURE 5-20: CARBON DIOXIDE OUTFLOW CONCENTRATIONS FOR PPS 1 AND PPS 5 (INDOOR AND OUTDOOR RIG) THE PLOTS REPRESENT THE 25TH PERCENTILE, MEDIAN AND THE 75TH PERCENTILE. THE WHISKERS REPRESENT THE 10TH AND 90TH PERCENTILES; SOLID CIRCLES REPRESENTS OUTLIERS (MARCH 2008 TO APRIL 2010, N = 113). 155
FIGURE 5-21: AMMONIA-NITROGEN CONCENTRATIONS FOR INFLOW 1 (GULLY POT LIQUOR) AND INFLOW 2 (GULLY POT LIQUOR AND DOG FAECES) (A) AND OUTFLOW CONCENTRATIONS FOR THE INDOOR AND OUTDOOR BINS (B). THE PLOTS REPRESENT THE 25TH PERCENTILE, MEDIAN AND THE 75TH PERCENTILE. THE WHISKERS REPRESENT THE 10TH AND 90TH PERCENTILES; SOLID CIRCLES REPRESENTS OUTLIERS AND STARS REPRESENTS EXTREME OUTLIERS (MARCH 2008 TO APRIL 2010, N = 113). 157
FIGURE 5-22: MEAN REMOVAL EFFICIENCIES WITH ERROR BARS FOR AMMONIA-NITROGEN DURING THE 1ST COOLING CYCLE (APRIL TO SEPTEMBER 2008), 1ST HEATING CYCLE (OCTOBER 2008 TO MARCH 2009), 2ND COOLING CYCLE (APRIL TO SEPTEMBER 2009) AND 2ND HEATING CYCLE (OCTOBER 2009 TO APRIL 2010) FOR INDOOR RIG (A) AND OUTDOOR RIG (B) (PPS1 TO PPS 6) RESPECTIVELY. 158
FIGURE 5-23: NITRATE-NITROGEN CONCENTRATIONS FOR INFLOW 1 (GULLY POT LIQUOR) AND INFLOW 2 (GULLY POT LIQUOR AND DOG FAECES) (A) AND OUTFLOW CONCENTRATIONS FOR THE INDOOR AND OUTDOOR BINS (B). THE PLOTS REPRESENT THE 25TH PERCENTILE, MEDIAN AND THE 75TH PERCENTILE. THE WHISKERS REPRESENT THE 10TH AND 90TH PERCENTILES; SOLID CIRCLES REPRESENTS OUTLIERS AND STARS REPRESENTS EXTREME OUTLIERS (MARCH 2008 TO APRIL 2010, N = 113). 160
FIGURE 5-24: MEAN REMOVAL EFFICIENCIES WITH ERROR BARS FOR NITRATE-NITROGEN DURING THE 1ST COOLING CYCLE (APRIL TO SEPTEMBER 2008), 1ST HEATING CYCLE (OCTOBER 2008 TO MARCH 2009), 2ND COOLING CYCLE (APRIL TO SEPTEMBER 2009) AND 2ND HEATING CYCLE (OCTOBER 2009 TO APRIL 2010) FOR INDOOR RIG (A) AND OUTDOOR RIG (B) (PPS1 TO PPS 6) RESPECTIVELY. 161
FIGURE 5-25: ORTHO-PHOSPHATE-PHOSPHOROUS CONCENTRATIONS FOR INFLOW 1 (GULLY POT LIQUOR) AND INFLOW 2 (GULLY POT LIQUOR AND DOG FAECES) (A) AND OUTFLOW CONCENTRATIONS FOR THE INDOOR AND OUTDOOR BINS (B). THE PLOTS REPRESENT THE 25TH PERCENTILE, MEDIAN AND THE 75TH PERCENTILE. THE WHISKERS REPRESENT THE 10TH AND 90TH PERCENTILES; SOLID CIRCLES REPRESENTS OUTLIERS AND STARS REPRESENTS EXTREME OUTLIERS (MARCH 2008 TO APRIL 2010, N = 113). 163
FIGURE 5-26: MEAN REMOVAL EFFICIENCIES WITH ERROR BARS FOR ORTHO-PHOSPHATE-PHOSPHOROUS DURING THE 1ST COOLING CYCLE (APRIL TO SEPTEMBER 2008), 1ST HEATING CYCLE (OCTOBER 2008 TO MARCH 2009), 2ND COOLING CYCLE (APRIL TO SEPTEMBER 2009) AND 2ND HEATING CYCLE (OCTOBER 2009 TO APRIL 2010) FOR INDOOR RIG (A) AND OUTDOOR RIG (B) (PPS1 TO PPS 6) RESPECTIVELY. 164

FIGURE 5-27: *ESCHERICHIA COLI* CONCENTRATIONS FOR INFLOW 1 (GULLY POT LIQUOR) AND INFLOW 2 (GULLY POT LIQUOR AND DOG FAECES) AND OUTFLOW CONCENTRATIONS FOR THE INDOOR AND OUTDOOR BINS. THE PLOTS REPRESENT THE 25TH PERCENTILE, MEDIAN AND THE 75TH PERCENTILE. THE WHISKERS REPRESENT THE 10TH AND 90TH PERCENTILES; SOLID CIRCLES REPRESENTS OUTLIERS AND STARS REPRESENTS EXTREME OUTLIERS (MARCH 2008 TO APRIL 2010, N = 113). 166
FIGURE 5-28: MEAN REMOVAL EFFICIENCIES WITH ERROR BARS FOR *ESCHERICHIA COLI* DURING THE 1ST COOLING CYCLE (APRIL TO SEPTEMBER 2008), 1ST HEATING CYCLE (OCTOBER 2008 TO MARCH 2009), 2ND COOLING CYCLE (APRIL TO SEPTEMBER 2009) AND 2ND HEATING CYCLE (OCTOBER 2009 TO APRIL 2010) FOR INDOOR RIG (A) AND OUTDOOR RIG (B) (PPS1 TO PPS 6) RESPECTIVELY. 167
FIGURE 5-29: *ENTEROCOCCI SP.* CONCENTRATIONS FOR INFLOW 1 (GULLY POT LIQUOR) AND INFLOW 2 (GULLY POT LIQUOR AND DOG FAECES) AND OUTFLOW CONCENTRATIONS FOR THE INDOOR AND OUTDOOR BINS. THE PLOTS REPRESENT THE 25TH PERCENTILE, MEDIAN AND THE 75TH PERCENTILE. THE WHISKERS REPRESENT THE 10TH AND 90TH PERCENTILES; SOLID CIRCLES REPRESENTS OUTLIERS (MARCH 2008 TO APRIL 2010, N = 113). 169
FIGURE 5-30: MEAN REMOVAL EFFICIENCIES WITH ERROR BARS FOR *ENTEROCOCCI SP.* DURING THE 1ST COOLING CYCLE (APRIL TO SEPTEMBER 2008), 1ST HEATING CYCLE (OCTOBER 2008 TO MARCH 2009), 2ND COOLING CYCLE (APRIL TO SEPTEMBER 2009) AND 2ND HEATING CYCLE (OCTOBER 2009 TO APRIL 2010) FOR INDOOR RIG (A) AND OUTDOOR RIG (B) (PPS1 TO PPS 6) RESPECTIVELY. 170
FIGURE 5-31: TOTAL COLIFORMS CONCENTRATIONS FOR INFLOW 1 (GULLY POT LIQUOR) AND INFLOW 2 (GULLY POT LIQUOR AND DOG FAECES) (A) AND OUTFLOW CONCENTRATIONS FOR THE INDOOR AND OUTDOOR BINS (B). THE PLOTS REPRESENT THE 25TH PERCENTILE, MEDIAN AND THE 75TH PERCENTILE. THE WHISKERS REPRESENT THE 10TH AND 90TH PERCENTILES; SOLID CIRCLES REPRESENTS OUTLIERS (MARCH 2008 TO APRIL 2010, N = 113). 172
FIGURE 5-32: MEAN REMOVAL EFFICIENCIES WITH ERROR BARS FOR TOTAL COLIFORMS DURING THE 1ST COOLING CYCLE (APRIL TO SEPTEMBER 2008), 1ST HEATING CYCLE (OCTOBER 2008 TO MARCH 2009), 2ND COOLING CYCLE (APRIL TO SEPTEMBER 2009) AND 2ND HEATING CYCLE (OCTOBER 2009 TO APRIL 2010) FOR (A) INDOOR RIG AND (B) OUTDOOR RIG (PPS1 TO PPS 6) RESPECTIVELY. 174
FIGURE 5-33: TOTAL HETEROTROPHIC BACTERIA CONCENTRATIONS FOR INFLOW 1 (GULLY POT LIQUOR) AND INFLOW 2 (GULLY POT LIQUOR AND DOG FAECES) AND OUTFLOW CONCENTRATIONS FOR THE INDOOR AND OUTDOOR BINS (B). THE PLOTS REPRESENT THE 25TH PERCENTILE, MEDIAN AND THE 75TH PERCENTILE. THE WHISKERS REPRESENT THE 10TH AND 90TH PERCENTILES; SOLID CIRCLES REPRESENTS OUTLIERS (MARCH 2008 TO APRIL 2010, N = 113). 175
FIGURE 5-34: MEAN REMOVAL EFFICIENCIES WITH ERROR BARS FOR TOTAL HETEROTROPHIC BACTERIA (THB) DURING THE 1ST COOLING CYCLE (APRIL TO SEPTEMBER 2008), 1ST HEATING CYCLE (OCTOBER 2008 TO MARCH 2009), 2ND COOLING CYCLE (APRIL TO SEPTEMBER 2009) AND 2ND HEATING CYCLE (OCTOBER 2009 TO APRIL 2010) FOR (A) INDOOR RIG AND (B) OUTDOOR RIG (PPS1 TO PPS 6) RESPECTIVELY. 176
FIGURE 5-35: *SALMONELLA SP.* CONCENTRATIONS FOR INFLOW 1 (GULLY POT LIQUOR) AND INFLOW 2 (GULLY POT LIQUOR AND DOG FAECES) AND OUTFLOW CONCENTRATIONS FOR THE INDOOR AND OUTDOOR BINS. THE PLOTS REPRESENT THE 25TH PERCENTILE, MEDIAN AND THE 75TH PERCENTILE. THE WHISKERS REPRESENT THE 10TH AND 90TH PERCENTILES; SOLID CIRCLES REPRESENTS OUTLIERS (MARCH 2008 TO APRIL 2010, N = 113). 178
FIGURE 5-36: MEAN REMOVAL EFFICIENCIES WITH ERROR BARS FOR *SALMONELLA SP.* DURING THE 1ST COOLING CYCLE (APRIL TO SEPTEMBER 2008), 1ST HEATING CYCLE (OCTOBER 2008 TO MARCH 2009), 2ND COOLING CYCLE (APRIL TO SEPTEMBER 2009) AND 2ND HEATING CYCLE (OCTOBER 2009 TO APRIL 2010) FOR (A) INDOOR RIG AND (B) OUTDOOR RIG (PPS1 TO PPS 6) RESPECTIVELY. 179
FIGURE 5-37: *SHIGELLA SP.* CONCENTRATIONS FOR INFLOW 1 (GULLY POT LIQUOR) AND INFLOW 2 (GULLY POT LIQUOR AND DOG FAECES) AND OUTFLOW CONCENTRATIONS FOR THE INDOOR AND OUTDOOR BINS. THE PLOTS REPRESENT THE 25TH PERCENTILE, MEDIAN AND THE 75TH PERCENTILE. THE WHISKERS REPRESENT THE 10TH AND 90TH PERCENTILES; SOLID CIRCLES REPRESENTS OUTLIERS (MARCH 2008 TO APRIL 2010, N = 113). 181
FIGURE 5-38: MEAN REMOVAL EFFICIENCIES WITH ERROR BARS FOR *SALMONELLA SP.* DURING THE 1ST COOLING CYCLE (APRIL TO SEPTEMBER 2008), 1ST HEATING CYCLE (OCTOBER 2008 TO MARCH

2009), 2ND COOLING CYCLE (APRIL TO SEPTEMBER 2009) AND 2ND HEATING CYCLE (OCTOBER 2009 TO APRIL 2010) FOR (A) INDOOR RIG AND (B) OUTDOOR RIG (PPS1 TO PPS 6) RESPECTIVELY. 182
FIGURE 5-39: GRAM STAINING RESULTS FOR (A) INFLOW 2 (NOVEMBER 2008) (B) INFLOW 1 (NOVEMBER 2008), (C) INFLOW 2 (MAY 2009) AND (D) INFLOW 1 (MAY 2009) 1
FIGURE 5-40: CORRESPONDING GRAM STAINING RESULTS FOR (A) PPS 4 (INDOOR RIG) EFFLUENT (NOVEMBER 2008), (B) PPS 2 (INDOOR RIG) EFFLUENT (NOVEMBER 2008), (C) PPS 4 (INDOOR RIG) EFFLUENT (MAY 2009), (D) PPS 2 (INDOOR RIG EFFLUENT) INFLOW 2 (MAY 2009)..... 187
FIGURE 5-41: PHYLOGENETIC TREE ILLUSTRATING THE BACTERIAL ISOLATES PRESENT IN THE SATURATED ZONE OF THE EXPERIMENTAL PERMEABLE PAVEMENT SYSTEM AND THE CLOSEST RELATED ORGANISMS (TABLE 5-7). *METHANOSPIRILLUM HUNGATEI* WAS ADDED AS THE OUTLIER ORGANISM. 189
FIGURE 5-42: DENATURING GRADIENT GEL ELECTROPHORESIS (DGGE) GEL SHOWING THE BACTERIAL COMMUNITIES IN THE INFLOW AND OUTFLOW OF THE EXPERIMENTAL PERMEABLE PAVEMENT SYSTEM. I AND I+F REPRESENT BACTERIAL COMMUNITIES IN THE INFLOW WITH AND WITHOUT DOG FAECES, RESPECTIVELY. THE POSITIONS TO WHICH THE BANDS FROM THE KNOWN ISOLATES HAVE MIGRATED IN THE GEL ARE INDICATED BY ARROWS. THESE ISOLATES ARE INDICATED IN THE INFLOW AND OUTFLOW COMMUNITIES, REPRESENTED BY OPEN ELLIPSES. 191
FIGURE 5-43: OVERALL GEOTHERMAL COOLING TEMPERATURES OF SUB-BASE ZONE FOR PPS DURING 1ST AND 2ND COOLING CYCLES. THE PLOTS REPRESENT THE 25TH PERCENTILE, MEDIAN AND THE 75TH PERCENTILE. THE WHISKERS REPRESENT THE 10TH AND 90TH PERCENTILES; SOLID CIRCLES REPRESENTS OUTLIERS (MARCH 2008 TO APRIL 2010, N = 113). 195
FIGURE 5-44: OVERALL GEOTHERMAL HEATING TEMPERATURES OF SUB-BASE ZONE FOR PPS DURING 1ST AND 2ND HEATING CYCLES. THE PLOTS REPRESENT THE 25TH PERCENTILE, MEDIAN AND THE 75TH PERCENTILE. THE WHISKERS REPRESENT THE 10TH AND 90TH PERCENTILES; SOLID CIRCLES REPRESENTS OUTLIERS (MARCH 2008 TO APRIL 2010, N = 113). 195
FIGURE 5-45: OVERALL ENERGY EFFICIENCY RATIO (EER) FOR INDOOR AND OUTDOOR RIGS FOR BOTH COOLING CYCLES. THE PLOTS REPRESENT THE 25TH PERCENTILE, MEDIAN AND THE 75TH PERCENTILE. THE WHISKERS REPRESENT THE 10TH AND 90TH PERCENTILES; SOLID CIRCLES REPRESENTS OUTLIERS (MARCH 2008 TO APRIL 2010, N = 113). 197
FIGURE 5-46: OVERALL COEFFICIENT OF PERFORMANCE (COP) FOR INDOOR AND OUTDOOR RIGS FOR BOTH HEATING CYCLES. THE PLOTS REPRESENT THE 25TH PERCENTILE, MEDIAN AND THE 75TH PERCENTILE. THE WHISKERS REPRESENT THE 10TH AND 90TH PERCENTILES; SOLID CIRCLES REPRESENTS OUTLIERS AND STARS REPRESENTS EXTREME OUTLIERS (MARCH 2008 TO APRIL 2010, N = 113). 198
FIGURE 6-1: THE PHOTOCATALYTIC PROCESS WITH UV LIGHT AND TITANIUM DIOXIDE (TIO_2) ABSORBS ULTRAVIOLET (UV) RADIATION FROM EITHER SUNLIGHT OR ILLUMINATED SOURCE (UV LAMPS) AND PRODUCES TWO OXIDATION REACTANTS (I) HYDROXYL RADICALS AND SUPEROXIDE ANIONS WHICH DECOMPOSE TOXIC ORGANIC SUBSTANCES VIA OXIDATION. (ADAPTED FROM WIST *ET AL.,* 2002; HERRMANN, 2005) 202
FIGURE 6-2: SCHEMATIC OF THE PHOTOCATALYTIC EXPERIMENTAL APPARATUS FOR THE PHOTOCHEMICAL REACTORS (BATCH PROCESSES), UV TREATMENT ONLY, UV+TIO_2 IN IMMOBILISED AND SUSPENDED FORMS. 206
FIGURE 6-3: SURVIVAL OF TOTAL COLIFORMS (CFU/100ML) IN THE PRESENCE OF ULTRAVIOLGIHT LIGHT RADIATION ONLY (UV), IMMOBILISED AND SUSPENDED POWDERED FORM OF TIO_2 IN CONCENTRATIONS OF 200MG/L, 400MG/L AND 600MG/L. THE INITIAL VALUES OF TURBIDITY (4.2 NTU) AND TOTAL COLIFORMS (N_0= 9.54×10^5 +/- 2000 CFU *PER* 100 ML) FROM PPS 1 (OUTDOOR RIG) EFFLUENT. 208
FIGURE 6-4: SURVIVAL OF *E. COLI* IN THE PRESENCE OF ULTRAVIOLGIHT LIGHT RADIATION ONLY (UV), IMMOBILISED AND SUSPENDED POWDERED FORM OF TIO_2 IN CONCENTRATIONS OF 200MG/L, 400MG/L AND 600MG/L. THE INITIAL VALUES OF TURBIDITY (1.5NTU) AND *E. COLI* (N_0= 7.54×10^4 +/- 230 CFU *PER* 100 ML) FROM PPS 1 (OUTDOOR RIG) EFFLUENT. 210
FIGURE 6-5: SURVIVAL OF *ENTEROCOCCI SP.* IN THE PRESENCE OF ULTRA VIOLET LIGHT RADIATION ONLY (UV) IMMOBILISED AND SUSPENDED POWDERED FORM OF TIO_2 IN CONCENTRATIONS OF 200MG/L, 400MG/L AND 600MG/L. THE INITIAL VALUES OF TURBIDITY (5.4NTU) AND *ENTEROCOCCI SP.* (N_0= 3.90×10^3 +/- 170 CFU *PER* 100 ML) FROM PPS 1 (OUTDOOR RIG) EFFLUENT. 212

FIGURE 6-6: CONCEPTUAL SCHEMATIC OF PERMEABLE PAVEMENTS FOR INITIAL FILTRATION AND TREATMENT OF URBAN RUNOFF FOLLOWED BY PHOTOCATYLTIC DECONTAMINATION WITH SOLAR ENERGY. 214
FIGURE 7-1: SCHEMATIC OF WATER AND ENERGY BALANCE FOR GEOTHERMAL PAVING SYSTEM ENERGY AND TEMPERATURE MODEL. 217
FIGURE 7-2: (A) THE MODELLED, PREDICTED AND ENVIRONMENTAL TEMPERATURES FOR THE GEOTHERMAL PAVING SYSTEM (PPS 1 OUTDOOR RIG) IN A COOLING CYCLE PLOTTED AGAINST TIME. THE MODEL HAD A TENDENCY OF UNDER-PREDICTING THE SYSTEMS TEMPERATURE (AVERAGE BIAS OF 1.9 °C); (B) THE SCATTER PLOT FOR THE BEST-FIT LINE Y = 0.65X+3.2, THE CORRESPONDING CORRELATION COEFFICIENT R = 0.871, AND THE UNITY LINE Y = X FOR THE COOLING CYCLE MEASUREMENT OF THE MODEL'S ACCURACY. FOR GPS 1, THE MODEL WAS RUN FOR THE PERIOD (02/04/2009 TO 11/09/2009) WITH N = 40 SAMPLE POINTS. 234
FIGURE 7-3: (A) THE MODELLED, PREDICTED AND ENVIRONMENTAL TEMPERATURES FOR THE GEOTHERMAL PAVING SYSTEM (PPS 1 OUTDOOR RIG) IN A HEATING CYCLE PLOTTED AGAINST TIME. THE MODEL HAD A TENDENCY OF OVER-PREDICTING THE SYSTEMS TEMPERATURE (AVERAGE BIAS OF 0.64 °C); (B) THE SCATTER PLOT FOR THE BEST-FIT LINE Y = 0.72X + 5.2, THE CORRESPONDING CORRELATION COEFFICIENT, R = 0.947 AND THE UNITY LINE Y = X FOR THE HEATING CYCLE MEASUREMENT OF THE MODEL'S ACCURACY. FOR GPS 1, THE MODEL WAS RUN FOR THE PERIOD (01/10/2008 TO 08/04/2009) WITH N = 40 SAMPLE POINTS. 235
FIGURE 7-4: (A) THE MODELLED, PREDICTED AND ENVIRONMENTAL TEMPERATURES FOR THE GEOTHERMAL PAVING SYSTEM (PPS 4 OUTDOOR RIG) IN A COOLING CYCLE PLOTTED AGAINST TIME. THE MODEL HAD A TENDENCY OF UNDER-PREDICTING THE SYSTEMS TEMPERATURE (AVERAGE BIAS OF -0.75°C); (B) THE SCATTER PLOT FOR THE BEST-FIT LINE Y=0.87X +0.51, THE CORRESPONDING CORRELATION COEFFICIENT, R= 0.825 AND THE UNITY LINE Y=X FOR THE COOLING CYCLE FOR MEASUREMENT OF THE MODEL'S ACCURACY. FOR GPS 2, THE MODEL WAS RUN FOR THE PERIOD (02/04/2008 TO 11/09/2009) WITH N=40 SAMPLE POINTS. 236
FIGURE 7-5: (A) THE MODELLED, PREDICTED AND ENVIRONMENTAL TEMPERATURES FOR THE GEOTHERMAL PAVING SYSTEM (PPS 4 OUTDOOR RIG) IN A HEATING CYCLE PLOTTED AGAINST TIME. THE MODEL HAD A TENDENCY OF OVER-PREDICTING THE SYSTEMS TEMPERATURE (AVERAGE BIAS OF 1.46° C; (B) THE SCATTER PLOT FOR THE BEST-FIT LINE Y=1.02X, THE CORRESPONDING CORRELATION COEFFICIENT, R = 0.881 AND THE UNITY LINE Y = X FOR THE COOLING CYCLE FOR MEASURING THE MODEL'S ACCURACY. FOR GPS 2, THE MODEL WAS RUN FOR THE PERIOD (01/10/2008 TO 08/04/2009) WITH N=40 SAMPLE POINTS. 237
FIGURE 8-1: ARCHITECTURE AND STRUCTURE OF THE FEED-FORWARD BACK PROPAGATION NEURAL NETWORK MODEL 244
FIGURE 8-2: MATLAB OUTPUT FOR TRAINING PERIOD WITH QUASI-NEWTON ALGORITHM FOR BOD. 250
FIGURE 8-3: COMPARISON OF THE MEASURED (OBSERVED) AND PREDICTED BIOCHEMICAL OXYGEN DEMAND (BOD) CONCENTRATIONS. 253
FIGURE 8-4: LINEAR REGRESSION BETWEEN THE NETWORK OUTPUTS AND CORRESPONDING TARGETS FOR THE BIOCHEMICAL OXYGEN DEMAND (BOD) USING THE (A) LEVENBERG-MARQUARDT, (B) QUASI-NEWTON, AND (C) BAYESIAN REGULARIZATION ALGORITHMS 255
FIGURE 8-5: COMPARISON OF THE MEASURED (OBSERVED) AND PREDICTED AMMONIA-NITROGEN (NH_4-N) CONCENTRATIONS 256
FIGURE 8-6: LINEAR REGRESSION BETWEEN THE NETWORK OUTPUTS AND CORRESPONDING TARGETS FOR THE AMMONIA-NITROGEN (NH_4-N) USING THE (A) LEVENBERG-MARQUARDT, (B) QUASI-NEWTON, AND (C) BAYESIAN REGULARIZATION ALGORITHMS 258
FIGURE 8-7: COMPARISON OF THE MEASURED (OBSERVED) AND PREDICTED NITRATE-NITROGEN (NO_3-N) CONCENTRATIONS 259
FIGURE 8-8: LINEAR REGRESSION BETWEEN THE NETWORK OUTPUTS AND CORRESPONDING TARGETS FOR THE NITRATE-NITROGEN (NO_3-N) USING THE (A) LEVENBERG-MARQUARDT, (B) QUASI-NEWTON, AND (C) BAYESIAN REGULARIZATION ALGORITHMS 261
FIGURE 8-9: COMPARISON OF THE MEASURED (OBSERVED) AND PREDICTED ORTHO-PHOSPHATE-PHOSPHORUS (PO_4-N) CONCENTRATIONS 263
FIGURE 8- 10: LINEAR REGRESSION BETWEEN THE NETWORK OUTPUTS AND CORRESPONDING TARGETS FOR THE ORTHO-PHOSPHATE-PHOSPHORUS (PO_4-N) USING THE (A) LEVENBERG-MARQUARDT, (B) QUASI-NEWTON, AND (C) BAYESIAN REGULARIZATION ALGORITHMS 264
FIGURE 9-1: ILLUSTRATING THE KOHONEN SELF-ORGANISING MAP AND ITS NEIGHBORHOOD NETWORK. 269

FIGURE 9-2: COMPONENT PLANES AND U-MATRIX VISUALIZATIONS OF THE RELATIONSHIPS BETWEEN *ESCHERICHIA COLI* (CFU/100ML) AND GEOTHERMAL HEATING/COOLING TEMPERATURE (°C), WATER SAMPLE TEMPERATURE (°C), PH, ELECTROCONDUCTIVITY (MS/CM), TOTAL DISSOLVED SOLIDS (MG/L), SUSPENDED SOLIDS (MG/L), TURBIDITY (NTU), AND CHEMICAL OXYGEN DEMAND (MG/L) IN STORMWATER FOR PPS 4 (OUTDOOR RIG) THE COMBINED PERMEABLE PAVEMENT AND GEOTHERMAL HEAT PUMP SYSTEM. 275
FIGURE 9-3: COMPONENT PLANES AND U-MATRIX VISUALIZATIONS OF THE RELATIONSHIPS BETWEEN *ESCHERICHIA COLI* (CFU/100ML) AND WATER SAMPLE TEMPERATURE (°C), PH, ELECTROCONDUCTIVITY (MS/CM), TOTAL DISSOLVED SOLIDS (MG/L), SUSPENDED SOLIDS (MG/L), TURBIDITY (NTU), AND CHEMICAL OXYGEN DEMAND (MG/L) IN STORMWATER FOR PPS 6 (OUTDOOR RIG) THE STANDALONE PERMEABLE PAVEMENT SYSTEM. 276
FIGURE 9-4: COMPARISON OF THE ACTUAL AND PREDICTED EFFLUENT CONCENTRATIONS OF *ESCHERICHIA COLI* BY SELF-ORGANISING MAP (SOM) FOR (A) PPS 4(OUTDOOR RIG) PERMEABLE PAVEMENT COMBINED WITH GEOTHERMAL HEAT PUMP SYSTEM AND (B) PPS 6 (OUTDOOR RIG) STANDALONE PERMEABLE PAVEMENT SYSTEM. SAMPLE NUMBER N= 112 WEEKS FOR A 2 YEAR PERIOD FROM 4 MARCH 2008 TO 5 MARCH 2010). 277
FIGURE 9-5: COMPONENT PLANES AND U-MATRIX VISUALIZATIONS OF THE RELATIONSHIPS BETWEEN *ENTEROCOCCI SP.* (CFU/100ML) AND GEOTHERMAL HEATING/COOLING TEMPERATURES (°C), WATER SAMPLE TEMPERATURE (°C), PH, ELECTROCONDUCTIVITY (MS/CM), TOTAL DISSOLVED SOLIDS (MG/L), SUSPENDED SOLIDS (MG/L), TURBIDITY (NTU), AND CHEMICAL OXYGEN DEMAND (MG/L) IN STORMWATER FOR PPS 4 (OUTDOOR RIG) COMBINED PERMEABLE PAVEMENT AND GEOTHERMAL HEAT PUMP SYSTEMS. 279
FIGURE 9-6: COMPONENT PLANES AND U-MATRIX VISUALIZATIONS OF THE RELATIONSHIPS BETWEEN *ENTEROCOCCI SP.* (CFU/100ML) AND WATER SAMPLE TEMPERATURE (°C), PH, ELECTROCONDUCTIVITY (MS/CM), TOTAL DISSOLVED SOLIDS (MG/L), SUSPENDED SOLIDS (MG/L), TURBIDITY (NTU), AND CHEMICAL OXYGEN DEMAND (MG/L) IN STORMWATER FOR PPS 6 (OUTDOOR RIG) THE STANDALONE PERMEABLE PAVEMENT SYSTEM. 280
FIGURE 9-7: COMPARISON OF THE ACTUAL AND PREDICTED EFFLUENT CONCENTRATIONS OF *ENTEROCOCCI SP.* BY SELF-ORGANISING MAP (SOM) FOR (A) PPS 4 (OUTDOOR RIG) PERMEABLE PAVEMENT COMBINED WITH GEOTHERMAL HEAT PUMP SYSTEM AND (B) PPS 6 (OUTDOOR RIG) STANDALONE PERMEABLE PAVEMENT SYSTEM. SAMPLE NUMBER N= 112 WEEKS FOR A 2 YEAR PERIOD FROM 4 MARCH 2008 TO 5 MARCH 2010). 281
FIGURE 9-8: COMPONENT PLANES AND U-MATRIX VISUALIZATIONS OF THE RELATIONSHIPS BETWEEN TOTAL COLIFORMS (CFU/100ML) AND GEOTHERMAL HEATING/COOLING TEMPERATURES (°C), WATER SAMPLE TEMPERATURES (°C), PH, ELECTROCONDUCTIVITY (MS/CM), TOTAL DISSOLVED SOLIDS (MG/L), SUSPENDED SOLIDS (MG/L), TURBIDITY (NTU), AND CHEMICAL OXYGEN DEMAND (MG/L) IN STORMWATER FOR PPS 4 (OUTDOOR RIG) COMBINED GEOTHERMAL HEAT PUMPS AND PERMEABLE PAVEMENT SYSTEM. 283
FIGURE 9-9: COMPONENT PLANES AND U-MATRIX VISUALIZATIONS OF THE RELATIONSHIPS BETWEEN TOTAL COLIFORMS (CFU/100ML) AND WATER SAMPLE TEMPERATURE (°C), PH, ELECTROCONDUCTIVITY (MS/CM), TOTAL DISSOLVED SOLIDS (MG/L), SUSPENDED SOLIDS (MG/L), TURBIDITY (NTU), AND CHEMICAL OXYGEN DEMAND (MG/L) IN STORMWATER FOR PPS 6 (OUTDOOR RIG) STANDALONE PERMEABLE PAVEMENT SYSTEM. 284
FIGURE 9-10: COMPARISON OF THE ACTUAL AND PREDICTED EFFLUENT CONCENTRATIONS OF TOTAL COLIFORMS BY SELF-ORGANISING MAP (SOM) FOR (A) PPS 4 (OUTDOOR RIG) PERMEABLE PAVEMENT COMBINED WITH GEOTHERMAL HEAT PUMP SYSTEM AND (B) PPS 6 (OUTDOOR RIG) STANDALONE PERMEABLE PAVEMENT SYSTEM. SAMPLE NUMBER N= 112 WEEKS FOR A 2 YEAR PERIOD FROM 4 MARCH 2008 TO 5 MARCH 2010). 285

Chapter 1 Introduction

1.1 Background to the project

The availability of clean water is a development issue faced by billions globally (World Bank, 2010). Like energy, the need for clean water is increasing rapidly as supplies of traditional resources continue to diminish due to waste, pollution and over usage. The mass of high profile flooding incidents recently has highlighted the catastrophic damages associated with urban flooding. Urban development generally results in an increase of the area used for infrastructure including roads, roofs and other impermeable surfaces which increases the supply of energy and water resources (World Bank, 2010). Flood events are associated with urban creep, gradual deterioration of drainage infrastructure and climate change. The cumulative runoff from large numbers of impermeable areas can significantly increase flood risk, therefore a shift towards futuristic sustainable urban drainage systems (SUDS) is beneficial for source control, whereby urban runoff is dealt with at the source rather than downstream (CIRIA, 2007). Freshwater availability and energy supplies to meet the growing needs of humanity have raised responses to counter this challenge by the development of alternative sources of energy and water. With these increasing pressures on energy and water resources, the concept of 'dual' beneficial use of treated urban runoff with geothermal energy technologies presents an opportunity for water reuse and renewable energy which has never been more viable. Urban runoff often considered as low-quality water has the potential to supplement freshwater supplies (Bulter and Davies, 2004). The benefits of using urban runoff include protection of water resources, prevention of coastal pollution, recovery of nutrients for agriculture, augmenting river flow and vast economic savings for downstream water, wastewater, groundwater treatment, groundwater recharge and sustainability of water resources management (Angelakis and Bontoux, 2001). Given that the impact of urbanisation on stormwater is associated to the introduction of impervious areas, the adoption of permeable paved surfaces is an intuitive response to the

challenge of managing urban stormwater. The potential of permeable pavements to control urbanisation impacts have been recognised for several decades (Coupe, 2004; Scholz and Grabowiecki, 2007). Compared to many structural management practices, permeable pavements have a particular advantage of not requiring additional land area. In addition, permeable pavements are capable of controlling stormwater quantity as well as quality, making it potentially efficient in meeting key stormwater management objectives of peak discharge control, pollutant removal and runoff volume reduction (Pratt *et al.,* 1995; Pratt, 1999). The potential of permeable pavements is widely acknowledged and reported experience in practical field applications has shown great benefits. However, common cited deficiencies in permeable pavement serviceability include structural inferiority and cracking due to extreme load bearings and clogging as a result of pollutant accumulation (Ferguson, 2005).

The key element towards enhancement for the realisation of renewable energy technologies is accelerated technological advancement and subsequent cost reduction combined with novel applications for its deployment. Renewable energy sources have been used and continue to be used directly and indirectly in water supply applications. Renewable energy technologies have great potential to contribute towards improved energy security and reduction in greenhouse gas emissions (World Bank, 2010). The development and deployment of these technologies are important components for a sustainable future. Geothermal energy is available as heat is emitted from within the Earth. This form of renewable energy has been used in the form of hot pools and springs for bathing, balneology, heating and washing purposes in many parts of the world for thousands of years. Geothermal energy for direct heating and cooling applications is a mature technology with a long history in developed countries (International Energy Agency, 2006). Geothermal energy represents a large global potential in renewable resources and has proven its ability in producing electricity and heat for a variety of direct and indirect uses in many regions of the world. Geothermal (Ground Source) Heat Pumps (GHP) like permeable pavement systems (PPS) have provided good evidence of their workability in both industry and academic research over the last decade. GHP contributed greatly to an increase of approximately 35% from 2000 to 2005 for direct

heat usage from geothermal energy and demonstrated that GHP's can be utilised almost anywhere in the world for both heating and cooling (Lund *et al.,* 2005). Hanson Formpave, a leading manufacturer of concrete block pavers and permeable paving solutions, presented an industry-first research proposal that integrates permeable paving with the proven technology of geothermal heat pumps (GHP). The innovative and unique combination of the permeable paving with a ground source heat pump addresses domestic, industrial and commercial buildings in tackling the global climate change challenges with regard to flooding, pollution, rainwater recycling and harvesting, rising energy costs and dwindling reserves. The integration of these two key technologies delivers a unique and highly energy-efficient system for harvesting rainwater and managing floodwater, whilst using the earth's heat to provide a sustainable heat and cooling solution for the interior of the building (Hanson Formpave, 2009). The geothermal technology is installed within a paved area and therefore no extra land is required, maximising build potential. Geothermal paving was first installed at the Hanson Eco-House, BRE, Watford in 2007. Approximately 6 KW of heating or cooling energy can be produced from the $65m^2$ paving installation at the Eco-house and proves to be a surplus of energy to maintain a comfortable year round temperature, all with the added benefit of a water harvesting and storm management solution incorporated. The geothermal paving system works by installing slinky pipes into the voided sub-base of the permeable pavement structure in order to generate sufficient energy to allow the transfer (exchange) of heat into buildings during cold periods and out of the building in the summer months. There is an ambient temperature in the sub-grade area of 10 °C that creates the energy within the refrigerant to affect the heat exchange.

Although researchers have conducted experiments to determine the impact of permeable pavements on pollutant removal, little work has been carried out on the new concept of geothermal paving systems. There is inadequate knowledge on this novel pavement system, which integrates renewable energy devices such as geothermal heat pumps and permeable pavements, and its removal efficiencies with regards to urban water pollutants. Hanson Formpave Heidelberg Cement Group in collaboration with The University of Edinburgh required key aspects of the environmental performance for the geothermal paving systems to be addressed.

These included the monitoring of microbial pathogenic organisms, re-growth and/or degradation of hazardous waterborne bacteria, physical and chemical water parameters, energy efficiency and systems modelling.

The application of PPS to treat different categories of urban runoff has not been addressed widely and there is a lack of knowledge of the detailed removal efficacies for most stormwater contaminants. This thesis addresses pertinent issues such as renewable energy technologies (geothermal heat pumps) and how it can be effectively incorporated with urban runoff treatment applications such as permeable pavements. The geothermal paving technology is specifically designed for urban water recycling applications and environmental friendly heating and cooling of nearby buildings. The treatment performance of the laboratory scaled experiments for integrated permeable pavements and geothermal heat pumps is assessed along with the impact of these systems on the environment.

1.2. Rationale, aims and objectives of this research

The rationale of the research project is to assess the performance of geothermal paving systems (permeable pavements integrated with geothermal heat pumps) and standalone permeable pavement systems through studying its treatment performance of concentrated urban runoff (gully pot liquor and animal faeces) and determining its impact on the associate water courses.

This will provide information on the role of these structures for stormwater catchment and address the arguments of practitioners and researchers. The overall aim of this project is to enhance understanding of the pollutant removal processes for laboratory based PPS and combined PPS-GHP experimental bins.

Detailed monitoring of the pavements' water quality was carried out for twelve pavement systems that were designed to temporarily collect and treat urban runoff. This study evaluated the long-term assessment of various small-scaled PPS and the integration of GHP with the impact of these systems on surrounding water courses and for water recycling purposes. The application of molecular microbiological techniques provided an opportunity to gain insights of the diversity present in the effluent of the pavement systems and photocatalytic disinfection as a polishing

treatment and decontamination stage after water filtration via the pavements' structure.

The overall goal of the thesis is to assess the performance of standalone PPS and combined PPS and GHP treatment systems in terms of pollution control and to identify the main factors which influence the performance in order to increase the benefits and overcome the limitations of the novel pavement technology.

The specific research objectives are:

1. to identify practical applications and scenarios where the use of combined PPS and GHP and its environmentally sustainable benefits can be applied;
2. to assess the performance of laboratory-scaled PPS and combined PPS-GHP treating concentrated urban runoff (animal faeces and gully pot liquor) and receiving high loads of biochemical oxygen demand (BOD), chemical oxygen demand (COD) suspended solids (SS) and nutrients;
3. to investigate the microbial activities under varying temperature patterns for the PPS and combined PPS-GHP including the presence of *Legionella*, and the degradation or re-growth of *Escharichia coli*, *Enterococci sp.*, *Salmonella sp.*, *Shigella sp.*, total coliforms and total heterotrophic bacteria for both the standalone PPS and GPS.
4. to evaluate the efficiency of geothermal heating and cooling applications when integrated within PPS in terms of the Energy Efficiency Ratio (EER) for a cooling cycle and the Coefficient of Performance (COP) in a heating cycle.
5. to investigate the use of photocatalytic disinfection and decontamination with Titanium Dioxide (TiO_2) for further treatment and deactivation of pathogenic microorganisms from the effluent of PPS.
6. to quantify and assess the applications of thermogeologic models for combined PPS-GHP using the runge-kutta method.
7. to apply neural network models (backpropagation and self-organising maps) to predict water quality parameters to support management decisions.

1.3. Outline of thesis contents

This thesis consists of four major parts. The first part focuses on sustainable urban drainage, permeable pavement engineering and its impacts on water courses and geothermal heat pumps and a review of literature. The second part focuses on the experimental operations and both water quality treatment and energy efficiencies, while the third part covers further disinfection and decontamination of the stormwater effluent from the pavement systems. The fourth part focuses on the application of modeling techniques for the energy transfers and water quality parameters for the prediction of the pavements performance. The thesis is organised into ten chapters.

Chapter 1 Introduction

In this chapter, a brief background and the aims and objectives of this study are described.

Chapter 2 Sustainable Urban Drainage Systems and Permeable Pavements

This chapter presents a review of the literature relevant to sustainable urban drainage and permeable pavements engineering in the context of urban stormwater management, an overview of sustainable urban drainage systems (SUDS), their types and pollutant removal mechanisms. The components of permeable pavements, hydrology, costs and pollutant removal processes and applications of urban runoff remediation are also described in this chapter.

Chapter 3 Geothermal Heat Pumps (GHP)

A review of geothermal heat pumps (GHPs) research is also presented, comparing its advantages, and disadvantages to conventional heating and cooling systems, from an economic, energy efficiency and environmental (Green House Gas Reduction) point of view.

Chapter 4 Experimental Design and Methodology

This chapter describes the experimental study along with the design, data collection and subsequent analysis. Methods adopted to cover various water quality and energy efficiency of the combined systems are described. The impacts of permeable paving with geothermal heating and cooling on its water quality treatment are investigated.

Chapter 5 Overall Water Treatment and Energetic Performance

This chapter focuses on the performance treatment of the laboratory-scaled integrated permeable pavements and geothermal heating/cooling system in terms of the physiochemical and microbiological removal efficacies and the energetic performances of the cooling and heating cycles for combined PPS-GHP experimental bins. Molecular microbiological techniques such as Gram-staining and gene sequencing DGGE (Denaturing Gradient Gel Electrophoresis) with PCR (polymerase chain reaction) was used to study the bacterial community entering and leaving the pavement systems. The removal efficiencies with combined GHP were assessed to see if any influences or reductions of water treatment occurred. The impact and benefits of stormwater treatment for urban runoff recycling is also discussed.

Chapter 6 Photocatalytic Oxidation with Titanium Dioxide (TiO_2) for Decontamination and Disinfection

Further disinfection was applied to the effluent of the PPS for the production of clean and safe treated stormwater, free from bacterial pathogenic organisms. Photocatalytic disinfection with ultraviolet radiation in the presence of the photocatalyst titanium dioxide (TiO_2) was assessed as a viable decontamination process for high rates of disinfection against organic pollutants which may not be fully removed from filtration after exiting permeable pavements.

Chapter 7 Runge-Kutta methodology for simulation of temperature and energy balances.

This chapter focuses on the application of the 4th order runge-kutta methodology for modeling the energy and temperature fluxes for combined PPS and GHP (Outdoor rig). The energy and temperature balances were analysed for a geothermal cooling and heating cycle to determine the thermogeological relationships of the systems. The model utilised heat fluxes and energy balances using measured temperatures and external environmental factors.

Chapter 8 Use of Backprogpagation Neural Networks Models

This chapter outlines the application of artificial intelligent techniques such as neural networks with backpropagation feed forward applied to model nutrient pollutant concentrations. Various algorithms were assessed in predicting effluent concentrations for biochemical oxygen demand, ammonia-nitrogen, nitrate-nitrogen and ortho-phosphate-phosphorous. The application of artificial neural networks within PPS is a promising modelling tool for environmental assessment and management within the systems.

Chapter 9 Application of Kohonen Self-Organising Map Model

The chapter describes the application of another artificial intelligence technique to support integrated PPS and GHP management decisions. The application of the Kohonen Self-Organising Map (KSOM) in prediction waterborne bacterial pathogenic parameters that are expensive to monitor in real time is demonstrated.

Chapter 10 Conclusions and Recommendations

The final chapter presents the conclusions by summarising the key findings from this research and identifies areas for potential further research.

Chapter 2 Sustainable Urban Drainage and Permeable Pavements

This chapter gives an overview of the relevant background literature on the importance of sustainable urban drainage systems (SUDS) and urban runoff both from a quantity and water quality aspect. The environmental benefits of SUDS and permeable pavements have been reviewed by several researchers and major ones are highlighted. Key characteristics of permeable pavement systems from an engineering point of view are addressed.

2.1 Urban Runoff

Urban runoff is a major environmental concern for the prevention of water quality deterioration and controlling flow in mitigating flood damage. A critical part of stormwater engineering is the management of urban runoff. Urban runoff is defined as water flowing because of urbanisation and stormwater that does not infiltrate into the ground (Scholz, 2006a). Urban runoff is a critical concern from a water quantity and quality perspective. The main contributors of urban runoff are composed of water flows from landscape areas, driveways, streets, parking lots, roofs and other impervious surfaces (Scholz, 2006a). Typically, urban runoff contains a high but variable number of pathogens, nutrients and sediments that require removal before reuse. Many urban water contaminants are toxic, persistent and/or bioaccumulative, and may produce subtle ecological effects. This can endanger soils, groundwater and slowly flowing receiving waters when it is discharged. Entire ecosystems can be affected when urban runoff is discharged directly without retention and treatment. There is also uncertainty surrounding their adverse public health effects on human life (ASCE and WEF, 1998). Harmful constituents are emitted from fertilizers used for lawns and gardens, animal and bird faeces, various fluids and heavy metals that originate from vehicular traffic, street litter, herbicides and pesticides residue, and atmospheric contributors of air pollutants transported onto the drainage system (Scholz and Grabowiecki, 2007). Much research has been conducted to examine the overall water quality of urban runoff. The types of urban stormwater pollutants vary and expected pollutant loads are found to be directly related to the surrounding land use (Lee *et al.,* 2007). Insignificant developments have been made to improve the water quality associated with urban runoff.

Advancements in sustainable urban drainage systems (SUDS) research is enabling engineers and scientists to identify an increasing range of emerging contaminants in the environment and to recognize these at lower levels than previously possible. Engineers have subsequently started to monitor environmental contaminants removal within SUDS and subsequently using it for water reuse and reclamation purposes.

Urban runoff is increasingly recognized as a significant cause of water quality impairment (Pitt *et al.,* 1995; Reeves *et al.,* 2004; Taebi and Droste, 2004). One approach for addressing this problem is to capture and treat urban runoff before it reaches the ocean. Prevention and control of urban runoff pollution requires an understanding of the various pollutant categories, major urban sources and its effects. Table 2-1 lists the primary categories of urban runoff pollutants, pollutants associated with each category, typical runoff sources and potential effects. For municipalities urban storm-generated runoff and construction are the most prevalent sources; outlying agricultural activities also can play a significant role in many urban areas (ASCE and WEF, 1998; US EPA, 1993). The effects of urban runoff pollutants vary for different water resource types. The magnitude of the pollution load transported by urban runoff to receiving water bodies is comparable to that of untreated sewage in some cases. The highest concentration of pollutants in stormwater is measured during the initial stages of a storm event, during which time the stormwater exhibits a 'first flush' effect by initially cleansing away the bulk of pollutants deposited during the preceding dry-weather period. A given municipality's pollutants of concern, therefore, depend on the types of water resource in and downstream of the community, and their desired uses (ASCE and WEF, 1998). Runoff from residential areas tends to contain high concentrations of nitrogen, phosphorus and herbicides. Studies by Line *et al.,* (2002) for a combined anlaysis of site runoff from residential, golf course and construction sites were compared to runoff from a wooded lot, with the average total nitrogen, phosphorus and sediment load from the combined land uses demonstrating a 300 % increase when compared to that associated with the wooded lot. Streets and roads contribute approximately eight times the pollutant load when compared to other sources (Bannerman, *et al.,* 1993). The significance of road runoff to urban stormwater pollution results in a number of factors. Streets possess a high runoff coefficient due to the transportation medium

directly connected to the drainage system. Curbs and gutter systems along streets are designed for effective entrapment and retention of finer particles and streets sustain frequent deposition of local emissions and leaks from vehicles. While conditions are very site specific, the water resources generally most affected by certain pollutants were addressed in this research.

Table 2-1: Summary of urban runoff pollutants (adapted from US EPA, 1993; Campbell *et al., 2004*; Metcalf and Eddy, 2007)

Category	Parameters	Typical concentration ranges	Possible sources	Possible effects
Sediments	Organic and inorganic suspended solids; turbidity; dissolved solids	Suspended solids (100-300 mg/l); total solids (100-3000 mg/l); turbidity (110-340 NTU)	Construction sites; urban and agricultural runoff; sewer systems; sewer pipelines; landfills; septic tanks	High turbidity, habitat alternation, recreational and aesthetic loss, contaminant transportation, hydrology, bank erosion
Nutrients	Nitrates; nitrites; ammonia; organic nitrogen; phosphates; total phosphorus	Ammonia-nitrogen (0.1-10 mg/l); nitrate-nitrogen (0.01-10 mg/l); total nitrogen (0.1-50 mg/l); total phosphorus (0.01-5 mg/l)	Urban and agricultural runoff; landfills; septic tanks; atmospheric deposition; soil erosion	Surface waters: - algal overgrowth and blooms, ammonia toxicity. Ground water:- Nitrate toxicity
Pathogens	Total coliforms; faecal coliforms; faecal streptococci; *Escherichia coli*; Enterococcus; viruses	Total coliforms (10^6-10^9); faecal coliforms (10^3-10^7 CFU/100ml); *Escherichia coli* (10^2-10^7 CFU/100ml); faecal streptococci (10^2-10^6 CFU/100ml);	Urban runoff; agricultural runoff; septic systems; poor sanitary connections; combined sewer overflows; domestic and wild animals	Intestinal and gastrointestinal infections, ear infections, dysentery, typhoid fever, viral and hepatitis, recreational and aesthetic loss
Organic enrichment	BOD; COD; TOC; dissolved oxygen	BOD (10-15 mg/l); COD (73-94 mg/l); TOC (80-220 mg/l)	Urban runoff; agricultural runoff; landfills; septic tanks; atmospheric deposition; soil erosion	Dissolved oxygen depletion, odours, toxicity levels for fish and other aquatic life
Toxic pollutants	Toxic trace metals; toxic organics; poly-aromatic hydrocarbons	Total lead (0.01-5mg/l); total zinc (0.01-5 mg/l); total hydrocarbons (0.01-5mg/l)	Urban runoff; agricultural runoff; pesticides; herbicides; hazardous waste sites; landfills; oil spills; hydrocarbon disposals, industrial discharges	Bioaaccumulation in food chain organisms and potential toxicity to humans and other organisms

2.2. Sustainable Urban Drainage Systems (SUDS)

The natural response of catchment, infiltration, evaporation, attenuation, surface storage and reduced runoff characterises sustainable urban drainage (CIRIA, 2007). Sustainable urban drainage systems or SUDS is a concept that embraces varying types of surface water (stormwater) management solutions (DEFRA, 2007). SUDS can be described as an approach to managing stormwater events and rainfall practically, which replicates natural drainage. SUDS mimics natural catchment processes and can be viewed as a more sustainable approach when compared to traditional urban stormwater runoff piping and storage solutions. The idea of SUDS is to utilise catchment areas in the best possible scenario with different drainage techniques depending on land use and characteristics (CIRIA, 2007). The nature and extent of benefits for SUDS depends on local conditions. Extensive applications of SUDS will significantly reduce the volume of urban runoff into drainage and sewer systems and therefore lessen the runoff load at combined sewer overflows (CSO) and sewage treatment plants whereby due to urban creep, the design capacity would be not be able to bear the excessive stormwater. The integration of SUDS can contribute to reduction of pluvial flooding risks and incidents. SUDS provides means of treatment and managing urban diffuse pollution nearby or at the source, thereby the pollution content is managed and reduces downstream contamination risks caused by CSO surcharging. SUDS techniques can intercept urban runoff and remove pollutants before it re-enters into watercourses (rives, lakes, ocean).

Some SUDS techniques can provide an alternative source for non-potable water within domestic, industrial and commercial settings. This can aid meeting water efficiency targets. It also provides a route for additional recharging of aquifers in areas under water supply stresses, thus helping to make economical savings on new water resource investments. The reduction and limitation of volumetric flow, which is caused by SUDS, reduces the flow to wastewater treatment works and thereby reduces the associated energy costs for pumping (Bulter and Davies, 2004). Reduced pumping, storage facilities, and less diluted urban wastewater would result in a more efficient treatment of urban wastewater. Once more, a rise in urban population

would result in sewage and wastewater treatment plants reaching a limit to their capacity.

Astebol *et al.,* (2004) states that a central element of sustainable stormwater management is the utilisation of stormwater as a resource. SUDS mimics the natural environment, retaining water which will attract wildlife and creating stable habitats. Stormwater in open systems creates the basis for recreation and development of ecosystems with a diverse fauna and flora life. Ideally, SUDS should adopt the characteristics of water's behaviour in nature and adapt it to urban conditions and requirements (Astebol *et al.,* 2004). Sustainability exists in complex network urban drainage systems and implementation of SUDS serves to produce a long-term viable drainage system. The philosophy behind SUDS is environmentally successful because of the aspiration of future development in drainage which leads to an increase in biodiversity and reduced water pollution.

2.2.1. SUDS Techniques

The SUDS approach to drainage includes a wide range of methods. SUDS techniques includes (i) control of rainwater at the source, (ii) infiltration trenches and filter drains, (iii) swales and basins, (iv) ponds and wetlands.

2.2.1.1 Green (Vegetated) roofs

Green or vegetated roofs are multi-layered systems comprising of vegetation cover and/or landscaping above a drainage layer (Wong and Chen, 2009). The vegetative layer over the impermeable roof membrane attenuates the urban runoff and allows some evaporation of water. This endows the roof with hydrologic characteristics, which can be optimised to achieve water quantity and quality benefits (Wong and Chen, 2009). It intercepts and retains precipitation, which results in less surface runoff. The vegetation can range from low grass to large shrubs. The larger the plants, the greater the depth of growth medium required and the greater the imposed load. The overall thickness of green roofs may range from 2 to 6 inches and

contain multiple layers consisting of waterproofing, synthetic insulation, non-soil engineered growth median, fabrics and synthetic components (Wong and Chen, 2009). This provides significant rainfall retention and detention functions. For practical installation on conventional roof structures, lightweight materials are used for most engineered media. While some installations are open to public access, most extensive vegetated roof covers are for public viewing only.

2.2.1.2 Rainwater harvesting (water butts for runoff capture and reuse)

Rainwater from impermeable surfaces is stored and used. The purpose of rainwater harvesting is to reuse water and reduce the rates of surface runoff. It encompasses a runoff capture and reuse technique (Pearlstine, 2010). The rainwater harvested can be used for garden irrigation. Water butts include storage tanks, rain barrels and other similar devices that are used to capture stormwater from the roofs of buildings. According to Pearlstine, (2010) in many parts of the developing world, these systems serve as a primary water supply. These systems can reduce potable water requirements for applications such as irrigation and fire protection while reducing stormwater discharges. Typically, a water butt has a high-level overflow to maximise the storage of water for garden irrigation.

2.2.1.3 Filtration Trenches and Drains

Filtration trenches or drains are filled with gravel enclosed in a geotextile membrane with a perforated pipe running through a narrow channel. The purpose of this is to allow water to filter into the surrounding soil and into pipes, which transfers the water to a disposal unit. The trench is backfilled with graded stones and gravel to create an underground reservoir. Urban runoff diverted into the trench gradually infiltrates into the subsoil and eventually reaching the water table (US EPA, 1993). The stormwater runoff velocity is reduced and this creates an environment conducive for storage. These systems trap organic matter and oil residues which disintegrate by bacterial action with time (US EPA, 2002). Stormwater runoff that flows into a filter drain or trenches can soak away into the surrounding soil as a result of the packing

and grading of stones and gravel fills which traps particles thereby preventing pollutants from entering groundwater courses.

2.2.1.4 Filter strips

A filter strip is designed to slow down urban runoff and allow stormwater to soak into the topsoil if not too compacted (CIRIA, 2007) and adopts a natural vegetated form and is well situated between surface water bodies (wetlands, streams and lakes). They generally are placed in locations where stormwater runoff leaves a field, with the intention to filter sediment, organic matter, nutrients and chemicals from the runoff water. The entrapment of sediments and the establishment of vegetation, nutrients can be absorbed to the sediment that is deposited and remain on the field landscape enabling plant uptake. This buffering system improves infiltration and percolation, thus reducing stormwater runoff amounts (CIRIA, 2007). The vegetation in filter strips recycles entrapped nutrients in the harvested material and provides permanent habitats for many types of flora and fauna. They are useful in areas where both point and nonpoint source pollutation occurs; for residential, industrial and commercial uses such as parks, businesses, schools, urban development and water treatment facilities for areas with potential sediment erosion, leaching and runoff. Basically, filter strips can be applied where runoff from land areas outfalls to a water body.

2.2.1.5 Swales

Swales are grassed areas of depression, which guide surface runoff overland from the source area to a storage or discharge system. They impede surface water during times of runoff, simultaneously the grasses and subsequent vegetation act as buffers, which filters the stormwater (SEPA, 2005). They are wide, shallow like ditches that provide temporary storage, transport, treatment and infiltration for surface water and are designed to achieve a dry state between storm events to enhance their filtering capabilities (Burkhard *et al*., 2000). Their broad and shallow channels slow urban runoff, promote infiltration and filter pollutants and sediments

in the process of conveying stormwater runoff. Swales provide an environmentally - superiror alternative to conventional curbs and guttering conveyance systems while providing partial treatment (pretreatment) and partially distributing stormwater flows to subsequent stormwater management systems or SUDS. They can be incorporated into the landscape as roadside kerbs avoiding alternative conventional construction methods reducing materials and costs. Pollution removal is achieved by mechanical filtering through vegetation, adsorption onto vegetation and microbiological breakdown of organic matter in the upper layers of the soil. The various pollutant removal mechanisms of a swale include sedimentary filtering, filtering through a subsoil matrix, and infiltration into the underlying soils with the full array of infiltration-oriented pollutant removal mechanisms. SEPA, (1997) reports that a 30 to 60 m swale can remove 60 to 70 % of solids and 30 to 40 % of metals, hydrocarbons and bacteria in surface runoff.

2.2.1.6 Infiltration Basins

Infiltration basins are shallow impoundment that temporarily store and infiltrate urban runoff; over level, uncompacted and relatively permeable soils (Birch *et al.,* 2005). They are designed to retain water for a few hours to ensure a settlement of solids and provide short-term water storage and the settlement of solids ensures water filtration reducing contamination. The ability of infiltration basins to temporarily store and treat water provides a degree of risk reduction for both flooding and pollution downstream (Birch *et al.,* 2005). The design of infiltration basins allows stormwater retention, retards flows and allows water to percolate through a filter layer which typically comprises of porous materials such as gravel and crushed rock. The water may be directed to a surface water outfall or continue to percolate through into groundwater. For small catchments the design of infiltration basins are determined by the availability of land, and a narrow trench-like basin is usually more appropriate. The capacity can vary from large basins to multiple, smaller basins throughout a site. It uses the existing soil mantle to reduce the volume of stormwater runoff by infiltration and evapotranspiration. The quality of urban runoff is also enhanced by the natural cleansing processes of the existing soil mantle

in addition to the vegetation planted in the basins. Well efficient infiltrating basin can remove anywhere from 70 to 98 % of the pollutants found in stormwater depending on the constituents and site conditions (Birch *et al.,* 2005). They can be incorporated into new developments b preserving the existing vegetation and grassed areas which can be utilised increasing evapotranspiration in addition to encouraging infiltration.

2.2.1.7 Subsurface Infiltration Bed

Subsurface infiltration beds provide temporary storage and infiltration of stormwater runoff by introducing a storage media of varying types beneath the proposed surface grade (Mays, 2004). The beds normally consist of vegetated, highly pervious soil media underlain by a uniformly graded aggregate bed for temporary attenuation, and infiltration of stormwater runoff. These SUDS are ideally suited for expansive, generally flat open areas such as playing fields, meadows and lawns which are located nearby and downhill from impervious areas. The designs of subsurface infiltration beds can vary from stepped or terraced down sloping terrain provided that the base of the bed remains at a fixed level (Mays, 2004). Urban drainage from impermeable surfaces including parking lots, roads, walkways, and rooftops can be conveyed to the subsurface storage media whereby it can be then distributed via a network of perforated drainage pipes. The storage medium typically consists of clean-washed uniformly graded aggregate (stone, pea gravel, crushed rock and gravel). Subsurface infiltration features can act as a standalone SUDS reducing stormwater runoff volume, rates and quality control practices significantly. These systems can also maintain aquifer recharge, whilst preserving or creating valuable recreational areas and open space (Mays, 2004). They can also maintain aquifer recharge, while preserving or creating valuable open space and recreation areas. They have the added benefit of functioning year-round and is generally employed for temporary storage and infiltration of runoff in subsurface storage media.

2.2.1.8 Constructed Wetlands

Constructed wetlands (CWs) are engineered systems that utilize natural treatment processes to reduce the pollution levels in urban runoff, water and wastewater (Scholz, 2006 a). A CW cell is typically built by digging a shallow excavation, lining it with an impermeable material such as plastic liner or concrete, filling up the space with filter media such as soil, sand or gravel and installing an influent storage or feeding and effluent collection or disposal system. They may be built as part of a SUDS treatment train. CWs consist of shallow marsh systems planted with emergent vegetation that are designed to treat stormwater runoff. They can mitigate peak flow rates and reduce runoff volume. They also provide considerable aesthetic and wildlife benefits. A combination of plants, soils and microorganisms efficiently remove organic pollutants, nutrients and toxic contaminants in urban wastewater using a variety of physical, biological and chemical processes. There are two basic types of CWs: surface flow and subsurface flow. Surface flow wetlands are essentially shallow ponds planted with floating and emergent species, the water flow occurring almost entirely above the soil. The flow in subsurface flow wetlands occurs under the surface and within the soils planted with emergent species such as cattails (Typha), rushes (Juncus) and reeds (Phragmites) (Scholz, 2006 a). Subsurface flow is either horizontal with the water moving parallel to the surface, or vertical where the influent is distributed across the surface, percolates down the media and collects in a bottom layer. Subsurface wetlands are generally more efficient and require less land area. Compared with conventional treatment systems, constructed wetlands have lower energy and chemical requirements resulting in reduced capital, operating and maintenance costs.

2.2.1.9 Wet Ponds (Retention Basins)

Wet ponds (WPs) or retention basins are a type of SUDS used to manage stormwater runoff to prevent flooding and downstream erosion, improving water quality for adjacent water courses (US EPA, 2002). WPs are artificial lakes with surrounding vegetation and include a permanent pool of water in its design. They are frequently used for water quality improvement, groundwater recharge, flood

protection, aesthetic improvement or any combination of these. They include one or more forebays that trap course sediment, prevent short-circuiting, and facilitate maintenance. The pond's perimeter is generally covered by a dense stand of emergent wetland vegetation. While they do not achieve significant groundwater recharge or volume reduction, they can be effective for pollutant removal and peak rate mitigation (Scholz, 2006 a).

WPs can also provide aesthetic and wildlife benefits and require an adequate source of inflow to maintain the permanent water surface. They act as a replacement for the natural absorption of a forest or other natural process that is lost when an area is developed due to urbanisation. As such, these structures are designed to blend into neighbourhoods and are viewed as an amenity. Stormwater is typically channeled to WPs through a system of streets and/or parking lot storm drains, and a network of drainage channels or underground pipes. These systems are often landscaped with a variety of grasses, shrubs and/or wetland plants to provide bank stability and aesthetic benefits and also provides water quality benefits by removing soluble nutrients through uptake (Scholz, 2006 a).

2.2.1.10 Dry ponds

Dry ponds (DPs) consist of excavated, berm-encased or dished areas, lined with grass or permeable paving (Madge *et al.,* 2004). These systems operate as a retention basins (no fixed outlet with drainage by infiltration alone) or detention basins with forms of outflow drainage systems via an orifice or mechanically hydraulic controls into a surface water drainage system. DPs are often multifunctional; operating as a recreational area and are filled during exceptional storm events. They serve to control peak rates of stormwater runoff that provides temporary storage and prevention of downstream flooding impacts (Madge *et al.,* 2004). DPs have relatively low pollutant removal efficiencies because of re-erosion of previously deposited solids during filling. Applications of DPs include lower density residential areas, industries, commercial businesses and urban areas. Roof runoff sometimes connects directly into the DPs. In the event that the DP is overwhelmed in an intense storm event, an overflow mechanism (surcharge that additional runoff is safely conveyed by

capturing runoff at the source. They can dramatically reduce the increased volume of stormwater generated by urban runoff.

2.3 Permeable Pavement Engineering

Permeable pavement engineering is effectively providing a structural pavement suitable for pedestrians and vehicular traffic whilst allowing water to filter through the surfaces of the pavement for temporary storage, storm attenuation, dispersal to the ground or collection for stormwater reuse. In general, permeable pavements sometimes referred to as pervious pavements can be constructed of asphalt, concrete, ceramic or plastic. However, the research focuses on permeable pavements created with concrete block paving systems specifically designed for the purpose of sustainable urban drainage. Permeable concrete block pavements are particularly designed to provide a hard surface within a SUDS framework. The general principle of permeable pavement engineering with the use of concrete blocks is to collect, treat and infiltrate urban runoff to support groundwater recharge or direct treated stormwater to open water streams.

Figure 2-1: Permeable pavement surface with a stone reservoir underneath (from TecEco, 2009).

Traditional paved surfaces, such as impermeable asphalt and concrete, do not allow water to infiltrate and convert almost all rainfall into runoff. In conventional pavements, stormwater is allowed to run across the surface to gullies, which collect and direct it into pipes for rapid removal (Barrett *et al.,* 2006). On the contrary, concrete block permeable pavements have a dual role and act as the drainage system in addition to supporting traffic loads. Permeable pavements are suitable for a wide variety of applications including residential, commercial and industrial. However, these pavements are confined to light duty and infrequent usage even though the design capabilities are used for Heavy Goods Vehicles (HGV's) parking space provisions. Permeable pavement systems (PPS) are very useful in areas where sewers flow at capacity during storms owing to an increase in impervious areas from parking lots or buildings. In such scenarios, replacing existing drainage pipes with larger ones may not be economical or allowable because it merely transfers the additional stormwater runoff downstream, which can lead to erosion and flooding. If designed and implemented correctly, PPS allows a large portion of stormwater to infiltrate, thus reducing peak runoff volumes and flows (Andersen *et al*., 1999.) PPS are regarded as an effective tool in managing stormwater (Scholz and Graboweicki, 2007). Appropriate applications of PPS are as follows:

- Vehicular Access including residential and commercial driveways, roadway shoulders, crossovers and medians.
- Parking (Supermarkets, Shopping Malls, Universities, and Colleges etc.)
- Slope Stabilization and Erosion Control
- Golf Courses Cart paths and parking facilities
- Pedestrian Access
- Bicycle / Equestrian trails

- Land irrigation

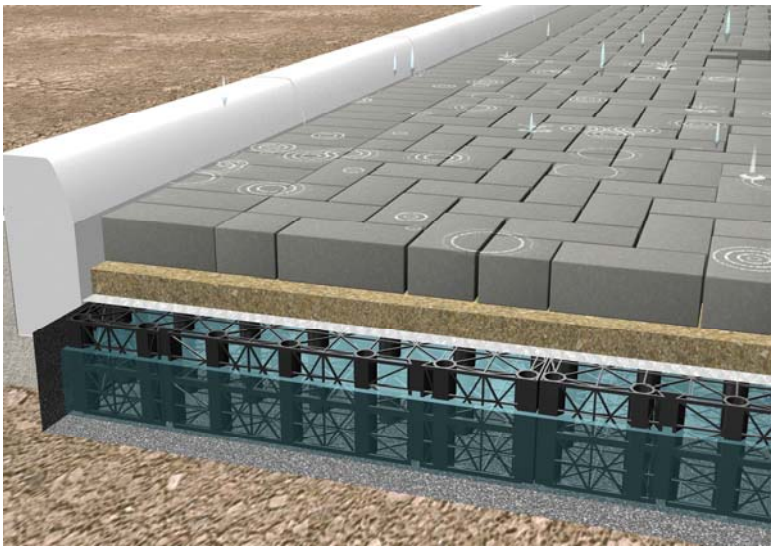

Figure 2-2: Schematic layout of a permeable paving parking bay consisting of a series of lattice plastic, cellular units, connected together to form a raft structure that replaces some or all of the permeable sub-base, depending upon the anticipated traffic loading (Interpave, 2010)

2.3.1 Permeable Pavement Structure and Design

A permeable pavement system (PPS) consists of a surface layer, overlying a sub-base layer which rests on existing soil (Pratt, 1999). One or more intermediate layers such as gravel and crushed stone or course fine sand may be included between the surface layer and the sub-base (Wilson, 2003). The essential function of the pavement surface is to support vehicular loads without undue deformation and to allow stormwater infiltration to the pavement's sub-base. The sub-base has a structural role in distributing the pavement's load to the underlying layers of gravel and soil, but also acts as a water storage layer and is sometimes referred to as the water saturation zone or reservoir course. Filtered stormwater may be transported from the pavement structure via infiltration to the underlying soil or be collected in a formal drainage system beneath the pavement surface. The surface layer of concrete block permeable pavements is modular. Modular permeable pavements are constructed from individual concrete, clay or plastic paving blocks, which acts as a structural matrix for unbound gravel, or soil, which is exposed at the surface (Newton, 2005). The use

of gravel is preferred to soil for the interstitial material, since soil is commonly subjected to compaction by vehicular traffic reducing the pavement's infiltration capacity (Pratt *et al.,* 1999). As seen in Figure 2-3, the components of PPS include the pervious concrete blocks, bedding layer course (pea gravel, small stone and sand), geotextile, layer of gravel and crushed rock and a possible extra geotextile bottom layer for extra buffering of water quality.

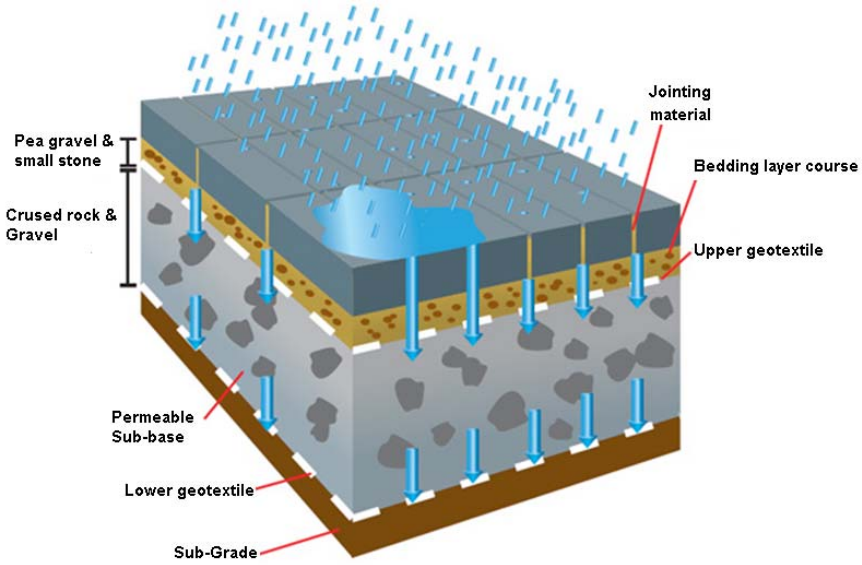

Figure 2-3: Schematic layout of permeable (pervious) pavement system (adapted from Interpave, 2010)

2.3.2 Porous Aggregates for Sub-base

Aggregate is any mass of particulate material such as gravel, crushed stone, crushed recycled bricks or decomposed granite. Single-sized particles create an aggregate mass with 30 to 40 % void space; such open-graded materials are extremely permeable to water (Newton, 2005). Aggregates are the most ubiquitous material in pavement design and construction and are the most common materials forming the subsequent layers of the pavement structure (Mallick and El-Korchi, 2009). Single-size aggregate is the principal component for porous concrete and pervious pavements, and is used as a porous fill in the open cells and joints of paving blocks, grids and geocells. Unbound open graded aggregate is used directly as a surface

course in very low-traffic bearing areas such as residential driveways, lightly used parking lots and pedestrian walkways (Mallick and El-Korchi, 2009). The sub-base zone is in contact for a large part of time, the strength and durability of aggregate particles when saturated and subjected to wetting and drying must be taken into account. For permeable pavement design in the U.K. aggregates should comply with British Standards BS EN 13242:2002 and BS 12629:2002 for unbound and hydraulically bound materials.

2.3.3 Geotextiles

Geotextiles are pervious polymeric materials such as geogrids, geomembranes and geocomposite. Geotextiles may be used in two locations within PPS, an optional upper geotextile at the laying course/coarse graded aggregate interface and between the laying course and the permeable sub-base. They are informally referred to as filter fabrics. Woven geotextiles tend to have both permeability and tensile strength whilst nonwoven models have high permeability but little tensile strength. The size of the openings or pores within geotextiles can vary from 0.02 to 0.002 inches, with the portion of the area in open pores varying up to about one third of the surface. In some permeable pavements, a woven geotextile under the base course can contribute to distributing the traffic load over soft subgrade. As the subgrade attempts to deform under a load the fabric is placed in tension and its tensile strength properities add support for the load. However, the presence of woven geotextiles does not allow a reduction in the required base thickness of pervious pavements. The geotextile functions as a bio-filter, which physically intercepts and digests organic matter present in urban runoff by biochemical reactions (Coupe *et al.,* 2003; Coupe, 2004). Geotextiles applications include layer or strata separation, reinforcement, filtration and drainage (Koerner *et al.,* 1994).

The susceptibility to clogging by biological growth or chemical precipiration within geotextiles has been identified (Korkut, 2003). The use of geotextiles to encourage biofilms and provide optimum conditions for urban runoff treatment has been well researched by Legret *et al.,* 1996; Pratt *et al.,* 1999; and Coupe, 2004. Geotextiles are one of the most important components within PPS (Newman, 2003,

Omoto *et al.,* 2003; Spicer *et al.,* 2006). A study by Elvidge and Raymond, (1999) found that increasing the mass per unit area of geotextiles reduces the amount of damage that occurred when in contact with open graded crushed aggregate. Geosynthetic layers for permeable pavement constructions are installed in according to British standards BS EN 13252:2001 and BS EN 13249:2001.

2.3.4 Types of Permeable Pavement Structures

There are principally three systems suitable for permeable pavements; these include total infiltration, partial infiltration and no infiltration. For total infiltration, the pavement allows all stormwater onto the surface to infiltrate down through the joints, voids between the concrete blocks, flowing through the constructed layers below, and eventually reaching the subgrade. Some retention of the urban runoff water will occur temporarily in the permeable sub-base layer allowing for initial storage before it passes through. This system is referred to as a 'Zero Discharge' PPS as no additional water from a development is discharged into the conventional drainage systems. Hence it reduces building and maintenance cost for pipes and gulleys (Interpave, 2010).

The partial infiltration PPS can be utilised in situations where the existing subgrade may not be capable of absorbing all the water. This system can therefore prevent the existing soils from loosing its stability. For partial infiltration, outlet pipes are connected to the permeable sub-base and allow the excess stormwater to be drained to other SUDS devices such as swales, filter drains or sewers. A fixed volume of stormwater is allowed to infiltrate down through the partial infiltration PPS, which in practice very frequently represents a large percentage of rainfall (Interpave, 2010).

The no-infiltration PPS allows for the complete capture of stormwater using an impermeable, flexible membrane placed on the top of the subgrade level and up the sides of the permeable sub-base to effectively form a storage reservoir. The no-infiltraton PPS can be applied to situations where the existing subgrade has low strength and low permeability and would therefore be damaged by the introduction of additional water (Interpave, 2010). This system can be utilised for urban runoff

harvesting to prevent water soaking into the ground in sensitive locations such as water extraction zones and prevent leakage, which can affect building's structural foundations. Effluent piping is constructed throughout the impermeable membrane at appropriate locations to transmit the stormwater to sewers, watercourses and other SUDS treatment. The outlet pipes are designed to restrict flow for temporary water storage within the pavement and discharge slowly. This system is particularly suitable for contaminated sites as it prevents pollutants from being washed further down into the subgrade where it can eventually enter groundwater. It can act as an underground retention/detention zone and the stored or captured water collected, cleansed, stored and reused for irrigation, washing of cars and toilet flushing.

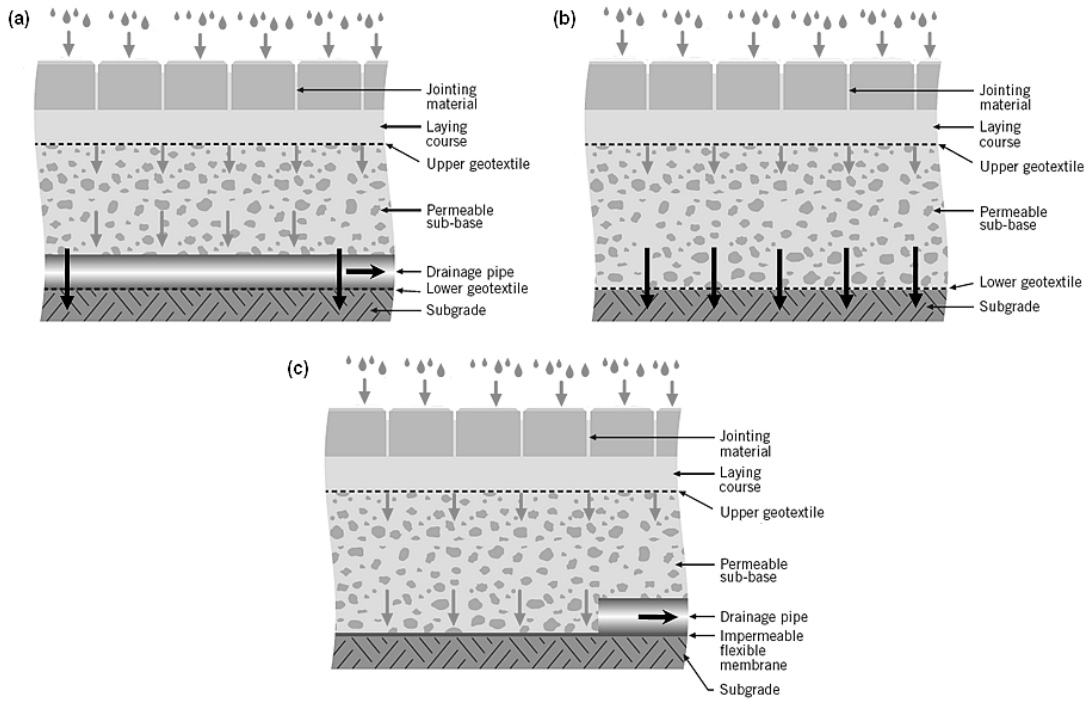

Figure 2-4: Various types of permeable pavement structures regarding stormwater runoff for (a) partial infiltration, (b) total infiltration and (c) no infiltration (adapted from Interpave, (2010)).

2.3.5 Pavement thickness design

Designing of the pavements thickness involves knowledge of the relationship between likely rainfall events, the occurrence of flooding and the structural requirements (Mallick and El-Korchi, 2009). It involves establishing the required reservoir capacity (minimum thickness of reservoir layer), estimating subgrade properties including the California Bearing Ratio (CBR) and strength of materials parameters, establishing the design traffic load, and design against rutting and cracking. The sub-base materials normally consist of crushed rock and gravel the modulus is around 100 to 150 MPa under the stress conditions applied. The potential to deform is best related to the strength parameters c (kPa) which represents the pressure exerted from vehicles onto the pavement and the angle of internal friction Φ values. For crushed rock and gravel the strength parameters c tends to be negligible and Φ around 45- 50° (Mallick and El-Korchi, 2009). The strength parameters also influence the upper permeable pavement design since they dictate how much protection the reservoir materials require to prevent deformation. Common concrete block pavements are traditionally rectangular with dimensions of 200 × 100 mm with a usual thickness of 60 to 80mm based on the structural load requirements for lightly trafficked areas (car parks, pedestrian areas) (Hanson Formpave, 2009).

2.3.6 Stress Loads

2.3.6.1 Corner Stresses

Load bearing stresses on permeable paving blocks due to traffic occur from corner loading, edge-loading and interior loading (Delatte, 2008). Stresses from corner loading are associated with corner breaks along the pavement while edge and interior stresses are associated with mid-transverse cracking stresses. Stresses depend on the load application, configuration, pavement thickness, modulus of subgrade reaction k and relative stiffness l (Delatte, 2008). Corner stress equations can be developed directly from equilibrium and are based on the conservative assumptions

that the load is placed at the corner of the pavement block from the standard bearing stress equation:

$$\sigma = \frac{Mc}{I}, \qquad [2\text{-}1]$$

Where σ is the yield stress, M= bending moment, c = outer radius of cylindrical area, and I=moment of inertia.

The failure zone is assumed to occur a distance 'x' from the corner and forms a crack length of '2x'. With a pavement thickness D,

$$D = 2c, \qquad [2\text{-}2]$$

and

$$I = \frac{bh^3}{12} \text{ Where } b = '2 \times X' \text{ and } D = h, \qquad [2\text{-}3]$$

The bending moment, M of the pavement is equal to the force 'P' times the distance 'X'. Therefore, M= P×X, the corner stresses becomes:

$$\sigma_C = \frac{Mc}{I} = \frac{P \times X(D/2)}{2 \times X(D^3 I \times 12)} = \frac{3P}{D^2}. \qquad [2\text{-}4]$$

This equation was updated by Westergaard, (1926) and subsequently by Ioannides *et al*., (1985) and Huang, (2004).

$$\sigma_C = \frac{3P}{D^2}\left[1 - \left(\frac{c}{l}\right)^{0.72}\right] = \frac{3P}{D^2}\left[1 - \left(\frac{1.772a}{l}\right)^{0.72}\right] \qquad [2\text{-}5]$$

where c = the side length of a square contact area, a = radius of a circle within the same contact area. In permeable pavement stress calculations, the load may be

considered to be evenly distributed as a uniform tire pressure ‘p’ over a circle radius ‘a’, therefore

$P = p\pi a^2$, rearranging a, $= \sqrt{\frac{P}{p\pi}}$ [2-6]

2.3.6.2 Edge loading stresses

For mid-pavement cracking, the edge-loading stresses are critical because they are much higher than the stresses due to interior loading. Once more, edge-loading equations developed by Westergaard, (1926), and further developed by Ioannides *et al.,* (1985) and Huang, (2004) found the empirical relation:

$$\sigma_e = \frac{0.803P}{D^2}\left[4\log\left(\frac{l}{a}\right) + 0.666\left(\frac{a}{l}\right) - 0.034\right]. \quad [2\text{-}7]$$

This equation assumed a Poisson’s ratio of concrete v = 0.15. Ioannides *et al.,* (1985) Huang, (2004) and Delatte, (2008) found that edge-loading stresses are approximately 42 % higher than corner loading stresses and mid-slab pavement cracking is more susceptible than corner breaks unless the pavement corners are heavily loaded or unsupported.

2.3.6.3 Interior loading stresses

The Westegaard, (1926) interior loading stress equation may be written as:

$$\sigma_i = \frac{0.316P}{D^2}\left[4\log\left(\frac{l}{a}\right) + 1.069\right] \quad [2\text{-}8]$$

Where b= a if a ≥ 1.724 D and otherwise

$$b = \sqrt{1.6a^2 + D^2} - 0.675D \quad [2\text{-}9]$$

This equation is discussed by Huang, (2004) and again assumes a Poisson's ratio of concrete ν = 0.15. Huang, (2004) and Delatte, (2008) found that interior-loading stresses are much lower that edge-loading stresses.

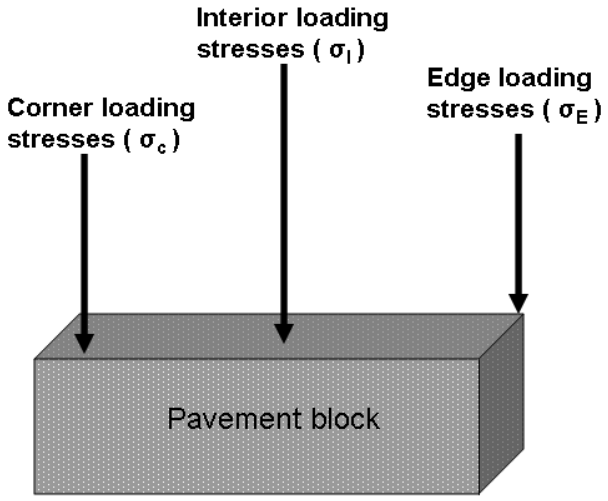

Figure 2-5: Stress loads on pavment block surface (adapted from Delatte, (2008)).

2.3.7 Sizing permeable (pervious) paving systems

Where the design objectives of a particular PPS are peak discharge attenuation or the capture and infiltration of a particular storm even, then the procedure includes:

(i) Selecting the design storm to capture for detention or infiltration,

(ii) Determining the detention volume: The required detention volume of a PPS is defined as the difference in the inflow and outflow volumes for the duration of a storm event (Argue, 2004). The inflow volume (V_i) will depend on the urban runoff source being routed through the PPS and may include: Rainfall onto the PPS only and a combination of rainfall onto the PPS and urban runoff from other impervious areas

The inflow volume for the design storm event on PPS is:

$$V_i = \left[\frac{A_s \times i}{10^3 \times 360} \right] \times D \qquad [2\text{-}10]$$

Where V_i is the inflow volume, A_s is the estimated surface area of paving (m^2), i is the average rainfall intensity for design storm event (mm/hr) and D is the duration of the storm (hr). The inflow for a combination of rainfall onto the PPS and urban runoff from other impervious areas is determined as the product of the design storm event and the storm duration.

$$V_i = Q_{DES} \times D \qquad [2\text{-}11]$$

Where V_i is the inflow volume (for a storm duration D) (m^3), Q_{DES} is the design storm flow for sizing using rational methods Q = CIA/360 (m^3/s), where C is the runoff coefficient, i is the average rainfall intensity for design storm event (m/hr), and A is the estimated surface area of paving (m^2). D is the storm duration (hrs × 3600 s/hr).

Outflow from the PPS is via the base and sometimes on the bottom sides of the pavement structure of the infiltration media and is dependent on the area and depth of the structure. It is calculated using the filtration rate through the filter layer media and the storm duration. The maxium filtration rate represents the maximum rate of flow through the paving system and is calculated by applying Darcy's equation as follow:

$$Q_{max} = K_{sat} \times A \times \left(\frac{h_{max} + d}{d} \right) \qquad [2\text{-}12]$$

Where Q_{max} is the maximum filtration rate (m^3/s), K_{sat} is the filter layer saturated hydraulic conductivity (m/s), A is the area of permeable paving (m^2), h_{max} is the depth of pondage above the soil filter (m) and D is the depth of the filter media within the pavement structure (m).

Given that no detention depth or ponding above the surface of the permeable paving and conditions are likely to be fully drained then

$$\left(\frac{h_{max}+d}{d}\right)=1 \qquad [2\text{-}13]$$

The outflow volume is calculates as:

$$V_o = Q_{max} \times D \qquad [2\text{-}14]$$

Where V_o is the outflow volume (m^3), Q_{max} is the maximum filtration rate (m^3/s) and D is the duration of the storm event. Thus the required detention volume (V_d) of a PPS can be computed as follows:

$$V_d = \left(\frac{V_i - V_o}{p}\right) \qquad [2\text{-}15]$$

Where V_d is the required detention volume (m^3), V_i is the inflow volume (m^3), V_o is the outflow volume (m^3) and p = porosity of the retention trench with gravel = 0.35. The depth of the PPS is determined from site constraints, soil properties and the structural requirements of the paving system.

The surface area can be determined and designed using two steps (i) calculating the surface area based on the volume and required depth and (ii) checking the surface area's capacity to infiltrate peak flows for design storm events. The surface area of the PPS can be determined by using the following equation (Argue, 2004)

$$A_S = \frac{Q_{peak}}{(1-B)\times K_{sat}} \qquad [2\text{-}16]$$

Where: Q_{peak} is the peak inflow to the permeable paving surface (m^3/s), B is the blockage factor and is estimated based on non-porous structural elements such as plastic and concrete grids, and K_{sat} is the saturated hydraulic conductivity of the paving surface.

2.3.8 Hydrology and hydraulics

PPS have been regarded as an effective tool for stormwater management and control because of their high surface infiltration rates, reduce runoff quantity and peak runoff rates and delay peak flows (Hunt *et al.,* 2002; Brattebo and Booth, 2003; Bean et *al.,* 2007). Figure 2-6 (Ferguson, 2005) summarizes major hydrologic features and processes that could occur in a pervious pavement. A pavement's hydrology begins at the surface with rainfall or snowmelt, which infiltrates through the pavement's surface. Movement of urban runoff through the porous system is controlled by surface runoff, infiltration through the pavement stones and aggregate, percolation through the unsaturated zone, lateral drainage at the base and deep percolation through the sub-grade. Three possible outcomes for precipitation reaching the surface of permeable pavements are infiltration to the base material, evaporation and runoff (James and von Langsdorff, 2003). Some additional stormwater may arrive as runoff from off-pavement areas. Water infiltrating the pavement surface may further infiltrate the subgrade soil; the remainder overflows at the elevation provided for in the pavement's construction. Storage in the pavement's reservoir takes up temporary differences between rates of inflow and outflow. Evaporation pulls water back into the atmosphere at every stage. Percolation represents the vertical gravitational flow of water from the unsaturated zone to the saturated zone of the base layer and represents the inflow source to the saturated zone. If systems are not lined, lateral inflow can occur from the surrounding areas (James and von Langsdorff, 2003). Base layer discharge signifies lateral flow from the saturated zone of the pavement's base to the receiving watercourse. Deep percolation through PPS represents limited losses from the saturated zone of the base (James and von Langsdorff, 2003).

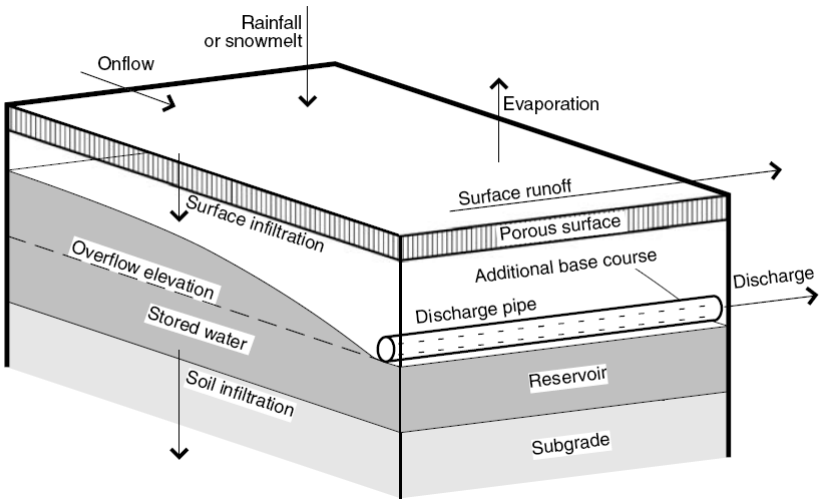

Figure 2-6: Hydrology and hydraulic features of permeable pavements (adapted from Ferguson, 2005).

In comparison to conventional paving surfaces (Asphalts and impervious concrete) permeable pavements, provide more effective peak flow reductions ranging up to 42 % and longer discharging times. There is also significant reduction of evaporation and surface water splashing (Booth and Leavitt, 1999; Pagotto *et al.,* 2000; Abbott *et al*., 2003). For areas where the underlying soil is not ideal for complete infiltration, the installation of under drains within the permeable pavement subsurface can yield reductions in outflow volumes and peak flow rates and delay the time to peak flow (Pratt *et al.,* 1989). In a controlled laboratory environment, Andersen *et al.,* (1999) carried out tests which showed that evaporation; drainage and retention within pervious pavement structures are mainly influenced by the particle size distribution of the bedding material and retention of water in the surface blocks.

Studies conducted by Valavala *et al.,* (2006) in South Carolina, USA, on a permeable pavement concrete laboratory experiment yielded negligible runoff for simulated rainfall events up to the 100-year frequency for unclogged pavement slabs ranging from 0 to 10 % slopes. The permeable pavement concrete slabs were 17 cm in thickness and underlain with a 15 cm thick sand bedding layer. During extremely high intensity events (20 to 47 cm/hour) no runoff was observed from the slabs with a 10 % slope. For the same high rainfall intensities, once more no runoff was observed for the 2 % sloped slabs (Valavala *et al.,* 2006).

Permeable pavements substantially reduced surface stormwater runoff quantities (Hunt *et al.,* 2002). For a permeable paving parking lot with a concrete grid paver in North Carolina, United States, Hunt *et al.,* (2002) found surface runoff to be dependent on rainfall intensity rather than volume. Furthermore, Hunt *et al.,* (2002) compared the hydrologic responses of various pavement sections including asphalt, pervious concrete and two types of interlocking concrete pavement for a 44-storm event. When compared to asphalt, all permeable pavement sections dramatically reduced surface runoff volumes with the pervious concrete and interlocking concrete pavement blocks having the highest mean runoff reduction from rainfall depth with 99.86 and 99.5 % respectively (Hunt *et al.,* 2002).

Concrete grid pavers and permeable interlocking concrete pavers were tested for infiltration at North Carolina State University, USA, with the age of pavements ranging from 6 months to 20 years (Bean *et al.,* 2007). Analysis of the data showed that periodic maintenance improved permeability on 13 out of 14 sites with a confidence level of 99.8%. Pavement sites constructed closely to loose fine particles had infiltration rates significantly less than sites free of loose fine particles. The infiltration rates of the permeable pavement site were comparable to that of grassed sandy loam soil (Bean *et al.,* 2007).

Brattebo and Booth, (2003) observed drainage through several types of porous and dense pavement surfaces at a parking lot in Renton, Washington, USA. They monitored flow during one winter rainy season where the rainfall was typically gentle and there were no long periods of freezing weather conditions or snow accumulation. Essentially all precipitation infiltrated the porous pavement surfaces (Brattebo and Booth, 2003).

Temporary storage within permeable pavement structures provides attenuation of stormwater inflows. In permeable pavement design for infiltration, the thickness of the reservoir course may be chosen to store a certain depth of rainfall for sufficient time to allow infiltration (Newton, 2005). The effectiveness of permeable pavements in attenuating peak discharges has been confirmed by field studies from Pratt *et al.,* (1995), who measured the hydrologic responses of modular permeable pavement car parks at the Nottingham Trent University, U.K. The pavement area consisted of Aquaflow blocks from Hanson Formpave designed to hold 16 cars with an area of 40

m long by 4.6 m wide and constructed on an impervious liner. The results from this study showed that peak effluent discharges to be approximately 30 % of the peak rainfall intensity whereas an impervious pavement would produce surface runoff closer to 90 %. The peak discharge was typically 5 to 10 times later than the peak rainfall, whereas for an impervious pavement on the same site would have a time of concentration of approximately 2 minutes (Pratt *et al.,* 1995).

The average volumetric runoff coefficient defined as the total runoff volume to the total rainfall volume for conventional pavements are typically of the order of 80 to 95 % (Rushton, 2001). Where infiltration occurs the volumetric runoff coefficients may be significantly lower (Legret and Colandini, 1999). These observations at Nottingham Trent University were confirmed and supplemented in Wheatley, England by Abbott and Comino-Mateos, (2003). They (Abott and Comino-Maeteos, 2003) monitored reservoir discharge from a pervious parking lot at a highway service station. An impervious geotextile membrane confined reservoir outflow to perforated drainage pipes where the effluent of the pavement was monitored. The reservoir aggregate consisted of substantial fines where abundant small pores were capable of retaining significant amounts of water. Table 2-2 summarises the observed discharges and the outflow discharges lags behind rainfall and continued at low rates after rainfall stopped. The delay occurred as a result of the slow movement of water through the reservoir's small pores. For a rainfall intensity of 0.5 inches/hour the peak discharge was only 0.01 inches per hour.

Table 2-2: Discharge from bottom of an open-jointed block parking lot in Wheatley, England (adapted from Abbott and Comino-Mateos, 2003)

	Range	Average
Time from start of rainfall to start of pipe drainage	5 minutes to 2 hours	
Time from peak rainfall to peak outflow	5 minutes to 9 hours	
Duration of outflow	5 to 31 times duration of rainfall	14 times duration of rainfall
Total water draining from each event	30 to 120 % of rainfall	67 % of rainfall
Peak rainfall intensity	0.19 inch/hour to 1.32 inch/hour	
Peak outflow rate	0.01 inch/hour to 0.15 inch/hour	

Evaporation may be expressed directly as the average rate of water loss from the PPS. Evaporation acts on water retained in the reservoir section of the permeable pavement structure as a thin film on wet rock surfaces, in capillary-sized openings at contact points between the bedding layers. The water required to re-wet the pavement structure and fill the small storage areas is often referred to as the initial loss. Initial loss is defined hydrologically as the amount of rainfall before runoff commences and is observed for both permeable and impermeable surfaces. Pratt *et al.,* (1995) reported an average initial loss for a drained pavement system of 2.4 to 3.2 mm depending on the type of sub-base material. Boyd *et al.,* (1993), found that storm event initial losses for impervious surfaces are generally around 1 mm. Macdonlad and Jefferies, (2001) reported an average initial loss of 0.8 mm for an impervious car park when compared to 5.6 mm for a porous pavement catchment with infiltration to a low permeability. Berry, (1995) found that evaporative losses from a drained pavement structure were limited by water availability and concrete surface blocks, which covered 85 % of the surface area in a modelled pavement structure, were found to significantly reduce evaporation.

Perez, (2000) investigated the effects of gravel sizes and sorting the efficiency and found that grain size and sorting through their effect on pore dimensions,

controls evaporation losses from the soils. Smaller particles have a large surface area to weight ratio and hence are capable of holding more water than larger particles. However, the smaller pore spaces in finer-grained gravels slowed down the rate of vapour diffusion (Perez, 2000).

2.3.9 Pollution Removal Processes and Water Quality

The large areas the pavements cover and the vehicles that use them make pavement surfaces a locus of urban pollutant generation. Permeable pavements have a desirable impact urban stormwater runoff quality. PPS effluent has shown to decrease concentrations of urban runoff pollutants. Most contaminants in urban stormwater are associated with particles (Dempsey *et al.,* 1993). Nevertheless, significant proportions of some contaminants such as nitrogen, heavy metals (zinc, copper and lead) may be present in a dissolved form (Newton, 2005). Several studies from Pratt *et al.,* (1989), (1995), (1999); Niemczynowicz, (1990); Legret and Colandini, (1999); Raimbault, (1997); Ruston, (2001); Mcdonald and Jefferies, (2001) and Brattebo and Booth, (2003); have reported significant water quality benefits from permeable pavement applications. The principal mechanisms for stormwater quality control by permeable pavements include (Newton, 2005; Scholz and Grabowiecki, 2009):

- Capture of water within the pavement structure for subsequent disposal by evaporation and infiltration to the underlying soils
- Sedimentation, filtration and adsorption of pollutants
- Biological assimilation and biodegradation of pollutants by microbial activity within the porous media.
- Volatilization and water transport.

The sub-base of a permeable pavement structure is essentially a gravel filter and mimics its treatment operations (Newton, 2005). With regards to the removal of particulate material in water and wastewater treatment applications, sedimentation is identified as the dominant removal process mechanism within coarse media filters (Ahsan and Alaerts, 1997). Filtration occurs for smaller particles and in dissolved

form through particle adhesion when in contact with the filter media. Adsorption of dissolved contaminants through the filter media and trapped particles within the porous media also occurs (Sansalone, 1999). Coarse media filtration is widely used in conventional water and wastewater treatment plants and reduces suspended solids from 30 to 90% (Chin, 2006). The efficiency of sedimentation and filtration processes is related to the hydraulics of the PPS, in particular with the velocity of flow through the pore spaces. With combined permeable pavements and impervious surfaces, the hydraulics has similarities to a horizontal roughing filter used for pretreatment in water treatment processes (Lebcir, 1992). The pervious pavement receives hydraulic and pollutant loadings that are intermittent and highly variable when compared to continuous, steady-flow operations of roughing filters. Permeable pavement traps solid particles on the pavement surfaces along with metal ions adsorbed to the particles (Balades *et al.,* 1995; Gerrits and James, 2003). Capture occurs with the settling of small aggregate particles with the contaminants lodging around them. Sansalone, (1999) suggested the use of oxide-coated sand as a bedding layer within porous pavements because it acts as a water-quality filter and can simultaneously adsorb dissolved metals out of solution and filter out solid particles.

Dierkes *et al.,* (2002) observed that heavy metal pollutions concentrations within a pervious pavement parking area decreased rapidly with the depth of pavement structure. Most heavy metals were captured in the top 2 cm of the void space fill media (Dierkes *et al.,* 2002). The analysis evaluated heavy metal reduction efficiencies of four pavements including concrete pavers with open infiltration joints, concrete pavers with greened joints (topsoil filled with planted grass), permeable concrete pavers and permeable concrete pavers with greened joints. All four pavements retained and degraded cadmium, copper, lead and zinc with the permeable concrete pavers and permeable concrete pavers with greened joints demonstrating the highest pollution retention capabilities with lead and copper being removed more effectively when compared to cadmium and zinc (Dierkes *et al.,* 2002).

Studies by Fach and Geiger, (2005) observed the pollution removal rates of cadmium, zinc, lead and copper for permeable concrete block paving and three variations of concrete block pavers; one paver designed with wide infiltration pores of 29mm, another with narrow pores of 3mm and pavers with a crushed brick

substrate infill. Permeable concrete had the highest average heavy metal removal efficiency of 96.5 % followed by block paving with brick substrate infill with a mean removal efficiency of 92.9 %. The infiltration of stormwater resulted in 63.1 % to 78.6 % mean removal rates for the heavy metals respectively, and there were no significant differences between these two types of permeable pavements. When the permeable pavements were set over a 4 cm crushed basalt or brick substrate roadbed and a 40 cm limestone base course, for all the pavements and substructures the average pollution removal rates were extremely high ranging from 96 to 99.8 % (Fach and Geiger, 2005).

In Reze, France, Legret and Colandini, (1999) examined and compared the pollutant loadings of runoff water either collected at the outlet of a porous pavement with a reservoir structure from a nearby catchment drained by a conventional separate sewage system. The pavement's aggregate base reservoir was separated from the subgrade by a geotextile and was drained at the bottom by a perforated pipe. The porous pavement discharged suspended solids at only 36 % of the initial concentration in the urban runoff. The adsorbed metals, cadmium, zinc, copper, and lead were reduced in concentration between 57 to 85 % respectively (Legret and Colandini, 1999). The heavy metals had primarily accumulated with the solid particles and were attached to the pavement surface and secondarily at the bottom of the base reservoir. Heavy metals (zinc, lead and copper) tend to be captured within the top layers of permeable pavements. Results from the field analysis of materials found that clogged permeable pavements had high concentrations of cadmium, zinc, lead and copper. The study found that these concentrations appeared to be correlated to traffic intensity and clogging materials with a finer particle distribution had the highest heavy metal concentrations (Legret and Colandini, 1999)

Brattebo and Booth, (2003) studied the long-term effectiveness of permeable pavements as an alternative to traditional impervious asphalt pavement, in a parking area at Renton, Washington, USA. A parking lot was constructed with four commercially-available permeable pavement systems including permeable interlocking concrete pavements (PICP), concrete grid pavers with grass (CGP), plastic grid pavers with grass and plastic grid pavers with gravel. Six years after installation, all four PPS showed no signs of wear and endured structurally. During

an 18 month monitoring period, 15 observable storm events were recorded whereby all rainfall infiltrated through each permeable section. Concentrations of zinc and copper were significantly lower for the PPS segments when compared to runoff from the asphalt with average removal rates of 90.4 % and 58.4 % of copper and zinc respectively. Lead effluent concentrations were undetectable whilst 72 % (copper) and 22 % (zinc) for the infiltrated water samples from the PPS were below the minimum detection limit whereas both limits were always exceeded by asphalt runoff.

Pratt *et al.,* (1995) observed similar retention and removal of solids and heavy metals at Nottingham Trent University parking lot, U.K, which was described earlier. The concentration of suspended solids discharging from all four types of permeable pavements ranged between 20 mg/l to 50 mg/l whereas the surface runoff from nearby impervious pavements was typically between 60 to 300 mg/l (Pratt *et al.,* 1995). The remaining solids and their attached heavy metals were trapped mostly within the pavement's bedding aggregate zone. The pavement's combination of reduced discharge volume (previously described) and reduced concentrations show that permeable pavement's particulate load was significantly lower when compared to impervious pavements.

Ruston, (2001) compared asphalt runoff to runoff from pervious pavements with a swale and found pollutant load reductions were observed for ammonia, nitrate and total nitrogen but an increase in loading for phosphorous attributed due to landscaping practices on the vegetated swale. Bean *et al.,* (2007) reported the nutrient removal capabilities of permeable pavements. At two sites in North Carolina, USA, water samples from permeable pavements were compared to runoff to an adjacent asphalt runoff. Total phosphorus, ammonia-nitrogen (NH_4-N), and total kjeldhal nitrogen were significantly lower that the outflow from the asphalt surface (Bean *et al.,* (2007). Average removal efficiencies for NH_4-N ranged from 86 % to 88 % and Nitrate-Nitrogen (NO_3-N) ranged from 48 to 65 % respectively (Bean, *et al.,* 2007). Kadurupokune and Jayasuriya, (2009) simulated a 17 year period of stormwater quality sampling on a laboratory scaled pervious pavement, using synthetic urban stormwater consisting of mean concentrations of 141 mg/l, 0.24 mg/l, 2.63 mg/l, and 20 mg/l for total suspended solids, total phosphorous, total

nitrogen and oil/greases respectively. The results showed an average removal efficiency of 96%, 95%, 63% and 94 % for these parameters (Kadurupokune and Jayasuriya, 2009).

Permeable pavements can function as in-situ bioreactors with regards to motor oil degradation (Pratt *et al.,* 1989, 1995; 1999). Pratt, (1999) identified filtration in the surface area and in particular, the geotextile layer between the surface and the sub-base as the primary mechanism for removal and biodegradation of particulates including motor oil. Long-term laboratory research conducted at Coventry University, U.K. has shown that over time, resilient, complex microbiological communities establish themselves within permeable pavements (Newman *et al.,* 2002). Geotextiles within permeable pavements enhances microbial growth and provides increased pollutant removal efficiency (Coupe, 2004). It was concluded that some degree of degradation occurred as a result of the elevated CO_2 levels and decrease O_2 measured within the pavement (Coupe, 2004). It separates heavy metals and micro-pollutants such as cadmium, zinc, copper and lead from the underlying soil, thereby preventing groundwater contamination (Legret *et al.,* 1996).

Oil and diesel motor fuels contaminate road surfaces. Booth *et al.,* (1998) showed that infiltrated water from PPS had total removal of motor oil when compared to 89 % of samples from the asphalt runoff area containing motor oil. Coupe *et al.,* (2003) showed that permeable pavements with geotextiles operate efficiently as a hydrocarbon trap and powerful in-situ bioreactor reducing hydrocarbon contamination by 98.7 %. Biodegradation within PPS geotextiles are enhanced by bacteria and fungi (Coupe *et al.,* 2003). When inoculated with microorganism, the protozoan population diversity increases rapidly when compared to similar non-inoculated systems. This leads to enhanced pollutant removal efficiencies. Coupe *et al.,* (2003) found that pavements with geotextiles contain protozoan communities such as testate amoebae, ciliates, flagellates and gymnamoebae which helps the biodegradation mechanisms. Newman *et al.,* (2002) monitored the biofilm development through scanning electron microscopy and revealed that a PPS can obtain high degrees of biodiversity due to the development of complex microbial compositions. Very large hydrocarbon spills can be contained due to absorption processes within permeable pavement structures (Newman *et al.,*

2002). Wilson *et al.,* (2003) incorporated an oil interceptor into a porous surface and tests were carried out analysing the worst-case scenario for combined pollution and rainfall events for pollutant retention within the PPS. The results demonstrated that the pervious system can contain hydrocarbons and offered improved water quality outflow.

Escherichia coli depletion in permeable pavement aggregate was assessed by Myers *et al.,* (2009). Twelve model permeable pavement storage reservoirs were filled in triplicate with dolomite, calcite and quartzite, three reservoirs contained no aggregate. The permeable pavements were spiked with rainwater containing freshly grown colonies of *Escherichia coli.* The results showed that sedimentation and adsorption are responsible for the reduction of *Escherichia coli*. There was no significant difference in the depletion of *Escherichia coli* found in reservoirs without aggregate and those filled with dolomite or calcite, however, the rate of depletion was found to be significantly lower in the quartzite filled reservoirs. Adsorption of the microorganism to fine matter and aggregate surfaces occurs from the reversible form of adsorption caused primarily by electrostatic attraction, van der Waals forces and hydrophobicity. Bacteria attached in this manner can detach from the surface and return to an aqueous phase (Myers *et al.,* (2009).

2.3.10 Clogging, Maintenance and Serviceability

Porous pavements can clog with time as a result of accumulation of fines in the surface void spaces (Balades *et al.,* 1995; Pratt *et al.,* 1995). Fine particle deposition is typically a result of moving vehicles, wear and tear of the pavement surfaces, or transport via wind and urban runoff from nearby soils. As these fine particles accumulate, a matrix forms within the permeable void spaces decreasing the infiltration rate (Balades *et al.,* 1995). For one analysis, infiltration rates declined up to 50 % of the initial rate after 3 years from the date of installment (Balades *et al.,* 1995). Modular pavement structures are much less susceptible to clogging than monolithic pavement structures (porous asphalt and pervious concrete) (ASCE and WEF, 1998). It provides the opportunity for maintenance by lifting surface blocks for reuse and replacing the sub-base material (Pratt *et al.,* 1989). The amount of

stormwater, which can pass through permeable pavement concrete blocks, is dependent on the infiltration rates of the joint filling, laying course and permeable sub-base materials. Geotextiles in the upper layers can also affect the infiltration rate. The percolations through joints have a typical value of 4000 mm/hr for newly laid block paving (Hanson Formpave, 2009). The permeable sub-base aggregates percolation rates are much higher averaging 40,000 mm/hr. A key consideration is the lifetime design infiltration of the entire pavement cross-sectional area including the subgrade. As seen in Figure 2-7, the infiltration rate decreases with time, but eventually stabilizes after 9 to 10 years in service.

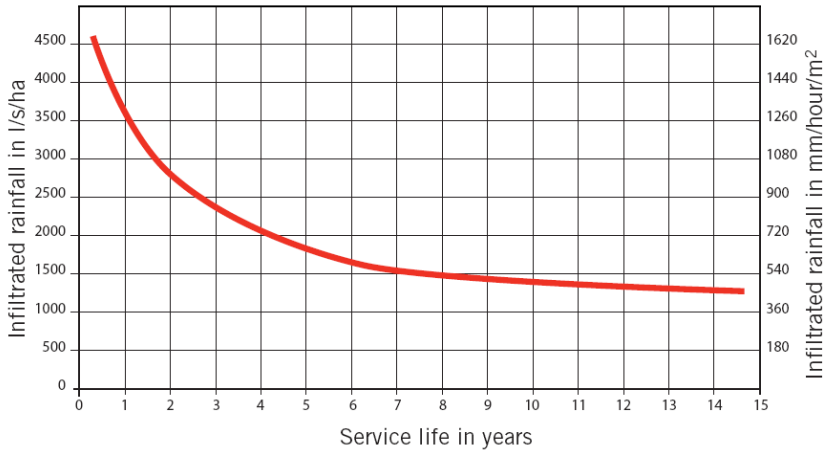

Figure 2-7: Infiltration of rainfall and service life of permeable pavements (adapted from Interpave, 2010)

Abbott and Comino-Mateos, (2001) reported results from tests conducted at a new car park, surfaced with small element concrete blocks. The infiltrations through the permeable block surface itself and through the gaps between the blocks were 550 mm/h and 27,000 mm/h respectively. At a similar car park, but with some years of usage, it was noted that the presence of dirt and oil spillage on the pavement surface significantly reduced the infiltration rates from both the block and the gaps between them. The surface infiltration rate of the permeable blocks was evaluated, both through the blocks themselves and via gaps between the blocks. There was a large variation in the block infiltrate rate (250 mm/hr to 14,000 mm/hr), which was similarly the case with test conducted on the gaps, however the infiltration rates at the gaps were 50 times higher (11,000 mm/hr to 229,000 mm/hr). The infiltration test when repeated after a 10-month interval revealed that some blocks had become

largely impermeable due to clogging, although the gaps between the blocks still performed well.

Wilson, (2002) conducted research at the University of Guelph, Canada, for particulate rate clogging analysis in a parking lot whereby the permeable pavement surface was applied street dust and dirt (particulates) and subjected to intense rain. Wilson, (2002) found that the quantities of sediment that can be applied without causing a decline in the performance of the pavers is determined by the porosity of the drainage cell fill material. Results from the experiments using a fill with 34 % porosity, suggests that the possibility of reduced maintenance than previously recommend can be applied. After applications of 1.4 kg /m^2 of permeable pavers, the average infiltration rate at the pavement surface declined to a rate below the inflow rates of 1/25-year design storm event of a 5-minute duration with an intensity of 230 mm/hour. After accumulation of 3.9 kg/m^2 onto the permeable pavements, the drainage cell materials became clogged and dysfunctional. Wilson, (2002) established that the permeable pavements should be maintained when the surface is affected by partial clogging and correspond to an accumulation between 1.4 and 3.9 kg/m^2 of street dust and dirt.

Dierkes *et al.,* (2002) carried out a field assessment for the effectiveness of maintenance and cleaning of a permeable pavement area in a schoolyard, Holte/Stukenbrock, Germany. The pavement was constructed in 1996 with an area of 1500 m^2. It was made of permeable concrete pavers with a filter later and bedded on pea gravel. To determine the cleaning efficiency, the infiltration capacity of the pavement was measured at 3 points before and after cleaning. The measurements were carried out using a drip-infiltrometer. The cleaning device operated with high pressure cleaning and a direct vacuum suction. In Germany, regulations for permeable pavements must provide an infiltration capacity ≥ 270 l /(s.ha) Dierkes *et al.,* (2002). For all points the infiltration capacity was below 1 mm/(s.ha), hence, the pavement was completely clogged and could not infiltrate the rainwater sufficiently. After the cleaning procedure the measurements of the infiltration rate at the three selected points were repeated. The new infiltration capacities post cleaning, were extremely high ranging from 1545 l /(s.ha) to 5276 l /(s.ha).

DayWater, (2003), identified that the infiltration rate on newly paved permeable pavements exceeds 1000mm/hr. Test results from a permeable pavement site in France, for a 700 m long street, which was rebuilt with permeable pavements and showed after 7 years since constructed, with remedial cleaning of the surface there was a reduction in permeability with time, with a loss of approximately 80% over the first 3 years. Observations on a concrete block surfacing at Shire Hall, Reading, U.K., indicated a mean infiltration rate of 2600 mm/hr, six years after installation without any maintenance (CIRIA, 2002).

Bean *et al.,* (2007) stated that the location of permeable pavement sites plays an essential role in surface clogging rates. Close proximity to disturbed soil sites can reduce the surface infiltration rate up to 90% when compared to pavement installations in stable watersheds (Bean *et al.,* 2007). With regular maintenance, clogging of permeable pavements can be reduced. Vacuum sweeping and/or pressure washing of the top layer so the void space materials can be removed, and infiltration capabilities of the pavement improved (Bean *et al.,* 2007). They (Bean *et al.,* 2007) showed that the mean infiltration rates were more than doubled for concrete grid pavers after maintenance had been simulated.

All evidence indicates that permeable pavements lose up to 90 % of their capacity to accept water through the surfaces in a few years, but the remaining 10% is more than sufficient to deal with storm events that occur. The surface infiltration rate is greatly reduced but is still capable of infiltrating water, and a design life of 20 years for permeable pavements would seem appropriate. The US EPA, (1999 a) recommends sweeping the pavements at least four times per year and hosing the top layer with high-pressure water to remove pavement clogging.

2.3.11. Reduction of Heat Island Effect

Permeable pavements can cause a reduction of thermal pollution (Ca and Aseada, 1997; Karasawa *et al.,* 2006). The amount of reflected solar radiation is reduced due to an increase in the amount of solar energy used in the adiabatic processes of evaporating moisture retained in the pavement voids. Over 90 % of the increase in temperature for urban areas is due to construction materials that absorb

and store solar heat without evapotranspirative cooling, and the other 10 % comes from active emissions of vehiciles, buildings and factories (Rosnefield *et al.,* 1997). Solid structures absorb solar heat and conduct it into the depth of materials making the structure into a thermal storage battery. When the solar heat intensities declines later in the day the solid construction materials re-emit their stored heat to the air, increasing the urban air temperature even after the sun has set (Asaeda *et al.,* 1996). Dense pavements contribute as much heat transfer as buildings to the heat-island formation because impermeable pavements have a high thermal inertia at the ground surface (Asaeda *et al.* 1996). Often overlooked are the importance of stormwater temperature and the growing problems of thermal pollution. Urban areas also produce a kind of thermal water pollution. The urban stormwater that drains off hot urban surfaces is correspondingly warm, raising the temperatures of nearby watercourses. Heated runoff, which reaches the receiving water environment, can have severe impacts on aquatic biota (Schueler, 1987). An increase in stormwater temperature above ambient levels can result in direct biological impacts, disruption of aquatic life cycles (fish populations), and increased levels of bacteria such as *Escherichia coli* (Armour, 1991). Van Buren *et al.,* (2000) at Queen's University, Kingston, Ontario, Canada studied the thermal enhancement of stormwater runoff from an asphalt test plot. A thermal energy balance approach using a one-dimensional heat equation mathematical model was applied successfully to predict the surface temperature and temperature gradients in asphalt during dry-weather and wet weather periods. Runoff temperatures collected at the outfall sewer from the parking lot area were cooler than measurements at the test plot. These differences were attributed to the cooling of the urban runoff in sewer pipes where sunlight was restricted.

Excessively high urban temperatures associated with the heat-island effect can aggravate air pollution in cities and densely populated areas. Heat accelerates chemical reactions in the atmosphere that transform emissions from cars and smokestacks into ozone. This effect can also cause a degree of discomfort for people outdoors and implicate heart-related health problems (Van Buren *et al.,* 2000).

The utilization of porous materials for the construction of pavements allows water exchange between the ground surface and the deep soil layers and thus

promotes evaporation and is an effective method to moderate thermal conditions on the pavement surface. This leads to the reduction of atmospheric heating rates as well as the infrared radiation emission, which directly affects pedestrians during the hot time of the day (Aeaeda and Ca, 2000). They (Asaeda and Ca, (2000), studied the heating effects on the ground surface of permeable pavements and its characteristics during hot summer weather conditions in Japan and impacts on the thermal environment when compared to traditional pavements from asphalt. At noon, the permeable surface was 9 °C cooler than a nearby dense asphalt surface; at 6:00 pm it was still 14 °C cooler and at midnight approximately 9 °C cooler. Porous materials have less thermal conductivity and thermal capacity than corresponding impervious materials (ASHRAE, 1993) and ought to conduct daytime heat downwards and store it internally but less effectively than impermeable (dense) materials. Because of evaporation for the porous pavement surface, the surface temperature is appreciably lower that non-porous pavement surfaces. Impermeable pavement surfaces absorb large amounts of incoming net radiation which increases its surrounding temperature and modifies the urban thermal environment unfavorably (Asaeda and Ca, 2000).

2.3.12. Comparative Costs Analysis of PPS and SUDS

Cost estimation, affordability and willingness to pay considerations and the financing issues in relation to the planning processes for SUDS such as PPS are economically important. Stormwater has an economic value and can be considered socially and economically good, as fresh water is finite and a vulnerable resource essential for life, development and the environment. The use of permeable surfaces have shown to improve water quality as a result of reduction in pollution and a reduction in peak flows to receiving waters as stated previously. The Chartered Institution of Water and Environmental Management (CIWEM, 2000) provided data on the extent of pollution in surface water outfalls and the costs associated with it. Overall, it provides a guide to the likely magnitude of pollution problems caused by untreated runoff from impermeable areas. The costs associated with diffuse pollution are summarised in Table 2-3. The pollutants that are relevant to urban surface water runoff and/or are known to be reduced by permeable surfaces are listed in Table 2-3

(Associated cost of pollution in surface water outfalls). Large vehicular oil spills, sediment loadings onto roadways and gully pot cleaning represents a huge portion of the financial cost required for cleaning and maintenance.

Table 2-3: Associated cost of pollutions in surface water outflalls (CIWEM, 2000)

Pollutants	Impacts	Capital & Associates Cost £	Cost £/year
	37 % of oil contamination incidents had no clearly identified source. Possible source from general surface water runoff		£ 500,000. Although this is considered to be a significant underestimate as it is based on costs recovered by Environment Agency U.K
Oil and hydrocarbons	Clean up costs for small spills	£ 20,000	Typically, 4800 incidents per year and 37% ascribed to surface water outfalls. Assuming 50 % are small ≈ £ 48 Million
	Clean up costs for moderate spills	£ 100,000	Typically, 4800 incidents per year and 37% ascribed to surface water outfalls. Assuming 50 % are moderate ≈ £ 240 Million
Suspended solids	Sediment problems in urban drainage systems		£ 50 to 60 Million
	Gully cleaning, drains and streets cleaning		£ 1 to 2 Million
Nitrogen	Achieving UK standards for potable water. Main source is agriculture		£ 16 Million
Phosphorous	Contamination of drinking water. Main source is agriculture		£ 55 Million

A review of the cost benefits of undertaking SUDS retrofit in urban areas was conducted by the Environmental Agency U.K in 2007 (Environment Agency, 2007). The study assessed the costs and benefits of various sustainable drainage systems (SUDS) most likely to be applicable for retrofitting within a period of 40 years. The scope of the analysis covered England and Wales and was applied to several different types of structures including schools, leisure centres, hospitals, low-rise flats, detached and semi-detached housing, rural and urban roads. The cost analysis involved the comparison of costs and benefits of a SUDS scheme with those of conventional or traditional approaches. The SUDS schemes that were selected in the cost benefit modelling analysis included permeable paving, infiltration trenches, filter drains, swales, green roods, rainwater harvesting and water butts. For each type of SUDS scheme evaluated in the cost benefit model, the relevant parameters and conditions for retrofitting were taken from national sources used in the U.K.

The costs in terms of both capital expenditure and operating expenditure were collected from a variety of available sources (Environment Agency, 2007). The installation of SUDS would have a direct impact on the flows in sewers either by direct disconnection of rainwater from the sewer systems or by reduction in the volumetric flow rate at which runoff enters the sewer system. The financial model assumed that converting 10 % of the total impermeable area to a pervious surface area would lead to "Greenfield flows" leading to a 90% reduction in internal flooding incidents. Reductions in flood events were assumed to be linearly related to the reduction in impervious areas and the reduction would not exceed 90 %. The results as shown in Table 2-4 suggested that the most important type of SUDS and vital for reducing the number of floods were permeable paving and rainwater harvesting (Environment Agency, 2007).

SUDS can improve the river water quality by reducing discharges from combined sewer overflows (CSOs) through a reduction in volume. As CSO spills due to drainage systems being overloaded, a comparatively small reduction in peak flows within the system greatly reduces the number of spills and subsequently a reduction in maintenance costs. Therefore, reducing the impermeable area would reduce the number of CSO's categorised for unsatisfactory performance (Environment Agency, 2007). Economic benefits would hence arise as the sewage companies would no

longer be required to upgrade these. Average costs of £51,000 per CSO upgrade were estimated. Reductions in the number being upgraded were once again assumed to be 90 % if the impermeable area was reduced by 10 %. However, unlike flooding incidents it was assumed that the reduction could increase to 98 % if 25 % of the impermeable area was removed. The use of some types of SUDS can also have a positive effect on the demand for potable water. Rainwater harvesting has the clear benefit of reducing potable water consumption, which remunerates water companies in their responsibility to ensure continuity of water supply, eases the volume of water to be treated and pumped; but also benefits the property owners via a reduction in the water bill for metered customers. Infiltration SUDS methods also has increased benefits for groundwater recharge, thus benefitting groundwater resources. The analysis assumed that full implementation of these SUDS would reduce demands for water from the supply network by 1.3 million m^3 per year. This would lead to an annual reduction in water rates of approximately £ 2,400 m per year, equating to a reduction in water bills of £ 21,477 m discounted over a 20-year period. From the results, the SUDS type shows clear evidence for economic benefits from permeable paving. Evidence suggests that on a long-term basis, permeable pavements has the added benefits of reduction in urban runoff and demand on potable water supply and consequently making it worthwhile to replace traditional paving where possible (Environment Agency, 2007).

Table 2-4: Total financial summary of cost-benefit analysis of SUDS (Environment Agency, 2007)

SUDS	Benefits (£' 000)	Costs (£' 000)	Benefits minus (-) costs (£' 000)	Benefits to cost ratio
Permeable paving	515,217	-896,603	1,411,820	*Very positive*
Rainwater harvesting	8,647,965	13,702,282	-5,054,317	*Neutral*
Water butt	733,075	325,824	407,251	*Very positive*
Swale	60,392	610,134	-549,742	*Very negative*
Infiltration trench	105,687	8,739,055	-8,633,368	*Very negative*
Filter drain	60,392	7,212,069	-7,151,676	*Very negative*

The potential cost advantages of concrete block permeable pavements are less well understood, and a report by Scott Wilson carried out an independent, comparative cost research for various pavement types used in different applications and ground conditions (Interpave/Scott Wilson, 2006). The cost analysis was carried out in two stages, including baseline investigations and comparison of pavements and drainage construction requirements and their initial construction cost. Scott Wilson used projects originally appointed as designers to give realistic and accurate designs reflecting topographical and drainage requirements. The projects were re-designed using various pavement types (permeable pavement concrete blocks, asphalt and unreinforced concrete pavements) and a range of different ground conditions expressed in California Bearing Ratio (CBR). Whole life costs (WLC) is a useful tool for establishing the most appropriate pavement design and maintenance solution. WLC is employed to assess the true costs of an asset or project over its design life and to assess the cost effectiveness of solutions. The monetary costs in the WLC analysis involves initial construction costs, user costs and maintenance cost. The WLC assessed the three pavement types. In each case two alternative subgrade conditions were considered, (i) a 3 % CBR representing a fairly poor quality subgrade and (ii) a 6 % CBR representing a reasonable quality subgrade. Each type

of pavement applications has different maintenance requirments driven by varying properties.

These factors for maintenance strategies met the requirements for each pavement type and application (Interpave/Scott Wilson, 2006). Costing for the maintenance strategies over a typical 40-year life have been combined with the initial construction costs from the initial stages when calculating the WLCs. The first application was supermarket and other car parks. In terms of initial costs, permeable concrete block pavements offer the lowest cost solution (£27/m^2) when compared to impermeable concrete paving and asphalt that had an approximate initial cost of £42/ m^2 and £44 m^2 respectively for the supermarket car park. Where ground conditions allow concrete block permeable pavements provided the lowest initial cost for applications including airport airside pavements, industrial estate roads, parking for warehouses and supermarket parking lots. As shown in Figure 2-8 the WLC for CBR values of both 3 % and 6 % the concrete block permeable pavements offers the lowest WLC and provides the most cost effective paving solution for a supermarket of 3438 m^2 in area. Similar results of the WLC occurred for the three other applications including airport airside pavements, industrial estate roads and parking for warehouses. Permeable block paving is considered to have significant environmental advantages over the impermeable asphalt and unreinforced concrete due to its performance as a sustainable drainage system (SUDS) and its inherent ability for reuse when being maintained.

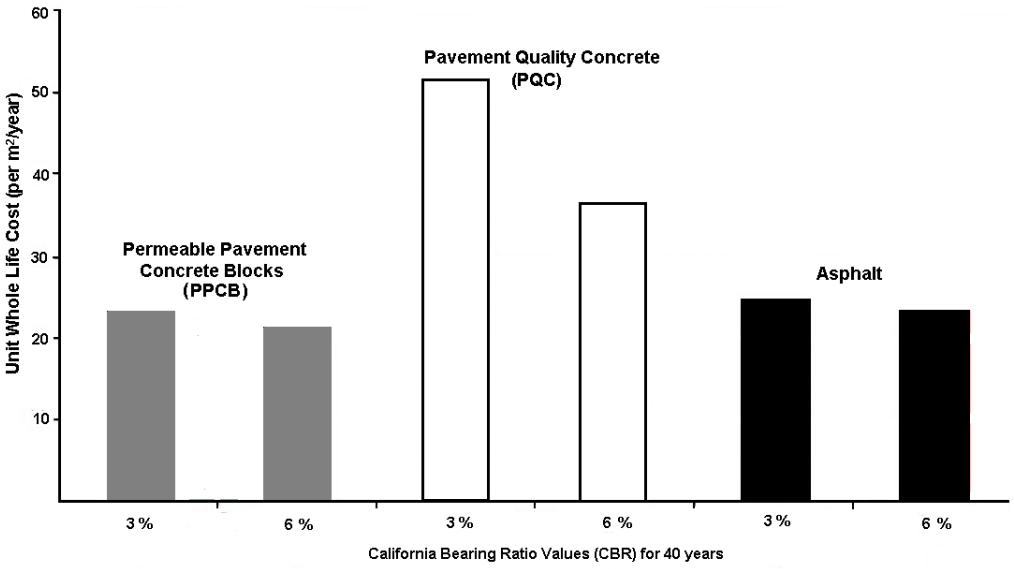

Figure 2-8: Unit whole life costs and pavement type for CBR of 3 % and 6 % (Interpave/Scott Wilson, 2006)**.**

Chapter 3 Geothermal Heat Pumps

This chapter outlines the importance of Geothermal (ground-source) heat pumps as a sustainable and renewable energy tool. The environmental and economic benefits of GHPs are presented with past research. Key aspects of GHPs are addressed and its importance for integration within permeable pavements.

3.1 Introduction

Geothermal heat pumps (GHPs) are considered a sustainable technology as it reclaims and recycles thermal energy from the Earth. GHPs are one of the most recognizable renewable energy applications around the globe today (Lund *et al.*, 2004**;** Curtis *et al.*, 2005). GHPs also referred to as ground source heat pumps (GSHP), Earth energy systems (EES) or geoexchange systems are recognised globally as energy-saving devices. They are regarded as a sustainable technology, as they reclaim and recycle thermal energy from the Earth (Lund *et al.*, 2004). Considering 46 % of solar energy is absorbed by the Earth, a feasible yet sustainable option is to utilise this abundant source of energy for heating and cooling applications. In contrast to other sources of heating and cooling energy that requires long distances to be transported, Earth energy is available on-site in massive quantities (Curtis *et al.,* 2005). GHPs are one of the fastest growing applications of renewable energy in the world with annual increases of 10 % in 30 countries since 1995 (Curtis *et al.,* 2005). This technology has further established itself as a highly efficient delivery mechanism for renewable heat and more importantly its role in carbon reduction. Geoexchange systems offer the lowest energy consumption, lowest greenhouse gas emissions and cheapest operating cost of any available technology for heating and air conditioning every type of building.

GHPs are an established technology, capable of providing high efficiencies for heating and cooling employing enormous renewable storage capacity of the ground (Omer, 2008). They have been progressively recognized as an alternative to fossil fuel systems; as a result, this technology offers a significant reduction in CO_2 emissions in relation to the cooling and heating applications of buildings (Healy and

Ugursal, 1997, Esen *et al.*, 2006). The United States Department of Energy (US DOE) stated that GHPs are the most energy efficient and environmentally clean of all the heating and cooling options available (US DOE, 2001; Hepbasli, 2005). In the United Kingdom, heating accounts for 47 % of the total carbon dioxide emissions of which 75 % is attributed to the domestic sector (Parliamentry Office of Science and Technology, U.K. 2010). In climates with a near balance in the annual heating and cooling loads, GHPs function essentially as a seasonal energy storage scheme (Phetteplace, 2007). Today GHPs are widely accepted as an established technology with approximately 1 million units installed worldwide since 2005 and approximately 1.7 million domestic and commercial units installed annually worldwide (Geothermal International, 2010). Today, GHP systems are one of the fastest growing applications of renewable energy in the world with most of the growth occurring in North America and Europe. Countries such as Japan and Turkey have increased the installation and applications of GHPs for residential and commercial buildings.

3.2 Energy source: The ground

GHP make use of the energy stored in the Earth's crust. The ground transports heat slowly and therefore has a high thermal storage capacity, its temperature changes slowly depending on the depth of measurements (Omer, 2008). As a consequence of the ground's low thermal conductivity, soil can transfer its heat from a cooling period to a heating period. Heat absorbed by the Earth during warmer periods can be effectively used during the winter months for colder climates (Banks, 2008). The yearly continuous cycle between air and soil temperatures results in thermal energy potential that can be harnessed to heat and cool a building. An additional thermal characteristic of the ground is that just a few meters of surface soil insulate the earth and groundwater below, minimising the amplitude in soil temperature in comparison with the temperature of the air above ground. Below 1 metre in the ground for the United Kingdom, the ground temperature remains at a fairly constant rate of 8 to 10 ° C all year round (Figure 3-1). This provides an adequate energy source for GHPs to generate heating and cooling comfortably. The

earth is warmer than the ambient air in winter and cooler than the ambient air in the summer (Banks, 2008). This warm earth and groundwater below the surface provides a free renewable source of energy that can easily provide enough energy year-round to heat and cool an average sub-urban residential home. A GHP transforms this Earth energy into the useful energy required for heating and cooling applications. It provides low temperature heat by extracting it from the ground or bodies of water and provides cooling by reversing the process. Its principal application is space heating and air conditioning in addition to domestic hot water uses.

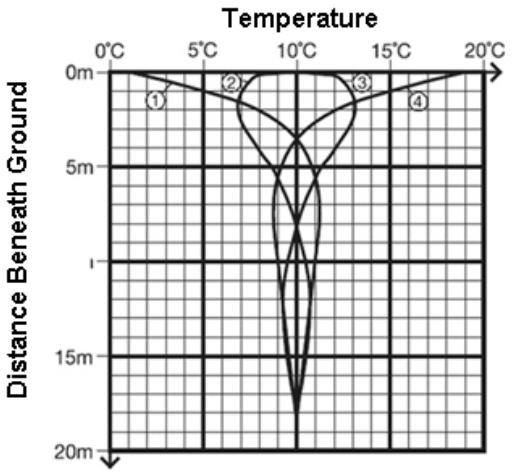

Figure 3-1: Distance beneath the ground and temperature profile in the U.K. during summer (1), autumn (2), winter 3 and spring (4) (adapted from Banks, 2008)

The two rock/soil properties that mostly affect the design of a geothermal heat pump system are the thermal conductivity (k_s) which measures the quantity of heat transmitted per unit area, per unit temperature gradient and in unit time and the thermal diffusivity (α) which is a measure of the grounds thermal conduction in relation to the thermal capacity. The most important difference is between soil and rock because rocks have significantly higher values for thermal conductivity and diffusivity (Rawlings and Sykulski, 1999). The moisture content of soil has a significant effect on its thermal properties. When water replaces the air between particles, it reduces the contact resistance. The thermal conductivity can vary form 0.25 $Wm^{-1}K^{-1}$ for dry soil to 2.5 $Wm^{-1}K^{-1}$ for wet soil (Rawlings and Sykulski, 1999). When heat is extracted, there will be a migration of moisture via diffusion

towards the heat exchanger and the thermal conductivity is increased. Water movement also has a significant impact on the heat transfer process through the ground as heat is transferred by convection due to moving water as well as conduction (Rawlings and Sykulski, 1999). In general, groundwater improves the heat exchange for GHPs, heat occurs through a dual mechanism of conduction in the aquifer material and convection in the ground itself (Banks, 2008). This thermal resistivity fluctuations further aid in shifting the heating or cooling loads to the season where it is needed. A GHP is used to concentrate and upgrade the readily available thermal energy from the ground before distributing it in a building through conventional ducts. It operates on the principles of a refrigerator or conventional air conditioning system in that it relies on an external source of electrical energy to concentrate the heat and shift the temperature. Typically, for every kilowatt (kW) of electricity used to operate a GHP system, 3 kW of renewable energy from the ground is drawn. Since a GHP system does not directly create any combustion byproducts and it draws additional free thermal energy from the ground it actually produces more energy that is uses. As a result, GHP efficiencies routinely average between 200 to 500 % over a season. GHP systems are more efficient than conventional heating systems and air-conditioning technologies and typically have lower maintenance costs (Rawlings and Sykulski, 1999; Banks, 2008). They require less space, especially when the heat transfer loops replaces voluminous air ducts and are not prone to vandalism like conventional rooftop units. Electrical power utility demand charges are reduced, as the electrical consumption for GHP is much lower than alternatives such as combustion or electrical resistance heating systems. Reductions in energy consumption between 30 to 70 % in the heating mode and 20 to 50 % in the cooling mode can be obtained.

3.3 Description of Geothermal Heat Pumps

A GHP system has three major components: (i) a heat pump, (ii) an earth connection and (iii) an interior heating or cooling distribution system.

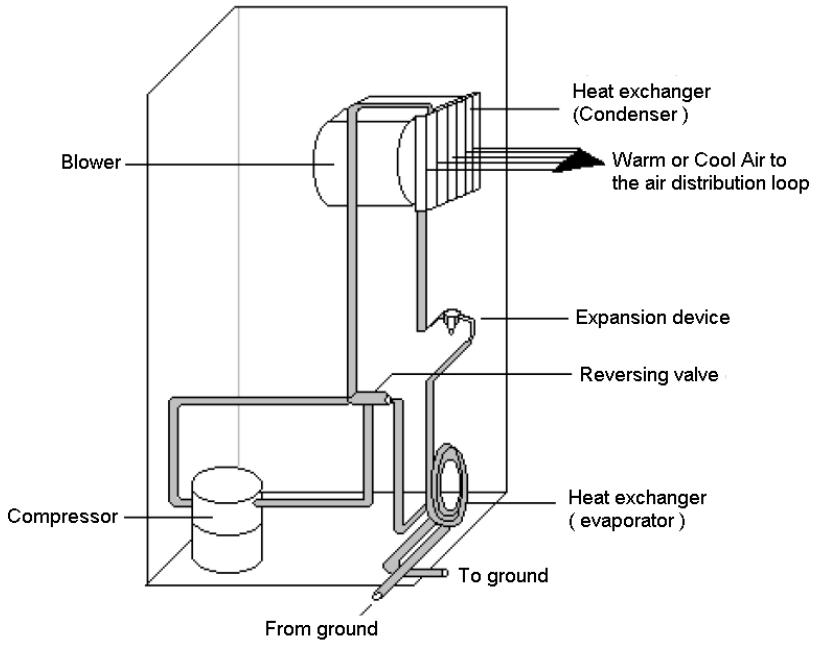

Figure 3-2: Domestic geothermal heat pump components for space heating and cooling (after Ochsner, (2007)**.**

3.3.1 Heat Pump

The heat pump transfers the heat between the heating and cooling distribution system and the earth connection. It is the basic building block for a GHP system. The heat pump may be an extended range unit, allowing lower entering fluid temperatures in a heating cycle and higher entering fluid temperatures in a cooling cycle. All components of the heat pump are in one enclosure exactly like a refrigerator, which includes the compressor, an earth connection to the refrigerant heat exchanger, controls, an air distribution system containing the air handler, duct fan, filter, refrigerant to air heat exchanger and condensate removal system for space heating and air conditioning. A typical packaged heat pump is shown in Figure 3-2. For larger commercial, institutional or industrial buildings multiple heat pump units are typically used in a distributed network connected to a common fluid loop, however for residential applications a single heat pump unit will suffice (Sanner *et al.,* 2003). The heat pump operates using the same thermodynamic cycle as a refrigerator. The heat uses compression and expansion of a refrigerant to drive heat flows between the inside of the building and the earth's connection. From the second

law of thermodynamics heat flows from a hotter to colder matter, but a heat pump draws heat from the ground and uses it to warm nearby buildings.

3.3.2 Earth connection

The earth connection transfers heat energy between the GHP system and the soil or groundwater. This comprises a wide variety of systems that uses the ground, groundwater, or surface water as a heat source and a heat sink. Common types of earth connection entails tubing buried in horizontal trenches or vertical boreholes (Figure 3-3). Alternatively, it can be submerged in a lake or pond. Earth connections come in two basic configurations (i) ground-coupled (closed loop) where an antifreeze mixture, water or another heat-transfer fluid is circulated from the heat pump around the tubing and back to the heat pump and (ii) a groundwater (open loop) system where the connection draws water from a well, or a body of water and transfers heat to or from the water and then returns it to the ground or the body of water. The type chosen depends upon the soil and rock type at the installation site, the land available and/or if a water-well can be drilled economically or is already on site. For all earth energy connections in a GHP system high-density polyethylene piping and fusion bonded pipe connections are used. Pipe diameters usually range between 20 mm to 40 mm. These pipe materials and pipe jointing methods now available can provide reliable, leak resistant loops that can be installed without requiring any maintenance for up to 50 years (Rawlings and Sykulski, 1999).

The American Society of Heating, Refrigerating and Air-Conditiong Engineers (ASHRAE, 1997) can distinguish geothermal heat pumps as having three main types of earth connection systems that has been adopted. The types of earth energy connection systems include:

- Ground-Coupled Heat Pumps (GCHPs)- This uses the ground as a heat source and heat sink with either vertical or horizontal ground heat exchangers;
- Groundwater Heat Pumps (GWHPs)- This uses underground (aquifer) water as a heat source and heat sink;

- Surface Water Heat Pumps (SWHPs)- These uses surface water bodies such as lakes, ponds and streams as a heat source and heat sink;

3.3.2.1 Ground-Coupled Heat Pumps (GCHPs)

In a GCHP system, a series of buried pipes circulates a heat transfer fluid in a closed loop, where the fluid never leaves the system but rather travels back and forth in a cyclic loop between the earth connection and the heat pump. This circulating fluid can be either water or an antifreeze solution if freezing temperatures are expected. The ground heat exchanger can make use of a series of deep vertical holes (boreholes) or a horizontal arrangement of pipes buried a few meters below the surface. Horizontal collectors are generally more appropriate for small installations such as residential and small commercial buildings where the collector pipe is buried in a trench at a dept between 0.25 to 1.8 m. A spiral coil can reduce the surface area required for horizontal earth connections and is sometimes referred to as a slinky coil installation. Vertical collectors are applied where land area is limited and require less pumping and pumping energy. The can be installed in most soil and rock types except alluvial gravel which has a low thermal conductivity. Boreholes are generally 100 to 150 mm in diameter and between 15 to 150 m deep and are drilled by rigs normally used for drilling wells. They contain either one or two loops of pipe with a U-bend at the bottom. After the pipe is inserted, the hole is backfilled and grouted. For deeper holes, problems can occur with backfilling, static pressure and insertion of the heat exchanger (ASHRAE, 1997).

3.3.2.2 Groundwater Heat Pumps (GWHPs)

Groundwater heat pump systems are open loop systems where they use a constant supply of groundwater as the heat transfer fluid. A GWHP earth connection consists of water wells were groundwater from an aquifer is pumped directly from the well to the heat pump's water connection to the refrigerant heat exchangers or to an intermediate heat exchanger. The intermediate heat exchanger transfers the heat

from the open groundwater loop to a closed building loop and thereby isolating the heat pump from the well water protecting the heat exchanger from potential fouling, abrasive or corrosive well water. After leaving the building, the water is pumped back into the same aquifer via a second well referred to as the injection well. The GWHPs were the first type of GHP which was developed and has been used successfully for decades (Banks, 2008). These are the simplest type of systems to install. Standing column wells are used for GWHP systems. Standing wells are typically 6 inches in diameter and may be as deep as 450 meters. For these systems, water from the bottom of the well is pumped to the building's heat exchanger and returns to the top of the same well. The well may also provide potable water supply. This system requires an abundant supply of ground water to work efficiently. However, this type of GHP is not used where the water table is especially deep since the power required for pumping renders the system prohibitively expensive (ASHRAE, 1997).

3.3.2.3 Surface Water Heat Pumps (SWHPs)

The surface water heat pumps are a viable and relatively low-cost GHP option. A series of coiled pipes are submerged below the surface of a lake or pond as the heat exchanger. This requires minimal piping and excavation; however, the pond or lake must be deep and large enough. The heat transfer fluid is pumped through the pipes in a closed loop avoiding adverse impacts on the aquatic ecosystem (ASHRAE, 1997).

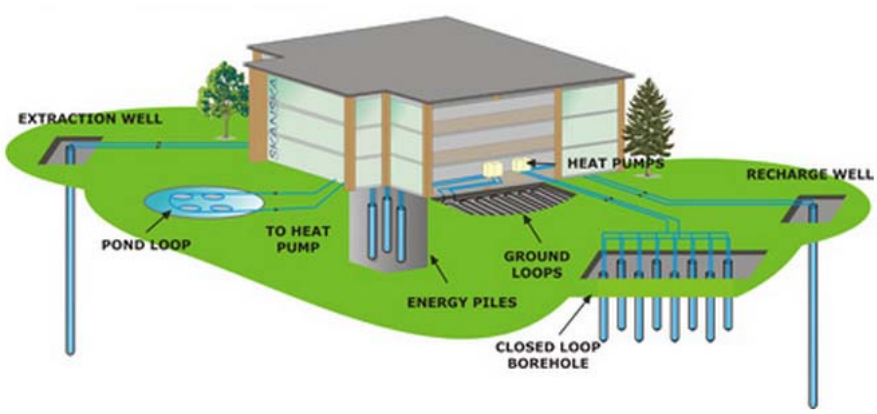

Figure 3-3: Various types of earth connection systems associated with GHPs (Geothermal International, 2010)

3.3.3 Interior heating or cooling distribution system

The heating-cooling distribution system delivers heating and cooling from the heat pump to the nearby building. It usually is designed similarly to an air duct distribution system for space conditioning, also a water loop systems (hydronic system which heat or cools floors and ceilings) can be incorporated. The distribution system consists mainly of air ducts, diffusers, fresh air supply systems and control components (ASHRAE, 1997).

3.4 Energetic Thermodynamic Performance

GHP's can function in two modes (i) a heating cycle and (ii) a cooling cycle. In a heating cycle, heat from the earth connection arrives at an earth connection to refrigerant heat exchanger (evaporator) (Figure 3-4). In the other side of the heat exchanger is the cold refrigerant in a liquid state. The refrigerant is colder that the temperature of the heat transfer fluid from the earth-connection therefore thermal energy flows into the refrigerant. This thermal energy causes the liquid refrigerant to evaporate; however, its temperature does not increase much. This gaseous, low pressure, low temperature refrigerant passes into an electrically-driven compressor (Figures 3-4). The refrigerant's pressure and consequently its temperatures are

raised. The high temperature, high pressure, gaseous output from the compressor is fed into a second heat exchanger (condenser). This high temperature liquid refrigerant then passes through an expansion valve (expander). The expander reduces the pressure of the refrigerant and consequently the temperature drops significantly. Finally, this low temperature liquid flows to the evaporator and the cycle starts again. From this process, the heat from the water or other heat transfer fluids in the earth connection is transferred to the air or water in the building.

One main significant difference between a GHP and a refrigerator is the GHP can run in both directions (heating and cooling). When in a cooling mode, the earth connection to refrigerant heat exchanger becomes the condenser and the refrigerant to air heat exchanger becomes the evaporator. This is accomplished through a reversing valve inside the heat pump. An auxiliary heat exchanger referred to as a desuperheater can be placed at the compressor's outlet to provide domestic hot water (Dieter and Stephan, 2006). It transfers excess heat from the compressed gas to water that circulates to a hot water tank. During a cooling cycle, when air-conditioning is applied frequently, the desuperheater can provide all the hot water needed for residential applications (Cengel and Boles, 2007). Residential heat pumps are also designed to provide hot water throughout the year in quantities sufficient to meet a household's requirement (Cengel and Boles, 2007).

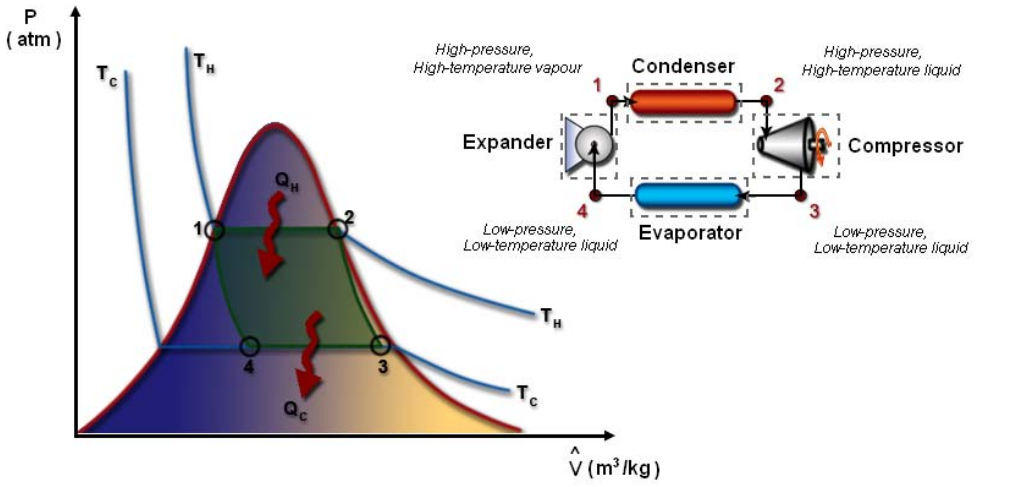

Figure 3-4: Thermodynamic cycle of geothermal heat pumps across compoments (Cengel and Boles, 2007)

GHPs can be assumed to follow a reversed cycle (Carnot cycle)**,** to supply heat at the elevated temperature**s** at the expense of work done by the heat pump (Cengel and Boles, 2007). In the Carnot Cycle a working fluid is taken through expansion-compression cycle, with portions of the cycle either thermally isolated or in contact with one of two thermal reservoirs at different temperatures. The final state of the fluid is unchanged after a cycle; the net result is taking heat from the hot reservoir at a higher temperature and converting part of the work to be done, while rejecting the rest of the energy as heat to the lower reservoir at temperature. The ratio of output to input measures the performance of a heat pump, namely heat supplied and heat rejected to work input.

To assess the energetic efficiency of the geothermal heat pump process, the ratio of the available useful heat produced by the system is compared to the energy that must be fed into the system (Wark, 1999). The efficiency of GHP units are described by the Coefficient of Performance ($COP_{heating}$) in the heating mode and the Energy Efficiency Ratio (EER) /$COP_{cooling}$ in the cooling mode (respectively in Europe), which is the ratio of the output energy divided by the input energy (work done by compressor and pumps). This has been shown to be the most appropriate method for assessing the energetic quality of a system (Healy and Ugursal, 1997, Hepbasli, 2005). The COP and EER in essence, depend on the difference in temperatures between the source of heat and the heating system that needs to be overcome (Hepbasli and Akdemir, 2004). For the experimental water-source geothermal heat pumps**,** the Energy Efficiency Ratio (EER) or $COP_{cooling}$ is the index, which defines the cooling performance. The heating performance during the heating mode is calculated by the Coefficient of Performance ($COP_{heating}$) index (Hepbasli, 2005, Cengel and Boles, 2007).

According to the first law of classical thermodynamics, in a reversible system: (Cengel and Boles, 2007)

$$Q_{(\text{Heat Supplied})} = Q_{(\text{Heat Rejected})} + W_{(\text{Net Work Input})} \quad (3\text{-}1)$$

Where Q is the useful heat supplied by the condenser and W is the work consumed by the compressor and pumps. The amount of work is always less then the heat supplied or heat rejected, and COP or EER, is thus always greater than unity i.e >0, indicating that the smaller the temperature difference between the upper and the lower reservoirs, the better the COP or EER is (Hepbasli *et al.*, 2003, Inalli and Esen, 2004).

The Heat supplied by the GHP unit in the heating mode can be described as in the equation:

$$Q_{HeatSupplied} = m_w C_{p,w}(T_{Max} - T_{Min}) \tag{3-2}$$

Where $C_{p,w}$ is the specific heat of the water, m_w is the mass flow rate of the water in the system and (T_{Max}-T_{Min}) is the temperature difference between the outlet and inlet of the GHP system. Similarly for the cooling mode,

$$Q_{Heat\ Re\ jected} = m_w C_{p,w}(T_{Min} - T_{Max}) \tag{3-3}$$

Negative heat removal rate indicates that heat is exiting the system. The Coefficient of Performance COP in a heating mode for a reversible inverse Carnot Cycle and the Energy Efficiency Ratio EER (Wark, 1999; Cengel and Boles, 2007) for the cooling mode is given by:

$$COP_{heating} = \frac{Q_{HeatSupplied}}{W_{NetWorkInput}} \tag{3-4}$$

$$\text{The Energy Efficiency Ratio EER or } COP_{cooling} = \frac{Q_{Heat\ Re\ jected}}{W_{NetWorkInput}} \tag{3-5}$$

By substituting the work done, $W_{Net\ Work\ Input}$ into equations (3-4) and (3-5),

$$COP_{heating} = \frac{Q_{HeatSuppiled}}{Q_{HeatSuppiled} - Q_{Heat\ Re\ jected}} \tag{3-6}$$

In addition,

$$\text{EER or } COP_{cooling} = \frac{Q_{HeatSuppiled}}{Q_{HeatSuppiled} - Q_{Heat\ Re\ jected}} \tag{3-7}$$

When the Geothermal Heat Pump is operating at the maximum theoretical efficiency (i.e. Carnot efficiency) (Hepbasli *et al.*, 2003; Hepbasli and Akdemir, 2004; Inalli and Esen, 2004; Hepbasli, 2005).

$$\frac{Q_{HeatSupplied}}{T_{Max}} = \frac{Q_{Heat\ Re\ jected}}{T_{Min}} \tag{3-8}$$

Where T_{Max} is the Maximum Temperature at the Hot Reservoir (Heat Supplied) and T_{Min} is the Minimum temperature at the Cold reservoir (Heat Rejected).

Therefore by substituting $\frac{Q_{HeatSupplied}}{Q_{Heat\ Re\ jected}} = \frac{T_{Max}}{T_{Min}}$ into equations (3-7) and (3-8)

$$COP_{heating} = \frac{T_{Max}}{T_{Max} - T_{Min}} \tag{3-9}$$

and similarly

$$\text{EER or } COP_{cooling} = \frac{T_{Min}}{T_{Max} - T_{Min}} \tag{3-10}$$

Using the maximum and minimum temperatures measured from the experimental rigs, assuming the simulated system operates in the ideal Carnot Cycle, the overall Coefficient of Performance for the heating cycle and Energy Efficiency

Ratio for the cooling cycle, were measured. The COP varies depending on the quality of the GHP unit and its operating conditions, in a heating mode COPs are in the range of 3 to 4.5 and in the cooling mode, performance generally is lower with a net EER of 2 to 3.5 (ASHRAE, 1997).

3.5 Greenhouse gas reduction, energy savings and economics benefits

Higher energy prices and environmental concerns regarding detrimental climate change have drawn increased attention to GHP systems. Hanova and Dowlatabadi, (2007), studied the delineate circumstances under which GHPs systems achieve net emission reductions for different electricity generation methods, heat pump efficiencies and heating load. In order to assess the environmental feasibility of GHPs a comparision of the emissions associated with the heat pump operation to conventional heating systems emissions were carried out. The overall potential for green house gases reductions is determined by lifecycle emissions of each energy source and the efficiency of energy conversion used to meet heating or cooling loads (Hanova and Dowlatabadi, 2007). Natural gas produces emissions of 51 kg CO_2e/GJ (US DOE, 1999), while oil is associated with emissions of 51 to 73 kg CO_2e/GJ (US DOE, 1999). The emissions associated with electric heat are dependent on electricity generation sources such as coal-fired power plants, which will yield larger emissions than renewable energy sources. Radiant electric elements achieve efficiencies close to 100%, with natural gas and oil systems achieving efficiencies of 95 % and 85 % respectively (for space and water heating, air conditioning). GHP systems commonly operate at efficiencies ranging from 200 to 500 %, which translates to the Energy Efficiency Ratio (EER) and Coefficient of Performance (COP) of 2 to 5 respectively. Using these efficiencies an environmental performance assessment for an annual heating load of 80 GJ using the mean heating load for a single detached house in Canada was conducted. The outcome of the analysis showed that GHPs relative to natural gas, oil and electric heating, the threshold of CO_2 intensity at which GHPs becomes environmentally feasible varies with the efficiency levels of the conventional systems and GHP systems. Hanova and Dowlatabadi, (2007) found that

GHP is a much more environmentally friendly system reducing the CO_2 emissions by 50 % if utilised as a heating and cooling application. The reduction in primary energy consumption leads to a reduction in greenhouse gases emissions.

Curtis *et al.,* (2005) stated that the reduction of CO_2 emissions has been easier to demonstrate. The coupling of GHPs to the current UK electricity grid can lead to reductions in overall CO_2 emissions of over 50% compared to conventional space heating technologies based on fossil fuels (Curtis *et al.,* 2005). This arises from the current generation mix on the UK grid. As the amount of CO_2 emitted by electricity generation falls, so the reduction in CO_2 emissions through the use of GHPs will increase. With the use of renewably derived electricity, there will be no CO_2 emissions associated with the provision of heating and cooling of a building. They (Curtis *et al.,* 2005) looked at the worldwide savings of tons of oil equivalent (TOE) and CO_2 for the estimated installed capacity of geothermal (ground-source) heat pumps in 2005. The annual geothermal energy used is 28,000 TJ (7,800 GWh) when compared this to the electrical energy generation using fuel oil at 30 % efficiency the savings are 15.4 million barrels of oil or 2.3 million TOE (Curtis *et al.,* 2005). Assuming the savings in the cooling mode are approximately the same number of operating hours per year as the heating requirements, these figures would double (Curtis *et al.,* 2005). GHPs save on energy and costs because the equipment operates more efficiently than conventional systems.

GHP systems offer economical alternatives of recovering heat from different sources for used in various industrial, commercial and residential applications. As the cost of energy continues to rise, it becomes imperative to save energy and improve overall energy efficiency. In this light, GHPs becomes a key component in an energy recovery system with great potential for energy saving. Improving heat pump performance, reliability, and its environmental impact has been an ongoing concern. Recent progress in heat pump systems have centred upon advanced cycle designs for both heat and work-actuated systems, improved cycle components (including choice of working fluid), and exploiting utilisation in a wider range of applications. For the heat pump to be an economical proposition, continuous efforts need to be devoted to improving its performance and reliability while discovering novel applications. Some recent research efforts by Mitsubishi Electric Europe Air Conditioning Systems

Division, Hertfordshire, England, have markedly improved the energy efficiency of heat pumps and Figure 3-6 shows at a higher efficiency less kg CO_2 per useful Kwh of thermal energy occurs and the running costs is reduced from a heating efficiency of 450% (COP of 4.5) to a COP of 350 %. For the same heating load, the GHP outperforms gas boilers, oil boilers and LPG boilers which operate at high efficiencies of 93, 91.2 and 86 % respectively. The costs associated per KWh of heating for GHPs are nearly 50 % less when compared to LPG boilers and oil boilers (Cool planet/Mitsubishi Electric, 2009).

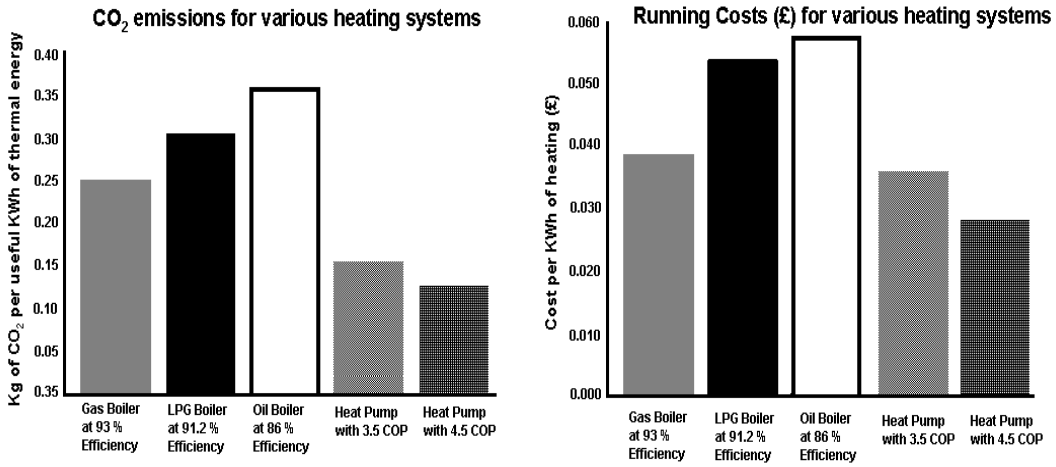

Figure 3-6: Comparison of CO_2 produced and cost per KWh for various heating systems (adapted from Cool planet/Mitsubishi Electric, 2009)

The capital cost for a GHP system consists of the equipment cost for the heat pump unit, the ground coils and the distribution system, the drilling or trenching costs and installation costs. The costs for the ground coil and its installation are specific to a GHP system and typically form 30 to 50 % of the total. The total costs for an installed ground collector ranges between US $45 to $60 per metre in North America and the running costs for electrically driven GHPs are 50 % less than conventional heating and cooling devices (US DOE, 1999). The maintenance costs for GHPs are low and results in a costs savings when compared to alternative systems. For the US and Canada the cost of maintenance for a commercial GHP system is between US $1.08 and $ 2.36/m^2/year when compared to a mean value of

5.38/m^2/year for an average commercial heating and cooling system (US DOE, 1999).

Esen *et al.,* (2006) performed an economic feasibility of GHP and compared it to natural gas, coal, fuel oil, liquid petrol gas, oil and electric resistance in Turkey (Table 3-1).

Table 3-1: Heating value, efficiencies, cost and consumption in Turkey (Esen *et al.,* 2006)

Energy medium	Average heating value	Mean efficiency (%)	Cost of unit of fuels	Consumption of fuel daily for heat load
Natural gas	8,250 kcal/m^3	91	0.154 Euro/m^3	3.18 m^3/day
Coal	6,000 kcal/kg	70	0.146 Euro/kg	4.38 kg/day
Fuel oil	9,700 kcal/kg	81	0.249 Euro/kg	2.71 kg/day
Liquid petrol gas	11,000 kcal/m^3	91	0.592 Euro/m^3	2.39 m^3/day
Oil	10,200 kcal/kg	85	0.618 Euro/kg	2.57 kg/day
Electric resistance	860 kcal/kW h	99	0.074 Euro/kW h	30.6 kW h/day
GHP	860 kcal/kW h	274	0.074 Euro/kW h	30.6 kW h/day

From the analysis, GHP is more cost effective than the heating systems using electric resistance, fuel oil, liquid petrol gas, coal and diesel oil. The comparison involves the efficiency of the device, the type of fuel used and the cost of the fuel. Esen *et al.,* (2006) found that GHP would have a payback period of 8.3 years against the electric resistance, 23.17 years against fuel oil, 12.43 years against liquid petrol gas, 35.68 years against natural gas, 20.75 years against coal and 10.31 years against diesel oil. Comparing the GHP with the conventional heating methods in Turkey, the heat pump is the more economical option (Table 3-1).

Similar studies were performed by Healy and Ugursal, (1997) assessing the economic benefits of ground source heating and cooling applications with conventional systems. The economic assessment evaluated the energy requirements for a house in Nova Scotia, Canada with a heating and cooling load of 22,800 kW h and 2300 kWh respectively. The analysis compared GHPs to electrical resistance heating and air conditioning as well as oil fired furnace and air conditioning systems. The annual heating costs for the GHP were found to be $590 Canadian compared to $1820 for the electric resistance and $1070 for the oil fired furnace. The fuel consumption was 7370 kWh for the GHP in a heating cycle for one year, which was 68% smaller than electric resistance heating and an oil fired furnace. The yearly

cooling costs were $ 55 Canadian for the GHP, $90 for the electric resistance and $90 for the oil fired furnace. The annual fuel consumption for the GHP in the cooling mode was 680 kWh when compared to 1140 kWh and 1141 kWh for the electric resistance and oil fired furnace respectively. The results indicate that GHPs is the least expensive to own and operate for heating and cooling a residential house in Canada for a 15 year period.

Other benefits of GHPs include quiet operations with virtually no noise production and no external fans, good aesthetics, there are no roof penetrations for commercial applications, high reliability when exposed to weather, inaccessible for vandalism, an increase in safety as no combustion or explosive gases are present within a building and produces no pollution.

3.6 Environmental Concerns

3.6.1 Water Quality

Legionnaire's disease is an acute bacterial infection of the lower respiratory tract resulting in bacterial pneumonia (WHO, 2004). The disease is associated to the bacterium *Legionella pneumophila* and is potentially fatal to the respiratory system (WHO, 2004). *Legionella* cannot be contracted by ingesting water (drinking), but can only be contracted through inhalation (breathing in steam) from small water vapours and micro droplets of water. *Legionella* exposure is most likely to occur via inhalation of aerosols, fine sprays, mists and other microscopic droplets of water or soil contaminated with the bacteria and entering into the lungs. *Legionella* are common warm water bacterial microorganism and primarily found in surface waters (lakes, ponds, rivers and streams) and can also be found in groundwater sources. *Legionella* tends to grow in biofilms on the surfaces of lakes, rivers and streams and can easily adapt to conditions within a water distribution system. The growth and amplification of Legionella occurs mainly in stagnant water conditions between a temperature of 20 to 48 ºC and a pH of 5 to 8.5 (WHO, 2004). Sediments scale deposits and biofilms also supports *Legionealla* growth microbiota including algae,

and other bacteria supply essential nutrients for the growth of *Legionella*. Hot water systems (tap faucets, showerheads, and sprayers); cooling towers, evaporative condensers, spas, humidifiers, fountains and hot springs are just a few examples of water systems which can serve as *Legionella* amplifiers (Marre *et al.,* 2002).

However, *Legionella* bacteria cannot survive at temperatures over 60 ºC but is progressively killed at temperatures above 46 ºC and at temperatures around 50 ºC the bacteria will be killed within hours, and at temperatures of around 60 ºC the bacteria is killed within minutes (Marre *et al.,* 2002). Cold stored water should be stored or transported within a GHP below 20 ºC for prevention of *Legionella* survival. A normal control systems and immersion heater will raise the temperature of the hot water to over 60 ºC periodically to pasteurise the stored hot water tank. To conserve on electricity this is timed so that the immersion heater raises the temperature to 60 ºC. The stored or distributed waters can be connected to a thermostatic mixing valve near to the points of outlet to ensure bathroom fittings have a temperature between 37 and 46 ºC respectively. Chlorination, UV irradiation, chemical biocides and ozonation can offer remedial or temporary disinfection by which planktoonic *Legionella* is eradicated from the water source (Marre *et al.,* 2002). A concentration of chlorination between 20 to 50 mg/l would be required to totally flush the system out from *Legionella*, Ultraviolet (UV) radiation with a spectrum range of 250 to 280 nm can disintegrate the nucleic acid structure of the *Legionella* bacteria's DNA and provide point-of-use rapid kill and sterilization (Marre *et al.,* 2002). Ozone dosages of 1 to 2 ppm dissolved in the water system acts as a strong oxidizer and an excellent microbiocide for effective removal of *Legionealla*. Biocides play an important role in microbiological control against *Legionella*, whereby the biodispersants loosen microbial deposits and promote cleanliness. Biodispersants promote biocide penetration of biofilms and removes the biofilms where *Legionella* flourish in its nutrient rich and diverse population of microbiota (Marre *et al.,* 2002).

Other water quality issues include potential leakage of the antifreeze solution, changes of temperature to the subsurface areas and contamination migration and turbidity effects associated with the installations of borings and trenches. The risk of groundwater contamination from a closed-loop GHP is very low. However, with an

antifreeze fluid that is circulated through the pipes, there is a small probability that exists for a leak or rupture to occur which can allow the antifreeze to escape. If the fluid is a polluting substance such as methanol or ethylene glycol there is a risk of soil and groundwater contamination. For this purpose, biodegradable refrigerants such as food grape propylene glycol are used today (Ochsner, 2007). The release of biodegradable antifreeze solutions does not require remediation actions. Additionally, because the cooling processes dominates (excess heat), antifreeze is often not required for GHP operations. With the change of pump motor failure and a leak there is little consequence to the environment as the motors on the heat pumps typically operate on vegetable or mineral oil, and additionally most heat pumps have an automatic shutoff device that activates if the system loses pressure.

Thermal pollution by most closed-loop GHP systems is likely to be negligible as the systems do not affect subsurface temperatures throughout the year and tend not to offset from a heating and cooling cycle. There is no long-term thermal imbalance, which will occur when the heating and cooling cycles are about the same period. Depending on the building type, the regional climate and whether a heating or cooling cycle will dominate, a GHP system will either cool or warm the subsurface until an equilibrium is reached. Consequences of thermal, chemical or biological of this long-term heat losses or heat gains need to be assessed initially before installation. It is recommended that an environmental impact assessment be carried out on larger sites where GHP systems are installed to assess any possible impacts to aquatic life or flora and fauna to the area (Ochsner, 2007).

3.6.2 Geologic Hazards

Sinkholes are the principal geologic hazard associated with the disturbance of the land surface. Trenches in carbonate areas may act as a french drains that change the local subsurface drainage conditions and accelerate the formation of sinkholes (Ochsner, 2007). This could cause subsidence of the area around the ground loop and around the structural foundations of a building. A GHP system that has a large number of poorly sealed borings can possibly alter the flow conditions and cause the collapse of dissolution features that have been slowly developing over time.

Alterations in the surface drainage can accelerate the formation of sinkholes and other collapsible features. Such transformations can damage the integrity of the GHP system. The removal of large quantities of groundwater for an open GHP system can enhance the formation of sinkholes (Ochsner, 2007). However, fewer problems occur if the groundwater is reinjected, the wells must still be properly constructed to avoid down-hole erosion.

Chapter 4 Experimental Design and Methodology

The investigations represented by the outlined objectives in Chapter 1 are the characteristics of urban stormwater reuse and SUDS technologies such as permeable pavements and its integrations with renewable energy tools (GHPs). In order to assess the combined PPS-GHP and standalone PPS, a small-scale laboratory design was setup.

4.1. Geothermal (combined PPS and GHPs) Paving Experiments

4.1.1 Design, construction and composition of experimental rigs

The integration of PPS and GHP included a tanked experimental rig. Due to the complexity of both systems, their design and installation was planned based on previous experiments found in literature as well as new proposed assumptions. These include:

- water quality analysis (physical, chemical and microbiological)
- type of systems (batch flow-tanked);
- integration of energy systems (GHP systems) with existing water saving tools.

The experimental site is located at The University of Edinburgh's Institute for Infrastructure and Environment Public Health Engineering and Ecological Engineering laboratories. In 2006, twelve experimental rigs were constructed with commercially available pervious (permeable) paving systems from Hanson Formpave. Each experimental pavement bin was filled with varying layers of standard pavement aggregates as per British Standards, (BS 882:1992) for construction and design including geotextiles and paving blocks. These twelve rigs were operated under controlled and uncontrolled conditions (internal and external rigs). An energy system was required to simulate the workability of GHPs. The need for an energy input to simulate heating and cooling throughout selected systems; heating and cooling coils were integrated at the base of four experimental bins;

where cooling was applied for a cooling mode (cycle) and heating switched on where specific temperatures were desired depending on the colder or warmer periods throughout the year. There was no direct contact between heat transferring water and water stored within the PPS sub-base during the experiment. Commercial 240-l wheelie-bins were used as the basic construction devices. The dimensions are maximum height-1070 mm; maximum length-730 mm; maximum width- 580 mm and maximum load weight (96 kg) were appropriate for this experiment. The bins mimicked impermeable tanked systems and provided suitable conditions for water collection (Figure 4-1). The indoor PPS was composed of six bins and placed in a temperature-controlled room with a mean ambient temperature of 15^{o}C. The outdoor rig was submerged within the ground and located outside the local laboratory building where atmospheric temperature conditions prevailed.

Commercially available aggregates were used for the construction of the sub-base. Their sizes were determined by the manufacturer of the system (Hanson Formpave, 2009), British Standards (British Standards Institution BS 882:1992) and Highway Agency specifications (Highways Agency, 2005). Typical road and pavement construction materials were used; including crushed gravel and rock with defined edges and sizes between 10 and 63 mm. Typical layer compositions consisted of permeable paving blocks (80 mm), clean 5 mm stone and pea gravel layer (50 mm), geotextile or composite layer (2 mm) a sub-base (crushed rock and gravel) (100mm), and finally the saturated water zone (500 mm) (Hanson Formpave, 2009) as shown in Table 4-1. The recommended standaridized depth of 350 to 400 mm is required for heating and cooling colis within the saturated water zone. However, this was altered for research purposes to integrate GHP (Figure 4-1). Though, sub-base depths depend on the individual application and can therefore vary subject to the environmental conditions and the discretion of the design engineer. For the experimental setup, it was decided to increase the lower sub-base to 500 mm, because GHP coils are required to be fully submerged in water to operate efficiently for optimal heat flux transfer and provide a more stable environment around the coils; increasing thermal conductivity. A system containing space filled with porous media under a constant head of water pressure delivers conditions similar to

submerged systems containing GHP installations (Water Furnace, 2008) while providing desirable conductivity for sufficient heat transfers.

Table 4-1: Pavement rig components and characteristics in experimentation

Depth (mm)	Pavement material	Thickness (mm)	Aggregate diameter (mm)
80	permeable paving block	80	-
> 130	clean stone/pea gravel	50	5
> 132	geotextile	2	-
> 232	Sub-base (Crushed rock and gravel)	100	5 to 20
>735	Lower sub-base and saturated water zone (heating/cooling coils submerged)	500	10 to 63

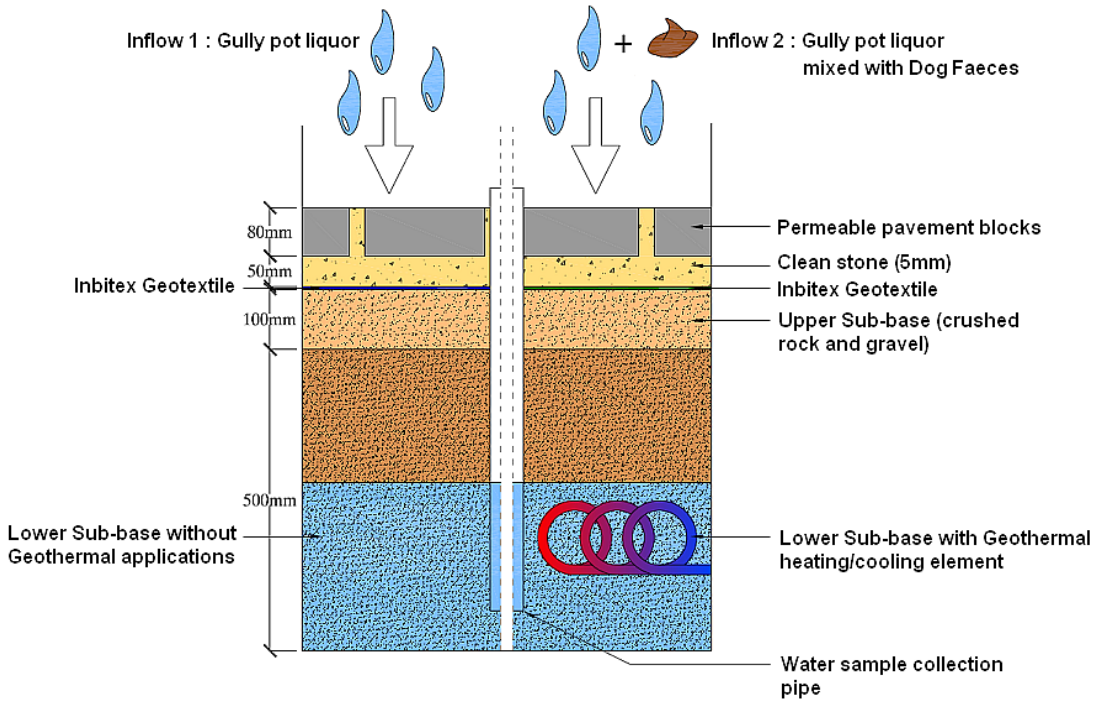

Figure 4-1: **Cross section of experimental permeable pavements and geothermal heat pumps (geothermal paving system) not drawn to scale.**

GHP simulation was achieved by installing reinforced 5-mm polypropylene tubes placed in the lower sub-base. Seven to nine loops were folded within the sub-

base saturated water zone of the pavements structure (total length of 10m). Both ends of each tube were located in a plastic water vessel. One end was connected to the pump and the end used as an orifice for discharges. The starting point of the system began with the pump directing water into the cooler; thereafter circulating through the coils located at the bottom of the bins and returning to the water vessel (Figure 4-2). This process is repeated for the heating cycle during which the water cooler is switched off and the water heater turned on. This arrangement provided closed circulation of water and achieved higher temperatures (between 20°C to 30°C) in a heating cycle and cooler temperatures (<10 °C) in a cooling mode. Aquarium heaters (VISITHERM, Aquarium Systems NEWA, Loughborough, UK) were used to achieve higher temperatures in the heating cycle (water heater) whilst In-line aquarium coolers (Titan 500, Aqua Medic, Bissendorf, Germany) were applied to decrease the temperatures within coils for the cooling mode (water cooler) (Figure 4-2). For both cycles, water circulated through the main water vessel and back to the subbase zone of the pavement structure, depending on the switching pattern. Digital liquid crystal display (LCD) aquarium thermometers (thermal electrodes) with a measurement range of (-50 to 70° C) were placed at the top and bottom of the tanked pavement system to measure geothermal heating and cooling temperatures. As shown in Figure 4-2, temperature measurements were recorded at the water vessel and at the base of pavement rig near the coils submerged under water with the thermal electrodes. Temperature recording times varied throughout the experiment depending on weekly laboratory analyses. The top consisted of permeable pavement blocks subsequently followed by the second layer located in the upper sub-base containing stones of diameters ranging between 5 and 20 mm and placed to a depth of 100 mm. Just above the upper sub-base, an inbitex geotextile membrane was installed (2mm thick). The geotextiles are specifically developed to retain pollutants in surface water run-off to prevent them washing into local watercourses or the underlying soils. The inbitex geotextile layer acts purely as a filter designed to remove sediments from urban runoff. This layer is placed strategically to prevent finer soils penetrating into the unbound layers of the pavement system and prevent siltation, while adding tensile resistance to the structure deterring subgrade deformation.

The Inbitex geotextile made of polyethylene and polypropylene fibres were placed in the top part of the upper-base, as this is the area that promotes microbial degradation of pollutants. Either an Inbitex geotextile on its own or an Inbitex geocomposite (together with an impermeable layer), were used in the experiments manufactured by Terram Geosynthetics, Gwent, UK. The main difference between these two types is the presence of the impermeable layer and the reinforcing grid made of plastic for the geocomposite. Due to the impermeable nature of the geocomposite layer, it was cut into smaller pieces and overlapped with the other layers to allow water percolation through the system avoiding evaporation and clogging. On the top of the geotextile, an additional 5 mm layer of pea-gravel is placed and covered with the permeable paving blocks provided by Hanson Formpave. Clean single-sized 3 mm pea-gravel was used as fill material to seal and fill the gaps between the individual permeable blocks. A water-sampling pipe was installed perpendicular to the layers of the pavement system, dissecting all aggregate layers to the bottom of the bins (Figure 4-1).

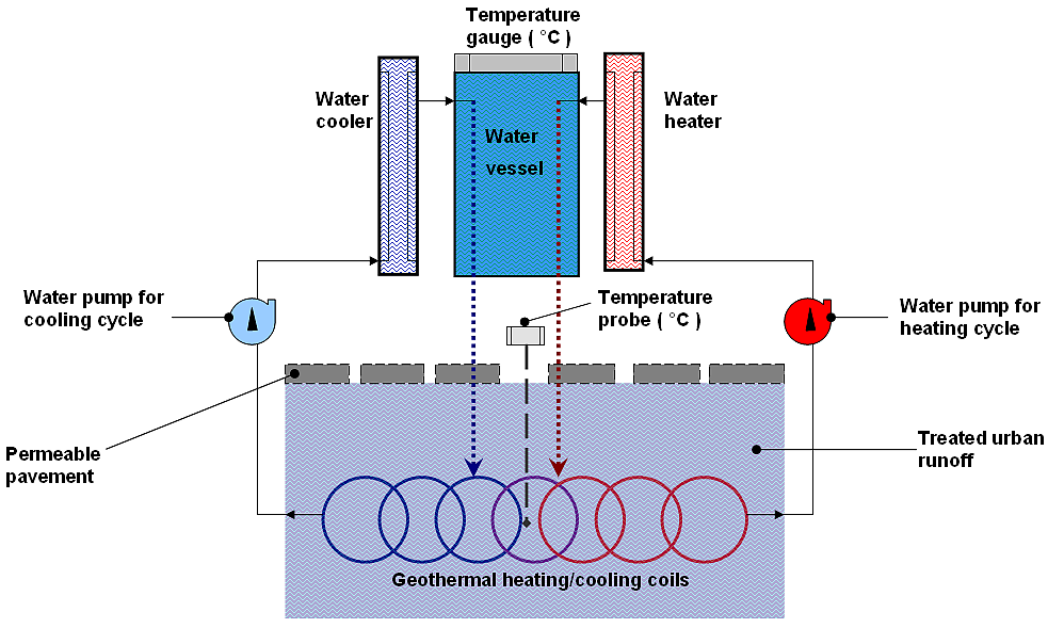

Figure 4-2: Schematic of simulated geothermal heating and cooling system showing the integration of permeable pavements with the water heater, water cooler, and polypropylene tubes placed in the lower sub-base saturated water zone.

4.1.2. Experimental design variations

Three main parameters were varied in the experimental rigs (i) geotextile type (geocomposite or geotextile layer); (ii) pollutant loadings and (iii) the presence of geothermal heating and cooling for both inside and outside systems. The two types of chosen pollutant loadings for highly concentrated urban stormwater included (a) gully pot liquor mixed with de-chlorinated tap water and (b) gully pot liquor mixed with dog faeces (*Canis lupus familiaris*) and de-chlorinated tap water. Four experimental pavement bins were integrated with geothermal heating and cooling applications, whilst two were standalone permeable pavement bins. Three bins were constructed with a geotextile layer and the other 3 hence, consisted of a geocomposite layer directly beneath the bedding layer. Carbon dioxide was monitored for two bins with geothermal heating and cooling coils, with the design variation being the presence of geotextile layer verses geocomposite and the type of concentrated stormwater runoff entering the system.

Table 4-2: Experimental design and variations for indoor and outdoor rigs.

Design feature	**Indoor rig**						**Outdoor rig**					
	1	*2*	*3*	*4*	*5*	*6*	*1*	*2*	*3*	*4*	*5*	*6*
Inbitex geotextile				◘	◘	◘				◘	◘	◘
Inbitex geocomposite	◘	◘	◘				◘	◘	◘			
Geothermal heating/cooling	◘	◘		◘	◘		◘	◘		◘	◘	
Dog faeces	◘			◘			◘			◘		
Gully pot liquor	◘	◘	◘	◘	◘	◘	◘	◘	◘	◘	◘	◘
Water temperatures (°C)	◘	◘	◘	◘	◘	◘	◘	◘	◘	◘	◘	◘
Geothermal temperatures (°C)	◘	◘		◘	◘		◘	◘		◘	◘	
CO_2 sampling (ppm)	◘				◘		◘				◘	

4.1.3 Selected pollutant loadings onto pavements

Public perceptions and acceptance of water reuse projects are recognised as the main ingredients of success for stormwater reuse. The psychological barrier and the risk perception is often related to public health issues arising from using water recycled from permeable pavements; which can all be removed by scientific research and findings to influence and comfort people that the treated recycled water is safe and free from contamination. One of the major concerns for permeable pavements and combined PPS-GHP identified by Hanson Formpave was the health and safety aspects of reusing water in warmer climate countries such as Spain or Australia, where the atmospheric temperature fluctuations may have an influence on the number of pathogenic microorganism. In Australia, for example it is not possible to recycle water which has been in contact with animal excrement. Experimental analysis can provide the relevant assessment for microbial levels and potential health risk to humans (Pond, 2005). The idea of using recycled water from a pavement which encounters animal faeces is not one many people would willingly accept. Therefore combined *Canis lupus familiaris* (dog) faeces and gully pot liquor was chosen to represent the extreme possible worst-case scenario on a permeable pavement surface.

Gully pots are small settling chambers or sumps located along the kerbs of road and paved surfaces to maintain sediments from road runoff before it enters the sewer systems (Bulter and Davies, 2004). Gully pots are normally covered with a protective cast iron grating. It is widely used in urban drainage networks and is the first point, which collects the runoff from roads and pavements where the initial treatment of runoff occurs. The gully pots are connected either to the storm sewer or to the sanitary sewer. Gully pots are one of the most common best management practices (BMPs) in the U.K, with more than 170 million gully pots installed (Memon and Butler, 2002).When stormwater is introduced into the chamber, it fills and the overflow is directed to traditional sewage treatment systems. The received stormwater runoff and pollutants deposited on road surfaces are washed off and drained into gully pots. The combined road surface pollutants and pot liquor results in a considerable degree of turbulent mixing, dilution and washout of dissolved and

sediment-attached pollutants. More dense sediments and attached pollutants settle in the gull pot under the influence of gravity and form a layer of sludge on the invert (Memon and Butler, 2002). This allows the sedimentation of heavier particles as well as an anaerobic process. The specific role and placement of gully pots is designed for the collection and entrapment of organic matter such as vegetation debris and urban runoff pollutants. Asphalt runoff is introduced into the chambers which contains polycyclic aromatic hydrocarbons (PAHs) originating from engine oil spills and metals from corroded car chassis. Ongoing chemical reactions in the gully pot chamber such as changes of forms for heavy metals, chemical oxygen demand (COD) reductions and ammonia nitrogen transformations form the beginning of pollution treatment (Butler and Davies, 2004). The design of gully pots has a direct impact on water quality and flow hydraulics entering into sewers as well as downstream watercourses as the biochemical processes increases the amount of dissolved pollutants in the liquor that is washed out during storm events (Memon and Butler, 2002; Bulter and Davies, 2004).

As a result of the complex nature and high organic pollutant loadings that exists in gully pots it was decided to select gully pot liquor as an excellent pollution source for experimentation. However because of the high density of pollutants and its chemical characteristics of gully pot liquor, a dilution ration with dechlorinated tap water of 1:10 was carried out.

Public perceptions with regards to animal faeces (dogs, cats, horses and birds) being exposed to permeable surfaces was selected as the second pollutant loading problem and incorporated into the experiments. Urine and faeces deposited on pavements from dogs, cats, birds or horses are not commonly assessed within urban drainage system (SUDS) because of its pathogenic nature. Canine faecal contamination contributes to environmental degradation and increases the exposure and health risk to humans (mainly children) to helminth infections. Furthermore, it can cause a series of health problems regarding recycled water from PPS if used for grey water purposes such as watering lawns, washing vehicles or toilet flushing (Scholz and Grabowiecki, 2007). In the U.K. by law, animal owners are responsible for cleaning up after their pets, especially while out walking their dogs; it is their responsibility to collect all faeces and then bury them in the garden or dispose of

them in a sealed bag in the general garbage. Dog faeces wash from pavements and driveways to the stormwater system directly into creeks, lakes and rivers, and pose a health threat. There were over 7.3 million dogs in Britain in 2003, and produced an estimated 1,000 tonnes of dog faeces per day (Environmental Campaigns, 2003). According to research conducted by Alderiso *et al*. (1996), non-human waste represents a significant source of bacterial contamination in urban watersheds. The Genetic studies by Alderiso *et al*. (1996) concluded that 95 % of the faecal coliforms found in urban stormwater were of non-human origin where the most important contributors being domestic cats and dogs. It has been estimated that for watersheds of up to twenty-square miles draining to small coastal bays, two days of droppings from a population of about 100 dogs would contribute enough bacteria and nutrients to temporarily close a bay for swimming and shell fishing and other recreational uses Alderiso *et al*. (1996). Pet waste from dogs can also be a factor in eutrophication of lakes and streams. The release of nutrients from the decay of dogs or cat faeces promotes weed and algae growth, limiting light penetration and the growth of aquatic vegetation. This in turn can reduce oxygen levels in the water, affecting fish and other aquatic organisms. One gram of dog faeces contains 23 million faecal coliforms and over 980 million faecal streptococci bacteria (van der Wel, 1995; Spicer, 2008). Studies by Olivieri *et al.,* (1977) in Baltimore, USA, found that dogs were the single most important source of faecal coliforms and faecal streptococci bacteria in urban stormwater from a highly urbanised area. In a more recent study conducted in Crane Creek, Florida, USA (Tyler, 2007), it was shown that residential lawns, driveways and streets were the main sources of pathogenic bacteria. For a population of 11,084 households in the analysis it was estimated that 40 % has a domestic dog and 40 % of dog owners do not pick up or clean after their pet's excretion. It was calculated that the total pet waste produced was approximately, 800,000 grams per day with 1.76×10^{12} faecal coliforms per day were deposited on the area with a dog producing 190.5 g of excretion per day (Tyler, 2007). Dog faeces are capable of transmitting many diseases, including leptospirosis, brucellosis, toxoplasmosis, tuberculosis and other diseases (Spicer, 2008). However, the greatest risk to public health from dog faeces is toxocariasis. The animal faeces consist of pathogenic organisms such as *Toxocara canis*, a roundworm leading to Toxocariasis

infection which causes blindness (Pond, 2005). It is a zoonotic disease that is spread via unwashed vegetables and dog faeces. Young children in particular are at risk due to their weaker immune systems and because they are more likely to be exposed. A puppy can pass as many as 15,000 eggs of *Toxocara canis* per gram of faeces, and they are a major source of environmental contamination. Additionally, the cost of collection and disposal of dog faeces by local authorities in the U.K amounted to £62,000 per annum between 2002 and 2003 (Environmental Campaigns, 2003). Milkovič *et al.,* (2009) conducted a study on the spatial distribution of canine faeces in Buenos Aires, Argentina suburbs and its implications for public health. The outcome of the research found that there was no spatial connection between the amounts of faecal contamination to grassed or non-grassed areas; low income and middle-income neighbourhoods; number of trees or standing objects. Favourable conditions for parasite eggs from the *Toxocara canis* bacteria causing the helminth infections were found on porous areas rather than impermeable surfaces, and faeces found on pavements represented an increased health risk to children.

A survey conducted by the Urban Water Research Group, The University of Edinburgh in the streets of Glasgow and Edinburgh area in 2006 found that the deposition rate of dog faeces were 3.51 g/m^2 and 3.32 g/m^2 for Glasgow and Edinburgh respectively. Water sampling was conducted weekly and the amount of added dog faeces on the two selected pavement systems ranged from 3.2 to 3.5g per bin per sampling event. The pollutant loading sequence is extremely high as it is highly improbable that dog faeces are deposited weekly on the same pavement surface. The sample number accounted for dog faeces loading was 113, which equates to 362 to 396 g for the indoor and outdoor rig. In the research, both indoor and outdoor rigs were operational for 26 months from March 2008.

The concentrated stormwater mixture was prepared by taking 0.5 litres of gully pot liquor from various gullies at the King's Building campus and mixed with dechlorinated tap water in a 1:10 ratio. Fresh dog faeces (approximately 6 grams) were collected from the Meadows Park and pavements in Edinburgh weekly. Approximately 3.2 to 3.5 g of dog faeces samples were weighed on a balance and mixed into a water-liquor mixture until all solids were dissolved. The same procedure was done for the gully-pot liquor and dechlorinated tap water without the

addition of dog faeces. The mixture was uniformly distributed over the pavement surfaces. Water residence times in the bins were estimated between 4 to 5 days. Before new spiking of the concentrated urban stormwater onto the pavements, effluent samples were collected weekly to prevent the oversaturation and mixture with the new pollutant dosing loads.

4.1.4. Geothermal heating/cooling operational conditions

The heating and cooling periods for the experimental rigs were controlled by timers, which switched on the heater or coolant to heat up or cool down the geothermal coils submerged beneath the pavement structure. The water pumps ran continuously, the coolers minimum temperature was set at 4°C and thermostats prevented overheating by switching the heaters off when a temperature of 35 °C is achieved. Two main switching patterns existed to mimic the heating and cooling applications of a supermarket in Scotland. Commercial buildings such as supermarkets prefer to have devices off as long as possible to conserve on energy. The type of running pattern was chosen for the experiment, as it is the most likely application for the combined PPS-GHP design. The on or off switching modules can be programmed up to six times daily and followed the annual heating and cooling periods of a supermarket in Edinburgh. The heating and cooling cycles were set as follows:

- Heating for a 6 month period (colder months in Scotland) October to March. The heating mode was switched on between the hours of 04:00 to 08:00, 09:00 to 11:00, 12:00 to 15:00, 16:00 to 18:00 and 19:00 to 23:00.
- Cooling for a 6 month period (warmer months in Scotland) April to September. The cooling mode was switched on between 11:00 to 12:00, 13:00 to 14:00, 15:00 to 18:00 and 19:00 to 20:00.

The geothermal heating and cooling cycles were selected based on the account for equipment safety such as overheating and economical constraints such as electricity costs escalate if the switching frequency is high.

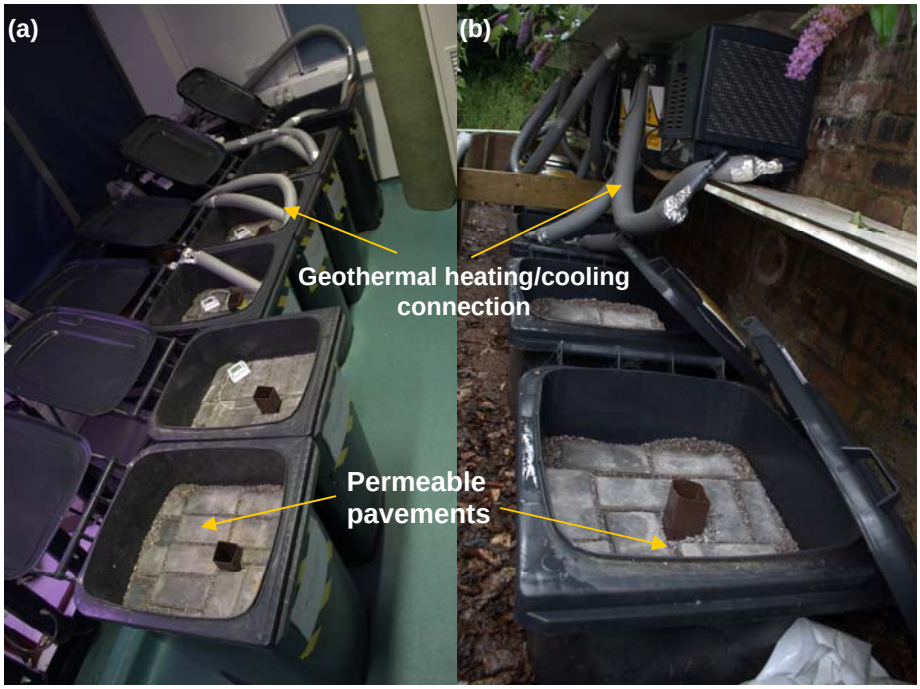

Figure 4-3: (a) Indoor and (b) Outdoor experimental bins for PPS and combined PPS-GHP

The indoor experimental rig was placed inside the ecological engineering laboratory at a fixed temperature of 15 °C and fixed humidity. The outdoor rig located outside the laboratories at the King's Buildings campus, The University of Edinburgh were subjected to external temperatures and humidity conditions. The bins were covered on the top surface and partially opened to avoid rainfall entering the outdoor rigs. The bins located outside were insulated with soil up to the pavement block levels to simulate natural soil conditions as shown in Figure 4-3.

4.2 Water Quality Parameters

The ecological integrity of water is made up of three components: physical, chemical, and biological (Chin, 2006).Water quality is assessed based on the present and future most beneficial uses of the water body and a set of water quality criteria that corresponds to the intended use of the water body (Chin, 2006). Some measures used to assess the suitability of water for various uses were analysed. The

interrelationships between the physical, chemical and biological measures are complex and alterations in the physiochemical conditions of water generally results in changes in the biological state (Chin, 2006). The quality of water is a function of either or both natural influences and human activities. The availability of stormwater and its physical, chemical and biological composition affects the ability of aquatic environments to sustain health ecosystems as water quality is eroded, organisms suffer and ecosystems can be lost. The quality of water from urban drainage systems such as permeable pavements is essential for regular, periodic monitoring in order to maintain healthy usable water for recycling and grey water purposes. Typically, water quality is determined by comparing the physical, chemical and microbiological characteristics of a water sample with water quality guidelines or standards. Water quality guidelines and standards such as the World Health Organisation (WHO), European Union Water Framework Directive or the United States Environmental Protection Agency (US EPA) are designed to enable the provision of clean and safe water protecting human health. These are usually based on scientifically assessed acceptable levels of toxicity both to humans and to aquatic organisms.

Water sampling was conducted weekly from the effluents of each pavement bin. All water quality sample analysis followed the American Health Public Association standard methods for the examination of water and wastewater (Clesceri *et al.,* 1998). The analysis took place in the ecological and public health laboratories at the Institute for Infrastructure and Environment under the supervision of Professor Miklas Scholz (Laboratory Director). The analysis of nutrients (ammonia-nitrogen, ortho-phosphate-phosphorous and nitrate-nitrogen) was conducted in the Crew Laboratory, School of Geosciences, The University of Edinburgh.

Experimental data were collected by monitoring the influent and effluent concentrations for both pavement systems for a 25 month period (10 March 2008 to 25 April 2010). The data was stored in a data base together with several input variables including: Inflow and outflow water temperature (°C), geothermal heating-cooling temperatures (°C), pH, electroconductivity (µS/cm), ammonia-nitrogen (NH_4-N) (mg/l), nitrate-nitrogen (NO_3-N) (mg/l), ortho-phosphate-phosphorous (PO_4-P), turbidity (NTU), suspended solids (mg/l), total dissolved solids (mg/l), total heterotrophic bacteria (CFU/100ml), *Escherichia coli* (CFU/100ml), *Enterococci sp.*

(CFU/100ml), total coliforms (CFU/100ml), *Salmonella sp*. (CFU/100ml), *Shigella sp*. (CFU/100ml), *Legionella sp*. (CFU/100ml), biochemical oxygen demand (BOD), (mg/l), chemical oxygen demand, (COD), (mg/l), dissolved oxygen (DO) (mg/l), redox potential (mV) and carbon dioxide (CO_2) (ppm).

4.2.1 Physiochemical Parameters

4.2.1.1 Temperature

Temperature can exert great control over aquatic communities. If the overall water body temperature of a system is altered, an aquatic community shift can be expected (Chin, 2006). In water above 30 °C, a suppression of all benthic organisms can be expected. In addition, different plankton groups will flourish under different temperatures. Metabolic rate and the reproductive activities of aquatic life are controlled by water temperature. Metabolic activity increases with a rise in temperature, thus increasing the demand for oxygen. However, an increase in water temperature also causes a decrease in oxygen levels, limiting the amount of oxygen available to these aquatic organisms. With a limited amount of oxygen available, aquatic life such as fishes in this system will become environmentally stressed. A rise in temperature can also provide conditions for the growth of disease-causing organisms. Temperature affects the rate of chemical reactions and the speed at which algae and aquatic plants photosynthesize; the metabolic rate of other organisms as well, as how pollutants, parasites and other pathogens interact with aquatic residents (Chin, 2006).

4.2.2.2 pH

In water, small number of water molecules (H_2O) dissociate and form hydrogen (H^+) and hydroxyl (OH^-) ions. If the relative proportion of the (H^+) ions is greater than the (OH^-) ions, the water is defined as acidic. However, if the (OH^-) ions dominate the water is defined being alkaline. The relative proportion of hydrogen

and hydroxyl ions is measured on a negative logarithmic.The pH scale ranges from 1 (very acidic) to 14 (very alkaline) with 7 being neutral and the standard pH of clean potable water (Carr and Neary, 2008). pH is one of the most common water quality tests performed. pH indicates the water sample's acidity or alkalinity, but is actually a measurement of the potential activity of the (H^+) or (OH^-) ions in the sample. The pH of an aquatic ecosystem is important because it is closely linked to biological productivity. pH values between 6.5 and 8.5 indicate good water quality. However, since some water courses are naturally acidic or basic, pH may not necessarily indicate pollution. The pH of natural water bodies affects biological and chemical reactions, controls the solubility of metal ions and affects aquatic life. Most natural waters have a pH near neutral with 95 % of all natural waters having a pH between 6 and 9 (Carr and Neary, 2008). A shift of pH in either direction from neutral may indicate the presence of a pollutant in the stream.

4.2.2.3 Biochemical Oxygen Demand (BOD)

One of the most commonly measured constituents of wastewater is the biochemical oxygen demand, or BOD (Metcalf and Eddy, 2007). Urban runoff is composed of a variety of inorganic and organic substances including faecal matter as well as detergents, soaps, fats, greases and food particles (ASCE and WEF,1998). Bacterial degradation results in the oxidation of organic molecules to stable inorganic compounds. The measure of the amount of oxygen used by aerobic bacteria during decomposition is called biochemical oxygen demand (BOD). BOD measures the amount of biochemically oxidisable organic matter present in water. Waste discharges that contain significant amounts of biodegradable organic matter have high BOD levels and consume significant amounts of oxygen. Biodegradable organic wastes are commonly associated with oxygen consumption in surface waters including human and animal excrements, food wastes and organic residuals from industrial operations. The BOD measures the mass of oxygen consumed per unit volume of water and is usually expressed in mg/l. BOD is the most commonly used parameter for determining the oxygen demand on the receiving water of a municipal or industrial discharge. BOD can also be used to evaluate the efficiency of treatment

processes, and is an indirect measure of biodegradable organic compounds in water. Elevated levels of BOD lower the concentration of dissolved oxygen in a water body and there is a potential for profound effects on the water body itself, detrimental to the resident aquatic life. BOD concentrations of < 5 mg/l can be considered to be moderately clean according to the US EPA, (2004 a) and concentrations of > 90 mg/l is very polluted with organic waste. Urban runoff high in BOD can deplete oxygen in receiving waters, causing deaths to aquatic life and variations in ecosystems (Scholz, 2006 b). The BOD_5, is measured by the quantity of oxygen consumed by microorganisms during a five-day period, and is the most common measure of the amount of biodegradable organic material in, or strength of the urban runoff wastewater (Metcalf and Eddy, 2007).

4.2.2.4 Chemical Oxygen Demand (COD)

The chemical oxygen demand (COD) is the amount of oxygen consumed when the substance in water is oxidized by a strong chemical oxidant. COD is a vital test for assessing the quality of effluents and wastewater prior to discharge. The COD test predicts the oxygen requirement of the effluent and is used for monitoring and control of discharges, and for assessing treatment plant performance. COD is based on the fact that nearly all organic compounds can be fully oxidized to carbon dioxide with a strong oxidizing agent under acidic conditions. It measures the amount of oxygen required to oxidize both biologically oxidisable and biologically non-oxidisable materials. The impact of effluents on receiving water courses can be predicted by the oxygen demand and because the removal of oxygen from the natural water reduces its ability to sustain aquatic life. The COD test is therefore performed as routine in laboratories of water utilities and industrial companies (Chin, 2006). COD measures the strength of a waste stream and gives an idea of the oxygen demands a particular industrial waste stream will have on the treatment plant US EPA, (2002; 2004 a). It is widely used to characterize the organic strength of water and pollution of natural waters. Domestic wastewater typically has a BOD_5/COD ratio of 0.4 to 0.5 (Metcalf and Eddy, 2007). Comparison of BOD and COD results can aid in identifying the occurrence of toxic conditions in a waste stream or indicate

the presence of biologically resistant or refractory waste. COD is an indicator of organics in the water, usually used in conjunction with BOD.

4.2.2.5 Suspended Solids

Suspended solids (SS) are an extremely important cause of water quality deterioration leading to aesthetic issues, higher costs of water treatment, a decline in the fisheries resource, and serious ecological degradation of aquatic environments (Bilotta and Brazier, 2008). The amount of suspended solids in water is an important measure of water quality. High levels of suspended solids are associated with soil erosion and wastewater effluent. Changes in soil erosion can be caused by changing rainfall, agricultural practice or increased construction activity. SS from combined sewer overflows (CSOs) and stormwater discharges represent a crucial parameter for evaluating wet-weather pollution in urban areas. An increase in concentrations of SS in water during rain events can have ecotoxic effects on aquatic organisms. Furthermore, major potentially harmful substances such as heavy metals, PAHs and organic matter are adsorbed onto SS and later settle on sediment. Water quality criteria for SS consequently enable the risk of wet-weather pollution to be assessed, to avoid detrimental effects on aquatic organisms. This parameter is a significant measurement as it depicts the effective and compliance of control measures. Large volumes of suspended sediment reduce light penetration, thereby suppressing photosynthetic activity of phytoplankton, algae, and macrophytes (Chin, 2006). This leads to fewer photosynthetic organisms available to serve as food sources for many aquatic organisms. As a result, overall aquatic life form populations may decline, resulting in decreased fish populations.

4.2.2.6 Turbidity

Turbidity monitoring is normally supplemented with direct, measurements of suspended solids. This allows the turbidity record to be checked and calibrated against SS, effectively building a rating-relationship between SS and turbidity, which would in turn provide a clearer picture of the exact magnitude of the SS problem

(Bilotta and Brazier, 2008). Turbidity refers to the clarity of water and is a result of organic and inorganic constituents in water (Carr and Neary, 2008). Organic particulates can harbour microorganism thereby increasing the possibility for waterborne diseases. Insoluble particulate impede the passage of light through water by scattering and absorbing rays. The interference of light passage gives a measurement of turbidity in water. The greater amount of sediments in water, the murkier it appears and the higher the measured turbidity. Water clarity is a major determinant of the condition and productivity of an aquatic system, and of the tractability of water for human consumption, recreation and manufacturing (source). Increased turbidity can change an ecosystem significantly. Sediment particles control the transport, reactivity and biological impacts of substances in the marine environment, and are a crucial link in interactions between the seabed, water column and the food chain. The most obvious effect of increased turbidity is a reduction in light available for photosynthesis which is similar to that of suspended solids.

High turbidities can transport contaminants and indicates the presence of particulate nutrients, heavy metals and potential toxicants (Bartram and Helmer, 1996). These conditions promote the growth of pathogens and waterborne diseases. Turbidity may be due to organic and/or inorganic constituents with organic particulates harbouring microorganisms. Thus, turbid conditions may increase the possibility for waterborne disease. Nonetheless, inorganic constituents have no notable health effects. The series of turbidity-induced changes that can occur in a water body may change the composition of an aquatic community. High concentrations of turbidity occur as a result of large volumes of suspended sediment and light penetration is reduced, thereby suppressing photosynthetic activity of phytoplankton, algae, and macrophytes. If turbidity is largely due to algae, light will not penetrate very far into the water, and primary production will be limited to the uppermost layers of water (U.S.EPA, 1993).

4.2.2.7 Dissolved Oxygen

Oxygen gets into water by diffusion from the surrounding air, by aeration (rapid movement), and as a waste product of photosynthesis. Dissolved oxygen (DO) is the

amount of molecular oxygen dissolved in water and is one of the most important parameters affecting the health of aquatic ecosystems, odours, fish mortality and aesthetic qualities of surface water (Bartram and Helmer, 1996). Discharges of oxidisable organic substances into water bodies' results in the consumption of oxygen and the depression of dissolved oxygen levels. Oxygen is required for metabolism of aerobic organisms and it influences inorganic chemical reactions. If DO levels fall too low, the effects on fish can range from a reduction in reproductive capacity to suffocation and death. Oxygen depletion in water courses create conditions in which iron and manganese can be solubilized and odour and taste problems may increase because of the release of anoxic and anaerobic degradation products such as hydrogen sulfide. DO is often used as an indicator of water quality such that high concentrations usually indicate good water quality and a low DO (< 2 mg/l) indicates poor water quality and thus would be difficult in sustaining many sensitive aquatic life (Bartram and Helmer, 1996). Pollutants such as sewage, agricultural or urban runoff result in the build up of organic matter and the consumption of dissolved oxygen by microbial decomposers as they break down the organic matter.

4.2.2.8 Redox potential

Redox potential sometimes referred to as oxidation-reduction potential is an electrical measurement that shows the tendency of a water or soil solution to transfer electrons to or from a reference electrode. In aqueous solutions, the redox potential is measures the tendency of the solution to either gain or lose electrons when it is subject to change by introduction of a new species. A solution with a higher (more positive) redox potential will have a tendency to gain electrons from the new water sample (to be reduced by oxidizing the new species) and a solution with a lower (more negative) reduction potential will have a tendency to lose electrons to the new species (i.e. to be oxidized by reducing the new species) (Carr and Neary, 2008). The transfer of electrons, between chemical compositions determines the redox potential of an aqueous solution. The redox potential represents an intensity factor and does not characterise the capacity of the system for oxidation or reduction. From this

measurement, estimatations of whether soil or water samples are aerobic, anaerobic, and the presence of chemical compounds such as iron oxides or nitrates have been chemically reduced or are present in their oxidized forms. The redox potential range in natural waters is limited in the negative range by reduction of H_2O to H_2 (gaseous state) and in the positive range by the oxidation of H_2O to O_2. At a pH of 7 to 8, the potential range averages from about -400 mV to +800 mV (Carr and Neary 2008).

4.2.2.9 Conductivity

Electroconductivity or conductivity is widely used to indicate the total ionized constituents of water. It is the ability of water to conduct electricity and is directly related to the sum of the cations (or anions), as determined chemically and is closely correlated, in general, with the total salt concentration (Carr and Neary, 2008). The unit of electroconductivity is microsiemen per centimetre (dS/cm) and is sometimes measured in terms of conductivity per unit length, and metres typically using microsiemens/cm (μS/cm). The conductivity of water is a more-or-less linear function of the concentration of dissolved ions. Conductivity indicates the presence of ions within the water from saline water or leaching. It can also indicate industrial discharges. Saline intrusions or landfill leaching into groundwater courses indicates a higher conductivity. Conductivity itself is not a human or aquatic health concern, but because it is easily measured, it serves as an indicator of other water quality problems. If the conductivity of a stream suddenly increases, it indicates that there is a source of dissolved ions in the vicinity. Therefore, conductivity measurements can be used as a rapid method to locate potential water quality problems.

4.2.2.10 Total Dissolved Solids

The total dissolved solids (TDS) in water consist of inorganic salts and dissolved materials. In natural waters, salts are chemical compounds comprised of anions such as carbonates, chlorides, sulphates, and nitrates and cations such as potassium (K), magnesium (Mg), calcium (Ca), and sodium (Na) (Carr and Neary, 2008). More harmful elements of TDS are pesticides arising from surface stormwater runoff.

Primary sources of TDS in receiving waters are redisential (urban) and agricultural runoff, leaching of soil contamination, and point source water pollution discharges from water, wastewater or industrial treatment plants, the chemicals used in the water/wastewater treatment processes, and the nature of the piping or construction materials for plumbing used to convey the water.

4.2.2.11 Nutrients – Nitrates (NO_3-N), Ammonia (NH_4-N) and Phosphates (PO_4-P)

Nutrients are elements essential for life. The major nutrients required for metabolisms and growth of organisms include carbon, hydrogen, oxygen, nitrogen, phosphorous, potassium, sulphur, magnesium and calcium. In aquatic systems nitrogen and phosphours are the two most essential nutrients that most commonly limit maximum biomass of algae and aquatic plants, which occurs when concentrations in the surrounding environment are below requirements for optimal growth of algae, plants and bacteria (US EPA, 1993; Metcalf and Eddy. 2007).

Through agricultural practices, urbanisation, industrialisation, and other alterations, humans have increased the nutrients load into biochemical cycles, especially nitrogen, ammonia and phosphorus (Peavy *et al*., 1985; US EPA, 1993; Metcalf and Eddy, 2007). Runoff can contain high concentrations of these nutrients and are regarded as a primary concern to water quality (Gromaire-Mertz *et al.,* 1999; Scholz, 2006 a). Nutrients are associated with agricultural and urban runoff, atmospheric deposition, leachate from landfills and septic systems, in addition to erosion. Both nitrogen and phosphorus are widely used as fertilizers are are mostly responsible for over enrichment of nutrients in surface waters (Rubin, 2001). Nitrogenous compounds in agricultural runoff are an important factor in causing eutrophication of recipient water bodies with an over-enrichment of the receiving waters, stimulating algal growth, causing unpleasant odours and detract from the aesthetic value of the water resource (Peavy *et al*., 1985; Metcalf and Eddy, 2007). Excessive plant growth associated with overenrichment of nutrients causes oxygen depletion, which results in increased stresses on aquatic organisms such as fishes.

Nitrogen is a nutrient that stimulates the growth of algae, and the oxidation of nitrogen species can consume significant amounts of oxygen. There are several forms of nitrogen that exists in water bodies including inorganic and organic forms and the concentration of each form is primarily mediated by biological activity. Nitrogen-fixation performed by cyanobacteria (blue-green algae) and certain bacteria converts dissolved molecular N_2 to ammonium (NH_4^+) (Peavy *et al*., 1985). Decomposers break down organic nitrogen to release ammonia (ammonification or deamination process). Aerobic bacteria (*nitrosomas* and *nitrobacter* bacteria) convert NH_4 to nitrate (NO_3^-) and nitrite (NO_2^-) through nitrification and anaerobic and facultative bacteria converts nitrate (NO_3^-) and nitrite (NO_2) to N_2 gas through denitrification (Figure4-4). Nitrate-nitrogen commonly originates in stromwater runoff from agricultural areas with heavy fertilizer usage, whereas inorganic nitrogen is commonly found in munipal wastewaters (Chin, 2006). Primary producers assimilate inorganic nitrogen N as NH_4^+ and NO_3^-, and organic N is returned to the inorganic nutrient pool through bacterial decomposition and excretion of NH_4^+ and amino acids by living organisms. Nitrates tend to travel very easily in surface water and groundwater and commonly originate from the nitrification of stormwater and wastewater discharges. Nitrogen deposits from stormwater or wastewater applications largely occurs as ammonium (NH_4^+), which can be adsorbed by negatively charges soil particles as it percolates through the ground or travels through surface water courses. Ammonia is the nitrogenous waste product for many organisms, and even more is released by bacteria breaking down dead decaying plants and animals or other nitrogenous animal wastes such as urea.

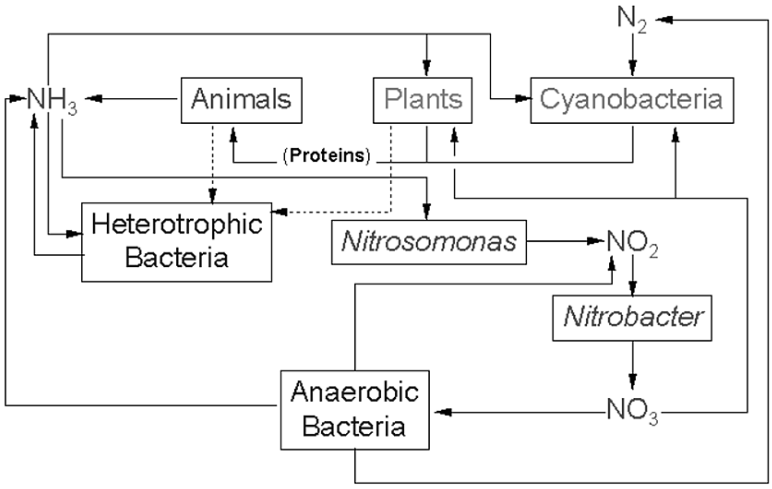

Figure 4-4: Schematic diagram of the Nitrogen Cycle in water. (adapted from Kiely, 1997 and Chin, 2006)

Phosphorous is present in natural waters primarily as phosphates which can be separated into inorganic and organic phosphates. The principal forms are organically bound phosphorus, polyphosphates, and orthophosphates (Peavy *et al*., 1985). Organically bound phosphorus originates from body and food waste and, upon biological decomposition of these solids, is converted to orthophosphates. Phosphates enters aquatic environments from the natural weathering of minerals in drainage basins, from biological decomposition, urban runoff from human activities such as polyphosphates are used in synthetic detergents, and used to contribute most inputs from dishwasher detergents that enter into the runoff (Scholz and Grabowiecki, 2009). Polyphosphates can be hydrolyzed to orthophosphates, thus the principal form of phosphorus in urban runoff can be assumed to be orthophosphates, although the other forms may exist. Oraganic phosphorus is typically available to plants as organophosphate (PO_4^{-3}). This compound is a common weathering product of igneous rock (Kiely, 1997). Other sources of organic phosphate are decaying animal bodies, animal wastes and bones of vertebrates and the accumulated excrement and remains of birds. Phosphorous is often the limiting factor for plant growth in aquatic systems. In many aquatic habitats, excessive phosphates lead to eutrophication. Heavy algal growth (blooms) are caused because the algae use the phosphates as soon as it becomes available (Kiely, 1997). This can cause problems whereby the algae as a result of the increase in respiration uses up all oxygen (O_2) in

the water. Human activities accelerates the process of eutrophication whereby phosphorous from agricultural runoff (phosphate fertilizers, animal wastes), human sewage, detergents enters a water system. Remedies to eutrophication by human activities include soil erosion control (much phosphorus is carried into aquatic systems bound to soil particles), careful and controlled applications of fertilizers and effective tertiary sewage treatment (removal of phosphorus and other nutrients). In many cases, nutrients from urban runoff originate from chemical fertilizers (containing ammonia and sometimes phosphates) and thus are in a dissolved form which algae in the receiving waters can readily utilise (Kiely, 1997).

4.2.3 Physiochemical water quality determinations

4.2.3.1Temperature, pH, total dissolved solids (TDS) and conductivity

A Hanna HI-991300 combined meter was used to measure pH, total dissolved solids, water sample temperatures and conductivity. During measurements of these variables, an electrode was gently stirred in the water sample until the meter reading on the digital display remained constant. The probe was washed with deionised water before and after each water sample analysis. The Hanna HI-991300 meter was calibrated weekly according to the manufactures' specifications using calibrating buffers. For pH, calibration the buffers ranged from a pH of 7 and 10, the electrodes were soaked in the buffer solution for 20 minutes until the accurate pH recorded. The fluctuations of temperatures changes with pH, and temperature compensation was done automatically on the electrode. The usage of buffer calibration solution eliminated errors in recording these variables.

4.2.3.2 Dissolved oxygen (DO) and redox potential determinations

Dissolved oxygen content was measured with a WTW Oxi 315i meter. Redox potential (ORP) recordings were carried out with a Hanna HI 98201 meter. The

water parameter instruments were calibrated on a weekly baisis using solutions supplied by the manufacturers (OxiCal air calibration vessel for DO and Hanna REDOX solution for platinum and gold ORP electrodes).

4.2.3.3 Suspended solids and Turbidity determinations

Suspended solids were determined using the total filterable residue, dried at 105° C (Clesceri *et al.,* 1998). The methodology involves filtration of approximately 100 water sample on a glass fibre filter. After filtration, the residue is transferred to a weighted dish and left for approximately 1 hour in an incubator at 105° C. After drying, the filter is cooled in a fume cupboard and weighed. The research samples (blank) were left in the incubator for a 24-hour period. The difference in weight of the clean filter and dried filter with residue being the mass of sediment in the water sample recorded as total suspended solids. A HACH 2100 N turbidity meter was used to measure turbidity (NTU). The turbidity meter has a resolution of 0.001 NTU and ranges from 0 to 4,000 NTU. Hach's patented StablCal Stabilized Formazin was used as the calibration solution and delivers precisely the concentration required. Calibration of the turbidity meter was carried out weekly to ensure accuracy in turbidity recordings.

4.2.3.4 Biochemical oxygen demand (BOD) determinations

The biochemical oxygen demand (BOD_5) (Nitification inhibitor N-Allylthiourera) was determined using the OxiTOP IS 12-6 system supplied by WTW, (Wissenschaftlich-Technische-Werkstatten GmbG, Wielheim, Germany). The system uses a piezo-resistive measure of pressure differences, from a respirometric method based on carbon dioxide produced within the bottle. A nutrient inhibitor was added to suppress the oxidation of ammonia to nitrates/nitrites. The pressure changes when sodium hydroxide transforms into sodium carbonate. Carbon Dioxide is then removed by sodium hydroxide tablets. The pressure changes were recorded by an electronic data logger and measured over a five-day period at a constant temperature of 20 °C. The amount of water samples used was approximately 0.5 litres for the

influent and effluents respectively. After 30 minutes of aeration with air pumps, a nutrient inhibitor was added to the samples, and bottles were incubated at a constant temperature of 20°C for five days. This method provided a simple operation, improved controllability and non-toxicity, with a measuring ranges of up to 4000 mg/l BOD. As the measured pressure is automatically converted, the values can be directly read as mg/l BOD.

4.2.3.5 Chemical oxygen demand (COD) determinations

COD was determined using the Palintest Tubetests System. Palintest Tubetests are integrated with the Palintest heater and photometer system to provide a complete COD measurement. COD analysis was performed using two Palintest Tubestes with product codes: PL450 and PL452 with the corresponding ranges of 150 mg/l and 400mg/l respectively. In the Palintest COD methodology, water samples are oxidized by digesting in a sealed reaction tube with sulphuric acid and potassium dichromate in the presence of a silver sulphate catalyst. This reaction occurs in the Palintest pre-prepared tubetests that consists of all the above necessary reagents. The amount of dichromate reduced is proportional to the COD. The absorbance of the COD samples is read with the Palintest 7000 Interface Photometer model. COD values were recorded as this model is a direct reading user-friendly photometer, pre-programmed for Palintest water analysis. The Palintest 7000 Interface Photometer brings a new dimension to COD water quality measurement as it replaces the traditional method whereby values were calculated using a calibration curve.

4.2.3.6 Nutrient determinations (PO_4, NH_4, NO_3)

Ortho-phosphate-phosphorous (PO_4), ammonia-nitrogen (NH_4) and nitrate-nitrogen (NO_3) were analysed in the School of Geosciences laboratories, The University of Edinburgh. Nutrients were analysed with traditional chemical methods (Clesceri *et al.,* 1998). Nitrate was reduced to nitrite by hydrazine in alkaline solution and determined at 550nm by a colorimetric method using a Bran Luebbe (Norderstedt, Germany) AA3 flow injection analyser (Bran and Luebbe, 1999), Bran

Luebbe AA3 Atoanalyser Methods : G-109-93 and 94, Bran and Luebbe, Norderstedt.

Ammonia coloured blue compounds were measured at 660 nm wavelength using the Bran Luebbe autoanalyser, model AA3. For the quantification of ammonia, the following reagents were used: ammonium molybdate, ammonia fluoride, antimony potassium tartrate, ascorbic acid, salicylate, hydrochloric acid, potassium dihyrdogen phosphate, dichloroisocynauric acid, calcium chloride, sodium chloride dehydrates, sodium dodecyl sulfate, sodium hydrogen carbonate, sulfuric acid and nitroprusside (catalyst).

Ortho-phosphate-phosphorus was measured with the ammonium molybdate method (Clesceri *et al.,* 1998). Ammonia molybdate, ascorbic acid and sulfuric acid were used. Ammonium molybdate and 0.5mol bicarbonate of soda were also used in the analyses performed by automated colorimetry with an AA3 colorimeter for all water samples at 660nm wavelength. Ortho-phosphate-phosphorus reacts with molybdate and ascorbic acid to form a blue compound. Antimony potassium tartrates are used as a catalyst.

4.3 Pathogenic Bacterial Microorganims

Sources of bacteria in urban runoff include sanitary sewer overflows, pets, and populations of urban wildlife such as birds. Bacteria are responsible for waterborne diseases such as cholera and typhoid. Pathogenic bacteria of particular concern to humans are *Salmonella*, *Shigella*, *Escherichia coli*, faecal streptococci (*Enterococci*) and *Legionella*.

4.3.1 Total Heterotrophic Bacteria

Heterotrophic microorganisms ingest biomass to obtain their energy and nutrition. In direct contrast, autotrophs are capable of assimilating diffuse, inorganic energy and materials, and using these to synthesize biochemicals (Sigee, 2005). All heterotrophs have an absolute dependence on the biological products of autotrophs

for their sustenance and depend on this as a source of nourishment. The presence of heterotrophic bacteria is not restricted to water. Total heterotrophic organisms can be found virtually everywhere in the environment, in air, foods consumed and in water courses (Sigee, 2005). Heterotrophic bacteria present in water sources can be either Gram-positive or Gram-negative (Sigee, 2005). Some are strictly aerobic, but many are facultative anaerobes (they can survive in both the presence and absence of oxygen). Many species of heterotrophic bacteria tolerate a wide range of environmental conditions: temperature, pH, salinity, etc. Most bacteria are heterotrophs, which includes all human pathogens and most of the bacteria associated with drinking water systems. However the total heterotrophic bacteria represents harmless heterotrophic organisms that does not reproduce in water systems and harmful pathogenic waterborne bacteria species hazardous to human health (Sigee, 2005). It was measured to indicate the harmless flora and predominant pathogens present entering and leaving the pavement systems.

4.3.2 Coliform bacteria and Escherichia coli

Coliform bacteria are described and grouped, based on their common origin or characteristics, as either total or faecal coliform. The total coliform group includes faecal coliform bacteria such as *Escherichia coli (E .coli)*, as well as other types of coliform bacteria that are naturally found in water and soil (Sigee, 2005). Faecal coliform bacteria exist in the intestines of warm blooded animals and humans, and are found in bodily waste, animal droppings, and naturally in soil. Most of faecal coliform in faecal matter (faeces) comprises 90 % of *E. coli*. The presence of total coliforms in water indicates contamination by human sewage or animal droppings, which contains other bacteria, viruses or disease causing organisms (National Research Council, 2004). Total coliform bacteria are considered as an indicator organism as their presence warns of the potential presence of disease causing organisms. The presence of total coliform bacteria in a water system indicates the vulnerability of contamination or experiencing bacterial regrowth.

Escherichia coli are recognised as a good indicator of faecal contamination. It is identified as the only species in the coliform group found exclusively in the intestinal

tract of humans and other warm-blooded animals and subsequently excreted in large numbers in faeces (approximately 10^9 per gram) (Department of National Health and Welfare, 1977). In addition to being faecal specific, *Escherichia coli* or *E. coli* do not usually multiply in the environment and have a life span on the same order of magnitude as those of other enteric bacterial pathogens, both of which are qualities of an ideal bacterial indicator (National Research Council, 2004). They are excreted in the faeces in high numbers, making detection possible even when greatly diluted. *E.coli* is a member of the coliform group, part of the family enterobacteriaceae, and is described as a facultative anaerobic, Gram-negative, non-spore-forming, rod-shaped bacterium. As a member of the enterobacteriaceae family, *E. coli* is naturally found in the intestines of humans and warm-blooded animals such as dogs. Unlike other bacteria in this family, *E. coli* does not usually occur naturally on plants or in soil and water. Within human and animal faeces, *E. coli* is present at a concentration of approximately 10^9 per gram (Edberg *et al.,* 2000) and comprises of approximately 1% of the total biomass in the large intestine (Leclerc *et al.,* 2001). Strains of *E. coli* bacteria can cause gastrointestinal illness along with other, more serious health problems. *E. coli* is generally sensitive to environmental stresses and its survival time in the environment is dependent on many factors, including temperature, exposure to sunlight, presence and types of other microflora, and the type of water involved (e.g., groundwater, surface water, stormwater, or treated distribution water). Generally, *E. coli* survives for about 4 to 12 weeks in water containing a moderate microflora at a temperature of 15 to 18 °C (Edberg *et al.,* 2000). Its presence in urban runoff stormwater indicates not only recent faecal contamination of the water but also the possible presence of intestinal disease-causing bacteria, viruses, and protozoa. The absence of *E. coli* in water generally indicates that the water is free of intestinal disease-causing bacteria. However, because *E. coli* is not as resistant to disinfection as intestinal viruses and protozoa, its absence does not necessarily indicate that intestinal viruses and protozoa are also absent.

4.3.3 Faecal Streptococci (Enterococci sp.)

The faeces of humans and animals contain large numbers of streptococcal bacteria that can be classified as belonging to the fecal streptococci group (Ashbolt *et al.,* 2001). The *Streptococcus faecalis* group (*enterococci*) has been under consideration as indicators of fecal pollution for many years. Cultural methods analogous to the coliform tests have been developed to determine the presence and concentration of these bacteria in water samples. The *Enterococci sp.* bacteria from the *Streptococcus faecalis* group is primarily found only in the faeces of warm-blooded animals and is now understood that some subtypes of this group are associated with insects (Ashbolt *et al.,* 2001). Their acceptance as a measure of faecal pollution from human and warm-blooded animal excreta has been due in part to the relatively high recovery rates in polluted waters. The enterococcus portion of the faecal streptococcus group is a valuable bacterial indicator for determining the extent of faecal contamination of water. The *Enterococci sp.* bacteria is a subset of the fecal streptococci group that includes the *Streptococcus faecalis, Streptococcus faecium, Streptococcus avium* and *Streptococcus gallinarum* of faecal streptococci. These groups of streptococci are considered to be more specific as indicators of the sanitary quality of recreational waters than the faecal streptococci group as a whole. *Enterococcic sp.* are facultative anaerobic organisms, (requiring no oxygen for metabolism), but can survive in oxygen-rich environments. *Enterococci sp.* are tolerant to a wide range of environmental conditions such as extreme temperatures in a range of 10 to 45°C, a pH of 4.5 to 10.0 and high sodium chloride concentrations (salt water). Clinical infections to humans caused by *Enterococcus* include urinary tract infections, bacteremia, bacterial endocarditis, diverticulitis, and meningitis. Furthermore, symptoms such as diarrhoea, dehydration, fever can occur because of the presence of this bacterium (Ashbolt *et al.,* 2001).

4.3.4 Salmonella sp.

Salmonella sp. is a Gram-negative facultative anaerobic rod-shaped bacterium in the same proteobacterial family as *Escherichia coli,* the family *Enterobacteriaceae.*

Salmonella sp. lives in the intestinal tracts of warm and cold-blooded animals. The bacteria are the cause of two diseases called salmonellosis (enteric fever or typhoid), resulting from bacterial invasion of the bloodstream, and acute gastroenteritis lasting between 1-7 days, resulting from a food borne infection/intoxication, with symptoms that include diarrhoea, abdominal pains, nausea, vomiting, and chills, leading to dehydration and headaches (Hunter,1997). Water, soil, animal faeces, raw meats and eggs can transmit *salmonella sp*. It constitutes a major public health burden and represents a significant cost in many developing countries. Millions of human cases are reported annually because of this bacteria and the diseases results in thousands of deaths (WHO, 2010). In general, it is thought that high numbers (between 10^5-10^6 cells) of salmonellae need to be consumed to cause illness. Most *Salmonella sp.* bacteria can grow over the temperature range 7 to 48 ºC, although growth is reduced at temperatures below 10 ºC. Although *Salmonella sp.* is unable to grow at refrigeration temperatures, the organism is able to survive for extended periods at chill temperatures, particularly under freezing conditions. The bacteria can grow over a range of pH values from 3.7- 9.5 under otherwise ideal conditions, but the optimum pH is 6.5 to 7.5. The bacteria cannot grow under very acidic conditions, but is able to survive for sometime in acidic environments. Survival times are dependant on type of acids present and temperature (chilled temperatures favours survival). *Salmonella sp.* is not especially resistant to sanitisers used in the food industry, but is able to form biofilms that may reduce the efficacy of a sanitizer if cleaning is inadequate. The bacteria is not particularly heat resistant and are usually inactivated by pasteurisation or equivalent heat processes. Within 1 to 10 minutes of pasteurisation at 60 ºC and <1 minute at 70 ºC, the bacteria is disintegrated (Hunter,1997).

4.3.5 Shigella sp.

Shigella sp. is a Gram-negative, nonmotile, non-spore forming, rod-shaped bacteria, very closely related to *Salmonella sp.* and *Escherichia coli* in the family *Enterobacteriaceae.* Shigellae bacterium is a major cause of diarrheoa and dysentery-diarrhoea with blood and mucus in the stools throughout the world. It is transmitted by ingestion of contaminated food or water, or through person to person

contact. Shigellosis, also known as bacillary dysentery in its most severe manifestation, is a food borne illness caused by infection of the *Shigella sp* bacteria (Hunter, 1997). Apart from diarrhoea, further symptoms of *Shigella* infection include fever, abdominal cramps, and rectal pain (Hunter, 1997). Shigellosis can be treated with antibiotics, although some strains have developed drug resistance. The causative organism is frequently found in water polluted with faeces. The bacteria survive in a temperature range of 6-7 °C, to a maximum of 45 to 47 °C, a pH range of 4.8 to 9.3 and in the presence of sodium chloride (5.2%) salt conditions (Hunter,1997).In the developing world, *Shigella sp.* causes approximately 165 million cases of severe dysentery and more than 1 million deaths per year mostly in children (WHO, 2010).

4.3.6 Legionella sp.

As discussed previously, *Legionella* was assessed because of its occurrence in heating and cooling systems. The bacterium, which causes legionnaire's disease, is essential for monitoring the water quality from combined PPS-GHPs systems.

4.4 Microbiological analysis

Quantification of microbes was conducted within 24 hours after sample collection. Pour-Plate and Spread-Plate techniques were used (Maier *et al.,* 2000). Dilutions of the samples were prepared in duplicates and 1 ml of sample was poured into a sterile disposable Petri dishes. 15-20 ml of the medium agar was cooled to a temperature of 45 °C into the Petri dishes with sample. The samples were mixed and then incubated along with the blank plates (Maier *et al.,* 2000; Cappuccino and Sherman, 1996). Soon after incubation the number of colonies on the plates were recorded (CFU/ml).

Plate counts were done under microscope in a fume cupboard to prevent pathogenic organisms transmission on the researchers. Bacteria colonies were recorded as Colony Fomring Units (CFU) per 100 ml. The number of colonies varied from zero throughout the analysis (*Legionella*) to thousands. Where growth of bacterial colonies was extremely high and not possible to count colonies on the entire

plate, APHA methods for counting were implemented. The plate was divided into 4 quarters and further sub-divided into 8 segments. The number of CFU's in one segment was counted and multiplied by 8 giving the total number of bacteria per plate.

When water samples overgrew the dishes with coliforms (typically for total heterotrophic bacteria), water effluent samples were diluted with sterile water at a 1:10, 1:100, and 1:1000 ratios where appropriate. The diluted samples were placed on the agar plates and bacterial count recorded after incubation. On the other hand, for low number of colonies (usually for *Salmonella sp* and *Shigella sp*), 20 ml of water sample was passed through a glass fibre filter. The filtered paper was placed on the agar and incubates in the same way as spread samples. After incubation, the colonies were recorded under microscope. The results were multiplied by a factor of 5 in order to give the number of CFUs per 100ml.

Nutrient Agar, a non-selective growth medium and allows for the growth of a wide variety of oxygen-tolerant genera such as total heterotrophic bacteria, as one of the key water quality indicators (Maier *et al.,* 2000). This agar is composed of peptone (vegetable) and vegetable extract (Atlas, 1993). The nutrient agar was obtained in ready-made form from The School of Biological Sciences, University of Edinburgh.

MacConkey Agar allows for the detection and isolation of *Salmonella* and *Shigella*. It consists of peptone, lactose, bile salts, sodium chloride, neutral read and crystal violet. The Slanetz and Bartley Agar was used to favour the growth of *Enterococci sp. where* colonies were identified by their red or pink colour (Tejedor, 2001). The Slanetz and Bartley medium consist of tryotose, yeast extract, glucose, di-potassium hydrogen phosphate, sodium azide, and tetrazolium chloride Atlas, 1993). Eosin methylene blue (EMB) agar was used for the detection of *E.coli* and Total coliforms, where *E.coli* colonies are identified by a blue-black colour with green metallic sheen (Maier *et al.,* 2000). The EMB agar composition includes peptone, lactose di-potassium hydrogen phosphate, eosin Y, and methylene blue.

Legionella glycine vancomycim polymixin cyclohexamide (GVPC) agar was specially developed for the isolation of most *Legionella* species, notably those responsible for infections such as *Legionella pneumophila*, which is the species most

frequently involved in Pontiac fever. This selective medium consists of charcoal yeast extract, potassium hydroxide, ferric pyrophosphate, cysteine hydrochloric acid and ketoglutarate, which enables the enumeration of *Legionella* in water according to published standards.

All culture media for growing of total heterotrophic bacteria, *E. coli,* total coliforms, *Enterococci sp., Salmonella sp., Shigella sp.* and *Legionella* were ordered from Oxoid Ltd (Solar House, Mercers Row, Cambridge, United Kingdom). Petri plates, filter papers (MF 200 with diameter of 125 mm) and primers were supplied by Fisher Scientific UK (Bishop Meadow Road, Loughborough, United Kingdom). Nutrient Agar plates and eosin methylene blue agar plates were incubated at 36°C ± 1°C for 2 d. Slanetz and bartley agar plates were kept at 45ºC for 5 d. The *Legionella* GVPC agar plates were incubated and inoculated in a moist chamber at 36°C ± 1°C for 10 days, and examined at intervals between 1 and 2 days during the incubation period.

4.4.1 Gram staining Analysis

The Gram stain is routinely used as an initial procedure in the identification of an unknown bacterial species. The Gram staining method is a differential staining method of differentiating bacterial species into two large groups (Gram-positive and Gram-negative) based on the chemical and physical properties of their cell walls. This reaction divides the eubacteria into two fundamental groups according to their stainability and is one of the basic foundations on which bacterial identification is built. 2 to 3 drops of the water sample is added onto a glass slide. It is spread evenly on the slide to form a thin smear, which is done by sliding the edge of another glass slide across the glass slide containing the water sample. It is then allowed to air dry. The smear is heat fixed quickly passing it 2-3 times through a flame; it is not overheated to avoid distortion (Clesceri *et al.,* 1998).

The smear on the glass slide is covered with crystal violet, after 30 seconds, the primary stain (crystal violet) renders all the bacteria uniformly violet. Crystal violet (CV) dissociates in aqueous solutions into CV+ and chloride (Cl–) ions. These ions penetrate through the cell wall and cell membrane of both gram-positive and gram-

negative cells. The CV+ ion interacts with negatively charged components of bacterial cells to stain the cells purple. After a minute of exposure to the staining solution, the slide is washed in distilled water. The smear is treated with few drop of Iodine and allowed to act for a minute. Iodine serves as a mordant, in the form of negatively charged ions, interacts with CV+ to form large complexes of crystal violet and iodine (CV–I complexes) within the inner and outer layers of the cell. Iodine acts as a trapping agent to retain the purple crystal violet colour in the cell. After 3 seconds, the iodine is gently rinsed off with distilled water. Thereafter, decolourisation occurs by adding alcohol or acetone to the smear while holding the slide at an angle to allow the declouriser to drain. The process of decolorization is fairly quick and does not exceed 30 seconds for thin smears. Acetone, a potent decolorizer decolorizes the smear in 2-3 seconds. After the smear is decolorized, it is washed in distilled water without any delay. The smear is finally treated with few drops of counterstain with dilute safranin. The slide is washed again in distilled water; excess water is removed using a blotting paper, dried in air and heat fixed before observing under microscope. Those bacteria that hold on to primary dye iodine complex and remain violet are called Gram positive and those, which get decolorized and subsequently take up counterstain (pink/red) are called Gram negative.

4.4.2 Molecular Microbiology

Advances in molecular techniques have resulted in a number of new detection methods that depend on the recognition of specific gene sequences. Such methods are rapid and tailored to detect specific strains of organisms on one hand or a group of organisms on the other. Figure 4-5 provides a general overview of the key molecular microbiological techniques. Colonies from selective plates were subcultured on Nutrient Agar to test for purity. The organisms were then identified by sequencing of the 16S ribosomal ribonucleic acid (rRNA) gene. The 16S rRNA gene was obtained by polymerase chain reaction (PCR) amplification using 'universal' bacterial primers (Weisburgh *et al.,* 1991). PCR was performed in a total reaction volume of 50 µl containing 34 µl water, 10 µl reaction buffer, 2 µl primer

mixture fD1 + rD1 (10 pmol/µl each), 1 µl dNTP mixture (10 mM each), 2 µl cell suspension and 1µl Taq polymerase.

Rather than purifying genomic DNA for use as a template, a suspension of cells in sterile water was added directly to the PCR reaction to act as a template; release of DNA from cells during the heating stages is sufficient to provide a template for the amplification, greatly reducing the amount of sample preparation required and opportunities for contamination with exogenous bacterial DNA. The primer sequences used were fD1: agagtttgatcctggctcag and rD1: aaggaggtgatccagcc. The cycling conditions were as follows: denaturation at 95ºC for 2 min, followed by 30 cycles at 95ºC for 0.5 min, annealing at 58ºC for 0.5 min and extension at 72ºC for 1.5 min, a final extension step of 72ºC for 10 min. Samples were kept at 4ºC until further analysis.

The PCR products were analysed by agarose gel electrophoresis, and if a PCR product of the correct size was observed, the DNA was purified using standard techniques (Sambrook *et al.,* 2000). If no product was obtained, the PCR was repeated using a lower annealing temperature. After purification, the PCR products were submitted for sequencing by The University of Edinburgh Sequencing Service, using the same primers as for PCR. The analysis of sequence data and homology comparisons were performed using the Basic Local Alignment Search Tool (BLAST) located at the National Centre for Biotechnology Information NCBI, (2008). Phylogenetic relationships were inferred by the neighbour-joining method using the Molecular Evolutionary Genetics Analysis (MEGA) software version 4.0 Tamura *et al.,* (2007). In addition to identifying these isolates, it was desired to determine how common they were in the water microbial community. To accomplish this, DGGE was used to analyse community DNA. Total waterborne bacterial DNA was extracted from 1 ml of each water sample using an UltraClean™ soil and water DNA extraction kit (CamBio Ltd., UK) according to the manufacturer's protocol.

The bacterial 16 S rRNA genes were amplified from the community DNA or pure cultures as described above. Nested PCR primers 341f-GC (5'-CGCCCGCCGCGCCCCGCGCCCGTCCCGCCGCCCCCGCCCGCCTACGGGAG GCAGCAG-3 and 534R (5'-ATTACCGCGCTGCTGG-3') were then used to amplify the V# variable region of the bacterial 16 S rRNA gener from 1 µl of

purified 1500 bp first-round PCR product as described by Muyzer *et al.,* (1993). The PCR conditions used were initial denaturation at 95 ˚C for 5 minutes; 28 cycles of 94 ˚C for 1 minute, 64 ˚C for 1 minute, 72 ˚C for 1 minute 30 seconds; final extension at 72 ˚C for 10 minutes. Ten µl-samples of the extension products were loaded onto DGGE gels (McCaig *et al.,* 2001); containing a linear gradient of 30-70% denaturant [where 100% denaturant is defined as 7 M urea (42% w/v) and 40% (w/v) formamide]. Electrophoresis was carried out on a DCode Universal Mutation Detection System (Bio-Rad, Hertfordshire, UK) in 7 l of 1 x TAE buffer at a constant temperature of 60 ˚C for 960 min at 75 V. Silver staining of gels was carried out as described by Nicol *et al.,* (2005). The stained gel was scanned at 600 dpi using an Epson Perfection V700 scanner. The bands obtained from isolated bacteria were compared to community profiles to obtain an indication as to whether these potentially pathogenic organisms were in fact common in the community.

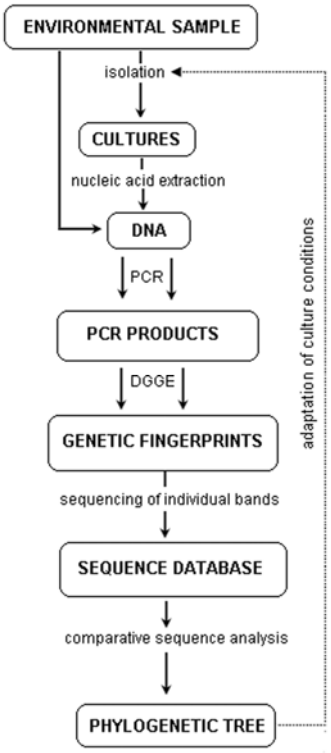

Figure 4-5: General overview of key molecular microbiological techniques. DNA, deoxyribonucleic acid; RNA, ribonucleic acid; PCR, polymerase chain reaction; RT-PCR, real-time polymerase chain reaction; DGGE, denaturing gradient gel electrophoresis; TGGE, Temperature gradient gel electrophoresis.

4.5 Carbon Dioxide (CO_2) gas monitoring

An indication of the level of microbial activity can be obtained from the quantity of CO_2 produced and reduction in oxygen concentrations. This is an indirect assessment of microbiological activity within the pavement systems. Four vertical tubes were installed in selected bins from both the indoor rig and outdoor rig respectively. The first tube was placed at the shallowest point within the pavement structure, the second tube was placed directly below the geotextile layer where the highest microbial activity is expected to occur, the third tube was placed in the upper part of the sub-base and the fourth placed a few centimetres below in the lower sub-base (partly submerges in filtered water). Sampling tubes were open at the bottom and sealed with black silicone rubber on the top. At the top of the silicone, a flexible tube was joined which formed a valve, which was opened during CO_2 sampling. The

CO_2 concentrations were recorded using an automated portable IRGA (Infra Red Gas Anlyser) (PP Systems, Hitchin, Hertfordshire, England, U.K).

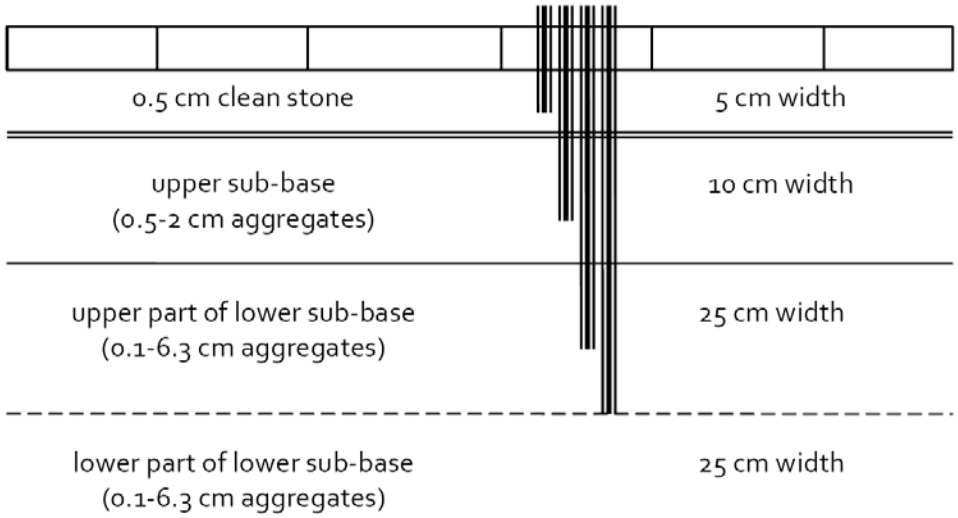

Figure 4-6: Carbon dioxide sampling points installed within PPS (not drawn to scale)

4.6 Energy Efficiency Analysis of Geothermal Heating and Cooling

Geothermal heat pumps sources of environmental energy are the ground or mediums thermally coupled to the ground as previously discussed. However, in our case the sub-base of a permeable pavement system acts as the thermal transfer mechanism. As the heat extracts heat energy flux form the water beneath the pavement, its temperature will drop. There is a theoretical limit of the efficiency of a GHP. Ideally, a geothermal heat pump works on the reverse principles of an ideal heat engine. Assuming that energy losses due to acoustic noises is negligible and that all extracted heat is efficiently transferred to a point of use, the efficiency η of the GHP can be defined as the ratio of heat delivered (H) at elevated temperature (T_1) to the work performed done (W). Therefore by using an idealised Carnot cycle as described previously in Chapter 3 (Banks, 2008):

$$\eta_{MAX} = H / W = T_1 /(T_1 - T_2) \tag{4-1}$$

Where T_2 is the lower temperature which is usually significantly below the environmental source temperature in order to ensure a kinetically rapid transfer of heat. The efficiency of the GHP in a heating mode is usually referred to as its Coefficient of Performance (COP) where (Banks, 2008):

$$COP_{Heating} = T_1 /(T_1 - T_2) \quad (4\text{-}2)$$

The GHP can be switched into reverse so that it can extract heat from the inside of a building and reject it to the ground or to ground-coupled medium such as the water beneath a permeable pavement system. The water in the saturated zone acquires heat from the GHP and its temperature increases a few degrees (°C) rather than decreases as in the heating mode. The COP in a cooling cycle is also referred to as the Energy Efficiency Ratio (EER) and is computed by (Banks, 2008):

$$EER[COP_{Cooling}] = T_2 /(T_1 - T_2) \quad (4\text{-}3)$$

4.7 Health and Safety Risks Assessment /Procedures

A risk assessment was completed and its content conveyed to other uses, the laboratory director (Dr. Miklas Scholz) and the institute's health and safety officer (Mr. Dereck Jardine) in the laboratory of the hazardous substances and description of work. Hazards were identifies using material safety data sheets (MSDS) for all proprietary (commercial) biological and chemical substances obtained from the suppliers.

Personal protective equipment (PPE) was worn at all times for water quality analysis (both physiochemical and microbiological). It is necessary to control and prevent exposure to hazardous substances. PPE included laboratory white coats made of a specialist cloth for body protection, eye safety spectacles and chemical resistant goggles, fully sealed waterproof shoes, and aloe vera disposable gloves (Fisher Scientific brand). Where appropriate (microbiological analysis) mechanical controls

such as local exhaust ventilation and fume cupboards are used. Chemical and biological waste was discarded to the appropriate waste disposal bins at the School of Biological Sciences, University of Edinburgh. A control of substance hazardous to heath regulations (COSHH) form under The University of Edinburgh regulations was assigned to all substances used during the research which covers hazardous substances used or produces, and a stated hazard classification.

Chapter 5 Overall Water Quality, Treatment and Energetic Performance

This chapter investigates the stormwater treatment potentials and mechanisms for physiochemical and microbiological water parameters for the integrated PPS with GHPs and standalone PPS. The overall variations of influent and effluent water quality are presented and performances of the experimental bins are assessed by evaluating the constituent concentrations. The average energetic efficiency for bins with GHPs were assessed by the EER and COP. The performance of the experimental systems were also statistically compared to examine differences in design (presence of geotextile, GHPs), location (environmental control systems) and types of urban runoff treated. Parts of this chapter have been published as articles in (the) International Journal of Sustainable Engineering, Environmental Technology, Environmental Progress and Sustainable Energy and The International Journal of Green Economics. The major objectives of this chapter are to assess the performance of laboratory-scaled permeable pavement and geothermal heating-cooling systems treating highly concentrated urban stormwater runoff and investigate the possiblities of stormwater reuse.

5.1. Inflow stormwater quality

Table 5-1 presents the minimum, maximum, mean, standard deviation and standard error of the mean inlet concentrations of the monitored water quality variables for inflows 1 (gully pot liquor) and inflow 2 (gully pot liquor mixed with dog faeces). Figure 5-1 illustrates the design variables for experimental statistical analysis. The overall statistical inflow concentrations and removal efficiencies for the pavement systems were calculated using the following:

$$\text{Mean, } \bar{x} = \frac{\sum x}{n} \tag{5-1}$$

Where ‘x’ is the recorded parameters and ‘n’ is the sample number.

$$\text{Standard deviation } \sigma = \sqrt{\frac{\sum \left(x - \bar{x}\right)^2}{n}} \tag{5-2}$$

$$\text{Standard error of the mean } \sigma_e = \frac{\sigma}{\sqrt{n}} \tag{5-3}$$

$$\text{The removal efficiency (\%)} = \left(\frac{C_{IN} - C_{OUT}}{C_{IN}} \right) \times 100 \qquad (5\text{-}4)$$

Where C_{IN} is the inflow (influent) concentration and C_{OUT} is the outflow (effluent concentration).

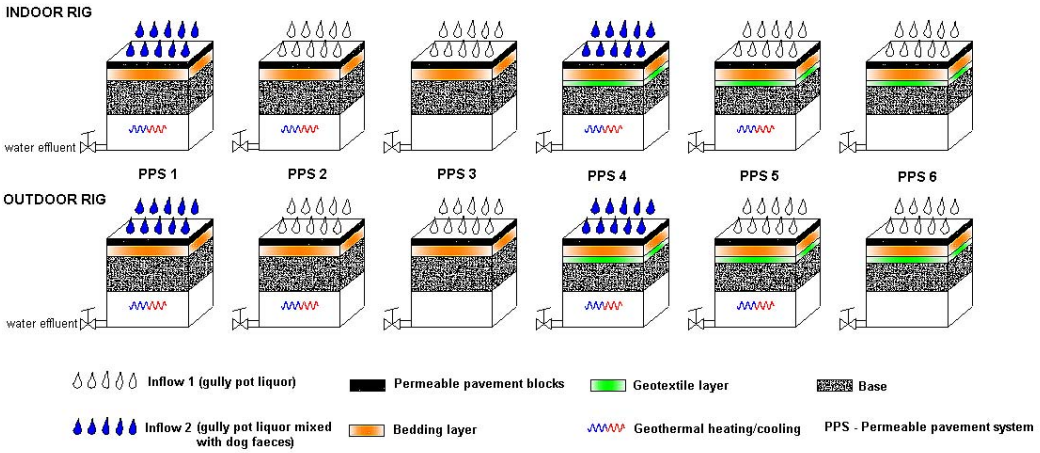

Figure 5-1: Experimental layout of indoor and outdoor rigs with design variables for statistical analyses.

Table 5-1: Overall influent concentrations for inflow 1 (gully pot liquor) and inflow 2 in brackets (gully pot liquor mixed with dog faeces) from March 2008 to April 2010 (sample number n = 113)

Water Quality Parameters	Minimum	Maximum	Mean	Std. Error of Mean	Std. Deviation
Temperature (°C)	14.20 (14.40)	28.60 (29.10)	20.93 (21.66)	0.32 (0.28)	3.38 (3.06)
pH	6.19 (6.42)	8.76 (8.49)	7.14 (7.29)	0.05 (0.04)	0.49 (0.43)
Electroconductivity (µS/cm)	339.86 (362.27)	1065.18 (982.66)	455.87 (584.29)	13.02 (11.95)	138.49 (127.07)
Redox potential (mV)	162.0 (196.20)	459.10 (451.30)	336.58 (332.51)	6.23 (4.94)	66.18 (52.47)
NO_3-N (mg/l)	0.31 (0.08)	5.13 (9.76)	1.74 (1.85)	0.11 (0.14)	1.20 (1.46)
NH_4-N (mg/l)	0.06 (0.31)	6.60 (11.81)	0.99 (2.80)	0.12 (0.21)	1.23 (2.18)
PO_4-P (mg/l)	0.15 (0.66)	4.15 (30.0)	1.19 (5.98)	0.09 (0.67)	0.97 (7.16)
Total dissolved solids (ppm)	210.0 (219.0)	450.0 (477.0)	249.35 (281.15)	4.73 (4.81)	50.28 (51.15)
Suspended solids (mg/l)	10.0 (30.0)	440.0 (1020.0)	133.32 (254.67)	10.34 (16.90)	109.97 (179.69)
Turbidity (NTU)	13.0 (38.0)	563.0 (665.0)	161.51 (274.63)	12.02 (14.63)	127.76 (155.52)
E.Coli (CFU/100ml)	1.8×10^3 (2.51×10^3)	8.39×10^4 (9.30×10^4)	1.88×10^4 (3.62×10^4)	1.57×10^3 (1.79×10^3)	1.68×10^4 (1.91×10^4)
Enterococci sp (CFU/100ml)	3.3×10^2(1.08×10^3)	1.71×10^4 (1.89×10^4)	3.74×10^3 (7.37×10^3)	3.21×10^2 (3.57×10^2)	3.42×10^3 (3.79×10^3)
Total coliforms (CFU/100ml)	4.38×10^5 (4.56×10^5)	1.80×10^6 (1.95×10^6)	7.10×10^5 (1.01×10^6)	2.72×10^4 (3.05×10^4)	2.89×10^5 (3.25×10^5)
Salmonella sp (CFU/100ml)	516.0 (1321.60)	4.31×10^4 (5.52×10^5)	7.37×10^3 (1.13×10^5)	8.07×10^2(1.24×10^4)	8.58×10^3 (1.32×10^5)
Shigella sp (CFU/100ml)	2.06×10^2 (5.26×10^2)	1.72×10^4 (2.21×10^5)	2.95×10^3 (4.53×10^4)	3.23×10^2 (4.97×10^3)	3.44×10^3 (5.29×10^4)
THB (CFU/100ml)	4.0×10^3 (8.10×10^4)	4.50×10^7 (1.47×10^{10})	3.87×10^6 (4.12×10^8)	7.99×10^5 (1.88×10^8)	8.49×10^6 (2.0×10^9)
BOD (mg/l)	8.0 (30.0)	97.0 (341.0)	29.84 (118.42)	1.66 (7.26)	17.72 (77.18)
COD (mg/l)	27.0 (71.0)	267.0 (747.0)	85.68 (263.46)	4.51 (15.79)	47.92 (167.83)
Dissolved oxygen (mg/l)	5.10 (5.30)	11.70 (11.82)	8.91 (8.92)	0.15 (0.15)	1.58 (1.59)

5.2 Water reuse standards and guidelines.

There are no fixed standards or guidelines regarding sustainable urban drainage techniques and urban runoff treatment. However, alternative water reuse standards and guidelines which varied for the types of application, regional context and overall risk perception were compared to the water quality treatment performance of the pavement system. Nevertheless, depending on the project specifications for various SUDS applications there will be different water quality requirements, treatment process requirements, and criteria for operation and reliability. Nonetheless, the starting point for water reuse is ensuring public health and safety. For this reason, nutrient, sediments and microbiological parameters have received the most attention in water reuse regulations from the World Health Organisation (WHO), United States Environment Protection Agency (US EPA) and the EU European Commission Environment. Monitoring all pollutants is not realistic and therefore specific indicator organisms are monitored to minimise health risks. Table 8-3 provides a summary of water quality parameters of concern with respect to their significance in water reuse systems, as well as approximate ranges of each parameter in reclaimed water. The treatment of urban wastewater is typically designed to meet water quality objectives based on suspended solids or turbidity, organic content (BOD / COD), biological indicators (total or fecal coliforms which includes *E.coli*), nutrient levels (nitrogen and phosphorus) pH and dissolved oxygen.

Table 5-2: Guidelines for Reclaimed Water Quality and Treatment Requirements (European Commission Environment, 1991, 2006; US EPA, 2004 b).

Parameters	European Commission Environment	US EPA (Guidelines for non-potable water reuse)[c]
pH	(6 to 9)[a]	6 to 9
Dissolved oxygen	(8 mg/l to 12 mg/l)[a]	8 mg/l to 12 mg/l
Suspended solids	-	< 30 mg/l
Turbidity	(< 2 NTU)[a]	< 30 NTU
BOD_5	(< 25 mg/l)[b]	< 45 mg/l
COD	(< 125 mg/l)[b]	< 90 mg/l
Total coliforms	(< 500 CFU/100ml)[a,b]	< 200 CFU/100ml
Faecal coliforms	(<100 CFU/100ml)[a,b]	< 10^3 CFU/100ml
Total Nitrogen	(<15mg/l)[b]	< 30 mg/l
Total Phosphorus	(<2mg/l)[b]	< 20 mg/l

[a]European Commission Environment Urban Wastewater Treatment Directive (91/271/EEC)
[b]European Commission Environment Bathing Water Directive (2006/7/EEC)
[c]US EPA (2004 b) Guidelines for Water Reuse (EPA/625/R-04/108)

5.3 Statistical Analysis

The one-sample Kolmogorov-Smirnov goodness-of-fit test was used to test whether or not a given distribution is significantly different from one hypothesized based on the assumption of a normal distribution (Mac Berthouex and Brown, 2002). The observed distribution in the one-sample Kolmogorov-Smirnov test of normality is the distribution of the variable in the sample. If the raw data set did not follow a normal distribution, data was transformed using a simple linear transformation method and logarithmic transformation prior to statistical analysis (Mac Berthouex and Brown, 2002).

From Table 5-3 below, the environmental parameters for all bins (both indoor and outdoor) followed a normal distribution if $\alpha > 0.05$. On the contrary if $\alpha < 0.05$, the distribution did not follow normality and was therefore transformed prior to statistical analysis.

Table 5-3: One-sample Kolmogorov-Smirnov test for normality. For significance $\alpha > 0.05$ sample follows a normal distribution (in bold).

Parameters	Indoor rig						Outdoor rig					
	PPS 1	PPS 2	PPS 3	PPS 4	PPS 5	PPS 6	PPS 1	PPS 2	PPS 3	PPS 4	PPS 5	PPS 6
Water sample temperatures (°C)	**0.830**	**0.194**	**0.951**	**0.876**	**0.148**	**0.852**	**0.834**	**0.900**	**0.744**	**0.679**	**0.645**	**0.827**
Geothermal heating/cooling temperatures (°C)	0.000	0.000	–	0.000	0.000	–	0.000	0.000	–	0.000	0.000	–
pH	**0.062**	**0.078**	**0.606**	**0.071**	**0.163**	**0.731**	**0.560**	**0.079**	**0.697**	**0.872**	**0.123**	**0.052**
Electroconductivity (µS/cm)	0.000	0.000	0.003	0.002	0.001	0.000	0.000	**0.083**	0.000	0.000	0.002	0.182
Redox potential (mV)	**0.113**	**0.104**	**0.099**	**0.154**	**0.571**	**0.246**	**0.292**	**0.255**	**0.083**	**0.163**	**0.342**	**0.202**
NO_3-N (mg/l)	0.000	0.000	0.000	0.000	0.000	0.000	0.000	0.002	0.000	0.000	0.001	0.000
NH_4-N (mg/l)	0.000	0.000	0.000	0.000	0.000	0.000	0.000	0.000	0.000	0.000	0.000	0.000
PO_4-P mg/l	0.027	0.000	0.000	0.047	0.000	0.000	**0.067**	0.000	0.000	0.046	0.000	0.001
Total dissolved solids (ppm)	0.042	0.041	**0.068**	0.006	0.014	**0.424**	0.043	0.048	**0.330**	**0.351**	**0.079**	**0.093**
Suspended solids (mg/l)	0.001	0.000	0.004	0.000	0.000	0.006	0.000	0.000	0.000	0.000	0.000	0.000
Turbidity (NTU)	0.002	0.000	0.001	0.000	0.000	0.003	0.001	0.000	0.000	0.000	0.000	0.000
E.Coli (CFU/100ml)	**0.176**	0.014	0.001	0.002	0.028	0.000	**0.230**	0.019	0.010	0.020	0.000	0.000
Enterococci sp (CFU/100ml)	**0.138**	0.008	0.000	0.000	0.000	0.000	**0.240**	0.018	0.002	0.001	0.015	0.000
Total coliforms (CFU/100ml)	**0.175**	0.015	0.001	0.001	0.019	0.000	**0.233**	0.019	0.010	0.002	0.029	0.000
Salmonella sp (CFU/100ml)	**0.423**	0.018	0.003	**0.183**	0.001	0.005	**0.332**	**0.663**	0.023	0.001	**0.237**	0.022
Shigella sp (CFU/100ml)	**0.424**	0.019	0.003	**0.170**	0.001	0.000	**0.298**	**0.639**	0.021	0.001	**0.225**	0.024
THB (CFU/100ml)	0.000	0.000	0.000	0.000	0.000	0.000	0.000	0.000	0.000	0.000	0.000	0.000
BOD (mg/l)	0.000	0.000	0.000	0.000	0.000	0.000	0.000	0.000	0.001	0.000	0.001	0.000
COD (mg/l)	0.002	0.000	0.003	0.003	0.001	0.000	**0.051**	0.000	0.017	0.000	0.001	0.001
Dissolved oxygen (mg/l)	**0.176**	**0.281**	**0.091**	**0.081**	**0.095**	**0.113**	**0.989**	**0.799**	**0.120**	**0.202**	**0.456**	**0.530**
Carbon dioxide CO_2 (ppm)	0.000	–	–	–	0.000	–	0.000	–	–	–	0.000	–

Analysis of variance (Anova) is a statistical method of testing two or more variables to determine whether their sample means could have been obtained from populations with the same true mean (Mac Berthouex and Brown, 2002). If the water quality effluent variables are similar (from populations with the same mean), the variation within each permeable pavement treatment will be approximately the same as the variations between pavement rigs. Anova used from SPSS 17.0 Analytical Software (Statistical Package for the Social Sciences (SPSS) Headquarters, 233 S. Wacker Drive, Chicago, Illonois, USA) to uncover the main and interaction effects of categorical independent variables (factors) such as the presence of geotextiles, heating/cooling effects, carbon dioxide on interval dependent variables (water quality parameters). The main outcome is the direct effect of an independent variable on the dependent variable. An interaction effect is the joint effect of two or more independent variables on the dependent variable. The key statistics in Anova is the test of difference of group means, testing if the means of the groups formed by values of the independent variable (or combinations of values for multiple independent variables) are different enough not to have occurred by chance. Anova assumes (Mac Berthouex and Brown, 2002):

- the data is in numerical format representing samples from normally distributed populations
- the variances of the groups are similar
- the sample sizes of the groups are similar
- the groups should be independent

One-way Anova which has one independent variable was used to test the entire group of Indoor (PPS 1 to PPS6) versus the outdoor group (PPS1 to PPS6) (Table 5-4) and the effects of carbon dioxide production with PPS 1 versus PPS 5 for both indoor and outdoor respectively. To test the effects if any, for variations in pavement design for such as (i) treating gully pot liquor and gully pot liquor mixed with dog faeces, (ii) geotextile layer versus geocomposites, and (iii) presence of GHP, were all analysed with grouped paired Anova for a combined indoor and outdoor rigs respectively (Table 5-5). Grouped pairwise Anova comparisons at a significant level of $p = 0.05$ was applied to test the significant differences between heating and

cooling cycles for all water quality parameters effluents within both indoor and outdoor rigs collectively (PPS1, PPS 2, PPS 4 and PPS 5). The statistical tests for pairwise analysis indicate that the water quality variables for each bin (PPS1, PPS2, PPS3, and PPS 5) outflow concentrations differ significantly from each other when $p < 0.05$ during the heating and cooling cycles (Table 5-6).

Table 5-4: One way Anova between in indoor (PPS 1-PPS 6) and outdoor rig (PPS 1-PPS 6), significant values ($p < 0.05$) in bold.

Water quality parameters	Indoor rig & Outdoor rig		
	Sum of squares	F	Sig.
pH	7.45	133.98	**0.000**
Electroconductivity (µS/cm)	4.031×10^4	2.75	0.098
Redox potential (mV)	72.50	0.02	0.894
Nitrate-nitrogen (NO_3-N mg/l)	0.52	1.02	0.314
Ammonia-nitrogen (NH_4-N mg/l)	0.63	9.01	**0.003**
Ortho-phosphate-phosphorous (PO_4-P mg/l)	9.14	18.74	**0.000**
Total dissolved solids (ppm)	1.749×10^4	17.35	**0.000**
Suspended solids (mg/l)	1.561×10^3	3.26	0.072
Turbidity (NTU)	1.972×10^3	2.77	0.098
Escherichia coli (Log_{10} CFU/100ml)	7.19	40.85	**0.000**
Enterococci sp. (Log_{10} CFU/100ml)	5.98	32.40	**0.000**
Total Coliforms (Log_{10} CFU/100ml)	7.37	33.24	**0.000**
Salmonella sp. (Log_{10} CFU/100ml)	5.34	56.08	**0.000**
Shigella sp. (Log_{10} CFU/100ml)	5.53	56.04	**0.000**
Total heterotrophic bacteria (Log_{10} CFU/100ml)	12.36	1.07	0.302
Biochemical oxygen demand (BOD mg/l)	349.39	26.88	**0.000**
Chemical oxygen demand (COD mg/l)	54.52	0.63	0.43
Dissolved oxygen (mg/l)	0.05	0.03	0.85

Table 5-5: Paired Anova (Indoor and Outdoor rigs) between PPS structure variations and type of urban runoff treated, significant values ($p < 0.05$) in bold.

Water parameters	PPS (Indoor and Outdoor)					
	[a](1vs 2)	[a](4 vs 5)	[b](1 vs 4)	[b](2 vs 5)	[c](2 vs 3)	[c](5 vs 6)
pH	**0.000**	**0.000**	**0.000**	**0.000**	0.489	0.291
Electroconductivity (µS/cm)	**0.000**	**0.000**	**0.000**	**0.000**	0.246	0.179
Redox potential (mV)	0.719	0.196	0.154	0.234	0.351	0.406
NO_3-N (mg/l)	0.231	**0.000**	**0.000**	**0.030**	**0.000**	**0.001**
NH_4-N (mg/l)	**0.017**	0.112	**0.042**	**0.026**	0.428	0.881
PO_4-P (mg/l)	**0.000**	**0.000**	**0.046**	**0.000**	0.937	0.331
Total dissolved solids (ppm)	0.095	**0.000**	**0.000**	**0.000**	**0.000**	0.063
Suspended solids (mg/l)	0.245	0.086	**0.048**	**0.000**	0.579	**0.016**
Turbidity (NTU)	0.096	0.226	**0.034**	**0.001**	0.651	0.102
E. Coli (Log_{10} CFU/100ml)	**0.000**	**0.000**	**0.000**	**0.000**	**0.000**	**0.000**
Enterococci sp (Log_{10} CFU/100ml)	**0.000**	**0.000**	**0.000**	**0.000**	**0.000**	**0.000**
Total coliforms (CFU/100ml)	**0.000**	**0.000**	**0.000**	**0.000**	**0.000**	**0.000**
Salmonella sp (Log_{10} CFU/100ml)	0.241	0.219	**0.000**	**0.019**	0.955	**0.000**
Shigella sp (Log_{10} CFU/100ml)	0.239	0.219	**0.000**	**0.018**	0.959	**0.000**
THB (Log_{10} CFU/100ml)	**0.000**	**0.000**	**0.000**	**0.000**	0.553	0.633
BOD (mg/l)	0.372	**0.022**	**0.000**	**0.000**	0.164	**0.000**
COD (mg/l)	0.144	0.138	**0.000**	**0.000**	0.982	**0.000**
Dissolved oxygen (mg/l)	**0.000**	**0.000**	**0.000**	**0.000**	**0.000**	**0.000**

[a](Inflow 1 vs. Inflow 2), [b](Geotextile membrane vs. Geocomposite), [c](GHP vs. no GHP).

Table 5-6: Paired Anova between heating and cooling cycles for PPS 1, 2, 4 and 5 (Indoor and Outdoor rigs), significant values ($p<0.05$) in bold.

(A) heating cylces	(B) cooling cycles	Mean Difference (A-B)	Std. Error	Sig.[a]
pH		0.15	0.02	**0.000**
Electroconductivity (µS/cm)		3.15	6.09	0.605
Redox potential (mV)		33.63	4.31	**0.000**
PO_4-P (mg/l)		0.05	0.04	0.184
NH_4 -N (mg/l)		0.04	0.02	**0.009**
NO_3 -N (mg/l)		0.05	0.08	0.485
Total dissolved solids (ppm)		3.79	2.14	0.077
Suspended solids (mg/l)		6.46	1.48	**0.000**
Turbidity (NTU)		5.93	1.86	**0.001**
Dissolved oxygen (mg/l)		0.58	0.12	**0.000**
BOD (mg/l)		0.15	0.23	0.512
COD (mg/l)		1.82	0.57	**0.001**
Total coliforms (Log_{10} CFU/100ml)		2.29	2.00	**0.048**
Escherichia coli (Log_{10} CFU/100ml)		2.12	1.82	**0.048**
Enterococci sp (Log_{10} CFU/100ml)		1.47	1.13	**0.026**
Salmonella sp (Log_{10} CFU/100ml)		1.85	1.22	**0.000**
Shingallae sp (Log_{10} CFU/100ml)		1.45	0.83	**0.000**
THB (Log_{10} CFU/100ml)		4.59	4.69	0.425

5.4 Water Quality Results

5.4.1 Water Sample Temperature

Water sample temperature is a critical water quality and environmental parameter because it governs the presence and growth of aquatic pathogenic organisms. Water sample temperatures for inflow 1 (gully pot liquor) and inflow 2 (gully pot liquor mixed with dog faeces) were relatively stable throughout the analysis and ranged from (14.2 °C to 28.6 °C) and (14.40 °C to 29.10 °C) with a standard deviation of ± 3.38 and 3.06 respectively (Table 5-1). Overall mean water sample temperatures throughout the two-year period of analysis were 20.93 °C and 29.10 °C for inflow 1 and inflow 2 respectively. The effluent water sample temperatures describe the environmental conditions leaving the sub-base of the

pavement structure. Figure (5-2) shows the box and whiskers plots for the combined period of analysis. With regards to the indoor rig PPS1, 2, 4 and 5 temperatures ranged from 10 to 28 °C respectively. These bins were subjected to geothermal heating and cooling and showed no statistical differences to PPS 3 and PPS 6, which indicated that the heaters and coolers temperature range were not powerful enough when warming and cooling the water to achieve significant temperature variations from the outflow. Regarding the outdoor rigs, the pavement rigs showed similar outflow water temperatures throughout the analysis. Another contributing factor for similarities in outfow water temperatures is the surrounding environment and time of heating-cooling applications, whereby during the heating period, water heaters operated for 15 hours per day raising the water temperatures to (20 °C -25 °C) and the cooling period, water coolants operated for 10 hours lowering the water temperature from (4 °C – 8 °C). The time elapsed would result in convective and conductive heat transfer and losses of the water throughout the pavement structure allowing the effluent temperatures to achieve an ambient value of approximately 18°C as seen in figure (5-1). Higher water temperatures stresses water quality and reduces the potential of water to contain essential dissolved gases such as oxygen. Temperature influences the rates of chemical and biological reactions within the pavement system. Scholz and Grabowiecki, (2009) showed that increased water temperature within the sub-bases of permeable pavements increases the metabolic rates. Effluent water sample temperatures for all PPS (indoor rig and outdoor rig) followed normal distributions from the one-sample Kolmogorov-Smirnov test with $\alpha > 0.05$ (Table 5-3).

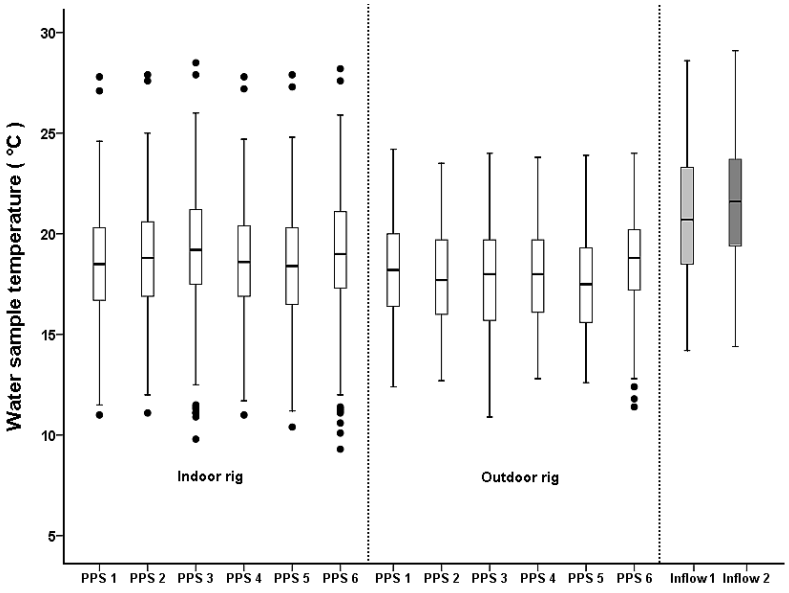

Figure 5-2: Water sample temperatures (°C) for inflow 1 (gully pot liquor), inflow 2 (gully pot liquor and dog faeces) and outflow for the indoor and outdoor bins. The plots represent the 25th percentile, median and the 75th percentile. The whiskers represent the 10th and 90th percentiles; solid circles represents outliers (March 2008 to April 2010, n = 113).

5.4.2 pH

pH measures the fraction of hydrogen (H^+) and hydroxyl (OH^-) ions within water quality determining the acidity or alkalinity state. pH as discussed earlier in the experimental methods section is closely linked to the biological productivity within an ecosystem. Alterations in pH may not give sound indications of contamination within the pavement systems but can sometimes be signs of poor water treatment or water pollution. The average pH for inflow 1 and inflow 2 were 7.14 ± 0.49 and 7.29 ± 0.43 (Table 5-1). pH values ranged for the gully pot mixture (inflow 1) from 6.19 to 8.76 and for the gully pot and dog faeces mixture (inflow 2) from 6.42 to 8.49 (Table 5-1). Figure 5-3 illustrates the box and whiskers plots for PPS 1 to PPS 6, indoor and outdoor rigs. It can be seen that pH values for the indoor rig varied from (6.6 to 8.4) and (6.3 to 7.7) for the indoor and outdoor rig respectively. pH outflow distributions followed normality from the one-sample Kolmogorov-Smirnov goodness-of-fit test for PPS 2, PPS 3, PPS 5 and PPS 6 from the indoor rig and PPS 1, PPS 3, PPS 4 and PPS 5 from the outdoor rig ($\alpha > 0.05$) Table (5-3). Generally, pH

values remained unaltered with small variations when compared to the influent urban runoff. Legret *et al.,* (1996) showed that pH did not vary from the inflow and outflow of pervious pavements from a 4-year urban runoff water quality analysis and the pH values were close to neutrality. Collins *et al.,* (2008) showed that there was no mobilization of pH from permeable pavement subsurface drainage and the pavement structure acts as a pH buffer within the range of 6-9.

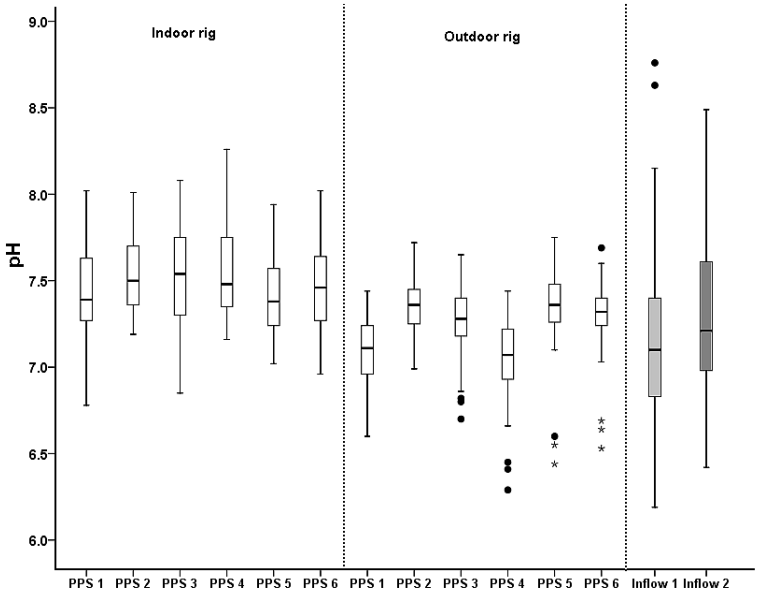

Figure 5-3: pH values for inflow 1 (gully pot liquor), inflow 2 (gully pot liquor and dog faeces) and outflow for the indoor and outdoor bins. The plots represent the 25th percentile, median and the 75th percentile. The whiskers represent the 10th and 90th percentiles; solid circles represents outliers and stars represents extreme outliers (March 2008 to April 2010, n = 113).

There was a significant difference between the indoor pH values and the outdoor pH values ($p < 0.01$) (Table 5-1). The pairwise Anova comparisons between heating and cooling cycles for PPS 1, 2, 4 and 5, pH values were also significantly different ($p<0.01$) (Table 5-5). Furthermore from the combined system approach (indoor and outdoor rigs), there were significant differences between the treatment of inflows 1 versus 2 (PPS 1 vs. PPS 2) and (PPS 4 vs. PPS 5) and the presence of geotextiles membranes versus geocomposites (PPS 1 vs. PPS 4) and (PPS 2 vs. PPS 5) ($p < 0.05$) (Table 5-5). Moreover, the integration of GHP showed no significant difference between (PPS 2 vs. PPS 3) and (PPS 5 vs. PPS 5) for pH outflow measurments. In addition, all pH effluent values met both the U.S. EPA, (2004)

guidelines for non-potable water reuse (EPA/625/R-04/108) U.S EPA and the European Commission Environment, (1991) urban wastewater treatment directive (91/271/EEC) standards.

5.4.3 Electroconductivity

Electroconductivity is a function of the concentration of dissolved ions present within the water sample. It is used to indicate high domestic or industrial discharges for water and wastewater treatment and indicates water quality problems. From Table (5-1) inflow 1 and inflow 2 had a mean electroconductivity of 455.87 μS/cm ± 138.49 μS/cm and 584.29 ± 127.07 μS/cm respectively. The influent urban runoff electroconductivity ranged from 339.86 μS/cm to 1065.18 μS/cm for the gully pot liquor (inflow 1) and 362.27 μS/cm to 982.66 μS/cm for the gully pot and dog faeces mixture (inflow 2) respectively (Table 5-1). Higher electroconductivity values were observed during the winter periods where deicing and salting of the roads occurred. Figure (5-4) illustrates the box and whiskers plots for effluent electroconductivity for the two-year period. Indoor rig (PPS 1 to PPS 6) mean outflow concentrations ranged from 166 μS/cm to 172 μS/cm respectively, with an overall reduction rate of (60 to 70%) and outdoor rig (PPS 1 to PPS 6) average outflow concentrations ranged from 120 μS/cm to 180 μS/cm respectively, with an overall reduction of (58 % to 77 %). One-sample Kolmogorov-Smirnov goodness-of-fit test for normality showed that only PPS 2 (outdoor rig) followed a normal distribution for electroconductivity effluent measurements ($\alpha > 0.05$).

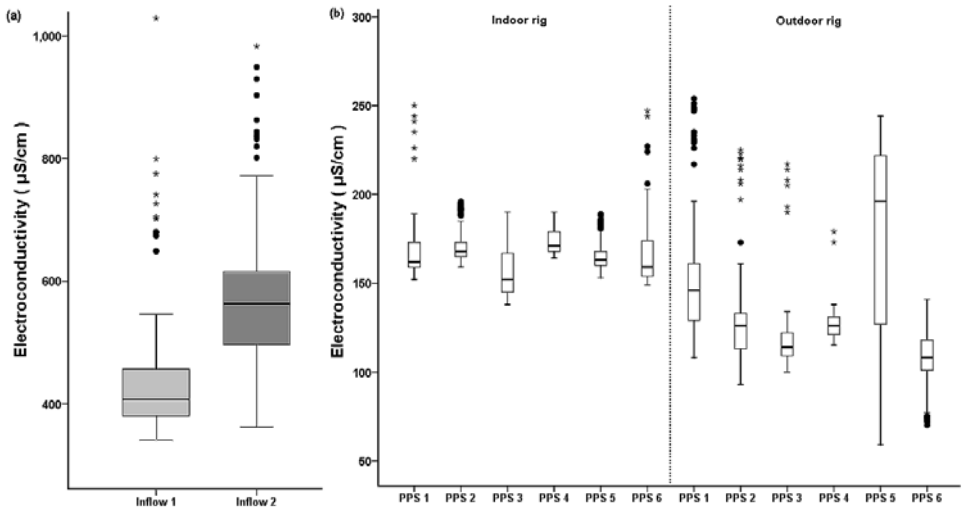

Figure 5-4: Electroconductivity concentrations for inflow 1 (gully pot liquor) and inflow 2 (gully pot liquor and dog faeces) (a) and outflow for the indoor and outdoor bins (b). The plots represent the 25th percentile, median and the 75th percentile. The whiskers represent the 10th and 90th percentiles (March 2008 to April 2010, n = 113).

Figure (5-5) (a) and (b) illustrates the mean and standard deviation removal rates throughout the biannual cooling and heating cycles for the indoor rig and outdoor rig respectively. It can be seen for the indoor rigs, mean removal efficiencies for PPS 1-PPS 6 followed a (69-70%)$^{1\text{-}I}$; (60%)$^{2\text{-}I}$; (63-65%)$^{3\text{-}I}$; (67-70%)$^{4\text{-}I}$; (61-62%)$^{5\text{-}I}$ and (61-62%)$^{6\text{-}I}$. The outdoor rigs periodic removal efficiencies during the cooling and heating cycles also performed relatively well in reducing electroconductivity with mean removal efficiencies ranging for (PPS 1 to PPS 6) (66-77%)$^{1\text{-}O}$; (65-74%)$^{2\text{-}O}$; (70-74%)$^{3\text{-}O}$; (75-79%)$^{4\text{-}O}$; (48-74%)$^{5\text{-}O}$ and (74-76%)$^{6\text{-}O}$.

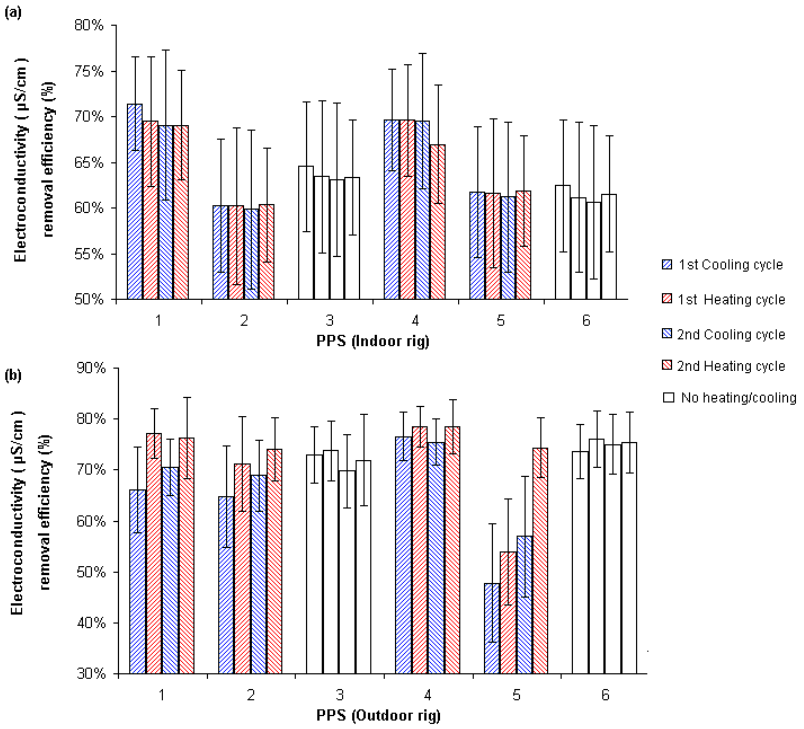

Figure 5-5: Mean removal efficiencies with error bars for electroconductivity during the 1st Cooling Cycle (April to September 2008), 1st Heating Cycle (October 2008 to March 2009), 2nd Cooling cycle (April to September 2009) and 2nd Heating cycle (October 2009 to April 2010) for indoor rig (a) and outdoor rig (b) (PPS1 to PPS 6) respectively.

There were no significant differences from the one-way Anova analysis between the effluent electroconductivity concentrations for indoor and outdoor rigs ($p > 0.05$). Table (5-4). The pair-wise Anova comparison between heating and cooling cycles for PPS 1, PPS 2, PPS 4 and PPS 5 also showed no statistical variation ($p > 0.05$) (Table 5-5). However, for the pair-wise comparison for combined (indoor and outdoor rigs) there were significant differences in the outflow measurement for electroconductivity between PPS 1 vs. PPS 2 and PPS 4 vs. PPS 5 (type of urban wastewater treated), PPS 1 vs. PPS 4 and PPS 2 vs. PPS 5 (presence of geotextile membrane and geocomposite layers) ($p < 0.05$). However, no statistical differences occurred with electroconductivity outflow concentrations in the presence of GHPs (Table 5-5) ($p > 0.05$).

5.4.4. Redox potential

Redox potential measures the availability of electrons for exchange between water samples. When redox potential is positive, there is enough dissolved oxygen present to allow metals and organic matter to be oxidised (Weiner, 2008). As discussed previously (Chapter 4), redox potential estimates where the water samples undergo aerobic or anaerobic conditions.

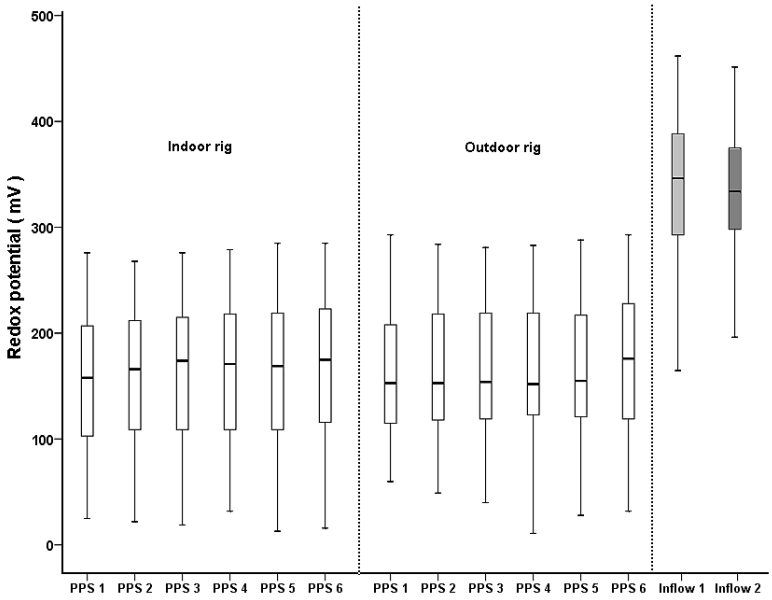

Figure 5-6: Redox potential concentrations for inflow 1 (gully pot liquor) and inflow 2 (gully pot liquor and dog faeces) and outflow for the indoor and outdoor bins. The plots represent the 25th percentile, median and the 75th percentile. The whiskers represent the 10th and 90th percentiles (March 2008 to April 2010, n = 113).

Presented in Table (5-1), inflows 1 and 2 redox potential measurements varied from 162 mV to 459 mV and 196 mV to 451 mV. Average redox potential readings were 336.58 ± 66.18 and 332.51 ± 52.47 for inflow 1 and inflow 2 respectively (Table 5-1). Figure (5-6) illustrates the box and whiskers plots for the influent and effluent measurement for (PPS 1 to PPS 6) indoor and outdoor rigs respectively. Mean redox potential outflow concentrations over the two-year period were (155 mV to 166 mV) and (158 mV to 166 mV) for the indoor and outdoor rigs respectively. Overall Mean removal efficiency for the two-year period ranged from (51 to 54 %) and (48 to 51 %) for the indoor and outdoor experimental bins. The effluent water

mean outflow shows a high positive redox potential, which indicates the aerobic state present within the pavement system. One-sample Kolmogorov-Smirnov test of normality showed $\alpha > 0.05$ for all experimental bins which followed a normal distribution for redox potential effluent concentrations.

Figure (5-7) illustrates the mean and standard deviation removal rates for the biannual cooling and heating cycles. It can be seen that the indoor rig (PPS 1 to PPS 6) followed a (49- 57%)$^{1\text{-}I}$; (50 -55)$^{2\text{-}I}$; (51-55)$^{3\text{-}I}$; (47-54%)$^{4\text{-}I}$; (50-56%)$^{5\text{-}I}$ and (50-57%)$^{6\text{-}I}$. The outdoor rigs periodic removal efficiency illustrated in (Figure 5-6) from the outdoor rig (PPS 1 to PPS 6) during the semiannual geothermal cooling and heating cycles showed a (43-59%)$^{1\text{-}O}$; (41-57%)$^{2\text{-}O}$; (39-58%)$^{3\text{-}O}$; (38-58%)$^{4\text{-}O}$; (41-62%)$^{5\text{-}O}$ and (39-57%)$^{6\text{-}O}$.

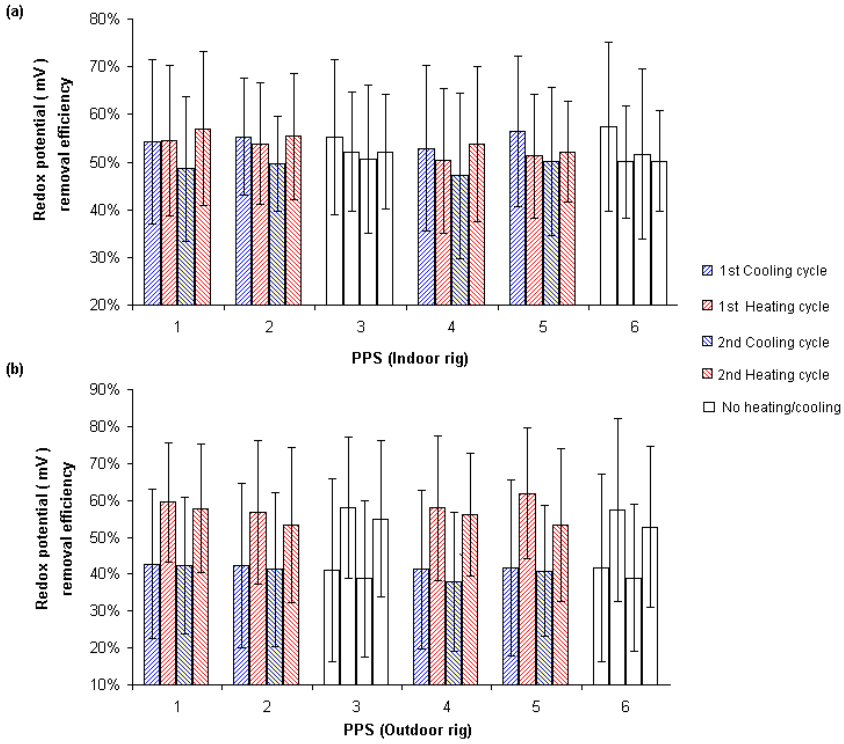

Figure 5-7: Mean removal efficiencies with error bars for redox potential during the 1st Cooling Cycle (April to September 2008), 1st Heating Cycle (October 2008 to March 2009), 2nd Cooling cycle (April to September 2009) and 2nd Heating cycle (October 2009 to April 2010) for indoor rig (a) and outdoor rig (b) (PPS1 to PPS 6) respectively.

One way Anova showed no statistical variation between indoor and outdoor rigs effluent redox potential measurements ($p > 0.05$) (Table 5-4). Pair-wise Anova comparison between the heating and cooling cycles (PPS 1, 2, 4 and 5) for the indoor

and outdoor rigs showed significant differences for redox potential outflow ($p < 0.05$) (Table 5-6). This occurred as a result of the outdoor rigs having almost a 10% difference for redox potential removal for the heating cycle. There were no statistical variations in pavement design (presence of geotextiles or GHPs) and the type of urban wastewater being treated with regards to effluent redox potential measurements ($p > 0.05$) (Table 5-5).

5.4.5 Sediments (Total dissolved solids, suspended solids and turbidity)

5.4.5.1 Total dissolved solids (TDS)

Elevated TDS concentrations are not hazardous to health but regulated from an aesthetic rather than health point of view. It is also used as an aggregate indicator of the presence of a broad array of chemical contaminants as discussed previously. Presented in Table (5-1), are the mean concentrations of TDS inflows 1 and 2 corresponding to 249.35 ppm ± 50.28 ppm and 281.15 ± 51.15 ppm respectively. TDS concentrations ranged from 210 ppm to 450 ppm and 219 ppm to 477 ppm for the gully pot liquor (inflow 1) and gully pot mixed with dog faeces mixture (inflow 2) (Table 5-1). Urban runoff stormwater generally has a TDS < 1000 ppm (US EPA, 2003). Figure (5-8) illustrates the box and whiskers plots for the 2-year period effluent TDS concentrations for indoor and outdoor rigs respectively. With regards to the indoor rig (PPS 1- PPS 6), effluent concentrations ranged from 61 to 91 ppm with a corresponding mean removal efficiency of 66 % to 78 %. The outdoor rigs showed similar removal efficiencies for TDS where outflow concentrations from the pavement structures ranged from 81ppm to 101 pm with an average removal efficiency of 60 to 70 % respectively. Nkwonata and Ochieng, (2010) showed that the average removal of TDS from a roughing filter (gravel based) treating industrial wastewater in South Africa is approximately 94 %. Kazemi Yazdi and Scholz, (2008) stated that combined biofiltration (plants and gravel based filter) lined with geotextiles was able to remove TDS from 28 to 96 % treating runoff from a car park in Edinburgh.

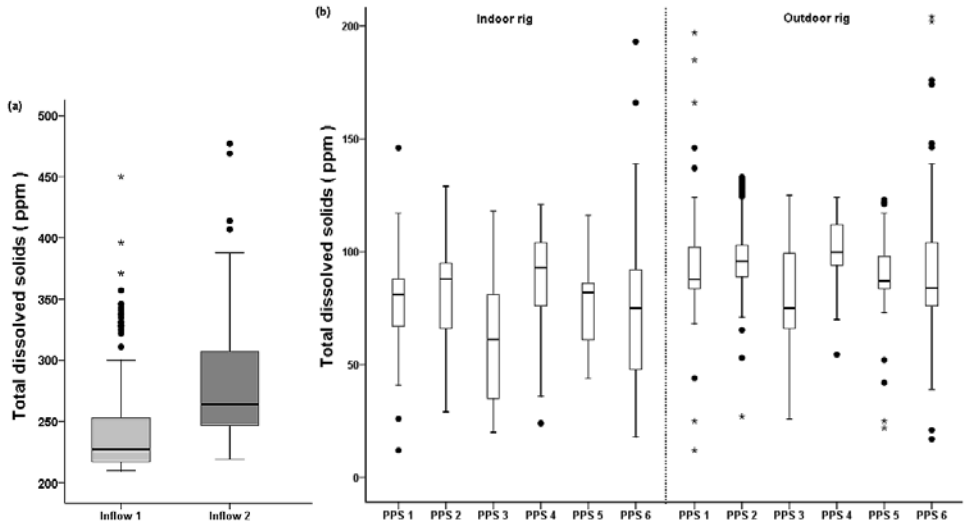

Figure 5-8: Total dissolved solids concentrations for inflow 1 (gully pot liquor) and inflow 2 (gully pot liquor and dog faeces) (a) and outflow for the indoor and outdoor bins (b). The plots represent the 25th percentile, median and the 75th percentile. The whiskers represent the 10th and 90th percentiles; solid circles represents outliers and stars represents extreme outliers (March 2008 to April 2010, n = 113).

The biannual cyclic (cooling and heating period) removal efficiencies for TDS are presented in Figure (5-9). With respect to the indoor rigs (PPS1 to PPS 6) showed removal efficiencies ranging from a (67-75%)$^{1\text{-}I}$; (63-73)$^{2\text{-}I}$; (72-86)$^{3\text{-}I}$; (62-72%)$^{4\text{-}I}$; (66-76%)$^{5\text{-}I}$ and (68-84%)$^{6\text{-}I}$. The results shown in Figure 5-6 from the outdoor rig (PPS 1 to PPS 6) during the semiannual geothermal cooling and heating cycles showed a (55-71%)$^{1\text{-}O}$; (50-64%)$^{2\text{-}O}$; (60-76%)$^{3\text{-}O}$; (56-69%)$^{4\text{-}O}$; (54-66%)$^{5\text{-}O}$ (55-75%)$^{6\text{-}O}$ removal efficiency.

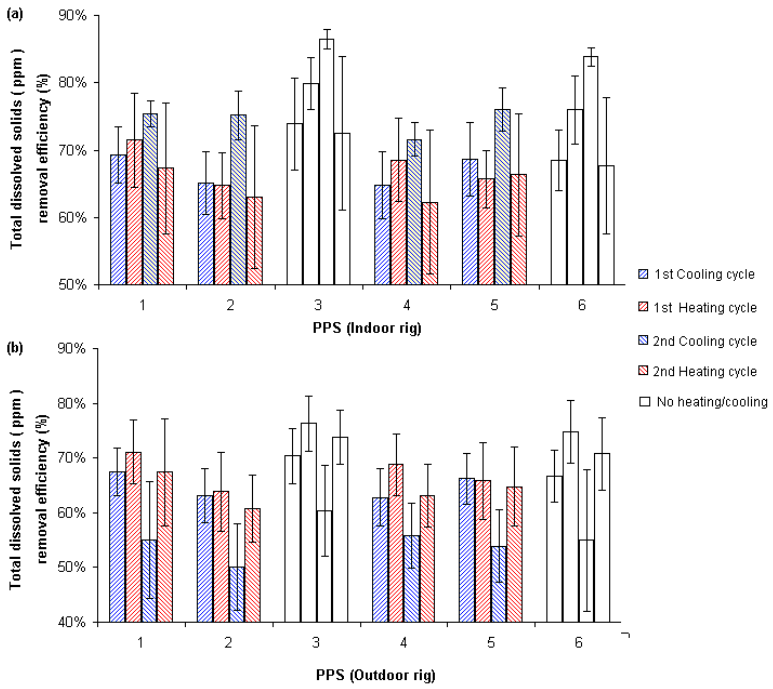

Figure 5-9: Mean removal efficiencies with error bars for total dissolved solids during the 1st Cooling Cycle (April to September 2008), 1st Heating Cycle (October 2008 to March 2009), 2nd Cooling cycle (April to September 2009) and 2nd Heating cycle (October 2009 to April 2010) for indoor rig (a) and outdoor rig (b) (PPS1 to PPS 6) respectively.

Anova analysis between the indoor rig and outdoor rigs for TDS effluent concentrations showed statistical variations ($p < 0.05$) (Table 5-4). Furthermore, variations in design factors for the pavement rigs such as the presence of geotextiles versus geocomposities (PPS 1 vs. PPS 4) and (PPS 2 vs. PPS 5), and the integration of GHP for (PPS 2 vs. PPS 3), and the type of urban stormwater being treated (PPS 4 vs. PPS 5) showed strong significant differences ($p < 0.01$). Nevertheless, comparisons between PPS 1 versus PPS 2 (treatment of different urban runoff) and PPS 5 versus PPS 6 (presence of GHPs) showed no statistical variations regarding outflow TDS concentrations (Table 5-5). However, there was no statistical variation between the heating cycles and cooling cycles for PPS 1, 2, 4 and 5 ($p > 0.05$) (Table 5-6).

5.4.5.2 Suspended solids

Water with high organic content typically consists of high suspended solids (SS); their *in-situ* decomposition can deplete levels of dissolved oxygen in the water, producing a critical oxygen shortage, which can lead to undesirable conditions for aquatic species as previously stated in Chapter 4.

Typical urban stormwater runoff SS concentrations are presented in Table (2-1), which ranges from 100 to 300 mg/l. However, typical composition of untreated domestic wastewater SS concentrations ranges from (120 to 1230 mg/l) (WHO, 2004; Metcalf and Eddy, 2007). From Table (5-1), SS concentrations for inflow 1 (gully pot liquor) and inflow 2 (gully pot liquor mixed with dog faeces) ranged from 10 to 440 mg/l and 30 to 1020 mg/l respectively. Average SS concentrations were 133 .32 mg/l ± 109.91 and 254.67 ± 179.69 (Table 5-1). This shows the large deviation for SS from the mean and concentration closely mimicked domestic urban wastewater rather than urban runoff stormwater.

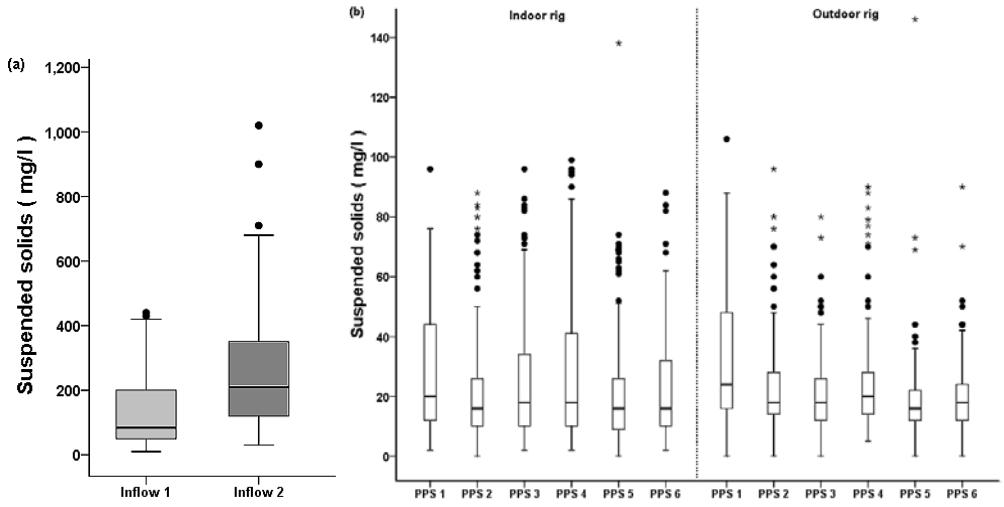

Figure 5-10: Suspended solids concentrations for inflow 1 (gully pot liquor) and inflow 2 (gully pot liquor and dog faeces) (a) and outflow for the indoor and outdoor bins (b). The plots represent the 25th percentile, median and the 75th percentile. The whiskers represent the 10th and 90th percentiles; solid circles represents outliers and stars represents extreme outliers (March 2008 to April 2010, n = 113).

Figure (5-10) presents the two-year influent and effluent concentrations of SS for (PPS 1- PPS 6) indoor and outdoor respectively. Mean effluent concentrations ranged from 23 to 28 mg/l for the indoor rig and 21 to 33 mg/l for the outdoor rig,

corresponding to an average removal rate of 72 to 86 % for the indoor systems and 73 to 84 % for the outdoor systems. Generally, SS met the US EPA guidelines for water reuse, which requires concentrations (< 30 mg/l). From the one sample Kolmogorov-Smirnov test of normality, (α <0.05) for all effluent concentrations, which states the outflow suspended solid concentrations did not follow a normal distribution. The overall reduction rate of SS from the pavement system is corroborated by Scholz and Grabowiecki, (2009). This finding is also supported by Kadurupokue and Jayasuriya, (2009) which showed a 95 % removal of suspended solids on a laboratory scaled PPS experiment. Permeable pavements have shown to cause a significant decrease in levels of suspended solids (> 90 %) (Pratt *et al.*, 1989; Pratt *et al*., 1995; James and Shahin, 1998; Brattebo and Booth, 2003; Collins *et al.,* 2008).

The mean biannual removal efficiencies during the cooling and heating cycles are presented in figure (5-10). For the indoor rig, (PPS 1 to PPS 6) showed removal efficiencies ranging from (76 - 90%)$^{1\text{-}I}$; (67-82%)$^{2\text{-}I}$; (62 -84%)$^{3\text{-}1}$;(79-94%)$^{4\text{-}I}$; (67-81%)$^{5\text{-}I}$ and (62-87%)$^{6\text{-}I}$. With respect to the outdoor rig, PPS 1-PPS 6 had a (66-86%)$^{1\text{-}O}$, (66 - 75 %)$^{2\text{-}O}$; (63 - 80 %)$^{3\text{-}O}$; (76 - 91% $^{4\text{-}O}$; (69 to 74 %)$^{5\text{-}O}$ and (71- 77 %)$^{6\text{-}O}$ removal efficiency between the cooling and heating periodic time (Figure 5-11).

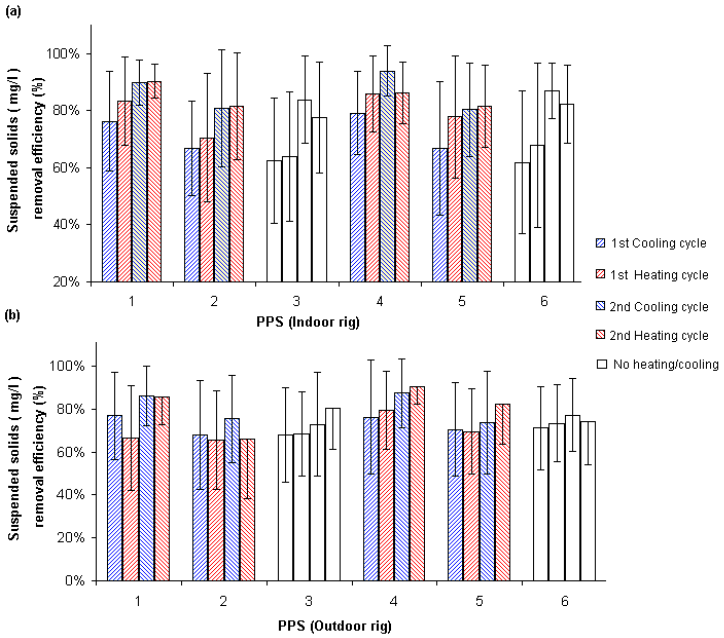

Figure 5-11: Mean removal efficiencies with error bars for suspended solids during the 1st Cooling Cycle (April to September 2008), 1st Heating Cycle (October 2008 to March 2009), 2nd Cooling cycle (April to September 2009) and 2nd Heating cycle (October 2009 to April 2010) for indoor rig (a) and outdoor rig (b) (PPS1 to PPS 6) respectively.

Anova statistical results showed that there was no statistical variation between indoor and outdoor rig effluent SS concentrations ($p > 0.05$) (Table 5-4). In addition, there were no statistical variations for the treatment of inflow 1 and inflow 2 (Table 5-4). However, the pair-wise statistical analysis between the heating and cooling cycles (PPS 1, 2, 4 and 5) indicated that the effluent concentrations were significantly different from each period ($p<0.01$) (Table 5-6). Effluent concentrations showed statistical differences between bins containing geotextiles versus bins with geocomposities (PPS 1 vs. PPS 4) and (PPS 2 vs. PPS 5) and variations between bins 5 and 6 with the varying design factor being the presence of GHP. Nevertheless comparisons between (PPS 2 vs. PPS 3) showed that the presence of GHP made no significant different to the effluent SS concentrations (Table 5-6).

5.4.5.3 Turbidity

Turbidity is often expressed collectively with suspended solids. This optical property cause by particle suspension in water is unlike SS because it expresses how much light is scattered by the water sample and not the weight of the suspended

material in the sample. The importance of turbidity is the potential of public health hazards regarding water reuse. The effectiveness of disinfection (chlorine, ultraviolet radiation and ozonation) largely depends on the disinfectant coming into contact with pathogenic organism. High turbidity values (>30 NTU) contains sediment particles in urban runoff which can shelter microorganisms and pathogens from disinfection. Table (2-1) shows typical turbidity values of urban stormwater runoff ranging from 110 to 340 NTU. Inflow 1 and inflow 2 concentrations ranged from (13 to 563 NTU) and (38 to 665 NTU) respectively (Table 5-1). Mean concentrations were 161.5 ± 127.76 and 274.63 ± 155.52 for inflows 1 and 2 respectively (Table 5-1). This shows a high variation between the two influent urban stormwater entering the pavement systems and shows high turbid conditions because of the extreme conditions of animal faeces and gully pot liquor composition.

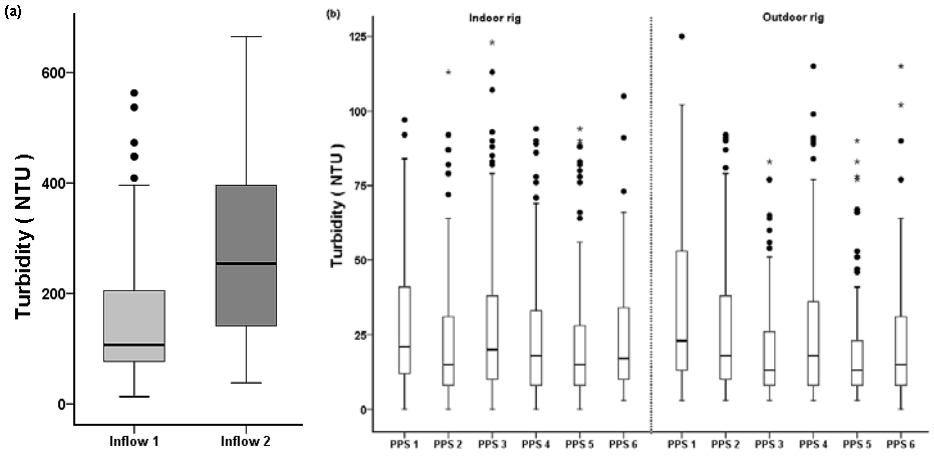

Figure 5-12: Turbidity concentrations for inflow 1 (gully pot liquor) and inflow 2 (gully pot liquor and dog faeces) (a) and outflow for the indoor and outdoor bins (b). The plots represent the 25th percentile, median and the 75th percentile. The whiskers represent the 10th and 90th percentiles; solid circles represents outliers and stars represents extreme outliers (March 2008 to April 2010, n = 113).

Figure (5-12) illustrates the box and whiskers plots with mean influent (a) and effluent (b) concentrations for PPS 1- PPS 6. Indoor rig outflow concentrations ranged from 24 to 29 NTU with a corresponding removal rate of 75 to 87 %. The outdoor rig (PPS 1-PPS 6) average outflow concentrations ranged from 19 to 34 NTU with a corresponding removal rate of (76 to 87 %). Effluent concentrations for turbidity with regards to the indoor and outdoor rigs did not follow a normal distribution ($\alpha < 0.05$) from the Kolmogorov-Smirnov test of normality. However, the

effluent concentrations did not meet the European Commission urban wastewater treatment directive standards (< 2 NTU) but met the US EPA guidelines for non-potable water reuse with regards to turbidity concentrations (< 30 NTU) (Table 5-2). This shows that permeable pavement systems are not designed for treating urban wastewater with high turbidity concentrations but shows extremely high reduction capabilities of turbidity. However, the standards set about by the US EPA and EU Urban Wastewater treatment directive are directed towards industrial process wastewater treatment plants and not urban drainage systems but merely used as a guide for water quality treatment.

Singhal *et al*. (2007) at The University of Auckland, New Zealand, examined the removal of sediments from a laboratory scaled pervious pavement setup and showed there was little effect of flow and sediment loading on particle retention from the effluent of the pavements, with tests showing sediment retention primarily occurred in the top 20 mm of the pavement column and retained sediments between 100–300 μm. Furthermore, Kim *et al.,* (2006) showed at the laboratory scale three permeable pavement rigs treating stormwater samples collected from Goyang-Si Gyeonggi-Do, Korea. Stormwater runoff showed had a mean concentration of 27 NTU reductions between the inflow and outflow with 70 % removal efficiency and found that turbidity is concentrated around the pavement void.

Figure (5-13) shows the biannual removal efficiencies of turbidity for the experimental bins undergoing geothermal cooling and heating applications and bins without GHPs. It can be seen for the indoor rig, (PPS 1 to PPS 6) the removal efficiencies ranged from (84 to 96 %)$^{1\text{-}I}$; (75 to 85 %)$^{2\text{-}I}$; (60 to 85 %)$^{3\text{-}I}$; (81 to 93 %)$^{4\text{-}I}$; relatively constant at (80%)$^{5\text{-}I}$ and (76 to 83 %)$^{6\text{-}I}$ respectively. Pertaining to the outdoor rigs (PPS 1 to PPS 6), periodic removal efficiencies ranged from (76 to 91 %)$^{1\text{-}O}$; (68 to 85 %)$^{2\text{-}O}$; (72 to 86 %)$^{3\text{-}O}$; (81 to 93 %)$^{4\text{-}O}$; (66 to 88 %)$^{5\text{-}O}$ and (68 to 81 %)$^{6\text{-}O}$ respectively.

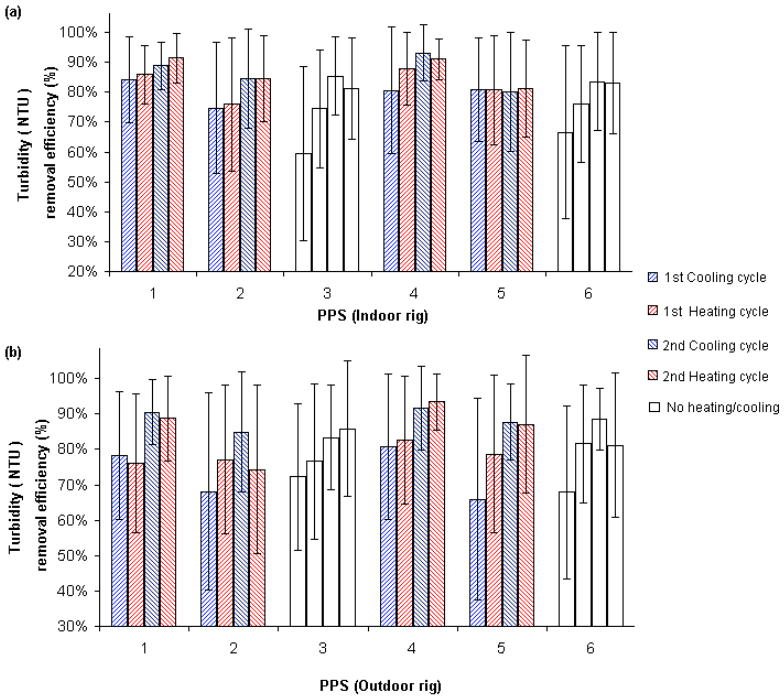

Figure 5-13: Mean removal efficiencies with error bars for Turbidity during the 1st Cooling Cycle (April to September 2008), 1st Heating Cycle (October 2008 to March 2009), 2nd Cooling cycle (April to September 2009) and 2nd Heating cycle (October 2009 to April 2010) for indoor rig (a) and outdoor rig (b) (PPS1 to PPS 6) respectively.

One-way Anova between indoor and outdoor rigs showed there was no statistical differences for turbidity effluent concentrations ($p>0.05$) and location of the bins and the environmental factors was invariant for the removal of turbidity (Table 5-4). Variations occurred between (PPS 1 and PPS 4), and (PPS 2 and PPS 5) which shows the design factor of the geotextile membranes resulted in significant differences for turbidity outflow concentrations ($p<0.01$) (Table 5-5). Nevertheless, the presence of GHPs or the type of urban runoff influent treated showed no statistical differences ($p >0.05$) (Table 5-5). Furthermore, Anova analysis showed strong statistical variations between the heating and cooling cycles ($p <0.01$) for turbidity outflow concentrations (Table 5-6).

5.4.6 Organic content (BOD, COD, DO)

5.4.6.1 Biochemical Oxygen Demand (BOD)

BOD measures the rate of biological organism uptake of oxygen and high levels of BOD (> 45 mg/l) are indications of poor water quality and are often associated with urban or industrial pollution. As presented in Table (2-1) typical BOD concentrations range from 10-15mg/l for urban runoff. Table (5-1) presents the mean influent BOD concentrations for inflow 1 (gully pot liquor) and inflow 2 (gully pot liquor mixed with dog faeces). Concentrations ranged from (8-97 mg/l) and (30-341 mg/l) for inflows' 1 and 2 respectively (Table 5-1). Mean BOD inflow concentrations were 29.84 ± 17.72 mg/l and 118.42 ± 77.18 mg/l for inflows' 1 and 2 respectively. It can be noted that typical concentrations of BOD from untreated domestic wastewater range from 110-350 mg/l (WHO, 2004; Metcalf and Eddy, 2007) which closely matches that of inflow 2, mimicking urban wastewater and not urban stormwater runoff. The standard error of the mean for inflow 2 (7.26 mg/l) shows the larger variation of the mean concentrations when compared to inflow 1 (1.66 mg/l) (Table 5-1). Figure (5-14) illustrates the box and whiskers plots for BOD inflow and outflow concentrations for indoor and outdoor rigs respectively. The BOD concentrations ranged from (2 - 3mg/l) and (4 - 5.8 mg/l) with corresponding removal efficiencies of (87- 97 %) and (75- 96 %) respectively (Figure 5-14). From the one-sample Kolmogorov-Smirnov test of normality, $\alpha < 0.05$ for all effluent BOD concentrations indicating that none followed normality.

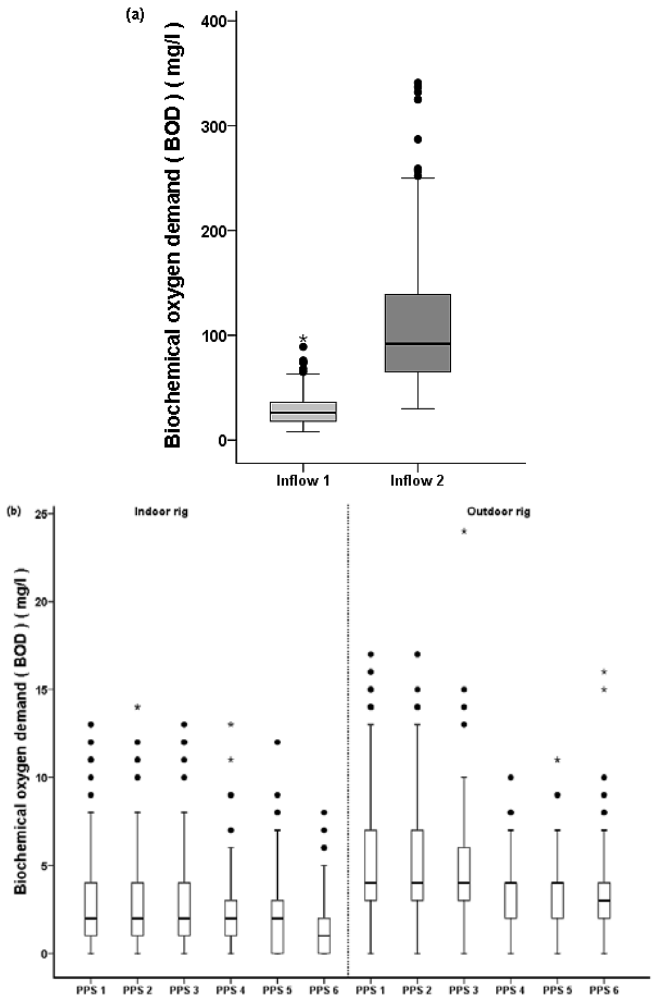

Figure 5-14: Biochemical oxygen demand concentrations for inflow 1 (gully pot liquor) and inflow 2 (gully pot liquor and dog faeces) (a) and outflow for the indoor and outdoor bins (b). The plots represent the 25th percentile, median and the 75th percentile. The whiskers represent the 10th and 90th percentiles; solid circles represents outliers and stars represents extreme outliers (March 2008 to April 2010, n = 113).

Biannual cyclic removal efficiencies (Figure 5-15) for indoor rigs (PPS 1 to PPS 6) ranged from (94 to 97 %)$^{1\text{-}I}$; (78 to 92 %)$^{2\text{-}I}$; (81 to 98 %)$^{3\text{-}I}$; (96 to 99 %)$^{4\text{-}I}$; (88 to 95 %)$^{5\text{-}I}$; and (89 to 95 %)$^{6\text{-}I}$. With regards to the outdoor rigs, average removal efficiencies throughout the cooling/heating cycles ranged from (92 to 94%)$^{1\text{-}O}$; (73 to 77 %)$^{2\text{-}O}$;(72 to 84 %)$^{3\text{-}O}$; (95 to 96 %)$^{4\text{-}O}$; (82 to 86 %)$^{5\text{-}O}$ and (82 to 86 %)$^{6\text{-}O}$. The overall reduction rate for BOD from the experimental results met the EC Commission Urban Wastewater Treatment Directive (< 25 mg/l) and the US EPA guidelines on water reuse (< 45 mg/l) and is corroborated by Scholz and Grobowiecki, (2009). Collins *et al.,* (2010) stated that mean BOD removal from a

PPS car park ranged from 60 to 80 %. The overall results agree with previous research conducted on multiple permeable pavement sites and laboratory based experiments. Macdonald and Jefferies, (2001) reported effluent concentrations of BOD (< 1.7 mg/l) from two different parking lots in Edinburgh, Scotland, constructed with permeable paving. Because of its functionality as an *in-situ* aerobic bioreactor (Pratt *et al.,* 1989, 1995, 1999; Coupe *et al.,* 2003; Coupe, 2004), BOD levels decrease and organic compounds decompose within PPS.

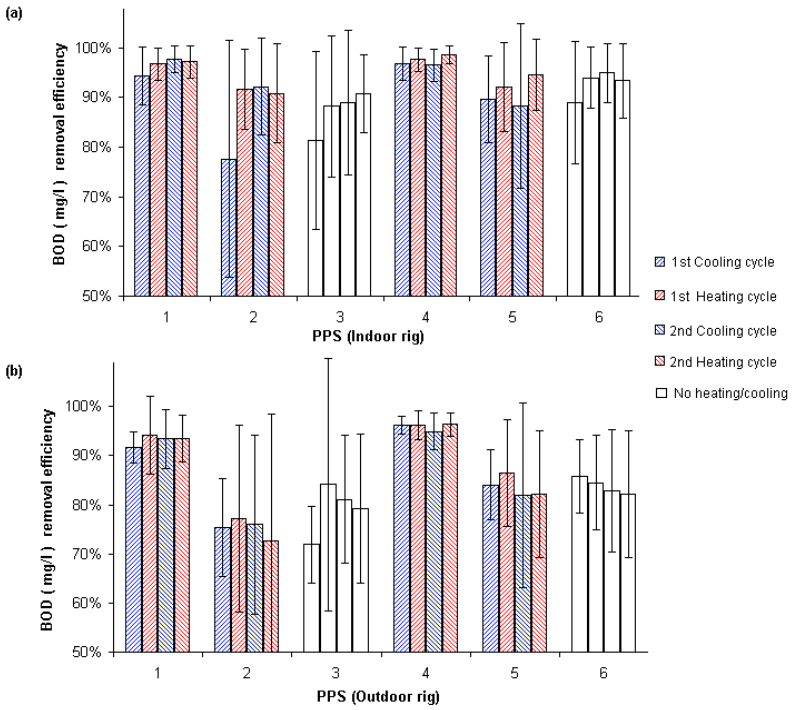

Figure 5-15: Mean removal efficiencies with error bars for Biochemical oxygen demand during the 1st Cooling Cycle (April to September 2008), 1st Heating Cycle (October 2008 to March 2009), 2nd Cooling cycle (April to September 2009) and 2nd Heating cycle (October 2009 to April 2010) for indoor rig (a) and outdoor rig (b) (PPS1 to PPS 6) respectively.

One-way Anova between indoor and outdoor rigs showed a strong statistical variation in effluent concentrations ($p < 0.01$) (Table 5-4). BOD effluent concentrations showed variations between (PPS 1 and PPS 4) and (PPS 2 and PPS 5) which represents the presence of geotextiles (PPS 4) and geocomposites (PPS 1). In addition, variations in concentrations of BOD occurred for (PPS 5 vs. PPS 6) ($p < 0.05$) and not (PPS 2 vs. PPS 3) ($p > 0.05$) which shows inconsistencies for BOD outflow concentrations when pavements systems are integrated with GHP.

Anova analysis between PPS 4 and PPS 5 which treated different types of runoff (inflows 1 and 2) saw statistical variations in BOD effluent concentrations ($p < 0.05$) but not (PPS 1 vs. PPS 2). However, during the heating and cooling cycles for PPS 1, PPS 2, PPS 4 and PPS 5, there were no statistical differences for BOD outflow concentrations ($p > 0.05$).

5.4.6.2 Chemical Oxygen Demand (COD)

COD is vital parameter for assessment of the quality of effluents from water prior to discharge from treatment. It measured the biodegradable organic matter. Typical concentrations range from 73-94 mg/l for urban runoff as shown in Table (2-1). Presented in Table (5-1) COD ranged from 27 to 267 mg/l and 71 to 747 mg/l for inflows 1 and 2 respectively. Domestic urban wastewater typical COD concentrations vary from 250 to 800 mg/l and shows once more that inflow 2 is closer to domestic urban wastewater characteristics rather than urban stormwater runoff (Metcalf and Eddy, 2007). Average COD influents were 86.68 ± 47.92 and 263.46 ± 167.83 for inflows 1 and 2 respectively (Table 5-1). Figure (5-16) shows the box and whiskers plot for the range of COD inflow and outflow concentrations from the pavement systems. Effluent COD for PPS 1 (outdoor rig) followed a normal distribution ($\alpha > 0.05$), however all other experimental bins outflow COD concentrations did not follow normality ($\alpha < 0.05$) from the one-sample Kolmogorov-Smirnov test.

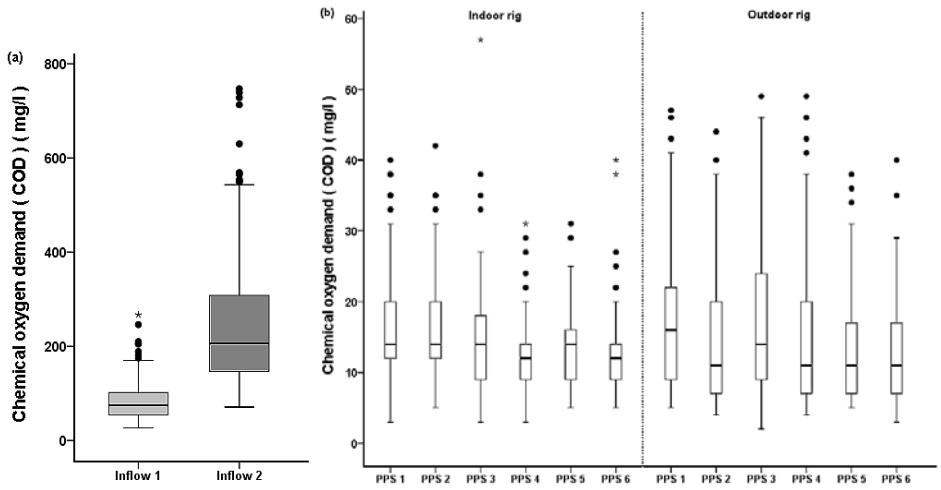

Figure 5-16: Chemical oxygen demand concentrations for inflow 1 (gully pot liquor) and inflow 2 (gully pot liquor and dog faeces) (a) and outflow for the indoor and outdoor bins (b). The plots represent the 25th percentile, median and the 75th percentile. The whiskers represent the 10th and 90th percentiles; solid circles represents outliers and stars represents extreme outliers (March 2008 to April 2010, n = 113).

Overall mean outflow concentrations ranged from 12-17 mg/l and 13-18 mg/l with corresponding removal efficiencies of 75-94 % and 74-92 % for indoor and outdoor rigs respectively. The outflow concentrations regarding COD removal met both the EU commission for urban wastewater treatment directive and the US EPA guidelines for water reuse throughout the analysis. Sorption of organic waste to colloidal solids within the pavement void matrix is a removal function of the pavement system. Angelakis and Bontoux, (2001) showed the effects of stormwater runoff quality was significantly improved (>46 %) when filtered through porous asphalted paving surfaces. Additionally, Berbee *et al.,* (1999) found that COD concentrations were 88 % lower from porous pavements (asphalt) when compared to urban runoff from conventional asphalt pavements. Likewise, stormwater that has infiltrated through porous pavement has been show to have an 80 - 90% reduction in chemical oxygen demand (COD) (Balades *et al.,* 1995). In aerobic processes, organic substances in the measurement of BOD and COD are oxidized into carbon dioxide, water, and new biomass cells are employed as a heterogeneous mixture of microorganisms with oxygen present. The water quality results from the research indicate that standalone PPS and combined PPS-GHP acts as *in situ* aerobic bioreactors and is effective in the treatment of concentrated urban runoff.

Biannual cyclic (cooling-heating period) mean removal efficiencies are illustrated in Figure (5-17). Indoor rigs ranged from (89-92 %)[1-I], (73-78%)[2-I]; (76-78%)[3-I]; (90-95 %)[4-I]; (78-82 %)[5-I]; and (78-80 %)[6-I]. With respect to the outdoor rig, mean removal efficiencies varied from (89 - 92 %)[1-O]; (73-84%)[2-O]; (70-77 %)[3-O]; (90-94 %)[4-O]; (79-82 %)[5-O] and (76-85 %)[6-O].

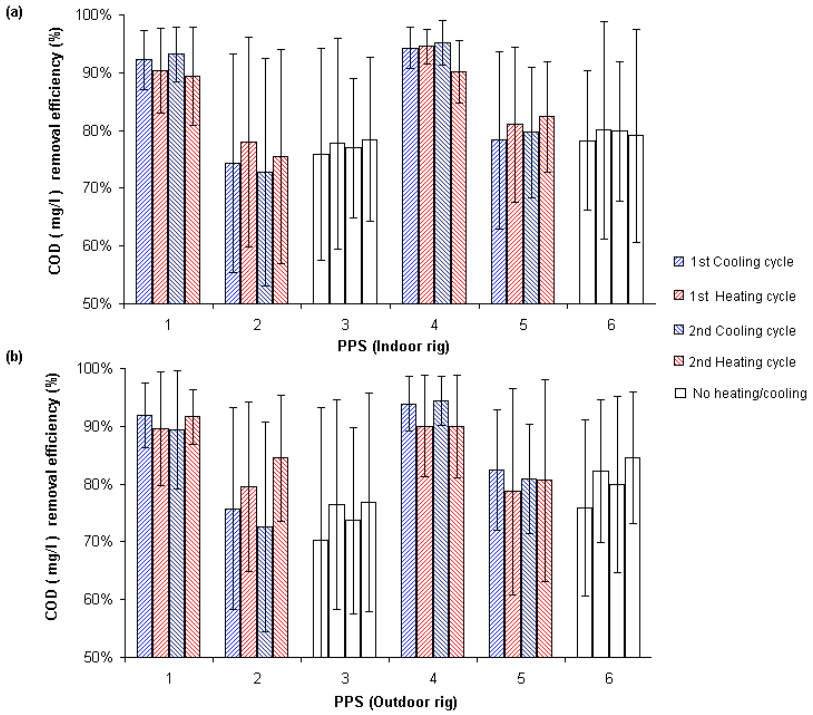

Figure 5-17: Mean removal efficiencies with error bars for Biochemical oxygen demand during the 1st Cooling Cycle (April to September 2008), 1st Heating Cycle (October 2008 to March 2009), 2nd Cooling cycle (April to September 2009) and 2nd Heating cycle (October 2009 to April 2010) for indoor rig (a) and outdoor rig (b) (PPS1 to PPS 6) respectively.

From Anova analysis, there was no statistical differences between the indoor rig and outdoor rig with respect to COD effluent concentrations ($p > 0.05$) (Table 5-4). The presence of geotextiles made a significant difference between (PPS 1 vs. PPS 4) and (PPS 2 vs. PPS 5) $p < 0.01$. The variations with the presence of GHP for (PPS 5 vs. PPS 6) also showed significant differences regarding COD concentrations. Nevertheless, this was not the case between (PPS 2 vs. PPS 3) which also contained GHP. There was no statistical variation for treating inflow 1 vs. inflow 2 ($p > 0.05$).

However, throughout the heating-cooling comparison, significant variations occurred ($p < 0.05$) (Table 5-6).

5.4.6.3 Dissolved Oxygen (DO)

Dissolved oxygen (DO) measures the health of water. There is a tendency for DO concentrations to range towards equilibrium or saturation in water. As a result of biological activity, changes in DO concentrations occur in addition to diffusion of the microscopic bubbles of oxygen gas (O_2). DO concentrations (< 1.5 mg/l) make water ecologically stressed for the survival of aquatic plants and wildlife (Bartram and Helmer, 1996). DO concentrations above (1.5 mg/l) are required to control odorous foul smells from water. An elevated level of DO (> 6mg/l) improves the taste of drinking water and removes bad odours (WHO, 2004).

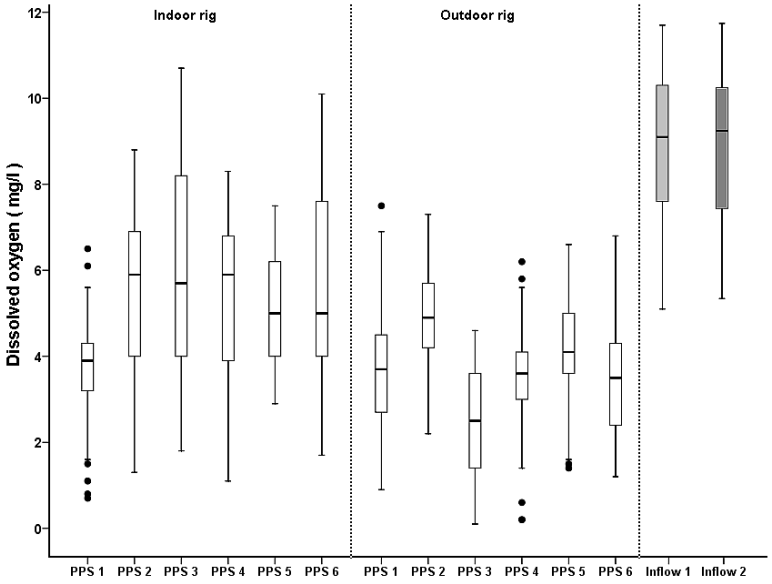

Figure 5-18: Dissolved oxygen concentrations for inflow 1 (gully pot liquor) and inflow 2 (gully pot liquor and dog faeces) and outflow for the indoor and outdoor bins. The plots represent the 25th percentile, median and the 75th percentile. The whiskers represent the 10th and 90th percentiles; solid circles represents outliers (March 2008 to April 2010, n = 113).

DO concentrations ranged from (5.10 to 11.70 mg/l) and (5.30 to 11.82 mg/l) for inflows 1 and 2 respectively (Table 5-1). Mean concentrations were 8.91± 1.58 mg/l with a standard error of the mean (0.15) and 8.92 ± 1.59 mg/l with a standard error of the mean (0.15) (Table 5-1). The lower DO concentrations can be accounted because of the location where urban runoff was selected (gully pots) where initial degradation of O_2 occurs. Figure (5-18) shows the range of DO concentrations from the box and whiskers plots. Mean DO for indoor and outdoor rigs ranged from (3.7 - 6.1 mg/l) and (2.5 - 4.9 mg/l) with corresponding deduction rates of (34 - 57 %) and (44 - 73%). All effluent DO concentrations followed a normal distribution ($\alpha > 0.05$) with the exception of PPS 4 and PPS 6 from the indoor rig ($\alpha < 0.05$) from the one sample Kolmogorov-Smirnov test (Table 5-3). However, the effluent concentrations did not meet the EC urban wastewater treatment directive and US EPA guidelines of DO concentrations ranging from 8-12 mg/l, but still produced odourless water quality (> 1.5 mg/l) according to the World Health Organisation standards (WHO, 2004).

Biannual reduction of DO throughout the cooling-heating period is illustrated in Figure (5-19). The indoor rig (PPS 1 to PPS 6) followed a (53-60 %)$^{1\text{-}I}$; (37-42 %)$^{2\text{-}I}$; (29-41 %)$^{3\text{-}I}$; (39-50 %)$^{4\text{-}I}$; (42-44%)$^{5\text{-}I}$; and (33-45 %)$^{6\text{-}I}$. With regards to the outdoor rig, mean removal efficiencies ranged from (51-63%)$^{1\text{-}O}$; (43-45 %)$^{2\text{-}O}$; (70-79 %)$^{3\text{-}O}$; (55-62%)$^{4\text{-}O}$; (48-54 %)$^{5\text{-}O}$ and (55-63 %)$^{6\text{-}O}$. The aerobic bioreactor conditions which resulted in high BOD and COD removal efficiencies is directly linked to the decrease in dissolved oxygen concentrations whereby microorganisms decompose the organic matter in the presence of oxygen, producing carbon dioxide. Aerobic treatment is a biological process occurring at the sub-base region of the PPS where the use of free or dissolved oxygen by microorganism (aerobes) degrades the organic waste present in the concentrated urban runoff. Since oxygen is available throughout the pavement system, aerobes acts as an electron acceptor and the biodegradation process is significantly accelerated (high BOD and COD reductions). The aerobic environment within PPS eliminates many pollutants present in stormwater (Pratt *et al.,* 1989, 1995, 1999) and the final discharge contains dissolved oxygen, which reduces the immediate oxygen demand on a receiving water body or prevents excessive aeration for improvement of the water quality from the pavement's effluent.

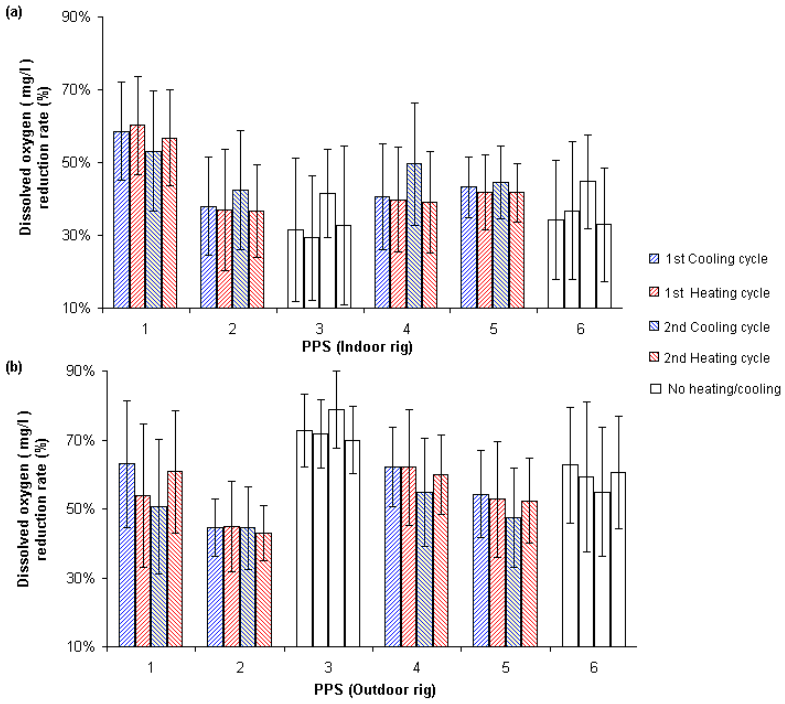

Figure 5-19: Mean removal efficiencies with error bars for Dissolved Oxygen during the 1st Cooling Cycle (April to September 2008), 1st Heating Cycle (October 2008 to March 2009), 2nd Cooling cycle (April to September 2009) and 2nd Heating cycle (October 2009 to April 2010) for indoor rig (a) and outdoor rig (b) (PPS1 to PPS 6) respectively.

From the Anova statistical analysis, between indoor and outdoor rigs there was no variation of DO effluent concentrations ($p > 0.05$) (Table 5-4). Furthermore, Variations in designs on the presence of geotextile (PPS 1 vs. PPS 4) and (PPS 2 vs. PPS 5), treatment of inflow 1 versus inflow 2, and the presence of GHP showed statistical variations ($p < 0.05$) (Table 5-5). Pair-wise Anova analysis between the heating and cooling cycles (PPS 1, 2, 4 and 5) showed a significant difference ($p<0.05$) regarding DO outflow concentrations. Increase in temperature (heating cycle) within water reduces its ability to retain oxygen molecules resulting in the variation of DO between geothermal heating and cooling periods.

5.4.7 Carbon Dioxide (CO_2)

Microbial activity within PPS and porous materials such as geotextiles has been measured under controlled and uncontrolled laboratory conditions (Newman *et al.,* 2002; Coupe *et al.,* 2003, Coupe, 2004). The determination of the CO_2 and/or O_2 produced allows the measurement for biological activity for the biodegradation processes occurring in PPS. Studies by Newman *et al.,* 2002; Neman, 2003; Coupe *et al.,* 2003; Coupe, 2004) showed that there are four major groups of protozoa mainly microflagellates, naked amoebae, testate amoebae and ciliates respiring producing CO_2 and responsible for the degradation of motor oil. The assessment of CO_2 evolution from microbiological activity present in soils can be made by respiration measurements using infrared gas analysers (Koizumi *et al.*, 1991).

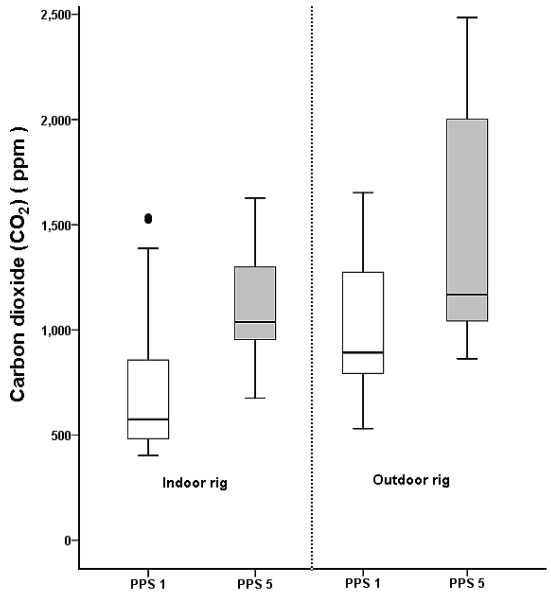

Figure 5-20: Carbon dioxide outflow concentrations for PPS 1 and PPS 5 (indoor and outdoor rig) The plots represent the 25th percentile, median and the 75th percentile. The whiskers represent the 10th and 90th percentiles; solid circles represents outliers (March 2008 to April 2010, n = 113).

Figure (5-20) shows the box and whiskers plots for CO_2 (ppm) evolution from PPS 1 and PPS 5 indoor and outdoor rigs respectively. Concentrations ranged from 403-1536 ppm and 526-1648 ppm for PPS 1 (indoor and outdoor), 676-1627 ppm, and 858-2481

ppm for PPS 5 (indoor and outdoor) respectively (Figure 5-20). One-way Anova showed a high significant difference ($p < 0.01$) between PPS 1 and PPS 5 for both indoor and outdoor rigs CO_2 produced respectively. The occurrence of higher concentrations of CO_2 (ppm) evolved for PPS 5 clearly demonstrates increased microbial activity in and around the geotextile level, when compared to the geocomposite layer in PPS 1. The results show that biodegradation does not only occur at the geotextile layer but evolves at a rapid rate when it is present. PPS 5 when compared to PPS 1 produced a higher percentage of approximately 35% CO_2. These findings are corroborated by Newman *et al.,* (2002); Coupe *et al.,* (2003); and Coupe, (2004) which showed that just above and beneath the geotextile layer within the PPS structure the highest volume of CO_2 is produced and O_2 is reduced which indicates a higher respiration rate for protozoa and aerobes in the biodegradation process of pollutants.

5.4.8 Nutrients (ammonia-nitrogen, nitrate-nitrogen and ortho-phosphate-phosphorous)

5.4.8.1 Ammonia-nitrogen (NH_4-N)

Total nitrogen in urban runoff comprises of organic nitrogen, ammonia-nitrogen, nitrite-nitrogen and nitrate-nitrogen. Nitrite (NO_2) is relatively short-lived in water and is quickly converted to nitrate (NO_3) by facultative bacteria, to a stable nitrogen form over a wide range of aquatic environmental conditions. The relationships are shown in equation (5-1) below.

$$\text{Total Nitrogen} = \text{Organic Nitrogen} + NH_4 + NO_3 + (NO_2 \Rightarrow NO_3) \qquad (5\text{-}1)$$

Ammonia-nitrogen composes of approximately two-thirds of the total nitrogen concentrations in domestic urban wastewater and urban runoff (Bartram and Helmer, 1996). NH_4 is toxic to aquatic organism and excessive concentrations in water contribute to eutrophication. Table (5-1) presents the ammonia-nitrogen concentrations which ranged from (0.06-6.60 mg/l) and (0.31-11.81 mg/l) for inflows 1 and 2 respectively. Mean concentrations were 0.99 ± 1.23 mg/l and 2.80 ± 2.18 mg/l for inflow 1 and 2 with corresponding standard error of the mean of 0.12 and 0.21 mg/l respectively (Table 5-1). As seen in Table (2-1) ammonia-nitrogen concentrations

from urban runoff ranges from 0.1-10mg/l, whilst average concentrations are approximately 25 mg/l from untreated urban domestic wastewater. Hence, the influent concentrations of NH_4 matched that of urban stormwater and not domestic wastewater.

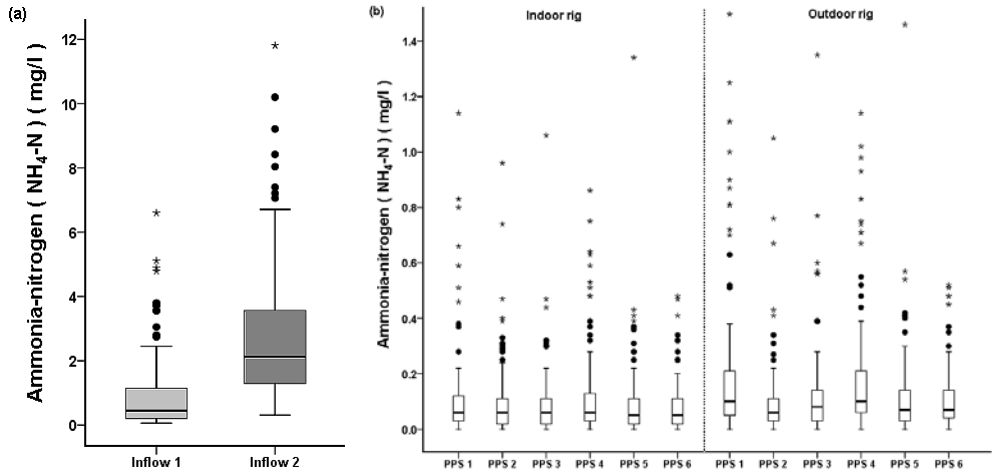

Figure 5-21: Ammonia-nitrogen concentrations for inflow 1 (gully pot liquor) and inflow 2 (gully pot liquor and dog faeces) (a) and outflow concentrations for the indoor and outdoor bins (b). The plots represent the 25th percentile, median and the 75th percentile. The whiskers represent the 10th and 90th percentiles; solid circles represents outliers and stars represents extreme outliers (March 2008 to April 2010, n = 113).

Figure (5-21) shows the box and whiskers plots for overall influent and effluent concentrations for NH_4-N (mg/l) from all experimental rigs. Mean effluent concentrations ranged from (0.09 - 0.12 mg/l) and (0.10 - 0.21 mg/l) with corresponding removal efficiencies of (78 - 94 %) and (74 - 90 %) for indoor and outdoor rigs respectively. From the one sample Kolmogorov-Smirnov test of normality (Table 5-3), no experimental bins effluent NH_4-N (mg/l) concentrations followed a normal distribution ($\alpha < 0.05$).

The biannual cyclic cooling-heating periods removal efficiency for the indoor rig (PPS 1 to PPS 6) followed (84-97 %)$^{1\text{-}I}$; (70-85 %)$^{2\text{-}I}$; (77-88 %)$^{3\text{-}I}$; (84-98 %)$^{4\text{-}I}$; (68-89%)$^{5\text{-}I}$ and (73-90%)$^{6\text{-}I}$ (Figure 5-22(a)) . With respect to the outdoor rig, removal efficiencies ranged from (81-96%)$^{1\text{-}O}$; (69-88 %)$^{2\text{-}O}$; (67-87 %)$^{3\text{-}O}$; (83-96 %)$^{4\text{-}O}$; (62-88 %)$^{5\text{-}O}$ and (67-88 %)$^{6\text{-}O}$ (figure 5-22(b)).

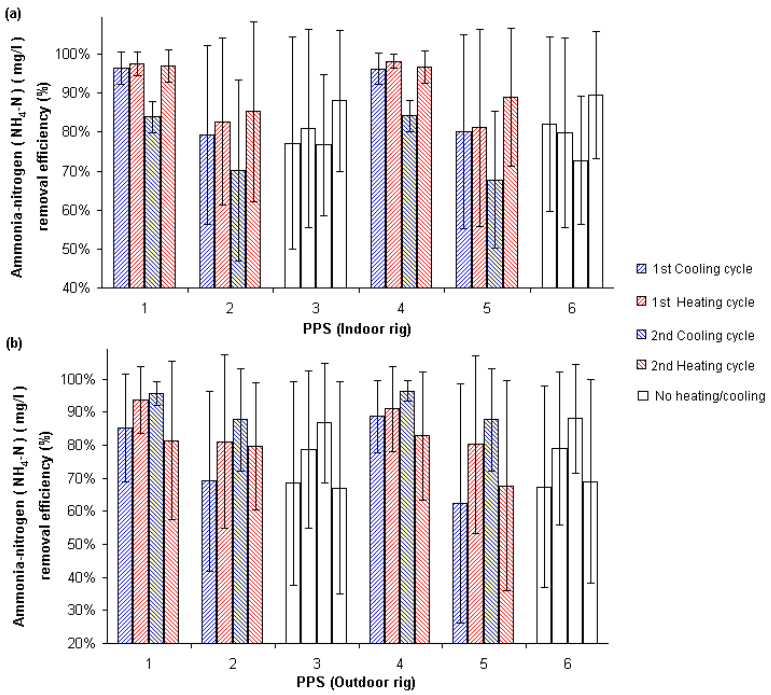

Figure 5-22: Mean removal efficiencies with error bars for Ammonia-Nitrogen during the 1st Cooling Cycle (April to September 2008), 1st Heating Cycle (October 2008 to March 2009), 2nd Cooling cycle (April to September 2009) and 2nd Heating cycle (October 2009 to April 2010) for indoor rig (a) and outdoor rig (b) (PPS1 to PPS 6) respectively.

Bean *et al.,* 2007 showed mean inflow runoff concentrations of NH_4-N > 0.35 mg/l reduced to < 0.05 mg/l with an average removal efficiency of 86 % through filtration and bacterial nitrification of ammonia levels within PPS. They (Bean *et al.,* (2007) showed for four permeable pavement sites in eastern North Carolina, USA, significantly reduced ($p < 0.05$) NH_4-N concentrations from stormwater runoff.

One-way Anova between indoor and outdoor rigs for the effluent NH_4-N (mg/l) concentrations showed statistical differences ($p < 0.05$) (Table 5-4). Furthermore, NH_4-N (mg/l) reductions saw significant variations between (PPS 1 vs. PPS 2) ($p < 0.05$) with the variable being the type of urban runoff being treated, however this was not the case for (PPS 4 vs. PPS 5) ($p > 0.05$) which had similar layouts and treated separately inflows 1 and 2 (Table 5-5). Once more, the presence of geotextiles made a significant contribution for the removal of NH_4-N (mg/l) with regards to (PPS 1 vs. PPS 4) and (PPS 2 vs. PPS 5) ($p < 0.05$). The statistical analysis between the heating and cooling cycles (PPS 1, 2, 4 and 5) also showed significant differences for effluent NH4-N (mg/l) concentrations ($p < 0.05$) (Table 5-6).

5.4.8.2 Nitrate-Nitrogen (NO_3-N)

Nitrate-nitrogen in freshwater can cause oxygen depletion, with higher concentrations due to pesticides, fertilizers, decaying animals and vegetable matter and leachates from sludge. Denitrification is a dissimilatory microbial process that transforms NO_3^- to N_2O or N_2 gas, which is released to the atmosphere. Denitrification can involve the following reaction sequence, in which NO_3^- is used as a terminal electron acceptor (Chin, 2006):

$$NO_3^- \rightarrow NO_2^- \rightarrow NO \rightarrow N_2O \rightarrow N_2 \quad (5\text{-}2)$$

WHO, (2010) reports that the primary health concern to humanity regarding nitrate and nitrite is the formation of methaemoglobinaemia or "blue-baby syndrome". This occurs as nitrate is reduced to nitrite in the stomach of infants (< 3 months old) oxidizing haemoglobin (Hb) to methaemoglobin (metHb). The process precents oxygen transport around the body causing cyanosis and at higher concentrations asphyxia.

As shown in Table (2-1), typical nitrate-nitrogen concentrations vary from 0.01-10 mg/l in urban runoff. From Table (5-1) inflows, 1 and 2 NO_3-N (mg/l) concentrations ranged from 0.31-.13 mg/l and 0.08-9.76 mg/l respectively. Mean influent concentrations were (1.74 ± 1.20 mg/l) and (1.85 ± 1.46 mg/l) with a standard error of the mean (6.23 and 4.94 mg/l) for inflows 1 and 2 in that order (Table 5-1). The inflow concentrations lie within the range of typical NO_3-N concentrations for urban runoff (Table 2-1).

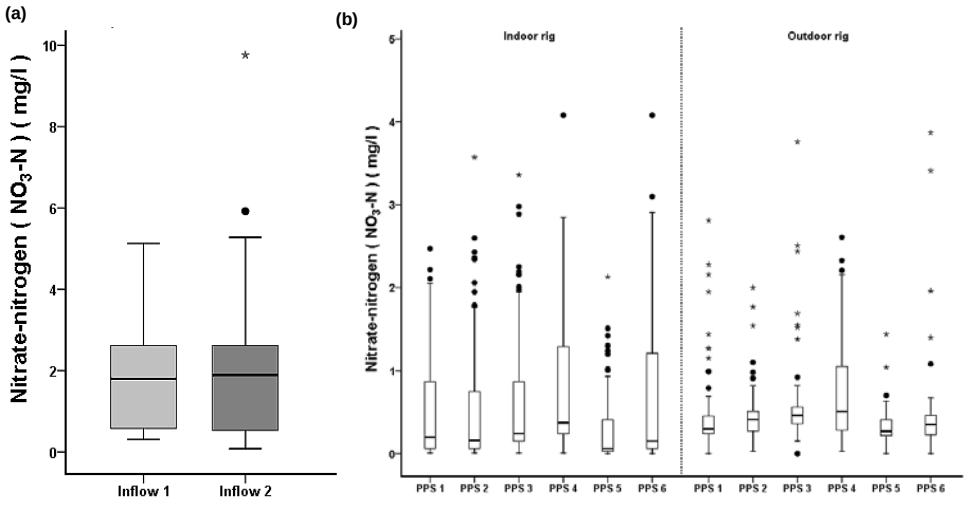

Figure 5-23: Nitrate-nitrogen concentrations for inflow 1 (gully pot liquor) and inflow 2 (gully pot liquor and dog faeces) (a) and outflow concentrations for the indoor and outdoor bins (b). The plots represent the 25th percentile, median and the 75th percentile. The whiskers represent the 10th and 90th percentiles; solid circles represents outliers and stars represents extreme outliers (March 2008 to April 2010, n = 113).

From the box and whiskers plots illustrated in Figure (5-23), mean outflow concentrations ranged from (0.29 - 0.77 mg/l) and (0.32 - 0.69 mg/l) for indoor and outdoor rigs with corresponding removal efficiencies of (54 - 83 %) and (52 - 71 %). The lower removal rates of NO_3-N are a result of NH_4-N transformations to NO_3-N due to nitrification (Scholz and Grabowiecki, 2009). However, like ammonia-nitrogen, nitrate-nitrogen is removed via adsorption and denitrifictaion. NH_4-N and NO_3-N is also assimilated by microorganisms within urban drainage systems (Collins *et al.,* 2010). Paggotto *et al.,* (2000) reported a 68.7 % and 73.0 % removal of NO_3-N and NH_4-N in Nantes, France where porous asphalt 30 mm thick was compared to conventional asphalt and found that the main phenomenon responsible for the retention of these pollutants by porous pavements was the filtering function. Carles river watershed association in Weston, Massachusetts, USA noted that permeable pavements are effective in eliminating nitrate-nitrogen (> 30 %). Gilbert and Claugen, (2006) compared the stormwater runoff quality and quantity from porous asphalt, permeable pavements and crushed stones for driveways in Waterford, Connecticut, USA. Mean inflow of NO_3-N was 0.6 mg/l, NH_4-N (0.18 mg/l) and total phosphorous (0.24 mg/l), the study found that permeable pavement driveways contained a significantly lower concentration of the measured pollutants (> 80 % removal rate, $p < 0.05$).

The combined NH_4-N and NO_3-N concentrations multiplied by a factor of 2 is still less than the required concentrations from the EC urban wastewater treatment directive (< 15mg/l) and the US EPA guidelines for non-potable water reuse (< 30 mg/l) which shows the benefits of SUDS schemes such as PPS in retaining and removing nutrients present in urban stormwater runoff.

The biannual removal efficiencies during the geothermal cooling and heating applications for the indoor rig (PPS 1 to PPS 6) illustrated in Figure 5-24 ranged from (65-77 %)$^{1\text{-}I}$; (60-77 %)$^{2\text{-}I}$; (60-64 %)$^{3\text{-}I}$; (47-64 %)$^{4\text{-}I}$; (78-91 %)$^{5\text{-}I}$ and (57-81 %)$^{6\text{-}I}$. With respect to the outdoor rigs, removal efficiencies ranged from (48-81 %)$^{1\text{-}O}$; (31-82 %)$^{2\text{-}O}$; (23-80 %)$^{3\text{-}O}$; (36-69 %)$^{4\text{-}O}$; (51-89 %)$^{5\text{-}O}$ and (54-83 %)$^{6\text{-}O}$. From the one-sample Kolmogorov-Smirnov test, ($\alpha < 0.05$) for all experimental bins (indoor and outdoor rig) NO_3-N concentrations and therefore did not follow normality.

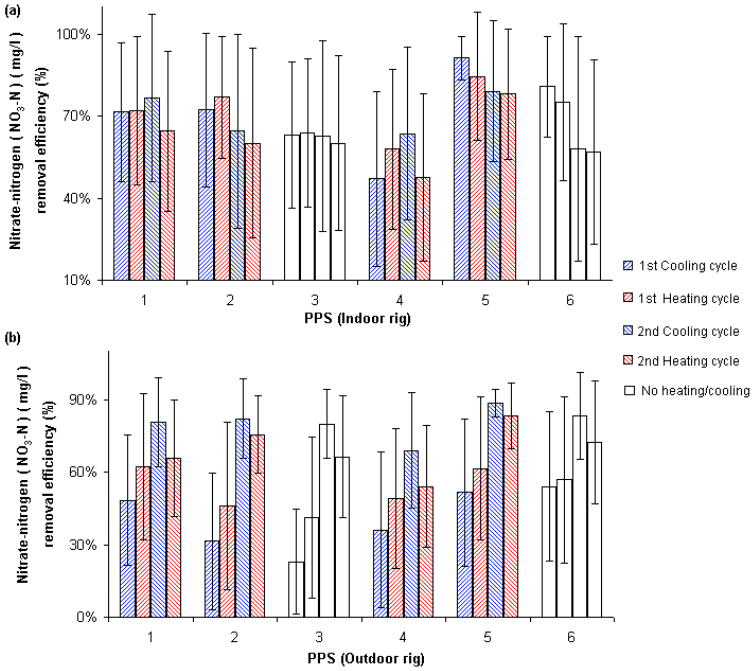

Figure 5-24: Mean removal efficiencies with error bars for Nitrate-Nitrogen during the 1st Cooling Cycle (April to September 2008), 1st Heating Cycle (October 2008 to March 2009), 2nd Cooling cycle (April to September 2009) and 2nd Heating cycle (October 2009 to April 2010) for indoor rig (a) and outdoor rig (b) (PPS1 to PPS 6) respectively.

From the one-way Anova analysis, between indoor and outdoor rigs as well as throughout the heating and cooling cycles (PPS 1, 2, 4 and 5) there was no significant variation for NO_3-N (mg/l) effluent concentrations ($p > 0.05$) (Table 5-4

and Table 5-6). Statistical variations occurred between (PPS 4 vs. PPS 5) for combined indoor and outdoor with regards to the NO_3-N effluent concentrations with the variable factor being the type of urban runoff being treated (inflow 1 and inflow 2) (Table 5-5). The presence of geotextile showed statistical variations in outflow concentrations between PPS 1 and PPS 4, as well as PPS 2 and PPS 3. Variations occurred for PPS 2 versus PPS 3 but not for PPS 5 versus PPS 6 with the variable factor being the presence of GHP (Table 5-5).

5.4.8.3 Ortho-Phosphate-Phosphorous

Phosphorous is a key metabolic nutrient in water and is available in relatively small amount in most unpolluted surface waters. Inorganic phosphates often reach waters in various effluents (synthetic detergents), pesticides and fertilizers. Excessive concentrations of phosphorous affects aquatic ecosystems and can cause eutrophication with high blue-green algae productivity and nutrient enhancement as previously discussed.

From (Table 2-1), total phosphorous ranges from 0.1 - 5mg/l in concentration for urban runoff. The average concentration of total phosphorous in wastewater ranges from 10 - 25 mg/l (Metcalf and Eddy, 2007). Influent concentrations of ortho-phosphate-phosphorous ranged from 0.15 - 4.15 mg/l and 0.66- 30.0 mg/l for inflows 1 and 2 respectively (Table 5-1). The extreme outliers from 20 to 30.0 mg/l can be as a result of detergents settling into one of the gully pots where sampling occurred or the presence of dead decaying plants or animals. However, mean concentrations were (1.19 ± 0.97 mg/l) and (5.96 ± 7.16) for inflows 1 and 2. Corresponding mean standard error of the mean was 0.09 and 0.67 mg/l for inflows 1 and 2 (Table 5-1).

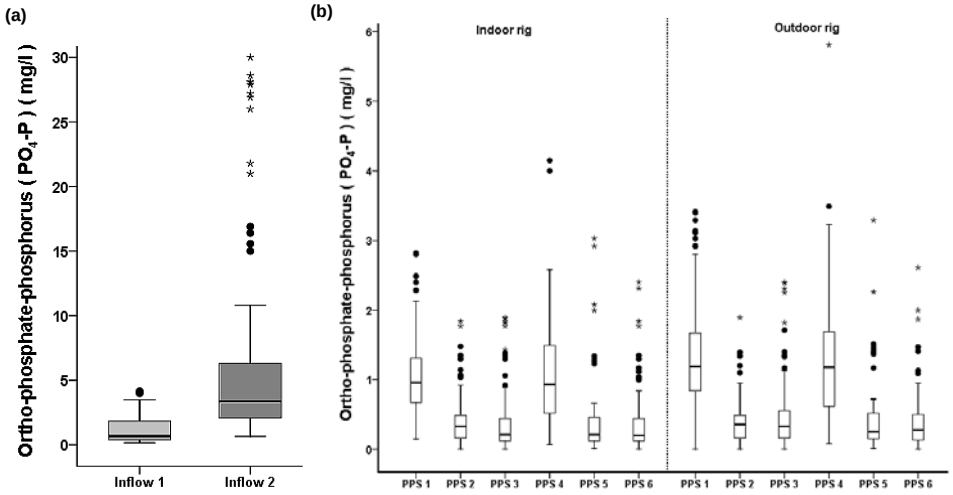

Figure 5-25: Ortho-phosphate-phosphorous concentrations for inflow 1 (gully pot liquor) and inflow 2 (gully pot liquor and dog faeces) (a) and outflow concentrations for the indoor and outdoor bins (b). The plots represent the 25th percentile, median and the 75th percentile. The whiskers represent the 10th and 90th percentiles; solid circles represents outliers and stars represents extreme outliers (March 2008 to April 2010, n = 113).

Overall inflow and outflow concentrations of PO_4-P are shown in Figure 5-25. Effluent concentrations ranged from (0.37-1.09 mg/l) and (0.39-1.37 mg/l) with corresponding removal efficiencies of (61 - 80 %) and (58 - 65 %) respectively. From the one-sample Kolmogorov-Smirnov test of normality, PPS 1 (outdoor) followed a normal distribution with regards to (PO_4-P) outflow concentrations ($\alpha > 0.05$). However, effluents from all other experimental systems for both indoor and outdoor rigs did not follow a normal distribution ($\alpha < 0.05$) (Table 5-3). Discharge limits for total phosphorous < 2mg/l, orthophosphates makes up approximately 70% of total phosphorous whilst polyphosphates contributed to the remaining 30 % (Metcalf and Eddy, 2007). From Table (5-2), 70 % of the EU urban wastewater treatment standards and US EPA non-potable water reuse guidelines gives an interpolated standard of <1.4 mg/l and <14 mg/l for PO_4-P respectively and shows that on average the effluent PO_4-P met the water quality requirements.

Water quality results from Bean *et al.,* (2007) supports high reduction of phosphorous concentrations from porous asphalted pavements. Results showed that mean removal efficiency of total phosphorous was > 42 % and orthophosphates > 63 % with effluent concentrations in the range of 0.01 - 0.28 mg/l and 0.03 - 0.98 mg/l at four sites in North Carolina, USA. Studies by Kim *et al.,* (2006) evaluated the effectiveness of concrete permeable pavements for water quality performances

regarding turbidity and nutrient removal (total nitrogen, NH_4-N, NO_3-N and total phosphorous). On average nutrients and turbidity were reduced to around 85 % from the water inflow and found that the suspended solids and phosphorus concentrated within the pavement voids (Kim *et al.,* 2006).

Biannual cyclic (geothermal heating/cooling) removal efficiencies for the indoor and outdoor rigs (PPS 1- PPS 6) are illustrated in Figure 5-26. The indoor rig followed a (60-69%)$^{1\text{-}I}$; (57-67%)$^{2\text{-}I}$; (65-73%)$^{3\text{-}I}$; (65-77%)$^{4\text{-}I}$; (64-73%)$^{5\text{-}I}$ and (66-70%)$^{6\text{-}I}$. Corresponding outdoor rig (PPS1 - PPS 6) removal efficiencies throughout the geothermal heating/cooling applications were (55-69%) $^{1\text{-}O}$; (49-65%)$^{2\text{-}O}$; (57-65%)$^{3\text{-}O}$; (48-70%)$^{4\text{-}O}$; (62-78%)$^{5\text{-}O}$; and (57-70%)$^{6\text{-}O}$. From figure 5-25, high removal efficiencies occurred for PPS 1, 2, 3 and 5 which contained GHPs and performed equivalently with PPS 3 and 6.

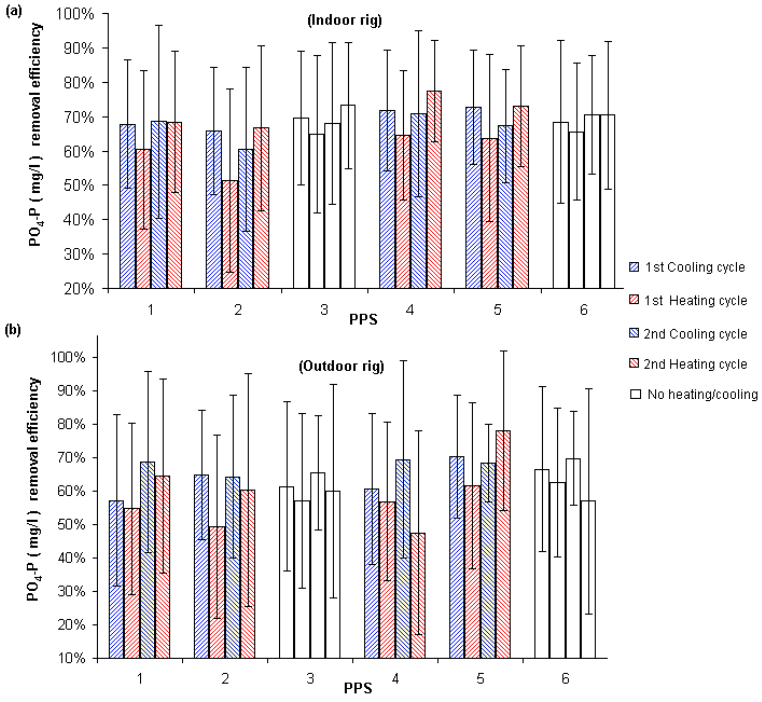

Figure 5-26: Mean removal efficiencies with error bars for Ortho-Phosphate-Phosphorous during the 1st Cooling Cycle (April to September 2008), 1st Heating Cycle (October 2008 to March 2009), 2nd Cooling cycle (April to September 2009) and 2nd Heating cycle (October 2009 to April 2010) for indoor rig (a) and outdoor rig (b) (PPS1 to PPS 6) respectively.

Statistical analysis between the indoor and outdoor rig regarding PO_4-P effluent concentrations saw a significant difference ($p<0.05$) (Table 5-4). With respect to the

different inflows being treated for similarly structured pavement systems, (PPS 1 vs. PPS 2) and (PPS 4 vs. PPS 5), there was a significant difference in the outflow concentrations ($p < 0.05$). Once more, the presence of a geotextile membrane played a significant role for PO_4-P retention with strong statistical variations between (PPS 1 vs. PPS 4) and (PPS 2 vs. PPS 5). Nevertheless, there was no significant differences throughout the heating and cooling cycles for PPS 1, 2, 3 and 5 regarding PO_4-P outflow concentrations ($p>0.05$) (Table 5-6).

5.4.9 Microbial pathogenic organisms

5.4.9.1 Escherichia Coli

Faecal coliforms are primarily 90 % *Escherichia coli* (Gerardi and Zimmerman, 2005). Typical ranges of *E.coli* bacterial cell colonies range from 10^2-10^7 CFU/100ml in urban runoff. According to the WHO, (2004) untreated domestic urban wastewater *E.coli* concentrations are around 10^3-10^8 CFU/100ml. As shown in Table (5-1), influent concentrations ranged from (1.8×10^3 to 9.3×10^4 CFU/100ml) and ($2.5 \times 10^3 - 9.3 \times 10^4$ CFU/100ml) for inflows 1 and 2 respectively. Mean concentrations were (1.88×10^4 CFU/100ml ± 1.68×10^4 CFU/100ml) and (3.62×10^4 CFU/100ml ± 1.91×10^4 CFU/) for inflows 1 and 2 in that order. Standard error of the mean was quite large for both inflows, showing the variation of *E.coli* concentrations entering the PPS (3.21×10^2 and 3.56×10^2) (Table 5-1).

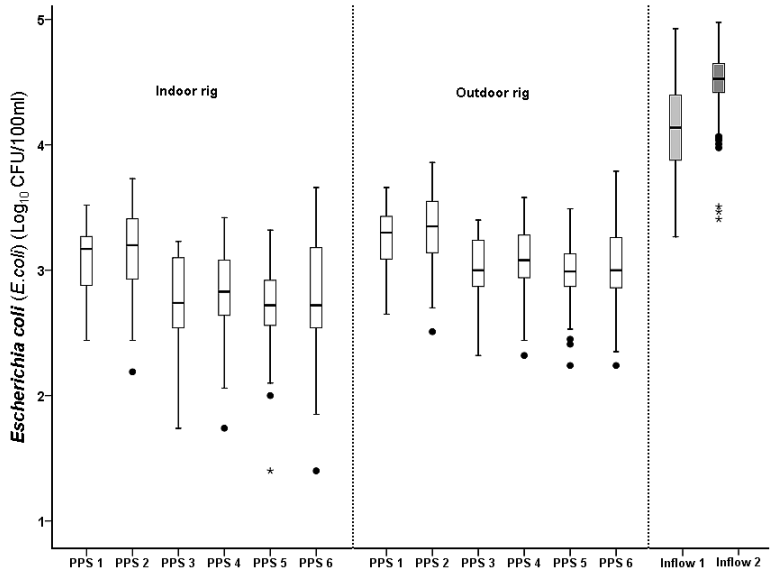

Figure 5-27: *Escherichia coli* concentrations for inflow 1 (gully pot liquor) and inflow 2 (gully pot liquor and dog faeces) and outflow concentrations for the indoor and outdoor bins. The plots represent the 25th percentile, median and the 75th percentile. The whiskers represent the 10th and 90th percentiles; solid circles represents outliers and stars represents extreme outliers (March 2008 to April 2010, n = 113).

Figure (5-27) illustrates the box and whiskers plot for the two-year data collection for effluent *E.coli* cell concentrations from the experimental bins. Overall mean outflow concentrations ranges from (2.72 to 3.18 $\log_{10}$ CFU/100ml) which corresponds to (7.37× 10^2 to 1.96 × 10^3 CFU/100ml) for the indoor rigs and (2.99 to 3.34 $\log_{10}$ CFU/100ml which corresponds to (1.12 × 10^3 CFU/100ml to 2.74 × 10^3 CFU/100ml). Overall equivalent removal efficacies ranged from (85-96 %) and (76-94 %) for indoor and outdoor rigs respectively. Nevertheless, according to the US EPA non-potable water reuse guidelines and the EU urban wastewater treatment standards a concentration of < 100 CFU/100ml and < 10^3 CFU/100ml of faecal coliforms are required. Regardless of the high retention and reduction rates of *E.coli*, the effluents did not meet 90 % of the treatment standards set aside by the US EPA and EU urban wastewater treatment directive. As a result of overloading and heavy contamination the drainage system did not retain all *E.coli* bacterial cells. This urges the need for further treatment and/or disinfection to fully remove this waterborne bacterium, before the filtered stormwater can be safely utilised.

From the one-sample Kolmogorov-Smirnov test of normality, effluent concentrations from PPS 1 (indoor and outdoor rig) followed a normal distribution. Outflow *E.coli* concentrations from all other experimental bins did not follow a normal distribution and therefore the dataset for all bins were transformed logarithmically before statistical analysis.

Throughout the biannual period (geothermal cooling/heating cycles); mean periodic removal efficiencies were generally high (Figure 5-28). Indoor rigs (PPS 1-PPS 6) followed a (95-96 %)$^{1\text{-}I}$; (84-87 %)$^{2\text{-}I}$; (92-95 %)$^{3\text{-}I}$; (96 %)$^{4\text{-}I}$; (92-96 %)$^{5\text{-}I}$; and (89-92 %)$^{6\text{-}I}$. With regards to the outdoor rig (PPS 1-6) reduction efficacies of *E.coli* followed a (90-91 %)$^{1\text{-}O}$; (73-77 %)$^{2\text{-}O}$; (88-90 %)$^{3\text{-}O}$; (94-95 %)$^{4\text{-}O}$; (89-91 %)$^{5\text{-}O}$ and (92-94 %)$^{6\text{-}O}$. It can be noted that PPS 3 and PPS 6 which were not integrated with geothermal heating and cooling applications performed on par with pavement systems (PPS 1, 2 3 and 5) that were combined with GHP for both the indoor and outdoor rigs.

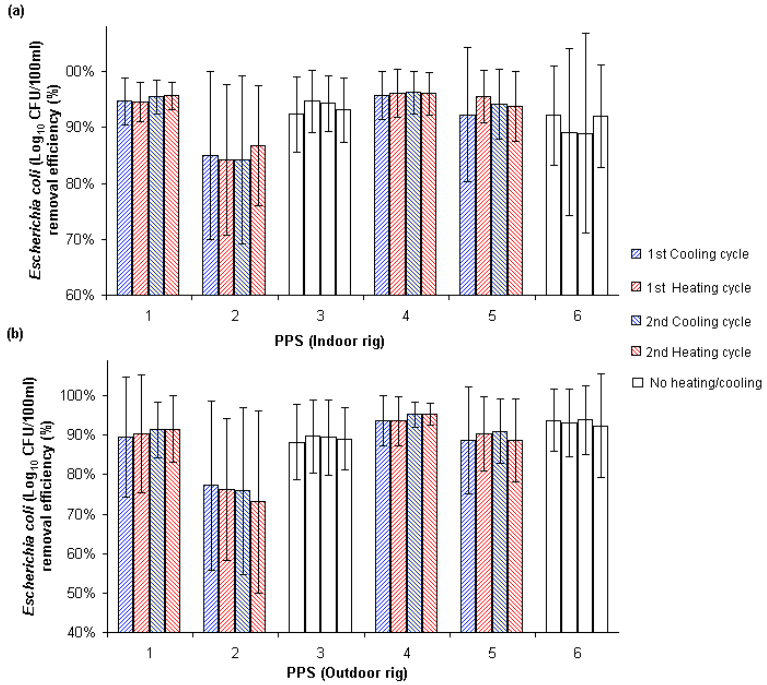

Figure 5-28: Mean removal efficiencies with error bars for *Escherichia coli* during the 1st Cooling Cycle (April to September 2008), 1st Heating Cycle (October 2008 to March 2009), 2nd Cooling cycle (April to September 2009) and 2nd Heating cycle (October 2009 to April 2010) for indoor rig (a) and outdoor rig (b) (PPS1 to PPS 6) respectively.

One-way Anova between the indoor and outdoor rigs showed a strong statistical variation for *E.coli* outflow concentrations ($p < 0.01$), which shows the effects of temperature and environmental conditions on the decline of these bacterial cell colonies (Table 5-4). With respect to the design variations in pavement systems, the presence of a geotextile membrane (PPS 1 vs. PPS 4) and (PPS 2 vs. PPS 5) for both indoor and outdoor rigs showed a significant difference of *E.coli* effluent concentrations ($p < 0.05$). The applications of geothermal heating and cooling (presence of GHP) also saw significant outflow concentrations between (PPS 2 vs. PPS 3) and (PPS 5 vs. PPS 6). In addition, the types of inflow 1 and 2 being treated by the same pavement design (PPS 1 vs PPS 2) and (PPS 4 vs PPS 5) showed significant variations for effluent *E.coli* concentrations. This is expected as inflow 2 spiked with dog faeces contains a higher concentration of *E.coli* bacterial cells than inflow 1 (gully pot liquor). Throughout the heating and cooling cycles, a significant difference occurred ($p<0.05$) for *E.coli* concentrations between (PPS 1, 2, 3 and 5) (Table 5-6).

5.4.9.2 Enterococci sp.

Faecal streptoccoci represents the larger group of bacteria which *Enterococci sp.* exists. Faecal streptococci bacterial cell concentrations range from around 10^2-10^6 CFU/100ml in urban runoff (Table 2-1). *Enterococci sp.* colonies varied from 3.3×10^2 to 1.71×10^4 CFU/100ml for inflow 1 and 1.08×10^3 to 1.89×10^4 CFU/100ml for inflow 2 (Table 5-1). Average concentrations were 3.74×10^3 CFU/100ml ± 3.42×10^3 CFU/100ml and 7.38×10^3 CFU/100ml ± 3.79×10^3 CFU/100ml. Standard error of the mean showed a large variation for both inflows (3.2×10^2 and 3.56×10^2 CFU/100ml) respectively (Table 5-1).

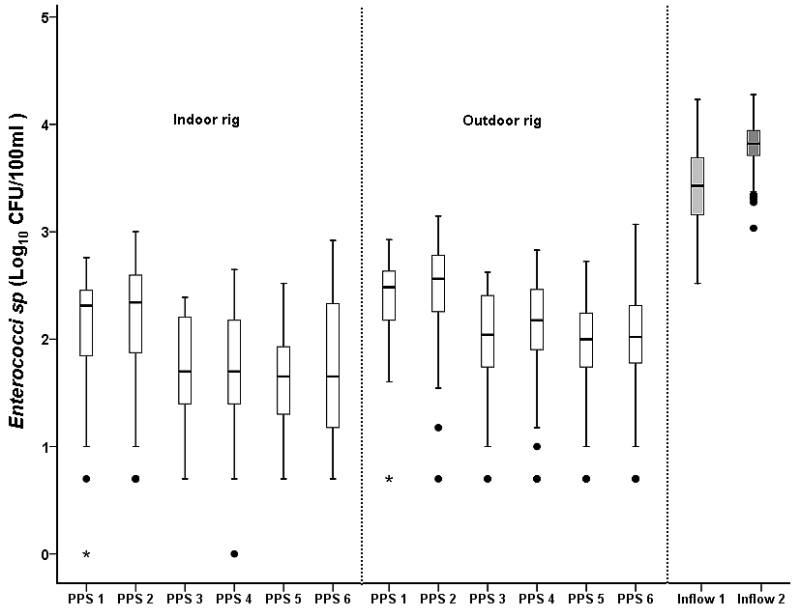

Figure 5-29: *Enterococci sp.* concentrations for inflow 1 (gully pot liquor) and inflow 2 (gully pot liquor and dog faeces) and outflow concentrations for the indoor and outdoor bins. The plots represent the 25th percentile, median and the 75th percentile. The whiskers represent the 10th and 90th percentiles; solid circles represents outliers (March 2008 to April 2010, n = 113).

Presented in Figure (5-29), the box and whiskers plots for influent and effluent cell concentrations of *Enterococci sp*. Overall outflow concentrations ranged from 1.60 to 2.23 $\log_{10}$ CFU/100ml corresponding to (8.3×10^1 to 3.0×10^2 CFU/100ml) for the indoor rig. Overall removal efficacies for *Enterococci sp.* ranged from 89-97 % for the indoor rig. Regarding the outdoor rig, effluent concentrations of *Enterococci sp.* ranged from 1.95-2.50 log10 CFU/100ml corresponding to (1.35×10^2 to 4.62×10^2 CFU/100ml) and equivalent removal efficiencies of 86 to 96 %. From one-sample Kolmogorov-Smirnov test of normality, PPS 1 (indoor and outdoor rigs) *Enterococci sp.* outflow concentrations followed a normal distribution ($\alpha > 0.05$), however, the other experimental bins did not show such distributions ($\alpha < 0.05$) (Table 5-3).

Biannual removal efficiencies throughout the cyclic geothermal cooling/heating periods for indoor rigs (PPS 1- PPS 6) followed a (97%)$^{1\text{-}I}$; (89-92 %)$^{2\text{-}I}$; (96-97 %)$^{3\text{-}I}$; (97-98 %)$^{4\text{-}I}$; (95-98 %)$^{5\text{-}I}$ and (93-95 %)$^{6\text{-}I}$ as shown in Figure (5-30). The outdoor rigs (PPS 1-PPS 6), followed suit, with extremely high reduction of *Enterococci sp.* bacteria with a (92-94 %)$^{1\text{-}O}$; (83-90%)$^{2\text{-}O}$; (92-94 %)$^{3\text{-}O}$; (96-97 %)$^{4\text{-}O}$; (91-95 %)$^{5\text{-}O}$ and (85-91%)$^{6\text{-}O}$ (Figure 5-30).

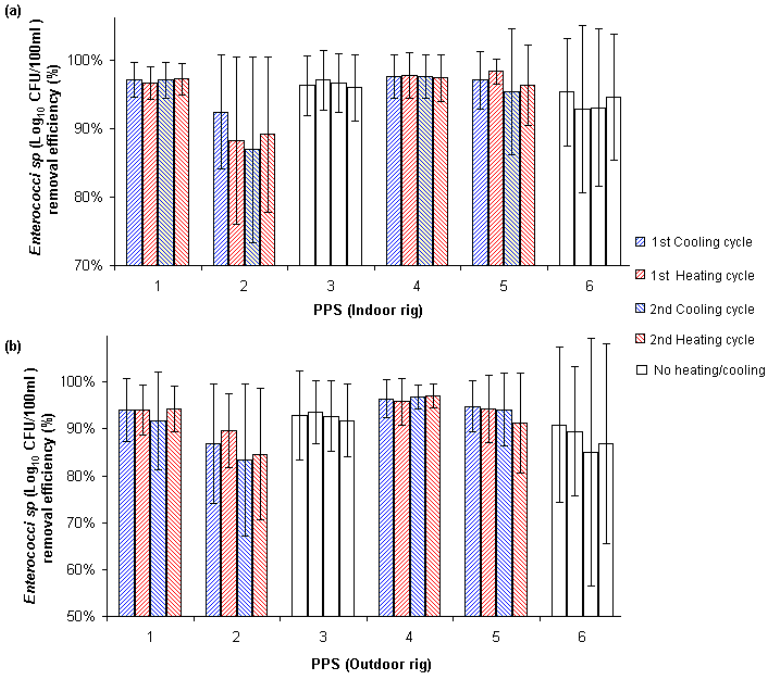

Figure 5-30: Mean removal efficiencies with error bars for *Enterococci sp.* during the 1st Cooling Cycle (April to September 2008), 1st Heating Cycle (October 2008 to March 2009), 2nd Cooling cycle (April to September 2009) and 2nd Heating cycle (October 2009 to April 2010) for indoor rig (a) and outdoor rig (b) (PPS1 to PPS 6) respectively.

One way Anova between indoor and outdoor rigs showed strong statistical differences with regards to *Enterococci sp.* outflow concentrations ($p < 0.05$) (Table 5-4). Statistical differences occurred for all design and variable parameters including the presence of geotextiles (PPS 1 vs. PPS 4) and (PPS 2 vs PPS 5); types of urban runoff being treated (PPS 1 vs PPS 2) and (PPS 4 vs PPS 5) and the integration of GHPs (PPS 2 vs 3) and (PPS 5 vs. PPS 6). Throughout the heating and cooling periods, *Enterococci sp.* concentrations also showed significant differences ($p <0.05$) for PPS 1, 2 3 and 5 (Table 5-6). The geotextile membrane creates a zone for protozoan communities, whereby aerobic biodegradation conditions exits, feeding on the *Enterococci sp.* bacterial. This aids the adsorption processes of enterococcis and its removal for an improved water quality effluent.

5.4.9.3 Total coliforms

Total coliform bacteria are indicators of the treatment efficacy and allowed detection of re-growth phenomena for the drainage system. Untreated domestic urban wastewater typical total coliform concentrations are 10^6-10^9 CFU/100ml. Similar concentrations exists in urban runoff (Table 2-1). As presented in Table (5-1), total coliforms bacterial colonies for inflows 1 and 2 ranged from 4.38×10^5 to 1.80×10^6 CFU/100ml and 4.56×10^5 to 1.95×10^6 CFU/100ml respectively. Overall mean total coliform bacterial cell concentrations were $7.10 \times 10^5 \pm (2.89 \times 10^5)$ CFU/100ml and $1.01 \times 10^6 \pm (3.25 \times 10^5)$ CFU/100ml for inflows 1 and 2 respectively. Standard errors of the means were 2.72×10^4 and 3.05×10^4 for influents 1 and 2 (Table 5-1). Larger bacterial concentrations of total coliforms is noted as a result of inflow 2 mixture containing dog faeces and the mean colony counts varying as the selection and sampling of dog faeces varied in quality and type (various dog excrements used). From one-sample Kolmogorov-Smirnov test of normality, PPS 1 (indoor and outdoor rigs) total coliforms outflow concentrations followed a normality ($\alpha > 0.05$), nevertheless, the other experimental bins did not show such distributions ($\alpha < 0.05$) (Table 5-3).

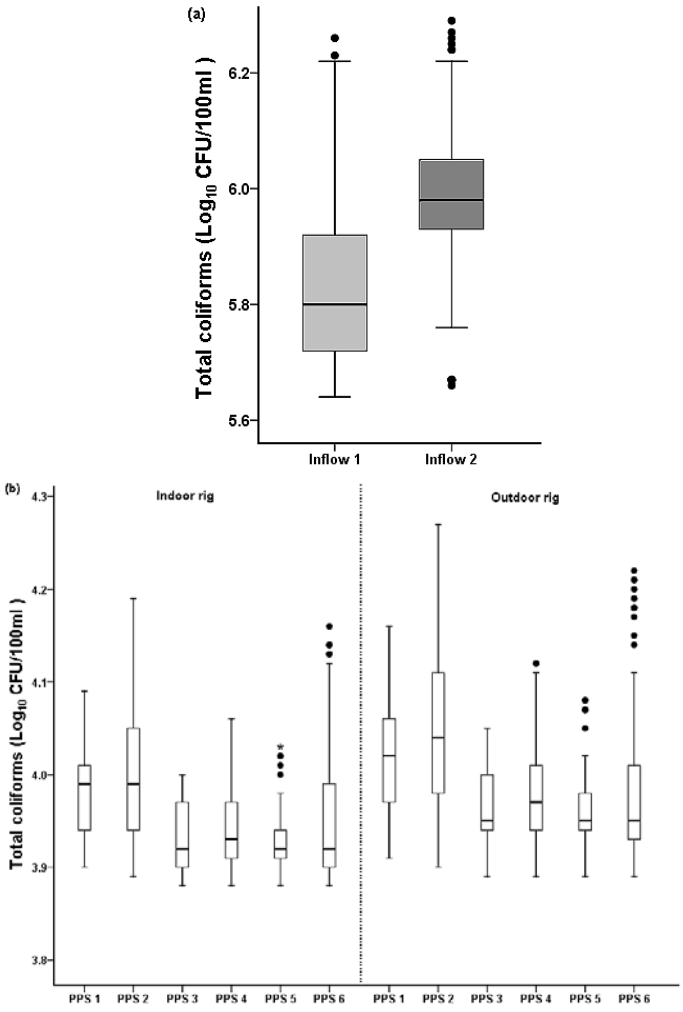

Figure 5-31: Total coliforms concentrations for inflow 1 (gully pot liquor) and inflow 2 (gully pot liquor and dog faeces) (a) and outflow concentrations for the indoor and outdoor bins (b). The plots represent the 25th percentile, median and the 75th percentile. The whiskers represent the 10th and 90th percentiles; solid circles represents outliers (March 2008 to April 2010, n = 113).

From the box and whiskers plots shown in Figure 5-31, mean outflow total coliforms were (3.92 $\log_{10}$ CFU/100ml to 4.01 $\log_{10}$ CFU/100ml) (8.49×10^3 to 1.04×10^4 CFU/100ml). Corresponding removal efficiencies were extremely high, ranging from 98-99% for the indoor rigs. Regarding the outdoor rig, total coliforms outflow concentrations ranges from 3.96 $\log_{10}$ CFU/100ml to 4.06 $\log_{10}$ CFU/100ml (9.18×10^3 to 1.16×10^4). Additionally, corresponding removal efficiencies ranged from 98 to 99 % for all experimental bins from the outdoor rig. Nevertheless, the effluent concentrations did show high removal rates but demonstrated that the PPS

systems could not meet the EU urban wastewater treatment directive and US EPA guidelines for non-potable water reuse with regards to total coliform bacterial coliforms (< 500 CFU/100ml and < 200 CFU/100ml) (Table 5-2). Once again this is a result of high water quality standards set about from the relevant agencies regarding bacterial pathogens after industralised process treatment, but still shows the need for further treatment and decontamination from the effluent of permeable pavements when encountering highly polluted stormwaters.

Throughout the geothermal heating-cooling cycles removal efficiencies showed a constant 98-99 % for both indoor and outdoor rigs (Figure 5-32). However, total coliforms showed statistical variances for all variations and types of inflows treated ($p < 0.05$) (Tables 5-4, 5-5 and 5-6). Taghizadeh *et al.,* (2007) carried out pilot studies with the feasibility of vertical porous concrete filters and the filtration of urban domestic wastewater. An adequate removal efficiency of about 90-100% of total coliforms was obtained, and the porous concrete filter's growth of biological mass, provides suitable screening and straining which were the predominant mechanisms for the removal of the bacteria (Taghizadeh *et al.,* 2007).

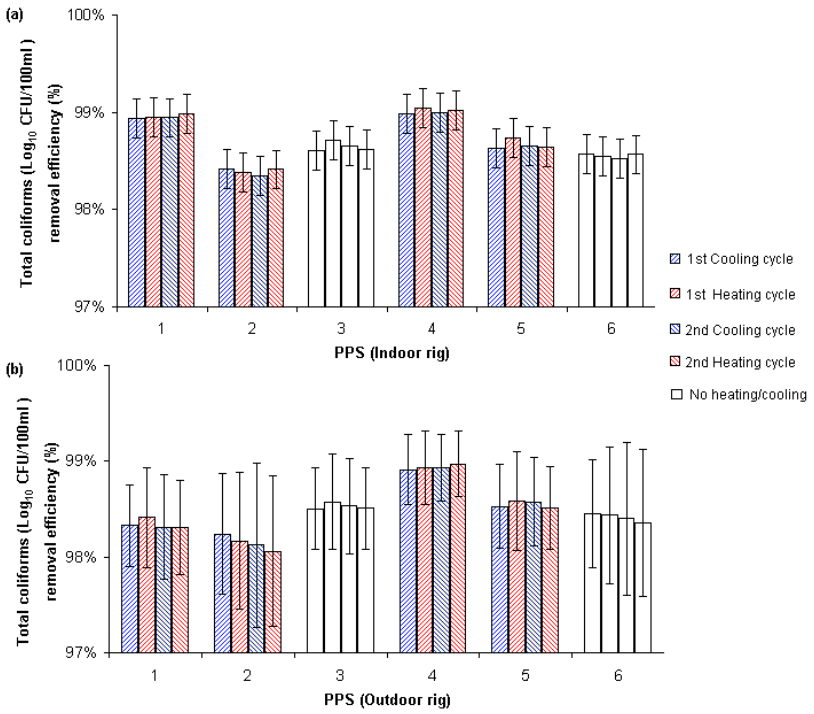

Figure 5-32: Mean removal efficiencies with error bars for Total Coliforms during the 1st Cooling Cycle (April to September 2008), 1st Heating Cycle (October 2008 to March 2009), 2nd Cooling cycle (April to September 2009) and 2nd Heating cycle (October 2009 to April 2010) for (a) indoor rig and (b) outdoor rig (PPS1 to PPS 6) respectively.

5.4.9.4 Total Heterotrophic Bacteria (THB)

As presented in Table (5-1), THB concentrations were the highest for all bacterium as it includes all heterotrophic bacteria present in the urban runoff samples. Concentrations ranged from (4.0×10^3) to (4.5×10^7) CFU/100ml and (8.10×10^4) to ($1.47 \times 10^{10)}$ CFU/100ml for inflows 1 and 2 respectively. Average influent concentrations were $3.87\times 10^6 \pm (8.49\times 10^6)$ CFU/100ml and $4.12 \times 10^8 \pm (2.0 \times 10^9)$ CFU/100ml for inflows 1 and 2. Standard error of the mean showed a large variation of (7.99×10^5 and 1.88×10^5 CFU/100ml) due to the fluctuation of bacterial cell concentrations, seasons and period whereby sampling occurred (Table 5-1). Overall mean inflow and outflow concentrations are illustrated in (Figure 5-33), ranged from 4.0-4.73 log10 CFU/100ml or (2.94×10^4 to 5.54×10^5) CFU/100ml with an overall corresponding removal efficiency of 75-96%. With respect to the outdoor rig, effluent concentrations of THB were (4.05-4.84 log10 CFU/100ml) (4.30×10^4 to 5.30×10^5 CFU/100ml). From the one-sample Kolmogrov-Smirnov test of normality,

THB effluent (CFU/100ml) did not follow a normal distribution for any experimental bins (α <0.05) (Table 5-3). Overall removal efficiencies for the outdoor rig with respect to THB ranged from 77-94% respectively.

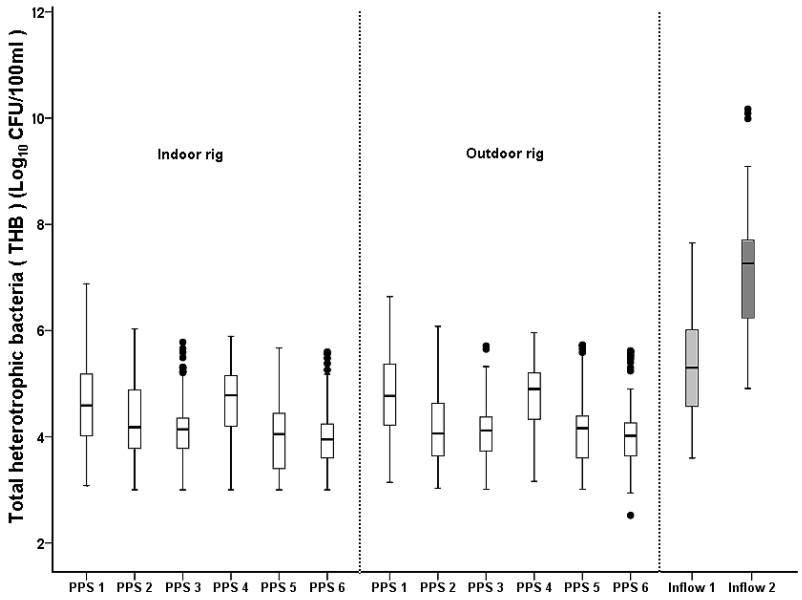

Figure 5-33: Total heterotrophic bacteria concentrations for inflow 1 (gully pot liquor) and inflow 2 (gully pot liquor and dog faeces) and outflow concentrations for the indoor and outdoor bins (b). The plots represent the 25th percentile, median and the 75th percentile. The whiskers represent the 10th and 90th percentiles; solid circles represents outliers (March 2008 to April 2010, n = 113).

Biannual (geothermal cyclic) removal efficiencies regarding the indoor and outdoor rigs (PPS 1-PPS 6) are presented in Figure 5-34. Indoor rigs followed a (95-97 %) $^{1\text{-}I}$; (72-77 %) $^{2\text{-}I}$; (77-81 %) $^{3\text{-}I}$; (95-96 %) $^{4\text{-}I}$; (88-89 %) $^{5\text{-}I}$; and (77-89 %) $^{6\text{-}I}$. With respect to the outdoor rig, removal efficacies followed a (93-95 %) $^{1\text{-}O}$; (75-82 %) $^{2\text{-}O}$; (77-82 %) $^{3\text{-}O}$; (91-95%) $^{4\text{-}O}$; (74-79%) $^{5\text{-}O}$; and (79-87%) $^{6\text{-}O}$. This shows the presence of geothermal heating or cooling did not affect the retention and degradation rates of total heterotrophic bacteria.

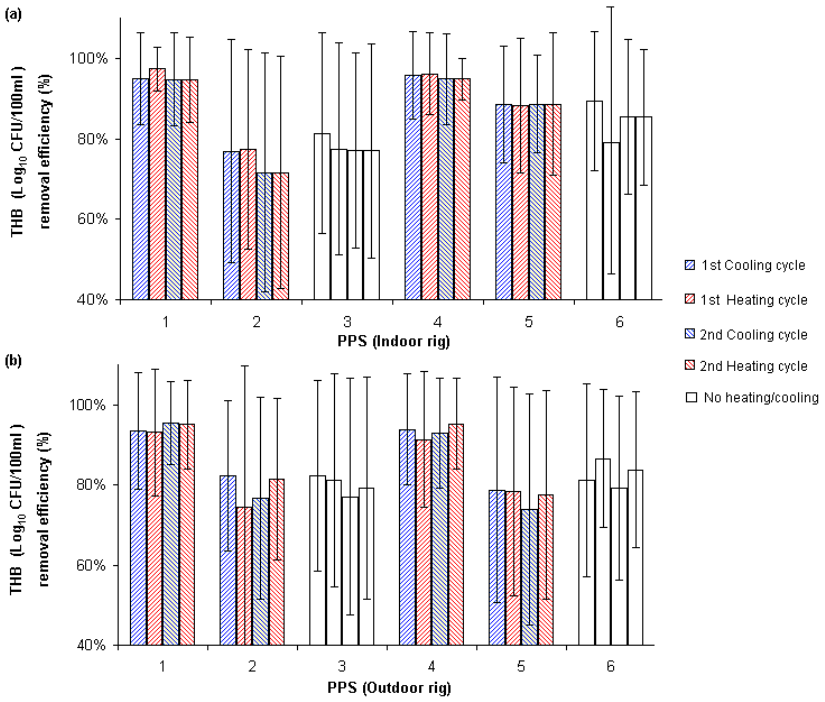

Figure 5-34: Mean removal efficiencies with error bars for Total Heterotrophic Bacteria (THB) during the 1st Cooling Cycle (April to September 2008), 1st Heating Cycle (October 2008 to March 2009), 2nd Cooling cycle (April to September 2009) and 2nd Heating cycle (October 2009 to April 2010) for (a) indoor rig and (b) outdoor rig (PPS1 to PPS 6) respectively**.**

One way Anova between indoor and outdoor rigs showed no significant differences for THB colonies exiting the systems ($p > 0.05$) (Table 5-4). However, when the type of inflows treated was statistically compared between PPS 1 vs. PPS 2 and PPS 4 vs. PPS 5 there were significant differences in the outflow concentrations ($p < 0.05$, Table 5-5). This is expected as inflow 2 (mixture of gully pot liquor and dog faeces) would naturally contain greater heterotrophic bacterial colonies. The presence of geotextiles showed statistical variations for THB outflow concentrations (PPS 1 vs. PPS 4) and (PPS 2 vs. PPS 5) (Table 5-5). Throughout the heating/cooling periods, for combined (PPS 1, 2, 3 and 5) there was also no significant differences regarding THB outflow concentrations ($p > 0.05$) (Table 5-6). This is a result of the greater microbial activities occurring in and around the geotextile layer, higher population of protozoan communities feeds on the heterotrophic organisms for sources of nutrients and energy. The presence of geothermal heating and cooling applications showed no effect on the effluent THB cell colonies ($p > 0.05$).

Studies by Stevik *et al.,* (2004) in Oslo, Norway showed *E.coli*, *Enterococci sp*. and total coliforms removed up to 90 % by gravity filters constructed of sand and gravel, treating wastewater from septic tanks. It was found that at the top of the filters, highest reduction rates for the selected waterborne bacteria (*E.coli*, total coliforms and faecal streptococci) occurred. A decrease in retention and enhanced residence time within the filter increases the likelihood for adsorption of the bacterial cells to the filter material (Stevik *et al.,* (2004).

5.4.9.5 Salmonella sp.

Salmonella sp. concentrations are generally low in urban runoff (< 10^4 CFU/100ml) (Gerardi and Zimmerman, 2005). However, due to the source of urban runoff concentrations of *Salmonella sp.* ranged from 5.16×10^2 to 4.31×10^4 CFU/100ml and 1.32×10^3 to 5.52×10^5 CFU/100ml (Table 5-1). Mean inflow concentrations were $7.37\times10^3 \pm (8.58\times10^3)$ CFU/100ml and $1.13\times10^5 \pm (1.32\times10^5)$ for inflows 1 and 2. Standard error of the mean was (807 and 1.24×10^4 CFU/100ml) which represent the variation of the mean (Table 5-1). From figure (5-35) it can be seen that the mean effluent concentrations for the indoor rig ranged from 2.46 - 2.60 $\log_{10}$ CFU/100ml (336 - 480 CFU/100ml). Overall removal efficiency for the indoor rigs was 84-96%. Regarding the outdoor rig, average outflow concentrations were 2.25 - 2.50 $\log_{10}$ CFU/100ml (221 - 285 CFU/100ml), with a corresponding removal efficiency of 88 - 97 % respectively. One-sample Kolmogorov test of normality showed that PPS 1 and 4 from the indoor rig, and PPS 1, 2 and 5 from the outdoor rigs, effluent of *Salmonella sp.* followed a normal distribution ($\alpha > 0.05$) (Table 5-3).

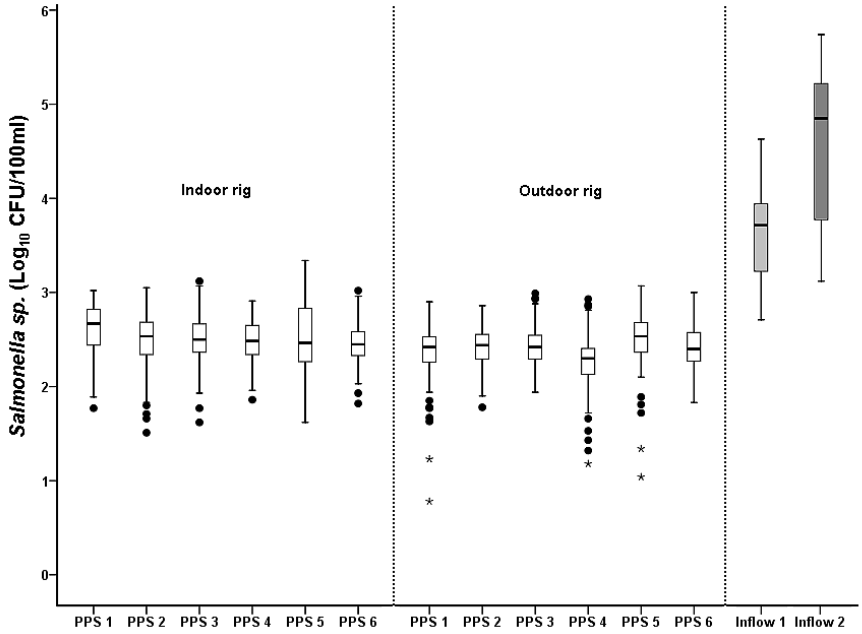

Figure 5-35: *Salmonella sp.* concentrations for inflow 1 (gully pot liquor) and inflow 2 (gully pot liquor and dog faeces) and outflow concentrations for the indoor and outdoor bins. The plots represent the 25th percentile, median and the 75th percentile. The whiskers represent the 10th and 90th percentiles; solid circles represents outliers (March 2008 to April 2010, n = 113).

Biannual cyclic removal efficiencies for the indoor and outdoor rigs (PPS 1-PPS 6) are presented in figure 5-36. Indoor rigs followed a (93-96 %)$^{1\text{-}I}$; (80-86%)$^{2\text{-}I}$; (85-88 %)$^{3\text{-}I}$; (95-97 %) $^{4\text{-}I}$; (82-88 %)$^{5\text{-}I}$; and (84-86 %)$^{6\text{-}I}$ removal efficiency. With respect to the outdoor rig, removal efficacies followed for (PPS 1-PPS 6), (96-97%)$^{1\text{-}O}$; (87-89%)$^{2\text{-}O}$; (89-91%)$^{3\text{-}O}$; (97-99%)$^{4\text{-}O}$; (85-88%)$^{5\text{-}O}$ and (86-89%)$^{6\text{-}O}$.

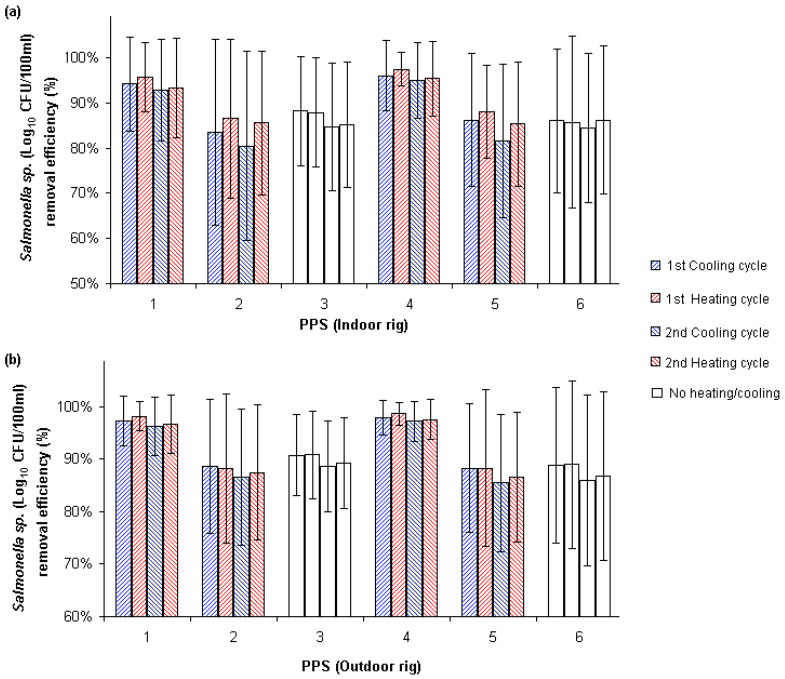

Figure 5-36: Mean removal efficiencies with error bars for *Salmonella sp.* during the 1st Cooling Cycle (April to September 2008), 1st Heating Cycle (October 2008 to March 2009), 2nd Cooling cycle (April to September 2009) and 2nd Heating cycle (October 2009 to April 2010) for (a) indoor rig and (b) outdoor rig (PPS1 to PPS 6) respectively.

One-way Anova between indoor and outdoor rigs, also showed statistical variations ($p < 0.01$, Table 5-4) for the outflow concentrations of *Salmonella sp.* Treatment and filtration of inflow1 versus inflow 2 carried out by Anova of PPS 1 versus PPS 2 and PPS 4 versus PPS 5 showed no significant differences ($p > 0.05$, Table 5-5).

Numerous urban runoff studies which detected *Salmonella* in low concentrations ($<10^4$ CFU/100ml) have not correlated this with the presence of faecal coliform observations. Once more, geotextile membranes showed a significant difference whereby biofilm production and assimilation of *Salmonella* by protozoan communities reduces this bacterial cell concentration (Table 5-5). Inconsistencies occurred with the presence of GHP and outflow *Salmonella* bacterial colonies for PPS 2 versus PPS 3 which showed significant variations ($p < 0.05$) and PPS 5 versus. PPS 6 whereby no statistical variations in the outflow occurred. Throughout heating and cooling periods for PPS 1, 2, 3 and 5; effluent concentrations of *Salmonella sp.* were significantly difference ($p < 0.01$, Table 5-6) which shows the effect on

temperature variation on the degradation and/or reproduction of this waterborne bacterium.

5.4.9.6 Shigella sp.

Shigella sp. species causes bacillary dysentery (bloody diarrhea) which is one of the primary human enteric diseases associated with this bacterium present in water as discussed previously. *Shigella sp.* inflow concentrations ranged from (2.06×10^2 to 1.72×10^4) CFU/100ml and (5.26×10^2 to 2.21×10^5) for inflows 1 and 2 respectively (Table 5-1). Mean inflow concentrations for inflows 1 and 2 were $2.95 \times 10^3 \pm (3.44 \times 10^3)$ CFU/100ml and $4.53 \times 10^3 \pm (5.29 \times 10^4)$ CFU/100ml. Standard error of the mean was 3.23×10^2 and 4.97×10^3 CFU/100ml for inflows 1 and 2 (Table 5-1) . As seen in Figure (5-37), the box and whiskers plots presents the inflow and outflow concentrations for the indoor and outdoor rigs regarding *Shigella sp.* bacterial cell concentrations. The indoor rig ranged from 2.06-2.20 log10 CFU/100ml (1.34×10^2 to 1.92×10^2) CFU/100ml. Overall removal efficacies for *Shigella sp.* regarding the indoor rigs were 85-94 %. With respect to the outdoor rig, effluent concentrations were 1.85 - 2.10 log10 CFU/100ml (8.8×10^1 to 1.52×10^2 CFU/100ml). The overall removal efficiencies for the outdoor rig regarding *Shigella sp.* ranged from 87 - 98 %. One sample Kolomogorov-Smirnov test of normality showed *Shigella sp.* outflow concentrations for PPS 1 and 4 from the indoor rig and PPS 1, 2 and 5 from the outdoor rig followed a normal distribution ($\alpha > 0.05$) (Table 5-3).

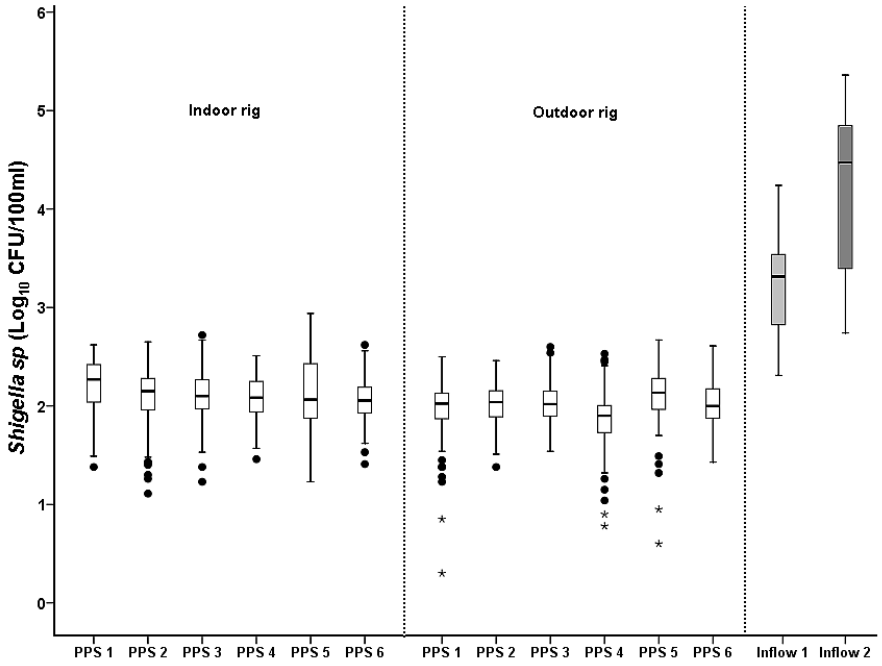

Figure 5-37: *Shigella sp.* concentrations for inflow 1 (gully pot liquor) and inflow 2 (gully pot liquor and dog faeces) and outflow concentrations for the indoor and outdoor bins. The plots represent the 25th percentile, median and the 75th percentile. The whiskers represent the 10th and 90th percentiles; solid circles represents outliers (March 2008 to April 2010, n = 113).

Biannual removal efficacies for the indoor and outdoor rigs (PPS 1- PPS 6) are illustrated in Figure 5-38. The removal efficacies for the indoor rig were as follows:- (93-96 %)$^{1\text{-}I}$; (87-89 %)$^{2\text{-}I}$; (89-91 %)$^{3\text{-}1}$; (97-99 %)$^{4\text{-}I}$; (85-88 %) $^{5\text{-}I}$; and (86-89 %) $^{6\text{-}I}$. With respect to the outdoor rigs, (PPS 1- PPS 6) removal efficiencies were as follows: - (96-98%)$^{1\text{-}O}$; (87-89%)$^{2\text{-}O}$; (89-91 %)$^{3\text{-}O}$; (97-99%)$^{4\text{-}O}$; (85-88%)$^{5\text{-}O}$; and (86-89%)$^{6\text{-}O}$. High reductions of *Shigella sp.* can be noted throughout each geothermal heating and cooling cycles.

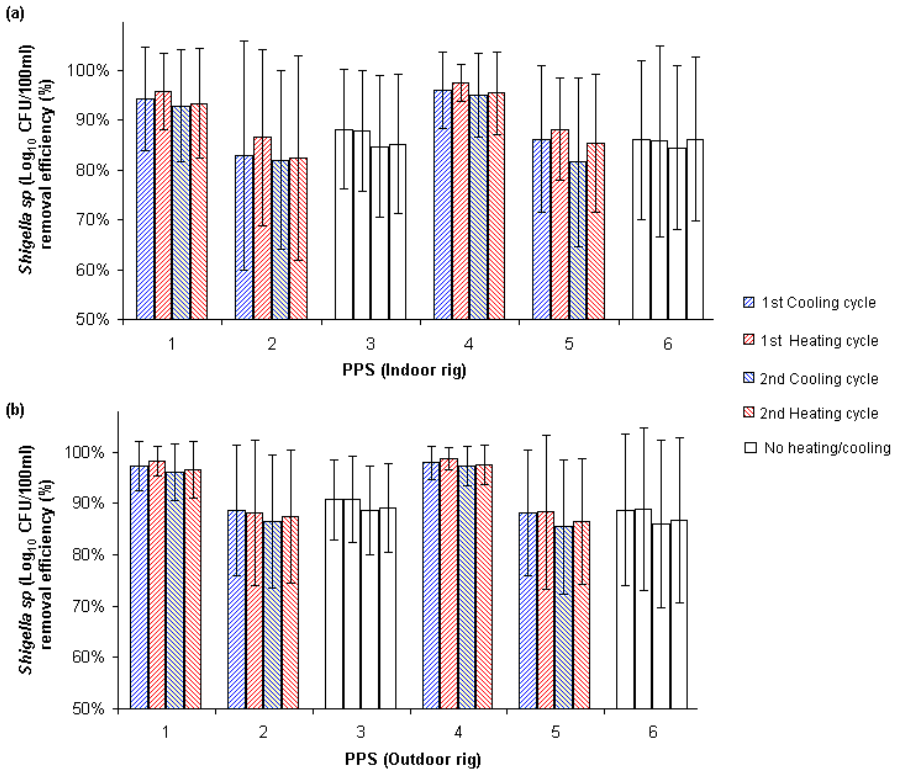

Figure 5-38: Mean removal efficiencies with error bars for *Salmonella sp.* during the 1st Cooling Cycle (April to September 2008), 1st Heating Cycle (October 2008 to March 2009), 2nd Cooling cycle (April to September 2009) and 2nd Heating cycle (October 2009 to April 2010) for (a) indoor rig and (b) outdoor rig (PPS1 to PPS 6) respectively.

One-way Anova between the indoor and outdoor rigs for Shigella effluent cell concentrations showed significant differences ($p < 0.01$, Table 5-4). However, there was no statistical variation between the treatment of inflows 1 and 2 regarding similarly structured pavement systems for *Shigella sp.* removal ($p > 0.05$, Table 5-5). The presence of geotextiles showed statistical variations for the dominant removal and increase in biodegradation of the waterborne bacterium ($p < 0.05$) for PPS 1 vs. PPS 4 and PPS 2 vs. PPS 5) (Table 5-5). Once more, inconsistencies occurred with the presence of GHP, whereby no statistical differences occurred between PPS 2 and PPS 3 ($p > 0.05$) but PPS 5 vs. PPS 6 showed variation ($p < 0.05$). Nevertheless, there was statistical variations regarding *Shigella sp.* effluent bacterial cell concentrations throughout the heating and cooling periods for PPS1, 2, 3 and 5 ($p < 0.01$) (Table 5-6).

5.5 Microbial removal processes within PPS.

Overall reductions of viruses and bacteria by sand-gravel based water filters are around 60-70 %. (WHO, 2004). The microbial quality of water is sometimes improved by holding or storing it undisturbed without mixing, as larger particles tend to settle out or sediment by gravity throughout filtration. Storing water at the sub-base of the permeable pavement for a few hours, sediment larger dense particles such as inorganic compounds whereby microbes and pathogenic organisms are associated to. Filter media and the filtration processes vary throughout the pavement system. Filtration through porous granular media is the most widely used physical method for water treatment. Granular media filters and slow-sand filters have moderate to high filtration effectiveness on water borne microbial pathogens (90-99%).

Ausland *et al.,* (2002) and Stevik *et al.,* (2004) found that filtration of wastewater through porous media (sand-gravel based aggregates) showed a 99.99% reduction of *E.coli*, faecal streptococci, and faecal coliforms from 70% of all effluent samples. The experiments found that increasing the hydraulic dosing rate of wastewater containing waterborne bacteria decreases the removal of the bacteria dramatically. A lower purification with increased inflows was observed (Stevik *et al.,* (2004); Ausland *et al.,* (2002). Indigenous bacteria and protozoa increase the purification of wastewater by antagonisms and grazing on the waterborne bacterium. Enhanced residence time within filters increases the likelihood of adhesion to the porous media. It was also observed from both experiments that there was no significant correlation of bacterial coliforms and temperature in the range of 2-17 ºC. The hydraulic sorptivity of the porous media within the filters produced steady state unsaturated flows throughout the filter volume and adsorption is a major bacterial immobilization process and is time dependent for filtration.

The straining mechanisms involve the physical blocking of movement through pores smaller than the bacterium, which occurs at the top layer of the permeable pavement blocks. Higher flow rates increase the average water suction in an unsaturated filter medium. This results in a greater transport through larger pores which decreases the effect of bacterial straining by porous material (Smith *et al.,* 1985). Through uniform distribution of urban runoff onto the pavement surfaces, the

negative effects of higher loading rates were reduced. However under real life conditions, with extensive rainfall and increased flows, the reduction in waterborne bacterial removal can occur for PPS. Flow patterns within the PPS will alter during its operations due to biomass formations within the porous media and around the geotextiles. This can change the hydraulic properties due to the accumulation of biomass from the growth of microorganism but the build up of biofilm can restrict particles and pollutants enhancing the effects of filtering within PPS.

Bacterial adsorption and attachment to porous media is a dominant mechanism for retention. Adsorption influences bacterial transport within porous media and factors that influences the adsorption of water borne bacterial cells to porous media includes the presence of organic matter, biofilm production, temperature, water flow velocities, ionic strength, species present, pH, hydrophobicity (incapable of dissolving in water), chemotaxix (directional movement of bacteria according to chemicals in their environment), electrostatic charges on cell surfaces and bacterial concentrations (Ausland *et al.,* 2002; Stevik *et al.,* 2004).

The rate of adsoption of bacteria increases linearly with cell concentration. Studies by Fletcher, (1977) observed that the number of attached cells increases with bacterial concentration until the filter media approaches saturation. An increase in bacterial concentrations led to an increase in the number of bacterial collisions with the media surface and hence an increase in opportunities for adhesion (Fletcher, 1977).

The survival of most water borne bacteria decreases with both low and high pH values. pH values lower than 3-4 and higher than 10-12 generally has a hostile effect on bacterial survival in water. The survival of *E.coli* adapts better to a more neutral to slightly alkaline conditions. However, the effluent pH shows mean values around 6-9 which presents pH conditions which may not influence the survival of pathogenic waterborne bacterium.

Organic matter content in the form of BOD and COD removal is closely associated to bacteria. Bacteria have an inability in lowering their nutrient requirements, and struggle to compete with other indigenous microorganisms in circumstances with low nutrient availability. Survival of pathogenic bacteria can be prolonged in water containing high organic matter, and in nutrient-limited

environments bacteria can change their metabolic activities from biosynthesis and reproduction to acquisition of energy for existing and survival biological functions (Gerardi and Zimmerman, 2005). Bacterial species survival differs between species. *Salmonella sp* species tends to have longer survival times that *E.coli*, whilst *Shigella sp* can die more rapidly. *Enterococci* species have much longer survival times than other bacterium (Gerardi and Zimmerman, 2005). Some intestinal bacteria may survive better due to their abilities in competition for nutrients with indigenous microorganisms and the production of spores which are more capable of surviving under unfavourable conditions.

Bacterium within the pavement systems undergoes aerobic biological treatment and is also subjected to predation and exposure to bacterial phages, protozoa and nematodes. According to Acea and Alexander, (1988) protozoa are the main predators of bacteria in soil and water. Tate, (1978) observed that the protozoan population increased six fold and the numbers of *E.coli* present in soil samples were significantly reduced.

5.5.1 Molecular Microbiology Results

5.5.1.1 Gram staining results

Figure 5-39, shows sample gram staining results for inflows 1 and 2. The two distinct purple and pink colours represent the Gram-positive rods and Gram-negative rods present within the water sample. Gram-negative bacteria are those bacteria that do not retain the crystal violet dye in the gram staining protocol and absorbs the counterstain colouring all Gram-negative bacteria with a red or pink colour, whilst the gram-positive bacteria shows the violet (purple) stains.

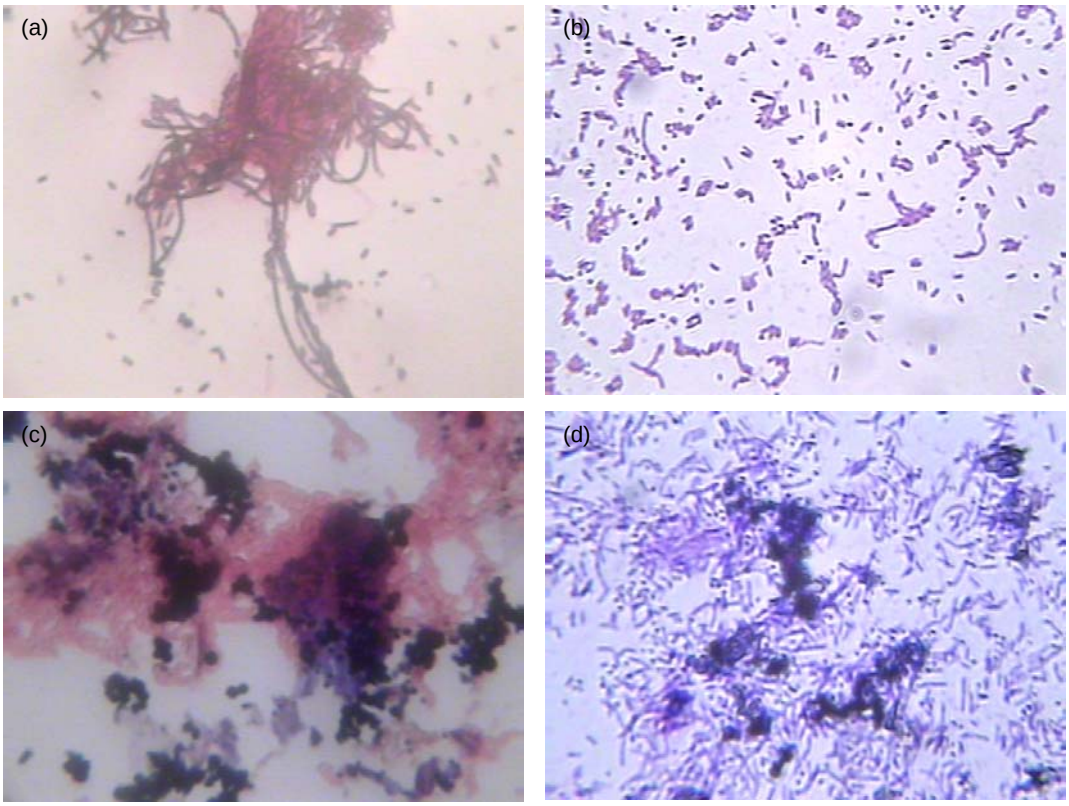

Figure 5-39: Gram staining results for (a) Inflow 2 (November 2008) (b) Inflow 1 (November 2008), (c) Inflow 2 (May 2009) and (d) Inflow 1 (May 2009)

Gram-positive rods include well known genera such as *Streptococcus* and *Enterococcus*. Gram-negative bacteria include *Escherichia coli*, *Salmonella*, *Shigella*, *Legionella* and other Enterobacteriaceae. The mixed gram-positive *enterococci* rods (purple-violet colour) and gram-negative bacilli (*Escherichia coli*, *Salmonella*, *Shigella*) pink stains were dominant with the gully pot and dog faeces mixture when compared to inflow 1 which shows higher concentrations of gram-positive rods.

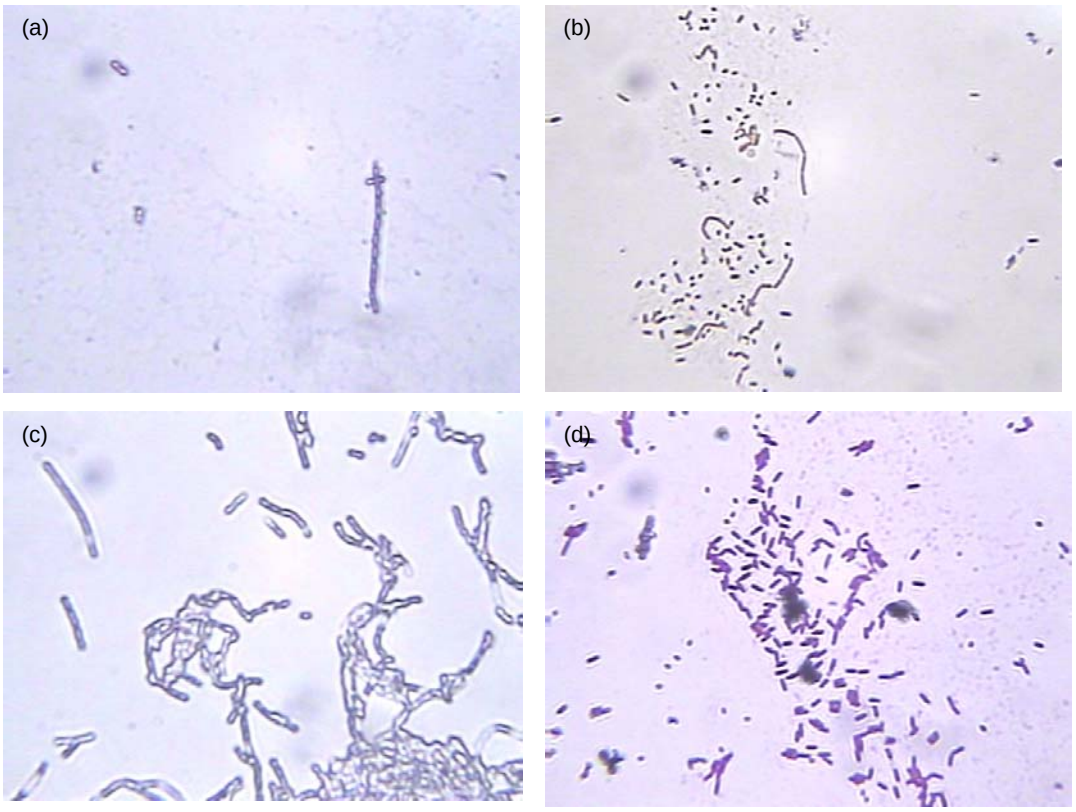

Figure 5-40: Corresponding Gram staining results for (a) PPS 4 (indoor rig) effluent (November 2008), (b) PPS 2 (indoor rig) effluent (November 2008), (c) PPS 4 (indoor rig) effluent (May 2009), (d) PPS 2 (indoor rig effluent) Inflow 2 (May 2009).

The effluent from PPS 4 (indoor rig) represents the high degradation rates of both Gram-positive and Gram-negative bacteria consumed and degraded within the pavement system and supports the findings from the agar plate count (Figure 5-40). However, effluent concentrations still showed cell colonies formation and bacteria

exiting the system. PPS 2 (indoor rig) shows a high reduction of Gram-negative bacteria which once more compliments the results of significant removal efficacies regarding waterborne bacterial pathogens (Figure 5-40).

5.5.1.2 Molecular microbiological results

Traditionally, the classification or taxonomy of microbiological organisms has been based on their morphology (i.e. their visible structure and form). The colony morphology of each isolated bacteria was studied on nutrient agar. A DGGE (denaturing gradient gel electrophoresis) analysis of PCR amplified 16 S rRNA gene fragments of bacteria was used to study the bacterial community and to compare the microbial diversity of the inflow and outflow samples. Moreover, the population diversity for the inflows in comparison to the outflows was assessed. Table 5-7 indicates the deoxyribonucleic acid (DNA) sequencing results, the bacterial strains present and similarity for the various experimental bins. Tables 5-7 and 5-8 indicate the presence of different organisms in different bins. However, the microbial ecology of most organisms within PPS is largely unknown.

The results of the phylogenetic analysis of the 16S rRNA sequences showed that bacterial isolates represented a diverse Gram positive and Gram negative heterotrophic bacteria community belonging to major phylogenetic groups represented by key bacteria such as *Brevundimonas* spp., *Pseudomonas* spp., *Aeromonas* spp., *Klebsiella* spp., Enterobacter spp., *Stenotrophomonas* spp. and *Bacillis* spp (Table 5-7). The most frequently identified genus was *Aeromonas* spp., followed by *Brevundimonas* spp. and *Bacillis* spp. on the same rank and *Enterobacter* spp. on the third place. In contrast, *Pseudomonas* spp., *Aeromonas* spp., *Bacillus* spp. *Brevundimonas* spp. and *Enterobacter* spp. were identified in the effluent of the inside and outside rigs. In addition, *Klebsiella* spp. and *Stenotrophomonas* spp. were only isolated and identified from effluents of the indoor and outdoor bins, respectively.

Figure 5-41 shows a neighbour-joining phylogenetic tree of the bacteria that were present in the saturated zone of the PPS, based on the 16S rRNA gene sequences of the isolates. The bands for selected strains, illustrating what organisms

are dominant in the saturated zone of the PPS, and outlines the neighbour joining method for comparative analysis of bacterial communities in the pavement system, indicating the most likely genetic relationships between 16S rDNA sequences from treated water samples (Figure 5-41). These heterotrophic bacteria were closely related to seven known bacterial species: *Brevundimonas* spp., *Pseudomonas* spp., *Aeromonas* spp., *Klebsiella* spp., *Enterobacter* spp., *Stenotrophomonas* spp. and *Bacillis* spp. (98 - 100% similarity; Table 5-7). Considering that the consequences of microbial interactions between these genera are largely unknown, this information is of little relevance for the system designer. Nevertheless, information on species presence or absence in the system helps to make an informed assessment on potential health risks. Information on persistence of microorganisms from sample to pavement is important since information on species presence or absence in the system helps to make an informed assessment on potential health risks.

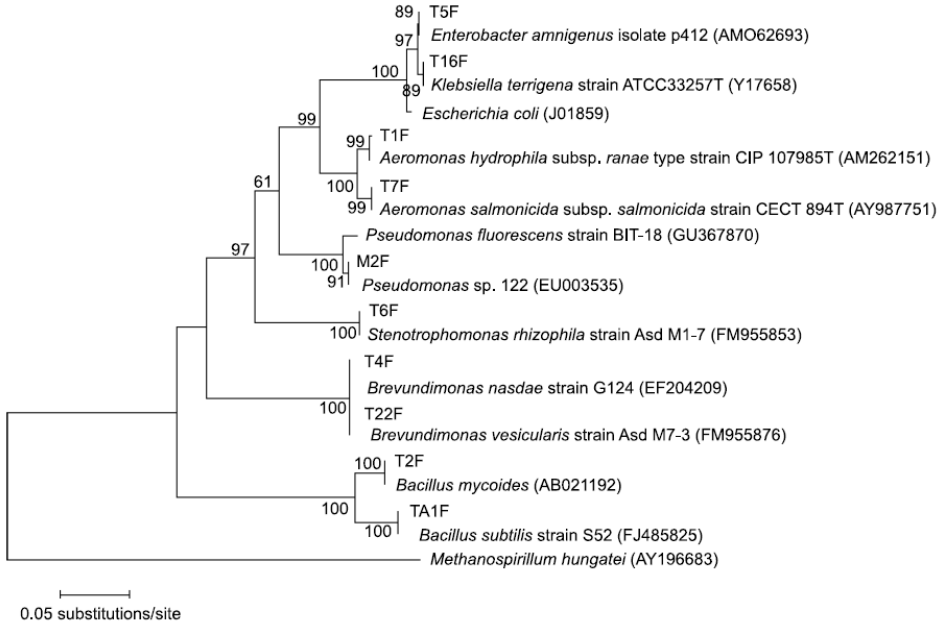

Figure 5-41: Phylogenetic tree illustrating the bacterial isolates present in the saturated zone of the experimental permeable pavement system and the closest related organisms (Table 5-7). *Methanospirillum hungatei* was added as the outlier organism.

Different colonies were isolated and identified by molecular microbiological techniques. Members of different phylogenetic groups were isolated from the experimental systems. Potentially pathogenic species such as *Mycobacterium porcinum* and *Aeromonas salmonicida* were found in some samples regardless of

contamination with animal faecal matter. Gram negative organisms were dominant among the isolates identified. Most frequently recovered bacterial isolates were of the genera *Bacillus*, *Brevundimonas*, *Pseudomonas* and *Aeromonas*.

The inflow waters contaminated with dog faeces and gully pot liquor contained *E. coli* and faecal Streptococci. Moreover, no growth of *Legionella sp.* was observed in the sub-base of the pavements. In contrast, *Pseudomonas* spp., *Aeromonas* spp., *Bacillus* spp. *Brevundimonas* spp. and *Enterobacter* spp. were identified in the inside and outside rigs. In addition, *Klebsiella* spp. and *Stenotrophomonas* spp. were only isolated and identified from the effluents of the indoor and outdoor rigs, respectively. A summary of the morphology and health significance of selected waterborne organisms is shown in Table 5-8.

Furthermore, DGGE fingerprinting of the bacterial communities in the twelve test bins and the two inflow samples (Figure 5-42) shows that the bacterial communities of the inflow with and without dog faeces were similar to each other, but despite this similarity, the outflow from the replicate bins showed very different outflow communities. There does not appear to be much similarity between the indoor and outdoor bins. The isolates were identified in the inflow and outflow, and are represented in Figure 5-42 by open ellipses. This showed that they were not necessarily the most abundant organisms in the communities. Bacterial communities are similarly diverse in both the inflow and outflow, showing 20 to 30 possible bacterial species in all communities. Molecular analysis has shown that the microbial diversity in the inflow and outflow is much higher than plating suggests. Further studies are required to determine the microbial community functionality and how this contributes to nutrient removal and bioremediation.

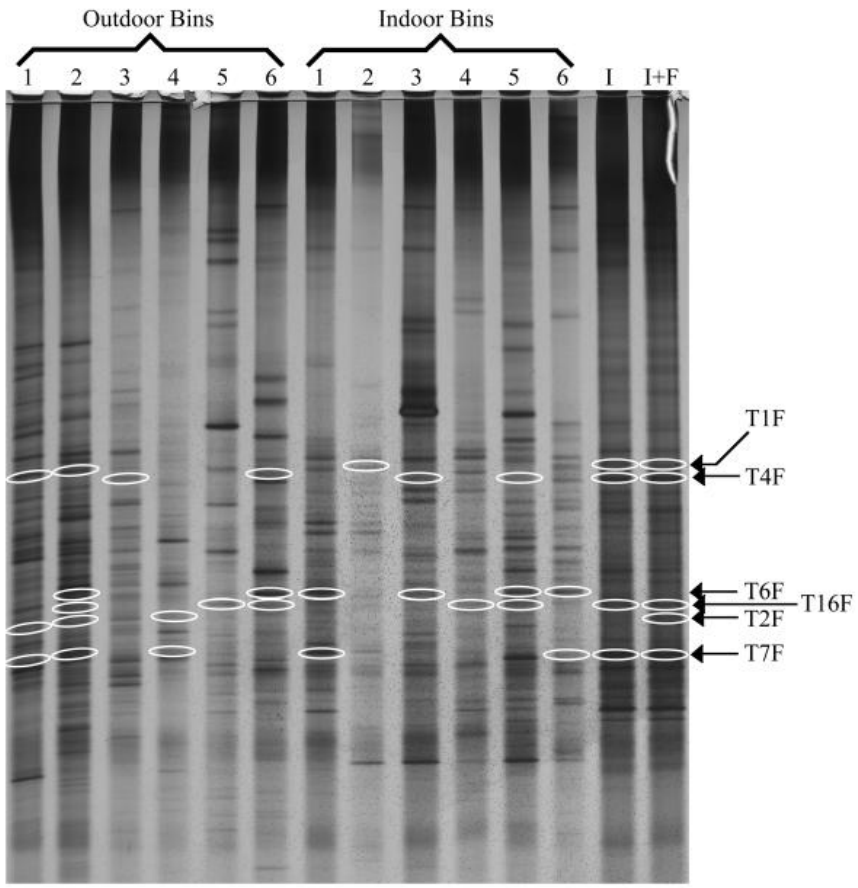

Figure 5-42: Denaturing gradient gel electrophoresis (DGGE) gel showing the bacterial communities in the inflow and outflow of the experimental permeable pavement system. I and I+F represent bacterial communities in the inflow with and without dog faeces, respectively. The positions to which the bands from the known isolates have migrated in the gel are indicated by arrows. These isolates are indicated in the inflow and outflow communities, represented by open ellipses.

Table 5-7: Deoxyribonucleic acid sequencing results for samples collected from indoor and outdoor rigs

Seq	Outdoor rig (PPS 1-6)						Indoor rig (PPS 1-6)						Inflow 1	Inflow 2	Accession no./ closest match	Similarity (%)	Strain
T1 F	x	x					x	±	x				x	x	AM262151.1	99	*A. hydrphila subp. ranea*
T2 F	±	±									x		x	x	AB021192.1	100	*Bacillus mycoides*
T4 F			X			x			x			±	x	x	FM955876.1	100	*Brevendimonas vesicularis*
T5 F	x				X	x			x	x	x		x	x	AM062693.1	99	*Enterobacter amniqenus*
T6 F											x		x	x	FM955853.1	100	*Stenotrophomonas rhizophila*
T7 F	x	x				x	x		x			x	x	x	AY987751.1	100	*A. salmonicida subsp. Salmonicida*
T16 F		x				x			x				±	x	Y17658.1	99	*Klebsiella terrigena*
22F		x		x	X	x					x		x	x	EF204209.1	99	*Brevendimonas nasada*
TA1 F	x	x					x			x	x		x	x	FJ485825.1	100	*Bacillus. subtilis*
M2 F		x	X				x				x		x	x	EU003535.1	98	*Pseudomonas sp.*

Blank = negative; ± =weekly positive; x= positive; X = strongly positive; A=*Aeromonas*

Table 5-8: Morphology and health significance of waterborne pathogens in the permeable pavement system

Sequence	Pathogen	Colony morphology on nutrient agar	Cells morphology	Health significance	Persistent in water supplies	Sources
T1 F	*Aeromonas hydrophila*	Irregular, entire, glistening, yellowish, off white colour and odour producing	Gram negative rods	High	High	Water and food
T2 F	*Bacillus mycoides*	Rhizoids, hairy and white spreaded	Gram positive rods	High	High	Water, soil and sewage
T4 F	*Brevendimonas vesicularis*	Orange small round raised	Gram negative rods	Low	Moderate	Wastewater
T5 F	*Enterobacter amniqenus*	Small, off white colour, round and raised colonies	Gram negative rods	High	High	Water and soil
T6 F	*Stenotrophomonas rhizophila*	White irregular, opaque, raised and creamy	Gram negative (small) rods	High	Moderate	Water, soil and plants
T7 F	*A. salmonicida subsp. Salmonicida*	Small white, round and rough colonies	Gram negative rods	High	May multiply	Wastewater and soil
T16 F	*Klebsiella terrigena*	Purple colour on Eosin methylene blue (EMB), large round and red on Mac. agar	Gram negative rods (single or in pairs)	High	Moderate	Water and soil
T22F	*Brevendimonas nasada*	Orange, small, round and raised	Gram negative rods	Low	Moderate	Wastewater and soil
TA1 F	*B. subtilis*	Small, white and rough colonies	Gram negative rods	High	Moderate	Wastewater and soil
M2F	*Pseudomonas spp.*	Small, white and rough colonies	Gram negative rods	High	May multiply	Wastewater and soil

5.6 Energetic performance of combined GHPs and PPS.

5.6.1 Geothermal heating/cooling sub-base temperatures

Geothermal heating/cooling temperatures are one of the most important water quality parameters in the experiments and was measured at 3 main points in the experimental rig. Figure 5-43 and 5-44 presents the geothermal cooling and heating cycles for PPS 1, 2, 4 and 5 throughout the 1st cooling cycle (April to September 2008), 1st heating cycle (October 2008 to March, 2009) and the 2nd cooling cycle (April to September 2009) and finally the last heating cycle (October 2009 to April 2010).The coolants prevented temperatures falling below 4°C throughout the geothermal cooling cycles and thermostats prevented overheating by switching off the heaters for temperatures $\geq$ 35°C. During the 1st cooling period, indoor rig temperatures (Figure 5-43) were relatively stable and varied between 4.5 to 9.8 ºC. Small fluctuations were caused by different cooling unit temperatures throughout the initial cycle. It can be seen that fluctuations and higher cooling temperatures occurred for PPS 1 and PPS 2 (outdoor rig) throughout the 1st cooling period. This can be a result of external environmental conditions affecting the temperatures through heat flux transfers across the pavement system into the saturated water zone at the sub-base. The second cooling cycle for both indoor and outdoor rigs showed consistencies in the sub-base water temperatures ranging from 4 to 10 ºC respectively.

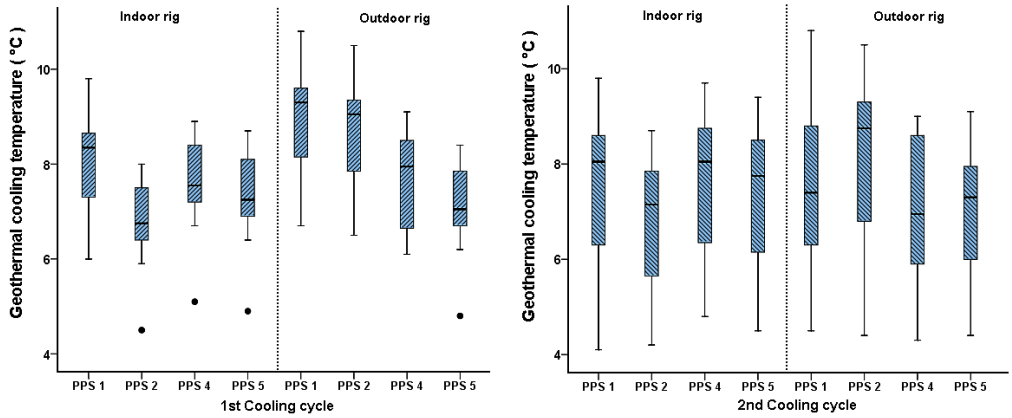

Figure 5-43: Overall geothermal cooling temperatures of sub-base zone for PPS during 1st and 2nd cooling cycles. The plots represent the 25th percentile, median and the 75th percentile. The whiskers represent the 10th and 90th percentiles; solid circles represents outliers (March 2008 to April 2010, n = 113).

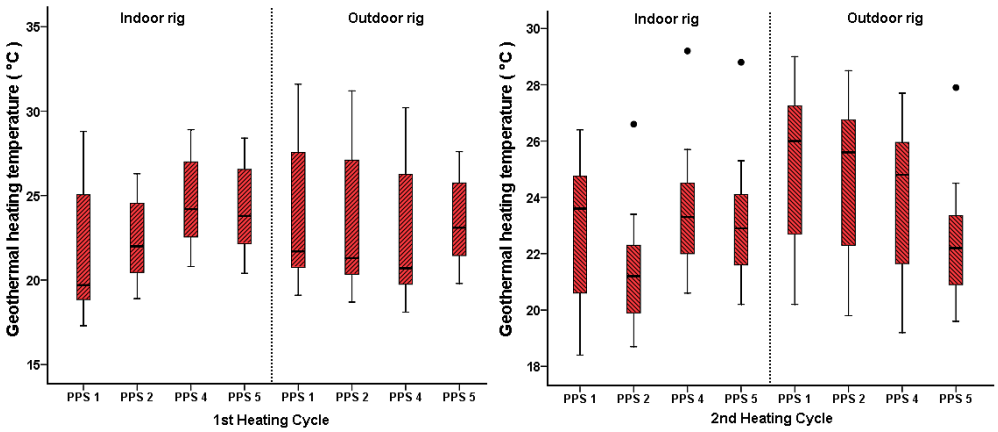

Figure 5-44: Overall geothermal heating temperatures of sub-base zone for PPS during 1st and 2nd heating cycles. The plots represent the 25th percentile, median and the 75th percentile. The whiskers represent the 10th and 90th percentiles; solid circles represents outliers (March 2008 to April 2010, n = 113).

Figure 5-44 illustrates the geothermal heating temperatures for the 1st and 2nd heating cycles, recorded for both the indoor and outdoor rigs. It can be seen that heating temperatures ranges from 17 to 32 °C for the 1st heating cycle and 18.5 to 29 °C for the 2nd heating cycle, regarding both the indoor and outdoor rigs. The large variations from the mean temperatures of 22 °C for PPS 1, 2 and 4 (outdoor rig) throughout the 1st heating cycle, can be a result of external temperatures and humidity changes which results in an overall change for the sub-base water temperatures. Temperatures at the sub-base zone of the experimental bins during both heating cycles followed the seasonal

temperature patterns of domestic heat pumps and mirrored the effects of GHP placed beneath a PPS during the colder months. Water vessel temperatures for all bins during the heating cycles followed similar temperature patterns with an average difference of 3 to 5 ^{o}C. The change in temperatures shows the variations of the heating/cooling coils installed beneath the pavement systems provided evidence on temperature distribution at the sub-base and fluctuations caused by GHP integration. Water temperature in bins with heating/cooling geothermal coils installed followed the vessel water temperature patterns indicating design accuracy and confirming actual temperature changes caused by the heating-cooling coils.

5.6.2 Energy Efficiency Ratio - Cooling Mode

The energy efficiency ratio (EER) measured the steady state cooling efficiency of the geothermal heat pump installed. The higher the EER, the more efficient the unit. The cooling operation modes were employed for the warmer months throughout the year in Edinburgh, Scotland. Figures 5-44 illustrates the overall cooling efficiency results for the two years of the sampled data set. The mean EER (equation 4-3) for both indoor and outdoor rigs for the combined cooling cycles was relatively stable throughout the analysis. The EER index shows a steady rate of 1.3 to 1.8 as a result of the accumulated heat rejected from the system biannually.

As the EER increases, less heat is supplied by the GHP or more heat is rejected by the system for the same amount of mechanical and electrical energy consumed by the pump. However, it should be noted that the total cooling energy consumption is much smaller in relation to the heating energy consumption and indicate a lower performance index when compared to the heating cycles (Figures 5-45), both for the indoor and outdoor rigs.

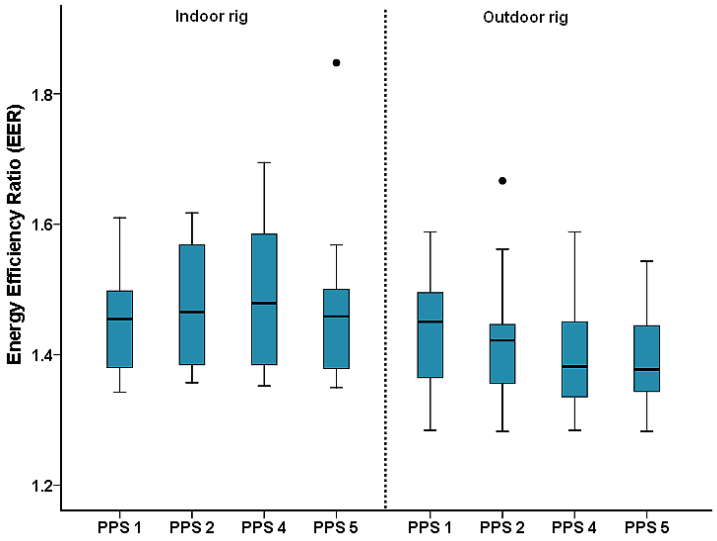

Figure 5-45: Overall energy efficiency ratio (EER) for indoor and outdoor rigs for both cooling cycles. The plots represent the 25th percentile, median and the 75th percentile. The whiskers represent the 10th and 90th percentiles; solid circles represents outliers (March 2008 to April 2010, n = 113).

As a GHP capacity size increases the heat pump energy is rejected and EER increases. The actual performance of the system during the cooling mode is a function of the water temperature produced by the GHP. It is clear from the mean EER performances that the simulated GHP can be categorized as acceptable, when compared to values of the US Department of Energy which ranges from 1.5 to 4 for heat pumps in a cooling cycle (US DOE, 2001). The heat rejection rate which is represented by the EER performance index factor represents the values of cooling performance found in Europe and North America. The values for both indoor and outdoor experimental rigs were found to be in the range of 1.3-1.8 for indoor bins and 1.5-5.5 for outdoor bins, demonstrating that system design was correct and efficient in the aspect of GHP installation within PPS.

Performance of the heat pumps during cooling is such that, at relatively moderate ambient temperatures, the ratio of heat energy output to electrical and mechanical energy consumed have shown, the efficiency of the system which operates in the outdoor (realistic) zone. However, at an ambient air temperature of 15.0 ºC, for the indoor rigs showed no significant performance decline, and no reduction in cooling capacity efficiencies of the installed systems.

5.6.3 Coefficient of Performance COP –Heating Mode.

The coefficient of performance (COP) (equation 4-2) is a measure of a heat pump's efficiency for heating applications. The higher the COP, the more efficient the heat pumps. To investigate the performance of the geothermal heat pump system further, the heating operation modes were employed for the colder periods throughout the year in Edinburgh Scotland (October to March). The GHPs inlet and outlet rigs follow the same pattern of temperature rise as in the case of the cooling mode. Figure 5-46 shows the box and whiskers plot for COP for the corresponding periods. Heating performance rather than cooling performance is normally considered in optimizing GHP's (Healy and Ugursal, 1997).

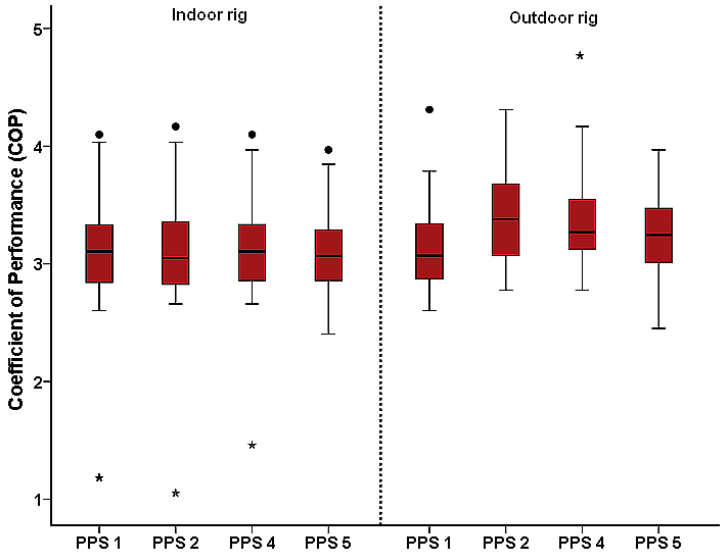

Figure 5-46: Overall Coefficient of Performance (COP) for indoor and outdoor rigs for both heating cycles. The plots represent the 25th percentile, median and the 75th percentile. The whiskers represent the 10th and 90th percentiles; solid circles represents outliers and stars represents extreme outliers (March 2008 to April 2010, n = 113).

The Coefficient of Performance is a key parameter for GHP's. The graphs of COP for both indoor and outdoor rigs illustrate benchmarks for the system in the heating capacity. It can be seen from Figure 5-45 that the system can be categorized as acceptable in the heating cycle. The actual performance of the system is a function of water temperature produced by the GHP. The values of $COP_{heating}$ were found to be 1.1-4.5 for the indoor rigs with extreme outliers occurring for PPS 1, 2 and 4, and

1.5-4.4 for the outdoor rigs respectively. It is noticed that the mean COP values remain relatively consistent around 3.1 to 3.5 for both indoor and outdoor systems. The system's COP varies with the difference between the saturated water temperatures. This difference can simply be defined as the temperature lift (the temperature difference between the source and sink). The lower this temperature difference the higher the COP. This trend is shown in Figure 5-45 and the results given for both indoor and outdoor rigs indicate that the COP of the heat pump increases with increasing temperature of the water entering, hence, higher entering water temperature. Therefore, a smaller temperature difference enhances the overall COP of the heat pump. Again by comparison based on the values of the US department of Energy (US DOE, 2001) the COP heating values for equivalent systems occurs in the range of 2 to 5 (Lund *et al.,* 2004.). As a result, the performance of the simulated system has proven comparable efficiencies to practical GHP units.

Table 5-9 provides the average heating and cooling performance indices calculated for the GHP system. These values are based on the GHP working all year round in the heating or cooling mode. The simulated geothermal heat pump design is thus feasible when it is applied to cooling and heating modes of operation within PPS.

Table 5-9: Average COP and EER Performance Index Ratios for the GHP system.

Location	EER- PPS 1	EER- PPS 2	EER-PPS 4	EER-PPS 5
Indoor	1.43	1.44	1.46	1.41
Outdoor	2.05	2.02	2.46	1.93
	COP-PPS 1	COP-PPS 2	COP-PPS 4	COP-PPS 5
Indoor	3.05	3.11	3.09	3.01
Outdoor	2.14	2.47	2.5	2.42

CHAPTER 6 Photocatalytic Oxidation with Titanium Dioxide (TiO2) for Decontamination and Disinfection.

The enhancement of permeable pavements by integration of titanium dioxide (TiO_2) under UV radiation for a photocatalytic reaction can provide high rates of disinfection against organic pollutants from contaminated urban runoff. Higher standards may be required for stormwater reuse and further treatment via disinfection. The disinfection effects of the TiO_2 photocatalytic reaction on stormwater with combined sustainable urban drainage techniques such as permeable pavements have not been evaluated. This chapter addresses the use of a small laboratory scaled TiO_2/UV photocatalytic reactor in a batch-process for the inactivation of waterborne bacterial microbes (total coliforms *Escherichia coli*, and *Enterococci sp.*).These three microbial groups from the effluents of PPS 1 (outdoor rig) have been used as indexes to test the disinfection efficiency of the combined urban drainage and photochemical treatment. The photo-degradation effects of TiO_2 on these microorganisms haven been examined and photocatalytic reactions between 80 and 100 minutes were required for the complete removal of *Escherichia coli,* total coliforms and *Enterococci sp.* The photocatalyst in suspension was more effective in the disinfection kinetics when compared to the immobilised setup. No bacterial growth was observed after illumination with TiO_2 and UV, after 24 h. Sections of this chapter is under review for the Water and Environment Journal.

6.1 Heterogeneous Photocatalytic processes with Titanium Dioxide (TiO_2)

Heterogeneous photocatalysis is a rapidly developing field in water and environmental engineering and an emerging technology (Shannon *et al.,* 2008). Their applications in oxidizing organic contaminants are still in the laboratory phases. It has a great potential to cope with the increasing pollution by stormwater. A heterogeneous photocatalytic system consists of semiconductor particles (photocatalyst) which are in close contact with a medium (liquid or gaseous) (Fujishima *et al.,* 2000). Exposing the catalyst to light excited states are generated which are capable in initiating subsequent processes like redox reactions and molecular transformations (Herrmann, 2005). In heterogeneous photocatalysis two or more phases are used in the photocatalytic reaction. A light source with semiconductor material is used to initiate the photoreaction (Herrmann, 2005). The catalysts can carry out substrate oxidations and reductions concurrently. UV light of long wavelengths (200-400 nm) can be used, as well as solar energy from sunlight (Soares *et al.,* 2007).

Heterogeneous photocatalysis using semiconductors such as titanium dioxide can be more appealing than conventional methods such as chlorination, ozone, and UV

disinfection for removing organic species in the environment. TiO_2 is known to have and excellent properties such as high ultraviolet absorption and high stability which allow it to be used in applications, such as the photocatalytic degradation of chemicals and organic pollutants in water and air (Fujishima *et al.,* 2000). The photocatalytic process gradually breaks down the contaminant molecules, resulting in no residue of the original material remaining and therefore no sludge in produced (Soares *et al.,* 2007). The photocatalyst is unchanged during the process and no consumable chemicals are required resulting in economic savings for an easier, less complicated disinfection system (Fujishima *et al.,* 2000; Herrmann, 2005; Soares *et al.,* 2007)

Heterogeneous photocatalytic processes (Salih, 2002) use certain metal oxides that can readily generate hydroxyl radicals on the surface of particles when absorbing UV light. The anatase crystalline form of TiO_2 has a low band-gap energy (approximately 3.2eV), which is almost equivalent to 200 to 400 nm wavelength of light, and the catalyst behaves as a classical semiconductor (Salih, 2002) where UV light is absorbed to promote electrons across the energy gap into the conduction band. Hence, the most important heterogenous photocatalytic processes is TiO_2-UV. Illumination of this photocatalyst in water in the range of 200-400nm generates electrons in the conduction band (Wang and Hong, 1999). These electrons form hydroxyl radicals, which can decompose organic compounds. The system presents a more advance reclamation and remediation technology, collecting the stormwater after it is filtered by permeable pavements. Zahraa *et al.,* (2006) showed that photocatalytic decolorization of municipal wastewater contaiminated with textile dyes proved to be effective for dye degradation when irradiated with UV light in the presence of air. Previous studies (Rincón and Pulgarin, 2003; Lonnen *et al.,* 2005) have reported that photocatalytic disinfection can be quenched by impurities in the water, particularly phosphates. Rincón and Pulgarin, (2003) reports reducions of almost 50% in photocatalytic activity for phosphate concentrations in the range of 0.2 to 2.0mmol/L. These phosphate levels are consistent with that of raw sewage and are much greater than the concentrations found in natural waters (Rincón and Pulgarin, 2003). Grzechulska *et al.,* (2000) tested the photocatalytic decomposition of oil in water and showed that complete oil decomposition was achieved just after 2

h of UV illumination with the photocatalyst (TiO_2) content of 0.5 g dm^{-3}. A simplified mechanism for the photo-activation of a semiconductor catalyst is presented in Figure 6-1.

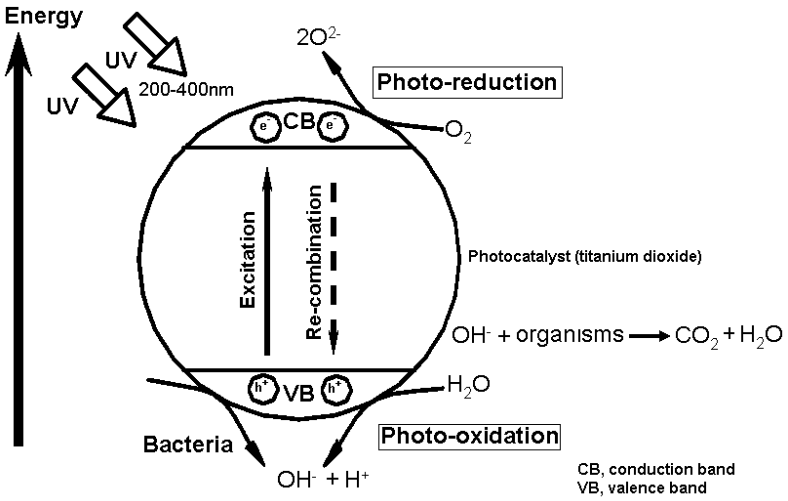

Figure 6-1: The photocatalytic process with UV light and Titanium dioxide (TIO_2) absorbs ultraviolet (UV) radiation from either sunlight or illuminated source (UV lamps) and produces two oxidation reactants (i) hydroxyl radicals and superoxide anions which decompose toxic organic substances via oxidation. (adapted from Wist *et al.,* 2002; Herrmann, 2005)

The valence band hole is strongly oxidizing, and the conduction band electron is strongly reducing (Herrmann, 2005). At the external surface, the excited electron and the hole can take part in redox reactions with adsorbed species such as water, hydroxide ion (OH−), organic compounds, or oxygen (Herrmann, 2005). The charges can react directly with adsorbed pollutants, but reactions with water are far more likely since the water molecules are far more populous than contaminant molecules. Oxidation of water or OH− by the hole produces the hydroxyl radical (•OH), an extremely powerful and indiscriminant oxidant (Wist *et al.,* 2002). The electron and hole can recombine, releasing the absorbed light energy as heat, with no chemical alterations (Wist *et al.,* 2002). The charges can still recombine, or they participate in redox reactions with adsorbed organic pollutants. Photooxidation, photoreduction, and adsorption occur on or near the particle surface as shown from Figure 6-1. The illumination of semiconductor particles such as TiO_2 generates e^-_{cb} and h^+_{vb} as described previously. An array of photochemical reactions occurs between water,

oxygen, organic molecules and contaminants which may be present in the system and is presented in Table 6-1.

Table 6-1: The principle photochemical reactions and mechanisms for titanium dioxide TiO_2 (after Wang and Hong, 1999; Rincón and Pulgarin, 2003).

Major photochemical reactions of TiO_2	Description	Reaction no.
$TiO_2 \rightarrow^{hv} TiO_2(h^+_{vb} + e^-_{cb})$	The first step involves ultraviolate (UV) light inducting the generation of a hole (h_{vb}^+) and electron (e^-_{cb}) pair in the valence band (vb) and conduction band (cb), respectively.	(I)
$O_2 + e^-_{cb} \rightarrow O_2\bullet^-$	The conduction band electron e^-_{cb} is available for electron transfer to reducible species that are adsorbed to the TiO_2 surface. The CB electron reduced oxygen to a $O_2\bullet^-$ radical.	(II)
$O_2\bullet^- + e^-_{cb} + 2H^+ \rightarrow H_2O_2$	Further reduction of the oxygen $O_2\bullet^-$ radical produces hydrogen peroxide (H_2O_2)	(III)
$O_2\bullet^- + H_2O_2 \rightarrow \bullet OH + OH^- + O_2$	The superoxide can react with H_2O_2 to produce the OH radical (Haber-Weiss reaction)	(IV)
$e^-_{cb} + H_2O_2 \rightarrow \bullet OH + OH^-$	Reduction of H_2O_2 by e^-_{cb} produces the OH radical	(V)
$h^+_{vb} + OH^- \rightarrow \bullet OH$	The VB hole abstracts electrons from absorbed oxidizable species or reacts with hydroxyl oxoanion (OH^-) or water (H_2O) to form the OH radical.	(VI)
$h^+_{vb} + H_2O \rightarrow H^+ \bullet OH$	The VB hole reacts with H_2O to form the OH radical.	(VII)
$2\bullet OH \rightarrow H_2O_2$	The recombination of OH radicals also produces H_2O_2 (oxidative pathway).	(VIII)

6.2 Research Aims and Objectives

The research objectives of this chapter are to assess a novel experimental design of combined permeable pavements and photocatalytic treatment system and to evaluate the disinfection efficiency of varying photocatalytic disinfection with combined sustainable urban drainage systems. The experimentation would provide interim knowledge on permeable pavements and photocatalytic disinfection and guidance as an appropriate technology for the implementation on stormwater recycling.

• Study at a lab scale experiment, in a batch process, the applications of combined permeable pavements and photocatalytic disinfection for the recycling of general urban stormwater runoff;

• Identify the concentrations of the photocatalyst Titanium Dioxide (TiO_2) that is capable of removing microbiological pollutant parameters such as Total coliforms, *E.coli*, and *Enterococci sp.* and as well as the inactivation rate constant for these microbes.

• Compare the performance of Titanium Dioxide (TiO_2) is a suspended or immobilised form for stormwater disinfection within the photocatalytic batch reactors.

6.3 Photocatalytic reactor and photochemical experiments

Titanium dioxide was used because of its low cost (£2.50) per kg in commercial quantities (Fisher Scientific UK Ltd, Bishop Meadow Road, Loughborough, Leicestershire, U.K.) and is readily available and conservative in nature as a photocatalyst. Anatase (TiO_2) was purchased from Fisher Scientific UK Ltd and used in all photochemical experiments. Pyrex glass beakers of 500ml were used as batch reactors. A UV lamp (Ultra-Violet Products Ltd Unit 1, Trinity Hall Farm Estate, Nuffield Road, Cambridge, UK) was employed as shown in Table 6-2. The lamp fitted the diameter of the glass beakers and was placed at the centre with a total distance of 5 cm from the surface of the water in order to enhance total incident irradiance. The irradiation experiments were performed at a fixed temperature of 20°C, and controlled humidity, all external lighting was controlled, whilst a control experiment (blank) was placed in the dark at the same temperature, with no applications of UV or photocatalyst disinfection. Anatase (TiO_2) catalyst concentrations was added in concentrations of 200 mg/l, 400 mg/l and 600 mg/l for both immobilised (fixed on glass) and suspended. Previous studies by Cho *et al.,* (2004) and Rincón and Pulgarin, (2003) has shown that concentrations of photocatalyst in this range and dosage have a high efficacy rate for protozoan, fungal and bacterial microbes in water. Immobilization was performed by evenly smearing a silicone adhesive on a glass plate and pressed against for uniformly spreading of the

catalyst in its anatase crystal powder form. Excess powdered TiO_2 was removed by tapping. After the glass plate was left overnight to dry in an incubator at 37 °C.

Table 6-2: UV lamps specifications used in photocatalytic reactor (Ultraviolet products Ltd Unit 1, Trinity Hall Farm Estate, Nuffield Road, Cambridge, UK).

Type	Unit	UV™ Lamps
λ wavelength (nm)	nm	200–400
Ratio UV-B/UV-A	-	<0.1 (%)
Electric power (W)	W	24
UV-A power (W)	W	8
Cap-base	-	2G11
Quartz length (mm)	mm	240
Total length (mm)	mm	260
Useful life (h)	h	5000
Ballast type	-	Electronic

The degradation rate was analysed by culture methods as described in Chapter 3. For analysing the indicator organisms, samples were taken from the influent and the effluent of PPS 1 (outdoor rig) and thereafter at regular intervals of 20 minutes from the photocatalytic disinfection experiments. The samples were analysed for total coliform, *E. coli*, and faecal streptococci. Water samples from the effluent of PPS 1 (outdoor rig) (pre-treated urban runoff) as well as samples after disinfection from UV and UV-TiO_2 were collected in 2 Litre sterile bottles and analysed within 2 h. The samples were diluted serially and cultured in triplicate to reduce the error margin.

The photocatalytic treatment was tested using artificial irradiation (UV) in a lab-scale reactor able to treat approximately 0.5 L of urban runoff wastewater. The photocatalytic reactor constitutes of a beaker (30 cm in height and 24 cm in diameter), a magnetic stirrer Anachem Ltd, Anachem House, Charles Street, Luton, Bedfordshire, United Kingdom) and the UV lamps fitted ontop (Figure 6-2). The filtered urban wastewater was collected from the permeable pavement rig and placed in the photochemical reactor (see Figure 6-2) where the photocatalytic oxidation took place under continuous stirring with a speed of 300 rpm to allow complete mixing and application of solar or artificial irradiation. Water sample microbes were identified by Pour-Plate and Spread-Plate techniques (Maier *et al.,* 2000), from the UV and photocatalytic treatments where plating efficiency was 98 %.

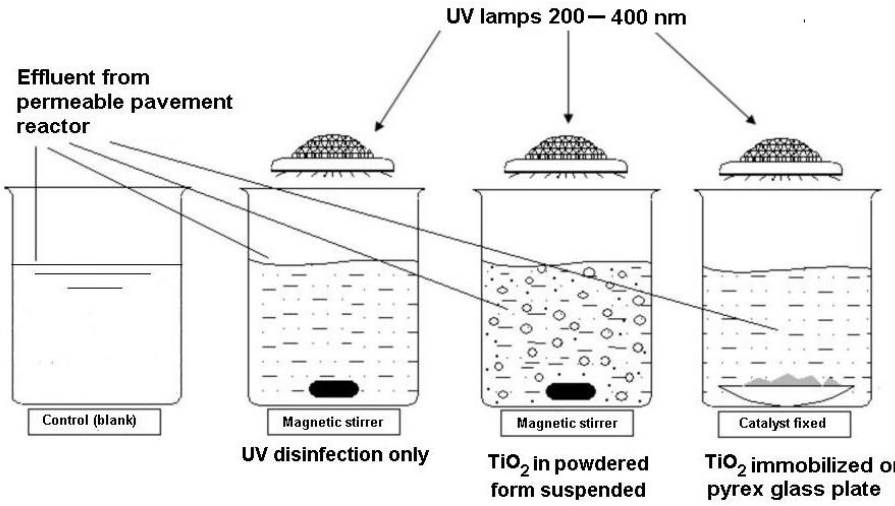

Figure 6-2: Schematic of the photocatalytic experimental apparatus for the photochemical reactors (batch processes), UV treatment only, UV+TiO_2 in immobilised and suspended forms.

6.4 Results and Discussion

6.4.1 The photocatalytic disinfection model (Chick-Watson model)

The photocatalytic disinfection processes has a complex mechanism; therefore the kinectic analysis of the photocatalytic bacterial inactivation can be analysed using empirical equations. Previous literature has reported that the Chick-Watson disinfection model is applicable to photocatalytic treatment of wastewater (Cho *et al.,* (2004); Fernández-Ibáñez *et al.,* 2009).

A disinfection kinetic model is usually required in order to compare the results obtained from different experimental conditions. The photochemical disinfection process for the experiments can be described by Chick-Watson Model,

$$\ln\frac{N}{N_o} = -kCT \quad \text{e} \tag{6-1}$$

- N_o is the initial microbial population (cfu/ml)
- N is the final microbial population (cfu/ml)
- k is the pseudo-first order inactivation rate constant (min^{-1})
- C is the OH radical concentration (mg/l)
- T, the inactivation time (min) of the microorganisms.

Linearization of Chick-Watson, the equation it becomes,

$$\frac{N}{N_o} = e^{-kCT} \tag{6-2}$$

Where e = number e (≈ 2.71828).

The inactivation pseudo-first order inactivation rate constant k (min^{-1}) was calculated for all experiments. The efficiency of disinfection is given by 100 × (N/N_0), which refers to the concentration ratio of the microbial pollutants in the water measured at any time, N, compared to the initial concentration, N_0. The higher the calculated value the more pronounced reduction in the microbial contaminant level, and, therefore, the better the photocatalytic inactivation efficiency (Fernández-Ibáñez *et al.,* 2009).

6.4.2 Total coliform photochemical deactivation

The effect of UV radiation on the viability of total coliforms is presented in figure 6-3. The experiment analysed UV radiation treatment only, UV with Titanium Dioxide in both suspended and immobilised forms. After 140 minutes the surviving fraction as a function of the time of UV exposure was negligible for approximately all the total coliforms present in the water, where inactivation was achieved by UV radiation only (Watts *et al.,* 1995). The germicidal effect of UV-radiation at wavelength ranging from 227 to 329 nm was known as early as 1900 (Watts *et al.,* 1995). Many researchers in the past have shown that UV is able to inactivate microorganism due to the synergistic effect from the infrared radiation. Figure 6-3 illustrates that after just 80 min heterogeneous photocatalysis with a concentration of 400 mg/l in the suspension form was responsible for the reduction of approximately 99.99% of the initial concentration of total coliforms in comparison to 400 mg/l in the immobilised form which took almost the same time as UV radiation for complete removal of total coliforms, however the inactivation processes was at a faster rate. The graphs in figure 6-3 indicate that within the first 20 to 40 minutes there is a sharp increase in the inactivation of the total coliform bacteria and after around 80 minutes time stabilization of the remaining total coliform bacteria occurred. As shown in

table 6-3 for the inactivation rate constants k (min^{-1}) for total coliforms, disinfection with UV radiation only resulted in the slowest inactivation rate (0.01563 min^{-1}) in comparison to both immobilised and suspended concentrations with the photocatalyst (TiO_2). Comparing the same concentrations for both immobilised and suspended, at 400 mg/l of TiO_2 , in the suspension form had the highest inactivation rate of (0.0744 min^{-1}) this was followed by a concentration of TiO_2 of 200 mg/l in the suspension form with an inactivation rate constant of 0.05058 min^{-1}. On average the catalyst in suspension at a concentration of 400 mg/l was 64% faster than that in its immobilised form, this was followed by a 40% difference in the rates for both 200 mg/l and 600 mg/l when compared to the immobilised form at the same concentrations. Comparing the results obtained in the experiments for total coliforms, it can be established that the photocatalytic disinfection process is a consequence of both the direct action of the UV on the microorganisms as well as the photocatalytic degradation from the excited photocatalyst particles. As shown in Figure 6-3 there is a synergistic effect of UV and oxidative species generated by the photoactivation of TiO_2 both in suspension and immobilised. A turbidity of 4.2 NTU did not affect the rates of disinfection for the total coliforms.

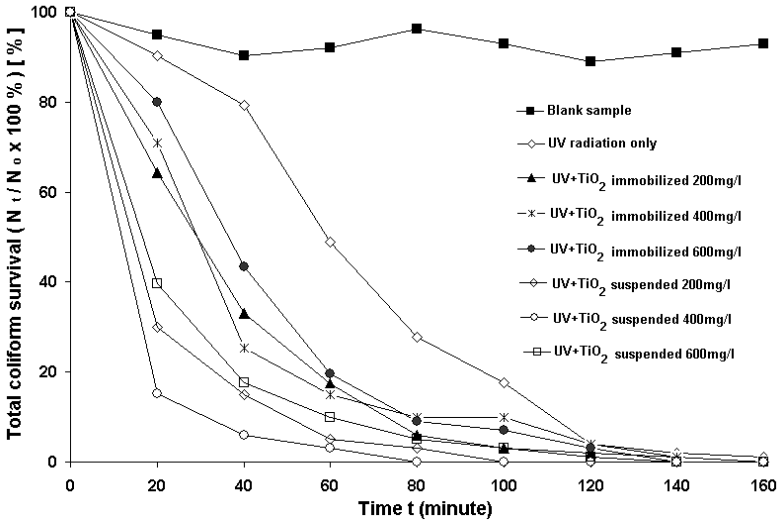

Figure 6-3: Survival of total coliforms (CFU/100ml) in the presence of ultraviolgiht light radiation only (UV), immobilised and suspended powdered form of TiO_2 in concentrations of 200mg/l, 400mg/l and 600mg/l. The initial values of turbidity (4.2 NTU) and total coliforms (N_0= 9.54 × 10^5 +/- 2000 CFU *per* 100 mL) from PPS 1 (outdoor rig) effluent.

6.4.3 *E.coli* photochemical deactivation

UV induced disinfection is well demonstrated in figure 6-4 for *E.coli*. The efficiency of the process for the decontamination of *E.coli* can be judged by the steep reductions in the number of viable bacteria cells remaining after exposure for 80 to 160 minutes. Just under three hours of exposure to UV and the photocatalyst were enough to reduce the number of survivors for this Gram-negative bacterium. This time is substantially reduced for application of the semi-conduction TiO_2. In the suspension form there is an increase in the disinfection capacity where the inactivation rates resembling that of the total coliform bacteria occurred. In suspension form at a concentration of 400 mg/l and 200 mg/l of TiO_2 the inactivation rates were 0.07637 min^{-1} and 0.07470 min^{-1} respectively. When TiO_2 was immobilised it was less efficient. This may be as a result of the localization of the TiO_2 with only microbes that are close to the TiO_2 being affected (Lonnen *et al.,* 2005) making suspended TiO_2 around 60% more effective that the immobilised form for disinfection of *E.coli*. The efficacy of the photocatalytic batch-process against waterborne bacteria such as *E.coli* has been significantly addressed. With the UV lamps energy inputs (8Watts) and a wavelength of 200 to 400 nm, performed reasonably well as expected for direct disinfection rates. The inactivation kinetics of *E.coli* is consistent with that reported by (Watts *et al.,* 1995; Lonnen *et al.,* 2005). Figure 6-4 shows that both systems are effective against the pathogenic organisms such as *E.coli* but with less energy and time required the implementation of photocatalyst may seem as more viable and economic. The inactivation rates achieved with TiO_2 (immobilised) was always less that that observed for the corresponding concentrations in suspension under similar conditions. This indicates that the advanced oxidative processes (AOPs) caused within the batch reactor by the UV, activated TiO_2 in the creation of a hostile environment that accelerates the microbial inactivation processes. The results displayed in Table 6-3 and Figure 6-4 clearly demonstrate that photocatylitic batch process reactors have been fitted with permeable pavements and the photocatalyst in suspension requires significantly less time and consequently smaller UV doses for the inactivation of *E.coli* microbial

species in urban runoff water when compared to UV treatment only in addition to a lesser extent TiO_2 in the immobilised form. When the *E. coli*-contaminated water was not exposed to irradiation (no photo-degradation took place), no change in the *E. coli* level was observed. The behavior of *E.coli* degradation indicated that the adsorption of microorganisms onto the TiO_2 surface shows that TiO_2 assisted photo-oxidation is the major process involved in the removal of *E. coli* in the water.

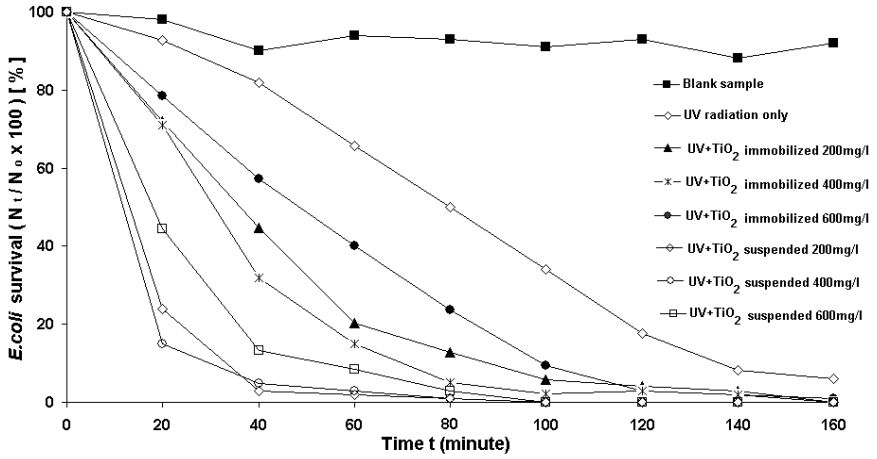

Figure 6-4: Survival of *E. coli* in the presence of ultraviolgiht light radiation only (UV), immobilised and suspended powdered form of TiO_2 in concentrations of 200mg/l, 400mg/l and 600mg/l. The initial values of turbidity (1.5NTU) and *E. coli* (N_0= 7.54 × 10^4 +/- 230 CFU *per* 100 mL) from PPS 1 (outdoor rig) effluent.

6.4.4 *Enterococci sp.* photochemical deactivation

The number of *Enterococci sp.* bacteria as a function of time during photocatalytic treatment is shown in figure 6-5. Reduction of the *Enterococci sp.* inactivation efficiency observed (Figure 6-5) followed Chick-Watson degradation kinetics. Lower efficiency in faecal streptoccoi inactivation was observed in immobilised forms which mimics the disinfection processes for both total coliforms and *E.coli*. UV and TiO_2 in suspensions concentrations of 400mg/l and 600mg/l had inactivation rate constants for *Enterococci sp.* of 0.05504 min^{-1} and 0.04401 min^{-1} respectively. These were 60 to 70% faster than those of similar concentrations in the immobilised form. It is seen again that after 80mins nearly all faecel streptococci present in the water samples were photo-degraded, when compared to just UV

radiation singly, going beyond 160 minutes for total removal of the microbe. Steady-state hydroxyl radical quantitation form the photocatalyst activity shows that the form in which the phototcatalyst (whether suspended or immobilised) is related to the disinfection activity for *Enterococci sp*. The photodegradation of *Enterococci sp.* was unaffected by the turbidity in the range of 1-5 NTU. There is an increase disinfection efficacy with a dosage between 400 to 600 mg/l in suspension.

Nevertheless the presence of TiO_2 in both forms enhanced the disinfection efficiency of *Enterococci sp.* to an appreciable extent. Some factors influencing the photocatalytic activity of TiO_2 in immobilised form would be the diminution of specific surface area of the catalyst to the *Enterococci sp.* bacteria and UV light (Herrera Melián *et al.,* 2000). In the immobilised form TiO_2 could enhance the recombination of photo-generated electron/holes pairs and the pathway followed by the UV light to reach the TiO_2 layers which are in contact with bacterial suspension as seen in Figure 6-5. As previously mentioned turbidity did not significantly affect the efficiency of inactivation for *Enterococci sp.* Particulate matter in suspension can affect the process of water disinfection because light scattering occurs, thereby filtering the ultraviolet radiation unto microorganism. Similar to the particles that cause turbidity, the microbial aggregates can affect the efficiency of disinfection because they serve as a support for pathogenic organisms, protecting against the dispersing radiation. In the case of heterogeneous photocatalysis, the active surface of the TiO_2 reactor can be reduced by the adsorption of particulate material, including aggregates of microorganisms (Herrera Melián *et al.,* 2000). Although the samples were taken from the permeable pavement reactor which initially came from natural sources, there was a significant decrease in the initial *Enterococci sp.* level, approximately 99.98 % (400 mg/l in suspension) after 80minutes and 91.38 % (N/N_o, UV only) inactivation after 160 minutes, were obtained for the water samples, respectively. These results are especially relevant because they indicate that the high efficiency of TiO_2-assisted disinfection achieved in urban runoff is very much effective in the removal of the *enterococci* bacterial species. The *Enterococci sp.* inactivation rate could also be dependent on the physical-chemical parameters of the water, as well as on the presence of biogenic and anthropogenic compounds. The

results indicate that the efficacy of the photocatalytic process is drastically affected as the concentrations are varied as well as the fixation or suspension form of TiO_2.

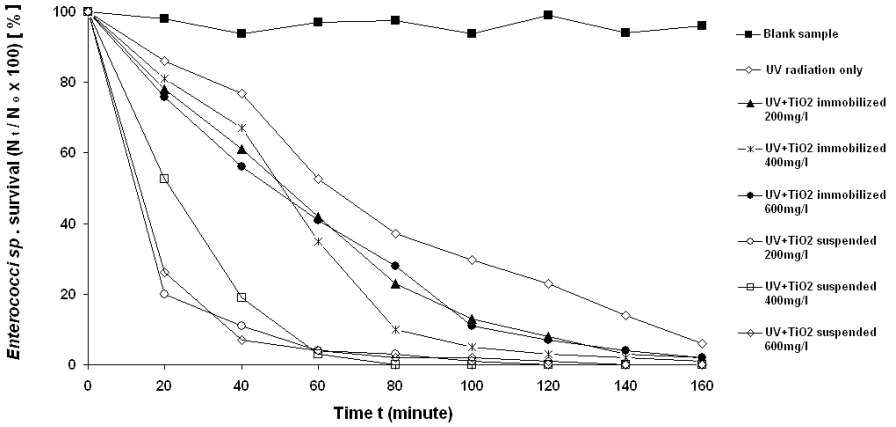

Figure 6-5: Survival of *Enterococci sp.* in the presence of ultra violet light radiation only (UV) immobilised and suspended powdered form of TiO_2 in concentrations of 200mg/l, 400mg/l and 600mg/l. The initial values of turbidity (5.4NTU) and *Enterococci sp.* (N_0= 3.90 × 10^3 +/- 170 CFU *per* 100 mL) from PPS 1 (outdoor rig) effluent.

Table 6-3: Inactivation rate constants *k* (min-1) for Total Coliforms, *E.coli* and *Enterococci sp*. with UV, UV and Titanium Dioxide in both immobilised and suspension.

System type	Treatment	Total Coliforms (min^{-1})	*E. Coli* (min^{-1})	*Enterococci sp.* (min^{-1})
	UV	0.01563	0.01209	0.01165
Immobilised (fixed on glass)	UV+TiO_2 (200 mg/L)	0.03027	0.02331	0.01855
	UV+TiO_2 (400 mg/L)	0.02693	0.02003	0.02197
	UV+TiO_2 (600 mg/L)	0.02437	0.03163	0.01884
Suspended	UV+TiO_2 (200 mg/L)	0.05058	0.07470	0.18260
	UV+TiO_2 (400 mg/L)	0.07440	0.07637	0.05504
	UV+TiO_2 (600 mg/L)	0.04005	0.04450	0.04401

6.5 Bacterial pollutants reappearance analysis

Total coliform, *E.coli* and Faecal streptoccoi experiements were carried out at the natural pH (7.5) for samples with and without TiO_2. After UV irradiation the UV-lamp was turned off and the sample was left at a controlled room temperature of 21.0

°C. The water samples were aerated (air-bubbled) for 3 hrs. After 24 hrs the bacterial reappearance was nil or almost insignificant for both experimental conditions (presence or absence of the photocatalyst).

6.6 Summary

Combined permeable pavements and photocatalysis oxidation have a great potential for the future of stormwater treatment. Further disinfection treatment with the batch process reactors was effective for the inactivation of total coliforms, *E.coli* and *Enterococci sp.* With an excellent correlation between TiO_2 and degradation rates of the microbial water pollutants, the findings suggest that TiO_2 photocatalyst is a viable process for disinfection of bacteria in urban water systems. The presence of TiO_2 enhanced the disinfection efficiency to an appreciable extent when compared to UV treatment only. The removal of organic matter from the permeable pavement reactor greatly improves the inactivation kinectics. With organic matter present within the photocatalytic batch process this would compete for hydroxyl radical oxidants therefore affecting the photochemical disinfection process. The heterogeneous photocatalytic experiments indicate that the OH radical is the primary species responsible for the microbes' inactivation. Calculations from the Chick-Watson model, with concentrations of 400 mg/l to 600mg/l of TiO_2 in the suspension form was more effective than the immobilised form which was on average 40-60% more effective with regards to the inactivation rate constants (k min^{-1}), totally removing the microbial pollutants within 80 minutes. The complete inactivation of the microbes from the stormwater indicates that photocatalysis represent an attractive means to decontaminate urban runoff. UV irradiation has proved to be an efficient source of light through the photocatalytic processes. This also shows with sun-bathed countries applications of permeable pavements and photocatayltic treatment is a feasible option for urban runoff disinfection.

Considering all the aspects discussed in this chapter and the continuous demand for sanitation technology with concomitant treatment and reuse purposes for stormwater, heterogeneous photocatalysis using TiO_2 must be considered as an attractive technology. It is important to emphasize that TiO_2 films can be produced

without access to specialized laboratory equipment. The main future challenges for using photocatalystic disinfection with combined permeable pavements in stormwater treatment could be the development of an efficient and low cost technology to promote sufficient treatment. As seen in figure 6-6, the use of renewable energy sources, such as solar energy and the adoption of such strategies for processes integration as a replacement to UV lamps integrated with permeable pavements can be applied. The use of solar irradiation with TiO_2 photocatalysis and permeable pavements (Figure 6-6) could result to an increase in efficiency for the produced hydroxyl radicals, causing a reduction in cost and energy. The application of separation steps such as permeable pavements which acts as both a sedimentation and filtration zone before the application of photocatalytic oxidation could achieve lover cost and sufficient organic compounds removal.

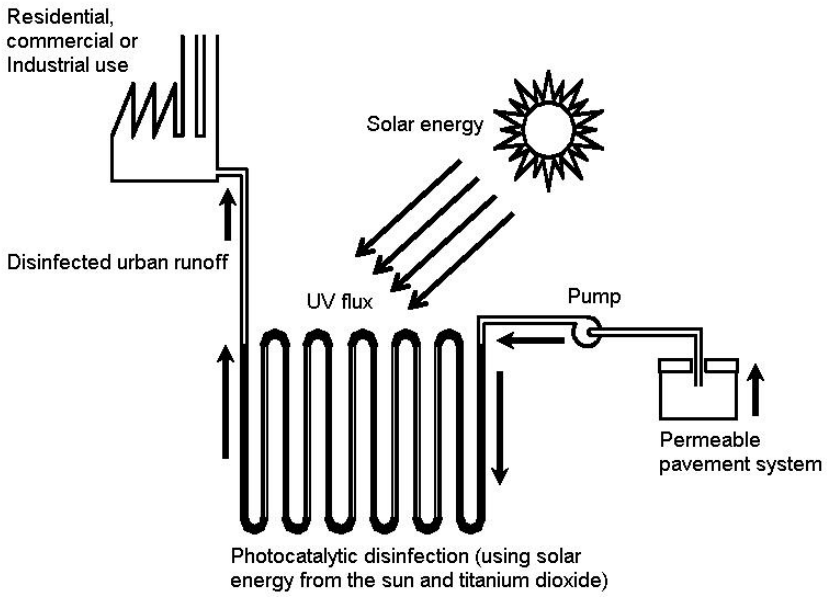

Figure 6-6: Conceptual schematic of permeable pavements for initial filtration and treatment of urban runoff followed by photocatyltic decontamination with solar energy.

Chapter 7 Runge-Kutta Methodology for Simulation of Temperature and Energy Balances

An energy and temperature balance was developed for two outdoor experimental permeable pavement bins which were subjected to geothermal heating and cooling (geothermal paving systems). The heat fluxes were analysed for a heating and cooling cycle to determine the thermogeological relationship for the systems. A 4th order Runge-Kutta numerical method was developed to model the heat fluxes and energy balance using measured temperature data and other environmental factors such as solar radiation, convection and evaporation heat fluxes for the outdoor pavement systems. The model was statistically tested for its validity and it can be concluded that the Runge-Kutta technique proved to be an effective and reliable simulation tool. Segments of this chapter have been accepted for publication in the International Journal of Road Materials and Pavement Design.

7.1. Justification of Thermogeological Model for Geothermal Pavement.

Water temperature is a critical parameter in urban runoff reuse and recycling. Survival of microbiological organisms and growth rates or degradation kinetics of bacterial parameters are linked to the environmental stresses that occur within water at varying temperatures which can affect the environmental impacts and degrade the sustainability of urban runoff reuse (Maier *et al.,* 2000). Furthermore, pathogens may thrive within a given temperature range (Maier *et al.,* 2000). The water temperature of permeable pavements systems can also affect management practices. Saturated water temperatures for the heating cycle in the aquifer zone of the pavement occurs beween 21 and 26 °C and in this mode has a moderately faster bacterial decomposition rates in this temperature range when compared to 4 to7 °C for the cooling mode (Coupe *et al.,* 2009); and enough dissolved oxygen to support the decomposition process (Pond, 2005). There are several reasons why temperature plays a pivotal role in the development of geothermal paving systems regarding urban runoff reuse. From commercial perspectives, applications of geothermal heat pumps for seasonal cycles (winter and summer) justify the control and monitoring of the treated stormwater's temperature at the sub-base of the pavement system. As a result of the risk of legionellosis, caused by the proliferation of *Legionella* bacteria

7.2 Modelling Methodology

The aquifer at the base of the permeable paving system will be in a form of dynamic hydrological and thermal equilibrium with the environment. In assessing the significance of heat exchange and water flow from the permeable pavements medium, Darcy's Law indicates that flow is dependent on both the hydraulic gradient and the hydraulic conductivity of materials (Banks, 2008) and is adopted to model the filtration and thermal processes. Darcy's equations are linked through suitably chosen conditions that describe the fluid across the surface of the porous media. It provides the simplest linear relation between velocity and pressure within the pavement media under the physically reasonable assumption that the water flow rates are usually very slow and all the inertial (non-linear) terms may be neglected. Heat transfer is dependent on the flow velocity and thermal properties of the pavement rig (Banks, 2008; Charbeneau, 2000). The porosity of the medium within permeable pavement systems is important in controlling the influence of hydraulic conductivity. Materials with higher porosity on average have a higher conductivity (Charbeneau, 2000).

7.3 Governing equations and parameterization of energy and temperature fluxes

Solar radiation and subsequent heat transfer will reach and warm the pavement's aquifer during the summer and convection processes are likely to occur to ensure the water is mixed homogenously throughout. As temperatures drop during the winter, cold water will sink to the base and the geothermal pavement system utilises this change in temperature with the heat exchanger (Chiasson, 1999). The solar radiation and thermal heat transfer fluxes are essential to the overall mechanisms with regards to the paving system energy it receives from the Earth's surface (Chiasson, 1999). Shortwave solar radiation that reaches the surface after atmospheric mixing may be rejected and or partially heat the ground. Thermal infrared radiation is emitted from both the surface and the atmosphere, with a net loss to the surface since the ground is usually warmer than the atmosphere above. The net radiative energy is used to

evaporate water (latent heat), to directly heat the atmosphere and to heat the deeper layers of the soil. Below the pavement surface through the various layers, surface heat diffusion takes place (Hermansson, 2001, 2004). Figure 7-1 illustrates the main processes and components of the energy and water exchange at the surface. The latent heat flux couples the surface energy with the water balance. If rain reaches the ground the water may be stored on the surface, infiltrate into the soil or be transported horizontally as surface runoff (Hermansson, 2001, 2004). These processes mainly depend on soil type and the total amount of water already stored in the soil column. Below the surface the water may reach greater depths through gravitational drainage and diffusion processes and may form interflow or groundwater runoff. When computing the thermal convective and conductive heat transfers of the pavement rigs the hydraulic properties (such as hydraulic conductivity, porosity and velocity) are required in addition to the thermal properties (including thermal conductivity and volumetric heat capacity) which are seen in Table 7-1.

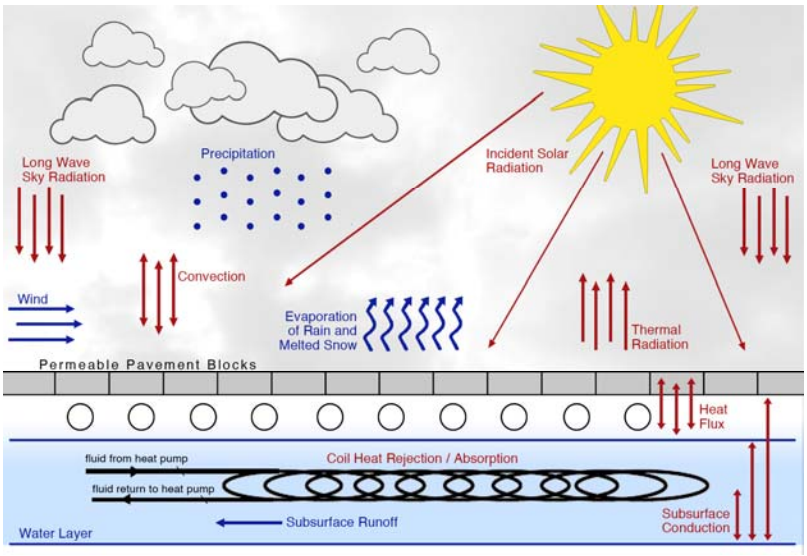

Figure 7-1: Schematic of water and energy balance for geothermal paving system energy and temperature model.

The conventional methodology of performing an energy balance requires the definition of a control volume. Therefore, for this research, all the filtered stormwater within the constructed aquifer zone is defined as the control volume and the thermal energy inertia contained by the geothermal paving system $E_{\text{Geothermal Permeable Pavement}}$ is the

total energy within the boundaries of the control volume. The amount of internal energy or thermal inertia inside the system at any time can be calculated as (Lamoureux *et al.,* 2006):

$$E_{\text{Geothermal Paving System}} = \rho\, V\, c_p\, \Delta T \qquad [7\text{-}1]$$

Where ρ is the density of the water at the sub-base of the pavement (kg/m^3), V is the volume of water in the system, c_p is the specific heat capacity of water (KJ/kg °C) and ΔT is the temperature fluctuations (°C).

Table7-1: Typical Values of Hydraulic and Thermal Properties of Permeable Pavement Systems (adapted from- Freeze and Cherry, 1979; Ling *et al*., 1993; Charbeneau, 2000; Hermansson, 2001, 2004; Banks, 2008; Herb *et al*., 2008.)

Permeable Pavement Medium	**Hydraulic Properties**			**Thermal Properties**	
	Hydraulic Conductivity K (m/s)	**Porosity n**	**Velocity *v* (m/yr)**	**Thermal Conductivity k (W/m°C)**	**Volumetric Heat Capacity $\rho_s c_s$ (J/m^3 °C)**
Permeable Pavement	1.0×10^{-6}	0.42	18.95×10^{4}	1.23	1.05×10^{6}
Geotextile	3.5×10^{-7}	0.52	3.21×10^{7}	0.98	2.23×10^{6}
Clean Stone /Pea Gravel	3.0×10^{-3}	0.38	1.26×10^{7}	0.8	1.40×10^{6}
Gravel (Base)	9.8×10^{-2}	0.31	3.05×10^{3}	0.8	1.40×10^{6}

It is assumed that the geothermal paving system is set up such that the temperature throughout the aquifer is the same for heating and cooling. The total energy in the geothermal paving system is the summation of the top surface and the sub-base aquifer zone (Lamoureux *et al.,* 2006):

$$E_{GPS} = E_{\text{surface}} + E_{\text{aquifer}} = (\rho\, V\, c_p\, \Delta T)_{\text{surface}} + (\rho\, V\, c_p\, \Delta T)_{\text{aquifer}} \qquad [7\text{-}2]$$

The governing equation of the model is an overall energy balance of the geothermal paving system using the lumped parameter approach:

$$q_{in} - q_{out} = \rho\, V\, c_p \frac{dT}{dt} \qquad [7\text{-}3]$$

Where q_{in} is the heat transfer to the permeable paving system, q_{out} is the heat flux leaving the pavement structure, dT/dt is the rate of change of temperature for the storm water runoff in the aquifer zone. If the temperature fluctuates in the constructed aquifer zone of the permeable pavement system, the amount of energy within the control volume also changes and is described by:

$$\left(\frac{dE}{dt}\right)_{GPS} = \left(\frac{d\rho c_p VT}{dt}\right)_{GPS} = \rho c_p \left[T\frac{dV}{dt} + V\frac{dT}{dt}\right]_{GPS} \qquad [7\text{-}4]$$

These fluctuations of temperature and thermal inertia are caused by absorption of solar radiation, heat exchange within the layers and structure of the permeable pavement system, heat fluxes with air as a result of convection, evaporation and black radiation, in addition to the bulk movement of water and transportation of energy across the control boundary system (Charbeneau, 2000; Herb *et al.,* 2008).

The heat movement vector quantities can be quantified and balanced with the rate at which energy within the system is changing (Mengelkamp *et al.,* 1999). A heat balance can be applied which is seen in Figure 7-1. The mathematical expression of the summation of heat transfer is schematically represented in Figure 7-4 and follows the expression:

$$\left(\frac{dE}{dt}\right)_{GPS} = q_{solar} - q_{thernal} + q_{sky} - q_{evap} + q_{snow/rain} \pm q_{conv} \pm q_{pps} - q_{seepage} \pm q_{coils} \pm q_{resp} \qquad [7\text{-}5]$$

E is the total energy at any given time (t) within the geothermal paving system. It is assumed that energy entering the system is positive (heat gain) whilst energy exiting the system is negative (heat loss). Rearranging equation [7-5] as a function of Temperature *T*, it becomes:

$$\left(\frac{dT}{dt}\right)_{GPS} = \frac{q_{solar} - q_{thernal} + q_{sky} - q_{evap} + q_{snow/rain} \pm q_{conv} \pm q_{pps} - q_{seepage} \pm q_{coils} \pm q_{resp}}{V\rho c_p} \qquad [7\text{-}6]$$

Where q_{solar} is the solar radiation heat gain to the geothermal paving system, $q_{thermal}$ is the thermal radiation heat transfer , q_{sky} is the radiative longwave emissions from the sky, q_{evap} is the heat and mass transfer as a result of evaporation throughout the pavement system as a result of the latent heat of fusion and vaporisation, $q_{snow/rain}$ is the sensible and latent heat fluxes resulting from the mass transfer of snow and rain, q_{conv} is the convection heat transfer at the pavement surface, q_{pps} is conduction heat flux across the permeable pavement medium in addition to the heat transfer due to inflow and outflow of urban runoff, $q_{seepage}$ is the internal energy of the liquid movement from seepage, q_{coils} are the heat exchange from the slinky coils at the base of the GPS in the aquifer zone for the heating and cooling cycles respectively, and q_{resp} is the metabolic heat rate from microbial respiration at the base of the permeable pavement structure.

The following assumptions were used to simply the solution of Equation [7-6]:

– The water density and specific heat capacity remained constant, regardless of the changes in water temperatures.

– The pavement's aquifer's volume was constant.

– The sky was cloudless when calculating the emitted atmospheric longwave radiation. Longwave radiation from a cloudless sky is the worst case scenario to ensure that the model did not under predict the thermal fluxes.

– The Hydraulic and Thermal properties of the permeable pavement medium were uniformly distributed.

– No evaporation occurred when the relative humidity of air is at or above 100 per cent.

– The concrete permeable pavement blocks had a solar reflectance value of 40 per cent.

– The heat flux for seepage through the pavement rig was ignored as it's a tanked system, however in practical geothermal paving systems seepage of urban runoff will occur.

7.3.1. Solar Radiation Heat Gain q_{solar}

Solar radiation heat gain is the net solar radiation absorbed by the paving system. It is assumed that all the solar radiation absorbed by the geothermal paving system becomes heat gain and is computed by (Duffie and Beckman, 2006):

$$q_{solar} = \alpha I \quad [7\text{-}7]$$

Where I is the solar radiation incident on the pavement surface and α is the absorptivity coefficient of the permeable pavement material. The absorptivity coefficient is computed for solar incidence angle (θ) using an empirical correlation (Duffie and Beckman, 2006). The model accepts solar radiation in the form of direct and diffused components in which case I is computed from:

$$I = I_{direct} \cos\theta + I_{diffuse} \quad [7\text{-}8]$$

The angle of incidence (θ) of the sun's rays is calculated at each time step from correlations given by Duffie and Beckman, (2006) and ASHRAE, (1997).

7.3.2. Heat Transfer through thermal radiation $q_{thermal}$

Thermal radiation can be viewed as the propagation of energy in the form of electromagnetic waves or discrete photons. No medium is required in its propagation form (source). Thermal radiation with wavelengths ranging from λ =0.2-1000 μm will be taken into account (Duffie and Beckman, 2006; Dieter and Stephan, 2006). The thermal heat transfer mechanisms is spilt into two major components, (i) The heat transfer from the aquifers surface throughout the system and (ii) the heat fluxes at the pavements top surface. For both heat transfers, the model uses a linearized radiation coefficient h_r defined as (Dieter and Stephan, 2006):

$$h_{r(aquifier)} = 4\varepsilon_w \sigma \left[\frac{T_{aquifer} + T_{sky}}{2} \right]^3 \text{ for the permeable pavement aquifer} \quad [7\text{-}9]$$

and

$$h_{r(pavement)} = 4\varepsilon_P\sigma\left[\frac{T_{pavement} + T_{sky}}{2}\right]^3 \text{ for the permeable pavement surface.} \quad [7\text{-}10]$$

Where ε_w and ε_p are the emissivity coefficients for the water in the constructed aquifer zone and the permeable pavement respectively. σ is the Stefan-Boltzman constant, $T_{aquifer}$ is the water temperature at the base of the pavement rig in absolute units, $T_{pavement}$ is the pavements surface temperature in absolute units and T_{sky} is computed from the relationship which relates sky temperature to the dew point temperature (T_{dp}) and the dry bulb temperature (T_{db}) (Van Buren *et al.,* 2000)

$$T_{Sky} = T_{db}\left[0.8 + \frac{T_{dp}}{240}\right]^{\frac{1}{4}} \quad [7\text{-}11]$$

All temperatures are in absolute units. The thermal radiation heat transfer ($q_{thermal}$) is then computed by (Van Buren *et al.,* 2000):

$$q_{thermal} = h_{r(aquifier)}A_{aquifer}\left(T_{sky} - T_{aquifer}\right) + h_{r(pavement)}A_{pavement}\left(T_{sky} - T_{pavement}\right) \quad [7\text{-}12]$$

7.3.3. Sky longwave radiation (q_{sky})

For a cloudless sky, the emissivity can be approximated with the following equation (Bliss, 1961; Diefenderfer *et al*., 2006):

$$\varepsilon_{sky} = \frac{1}{c_1 - c_2 T_{dew} + c_3 T_{dew}^2} \quad [7\text{-}13]$$

Where c_1 = 1.2488219, c_2 = -0.0060896701, c_3= 4.8502935 $\times 10^{-5}$ and T_{dew} is the dew temperature (°C).

The dew temperature is calculated from the following equation (Bliss, 1961):

$$T_{dew} = \frac{1}{\left(\frac{1}{T_{air} + 273}\right) - (1.846 \times 10^{-4})\ln(rh)} - 273 \quad [7\text{-}14]$$

T_{air} is the air temperature (°C), rh is the relative humidity. Using the apparent emissivity, the longwave sky radiation is expressed as (Bliss, 1961; Dieter and Stephan, 2006)

$$q_{sky} = \varepsilon_{sky} A_{pavement} \sigma (T_{air} + 273)^4 \quad [7\text{-}15]$$

T_{air} is the air temperature recorded in Degrees Celsius (°C),

7.3.4. Heat Transfer through Conduction q_{pps}

In practice, the properties of the geothermal paving system can vary tremendously as a result of the local climate, soil compositions and temperatures. Two properties of interest here are the thermal conductivity of the materials (k) and the volumetric specific heat (C_v). The rate at which heat is exchanged across the permeable pavement system can be described by Fourier's Law of heat conduction (Dieter and Stephan, 2006; Incropera *et al.,* 2007; Diefenderfer *et al.,* 2006):

$$q_{pps} = -k_n A \left.\frac{\partial T}{\partial z}\right|_{z=0} \quad [7\text{-}16]$$

Where k is the thermal conductivity of materials within the geothermal paving system (Table 7-1), A is the area of the aquifer (m^2), T is the temperature fluxes of the materials, z is the depth (m), $\left.\frac{\partial T}{\partial z}\right|_{z=0}$ is the temperature gradient across the geothermal paving system.

For the scenario where the water temperature and the flow characteristics along the permeable pavement medium remain constant (Dieter and Stephan, 2006; Incropera *et al.,* 2007):

$$-k_n A \left.\frac{\partial T}{\partial z}\right|_{z=0} = -hA\,(T_{pavement\ medium} - T_{Aquifer}) \quad [7\text{-}17]$$

Where *h* is the heat transfer coefficient ($W/m^2/K$). Setting the initial and final boundary conditions, it was assumed that the temperature throughout the pavement medium was initial the same at all depths for both heating and cooling cycles.

$$T_{\text{pavement medium}}(z, t) \approx T_{\text{initial}} \quad [7\text{-}18]$$

$$T(z = 0, t) \approx T_{\text{Aquifer}} \quad [7\text{-}19]$$

The solution to the heat diffusion equation with the boundary conditions (Alexandri and Jone, 2007):

$$\frac{T(z,t) - T_{\text{aquifer}}}{T_{\text{initial}} - T_{\text{aquifer}}} = \text{erf}\frac{z}{2\sqrt{\alpha t}} \quad [7\text{-}20]$$

Where erf is the Gauss error function, α is the thermal diffusivity and can be calculated from the pavement medium parameters where (Alexandri and Jone, 2007):

$$\alpha = \frac{k_p}{C_v} \ , \quad [7\text{-}21]$$

Where k_p is the pavement's mediums' thermal conductivity (W/m/K) and C_v is the volumetric specific heat ($J/m^3/K$).

7.3.5. Convection Heat Fluxes q_{conv}

This mechanism accounts for heat transfer at the geothermal pavement top and bottom (aquifer) surfaces due to free and forced convection. The convection coefficient (h_c) is a function of the Nusselt Number (Nu). For a pavement surface, correlations for a horizontal flat plate would be the most applicable, similarly for that of the aquifer's surface. In free convection heat transfer mechanism, the Nuzzelt Number (Nu) is correlated to the Rayleigh Number (Ra) where (Dieter and Stephan, 2006; Incropera *et al.,* 2007):

$$Ra = \frac{g\beta(\Delta T)L^3}{v\zeta} \quad [7\text{-}22]$$

Where g is the acceleration due to gravity, ζ is the thermal diffusivity of air, β is the volumetric thermal expansion coefficient of air, *v* is the kinematic viscosity of air, ΔT is the temperature difference between the GPS and the air and L is the length of the pavement system. In external free convection flows over a horizontal flat plate, the critical Rayleigh Number (Ra) is approximately 10^7 (Incropera *et al.,* 2007). Two empirical relations for the Nuzzelt Number (*Nu*) are used in the model for free convection for the upper surface of a heated plate and/or the lower surface of a cooled plate (Dieter and Stephan, 2006; Incropera *et al.,* 2007):

$$Nu = 0.54(Ra)^{[1/4]} \qquad (10^4 < Ra < 10^7) \text{ for laminar flow} \quad [7\text{-}23]$$

$$Nu = 0.15(Ra)^{[1/3]} \qquad (10^4 < Ra < 10^7) \text{ for turbulent flow} \quad [7\text{-}24]$$

The convection coefficient (h_c) for free convection can then be determined by:

$$h_c = \frac{(Nu)k}{L} \quad [7\text{-}25]$$

Where *k* is the thermal conductivity of air and L is the length of the pavement surface.

With regards to forced convection heat transfer, Nusselt number (Nu) is a function of Reynolds (Re) and Prandtl (Pr) Numbers. The Reynolds number is described as:

$$Re = \frac{\upsilon L}{v} \quad [7\text{-}26]$$

Where *v* is the wind speed, *υ* is the kinematic viscosity of air, and *L* is the length.

The Prandtl Number is defined as:

$$Pr = \frac{c_p\mu}{k} \quad [7\text{-}27]$$

Where c_p is the specific heat capacity of air, μ is the dynamic viscosity of air, and k is the thermal diffusivity of air.

For forced convection over a flat plate (pavement surface), the critical Reynolds Number is approximately 10^5 (Incropera *et al.,* 2007). Again, two empirical relations for the Nusselt number (Nu) are used in the model as described by Incropera *et al.,* (2007):

$$Nu = 0.664\,Re^{[1/2]}\,Pr^{[1/3]} \quad \text{for laminar flow regime} \qquad [7\text{-}28]$$

$$Nu = 0.037\,Re^{[4/5]}\,Pr^{[1/3]} \quad \text{for mixed and turbulent flow.} \qquad [7\text{-}29]$$

The convection coefficient (h_c) is then determined by equation [7-25]. The convection heat transfer across the geothermal paving system is computed by:

$$q_{convection} = h_{c(aquifier)} A_{aquifer} \left(T_{air} - T_{aquifer}\right) + h_{c(pavement)} A_{pavement} \left(T_{pavement} - T_{pavement}\right) \qquad [7\text{-}30]$$

Where T_{air} is the ambient air temperature and h_c is the maximum free and forced convection coefficient.

7.3.6. Heat Transfer due to Evaporation q_{evap}

This heat transfer mechanism contributes to the pavement cooling. The mass transfer of evaporating water (m'_w) at the pavement surface (Freeze and Cherry, 1979):

$$m'_w = h_d (w_{air} - w_{pavement-surf}) \qquad [7\text{-}31]$$

Where h_d is the mass transfer coefficient, w_{air} is the humidity ratio of the ambient air, and $w_{pavement\text{-}surf}$ is the humidity ratio of saturated air at the pavement surface. $w_{pavement\text{-}surf}$ is computed from psychometric charts and tables. The mass transfer coefficient (h_d) is defined using the Chilton-Colburn analogy (Tosun, 2007):

$$h_d = \frac{h_c}{c_p Le^{\frac{2}{3}}} \qquad [7\text{-}32]$$

Where h_c is the convection coefficient defined previously in Equation [7-25], c_p is the specific heat capacity of air and Le is the Lewis number and computed as (Tosun, 2007):

$$\mathrm{Le} = \frac{\alpha}{\mathrm{D}} \qquad [7\text{-}33]$$

Where α is the thermal diffusivity of air and D represents the diffusion coefficient and is computed as (Tosun, 2007):

$$\mathrm{D} = \frac{1.87 \times 10^{-10} \mathrm{T}^{2.072}}{\mathrm{P_{air}}} \qquad (280\mathrm{K} < \mathrm{T} < 450\mathrm{K}) \qquad [7\text{-}34]$$

Where P_{air} is the atmospheric pressure in atmospheres. The heat transfer due to evaporation (q_{evap}) is then computed by:

$$\mathrm{q_{evap}} = \mathrm{h_{fg}} \mathrm{A_{pavement}} \dot{\mathrm{m}}_{\mathrm{w}} \qquad [7\text{-}35]$$

Where h_{fg} is the latent heat of vaporization.

7.3.7. Rain and Snow Heat Fluxes $q_{snow/rain}$

The heat transfer mechanism includes both latent and sensible heat fluxes. The model uses a simple energy and mass balance of water at the pavement surface to account for the heat and mass transfer. The sensible heat flux as a result of snow or rainfall onto the pavement surface ($q'_{rain,\ snow}$) is given by:

$$\mathrm{q'_{rain,snow}} = \dot{\mathrm{m}}_{\mathrm{rain,snow}} \mathrm{c_p} \left(\mathrm{T_{air}} - \mathrm{T_{pavement}} \right) \qquad [7\text{-}36]$$

Where $\dot{m}_{rain,snow}$ the snowfall or rainfall in water equivalent mass per unit time per area of the pavement is calculated from a modified version of Equation [7-31] and c_p is the specific heat capacity of water at the air temperature.

7.3.8. Energy Associated with Movements of Water from Seepage (q_{seep})

The urban runoff water entering or leaving the geothermal paving system has an internal energy, as movement of liquid water across the system boundary represents

energy gains or losses. The rate of bulk energy moved across the system by water seepage can be calculated with the following equation (Freeze and Cherry, 1979):

$$q_{seepage} = \dot{m}_{water-seepage} c_p T_{aquifer} \quad [7\text{-}37]$$

Where $\dot{m}_{water-seepage}$ is the mass flow rate of water from seepage, c_p is the specific heat capacity of water and $T_{aquifer}$ is the water temperature in the aquifer zone. $\dot{m}_{water-seepage}$ can be calculated from Darcy's Equation (Carbeneau, 2000):

$$\dot{m}_{water-seepage} = k_{hyd} i A \quad [7\text{-}38]$$

Where k_{hyd} is the hydraulic conductivity (m/s), which can be assumed to be in the range of 10^{-11} to 10^{-9} cm/s, i is the hydraulic gradient (dimensionless) ≈ 0.001, and A is the area (m^2) of the aquifer (Carbeneau, 2000). As a result of the experiment being a tanked system, seepage losses were ignored, however in practical permeable pavement systems this must be taken into account for both water movements and energy losses.

7.3.9. Heat Transfer from slinky coils (q_{coils})

This heat transfer from the heating and cooling coils represents the heat flux occurring for both cycles. The heat flux from the coils can be computed from:

$$q_{coils} = U_{coils}(T_{coils} - T_{aquifer}) \quad [7\text{-}39]$$

Where U_{coils} is the overall heat transfer coefficient of the slinky coils and can be expressed as (Dieter and Stephan, 2006; Incropera *et al.,* 2007):

$$U_{coils} = \frac{1}{\frac{1}{h_{coils}} + \frac{l}{k_{coils}}}, \quad [7\text{-}40]$$

Where h_{coils} is the convection coefficient, k_{coils} is the thermal conductivity of the slinky coils material, and l_{coils} is the wall thickness of the coils. For the slinky coils the convection coefficient h_{coils} can be determined using Nusselt Number as laminar flow through a horizontal cylinder and is approximately 4.36 (Dieter and Stephan, 2006; Incropera *et al.,* 2007) computed as:

$$h_{coils} = \frac{4.36k}{D} \quad [7\text{-}41]$$

Where D is the inner diameter of the slinky coils (m).

7.3.10. Mircobial respiration (q_{resp})

Decomposition of organic matter is a source of energy within geothermal paving systems. The energy released within the urban runoff is a by-product of decomposer respiration (Datta, 2002). Chemically, the aerobic respiration of glucose can be described by (Datta, 2002)

$$C_6H_{12}O_6 + 6O_2 \rightarrow 6CO_2 + 6H_2O + \Delta H_c \quad [7\text{-}42]$$

Where ΔH_c is the heat of combustion for glucose = 16KJ/mol of glucose.

Permeable pavement systems without geotextiles consume 1 to 2g O_2/m^2/day whilst those with geotextiles consume 3 to 4g O_2/m^2/day (Tota-Maharaj and Scholz, 2010). Assuming that most of the generated energy comes from the decomposition of organic matter, the total energy produced by the anaerobic decomposers would be in the range of 82 to 163 J./m^2/day without geotextiles and approximately 325J./m^2/day with the presence of geotextiles. Factors which may cause alterations in the rate at which the aquifer respiration occurs include temperature, oxygen accessibility, pH and nutrient availability (Datta, 2002).

7.4 Solving the Overall Energy Balance Equation

Runge-Kutta integration is an extension methodology that allows a substantially improved accuracy for solving complex differential equations, without imposing a severe computational burden (Chapra, 2005). The idea is to step into the interval and evaluate derivatives, providing a more accurate solution with a smaller increase in computation derivation. Second order Runge-Kutta integration has an error that is proportional to the time step cubed for an integration step and proportional to the time step squared from the whole simulatation (Chapra, 2005). Fourth order Runge-Kutta integration has an error that is proportional to time step to the fifth power for an integration step and proportional to time step to the fourth power for the whole

simulation thus improving the computational efficiency reducing the error on which the Runge-Kutta techniques are built (Chapra, 2005).

The differential equation describing the overall energy balance of the geothermal paving system is rearranged in the form:

$$\left(\frac{dT}{dt}\right)_{GPS} = \frac{\sum q}{\rho V_{pps} c_p} = f(t,T) \quad [7\text{-}43]$$

Where T is the temperature, t is the time, and q is the energy vectors. The linear first-order differential equation is solved at each time step. To solve this differential equation, the 4th order Runge-Kutta numerical technique was used in Matlab 7.0 (The MathWorks Inc, Natick, Massachusetts, U.S.A). The 4th order Runge-Kutta numerical technique is recognized as an accurate method in evaluating and solving differential equations (Chapra, 2005). With the use of initial conditions, the Runge-Kutta technique evaluates the geothermal paving system aquifer's temperature with the following set of equations:

$$T(t+\Delta t) = T(t) + \frac{\xi_1 + 2\xi_2 + 2\xi_3 + \xi_4}{6} \quad [7\text{-}44]$$

$$\xi_1 = (\Delta t) f(t,T) \quad [7\text{-}45]$$

$$\xi_2 = (\Delta t) f\left(t + \frac{\Delta t}{2}, T + \frac{\xi_1}{2}\right) \quad [7\text{-}46]$$

$$\xi_3 = (\Delta t) f\left(t + \frac{\Delta t}{2}, T + \frac{\xi_2}{2}\right) \quad [7\text{-}47]$$

$$\xi_4 = (\Delta t) f(t + \Delta t, T + \xi_3) \quad [7\text{-}48]$$

Where T (Δt) is the average GPS temperature at the previous time step and ξ is the mean GPS temperature at the new time step (Chapra, 2005). The model was run and completed, and the output was analyzed with the measured data. A convergence criterion for the permeable pavement aquifer's temperature of 1 $\times 10^{-5}$ °C (1.8 $\times 10^{-5}$ °F) is used.

7.5 Validation of 4th order Runge-Kutta Numerical Analysis for modelling.

To compare the predicted and measured data, three statistical parameters were applied (i) The average bias, (ii) standard deviation of the average bias (iii) The Pearson's linear correlation coefficient, R and (iv) The coefficient of determination R^2. These techniques are an effective methodology in testing the precision of a simulation in heat and mass transfer (Lamoureux *et al.,* 2006).

The average bias μ is the bias measurement of how accurate the model is when estimating the actual geothermal paving system's temperature (i.e. the predicted temperature minus the measured temperature). The average bias is the mean of all the biases at every time step, for n time steps and is calculated as:

$$\mu_{bias} = \frac{\sum\left(T_{Predicted} - T_{Measured}\right)}{n} \qquad [7\text{-}49]$$

The standard deviation of the average bias measured the variations in the bias and is an indicator of the model's consistency.

$$S.D = \sqrt{\frac{\sum T_{Predicted} - T_{Measured} - \mu_{bias}}{n-1}} \qquad [7\text{-}50]$$

The Pearson's linear correlation coefficient R, between the measured and predicted temperatures was also calculated to view the model's data set in comparison to measured variables. The coefficient of correlation statistic evaluates the linear correlation between the measured and computed values. A positive correlation indicates that large predicted values are correlated with large observed values (US EPA, 1999 b). On the contrary, a negative correlation occurs when small values of one set are correlated with high values of the other data set. The coefficient of correlation is calculated by equation (7-51)

$$R = \frac{\sum_{i=1}^{N}(T_m - \overline{T}_m)(T_y - \overline{T}_y)}{\sqrt{\sum_{i=1}^{N}\left(T_m - \overline{T}_m\right)^2 \sum_{i=1}^{N}(T_y - \overline{T}_y)^2}} \qquad [7\text{-}51]$$

Where *R* is the coefficient of correlation, N is the total number of data records, T_m is the observed or measured value, $\overline{T}_m$ is the mean of the corresponding measured temperature variable, T_y is the predicted (computed) temperature variable, and $\overline{T}_y$ represents the mean of the corresponding predicted variable. When $R \approx 1$, the model predictions are near perfect, on the other hand when $R \approx 0$ the model has failed to predict the variable. The coefficient of determination, R^2 measures how good the prediction maybe when compared to the modelled values and gives information of the goodness of fit for the model and how the regression line approximates the measured temperature data points.

7.6. Results and Discussion

The validation and verification of the model process was compared by scatter plots of the modelled (predicted) data set versus the measured temperatures for both PPS 1 and PPS 4 (outdoor rig) in a heating and cooling mode. This comparison allowed the data to be checked for the accuracy of the simulation which included environmental heat fluxes and energy mechanisms across the pavement. Simulated and actual temperatures are shown in Figure 7-2(a) for PPS 1 in a cooling cycle for approximately six months. The Pearsons' correlation coefficient R = 0.871 and coefficient of determination R^2 (0.75) is statistically a very good link between the simulated points and measured data set (Figure 7-2 (b)). The equation y = 0.65 x + 3.2 represents a linear relationship between the predicted and measured temperatures, however when compared to the unity line y = x, the modelled values are offset several times, showing the level of error in prediction.

For the heating cycle for PPS 1, the temperatures successfully mimicked the measured data set illustrating that the 4^{th} order Runge-Kutta method supported the simulation with a relatively good accuracy and high Pearsons' Correlation Coefficient R = 0.947, and R^2 (0.89) Figure. 7-3 (a) shows the calculated and observed temporal variations of the treated urban runoff's temperature for PPS 4 from the experimental rig during April-September 2008. An assessment of the plots in Figure 7-3 (a), illustrates that the model cumulative heat rejected compares well to the measured heating element and GHP input. At the end of the 6-month test period,

the percent difference between the cumulative simulated heat rejected compared to the actual data is negligible. Nonetheless, Figure 7-3(b) the linear equation y = 0.72x + 5.2 and correlation coefficient (0.947) shows a good prediction but an overestimation which can be seen when compared to the line y = x.

Figure 7-4(a) depicts a slightly less efficient comparison between the calculated and observed diurnal variations of the temperature during the cooling mode for PPS 4. Since the water temperatures in the surface layer fluctuates to some extent more than that of PPS 1, because of the geotextile layer, the numerical model gives values that can differ from the observed surface temperatures. This model featured in Figure 7-4(a) is particularly good at simulating values of the water temperature. The model gave comparable results with the measurements for both data sets, suggesting that the model is capable of simulating however with some inaccuracies and variations as seen in Figure 7-4 (b) for a cooling cycle for the geothermal paving system.

Review of the plots in Figure 7-5 (a) and (b) shows again that the model temperatures compare favourably to some extent of the actual temperatures within a certain error range of approximately 2 °C. The Runge-Kutta analysis simulated the temperatures within 1.46 °C (34.63 °F) throughout the testing period. The correlation coefficient was 0.881 ($p<0.05$), and coefficient of determination (0.77) shows a near linear relationship between the predicted and measured temperatures for PPS 4 in the heating mode. On the other hand, there is an offset between the unity line (y = x) and the linear best-fit equation y = 0.65 x+ 3.2, which illustrates the margin of error occurred during simulation.

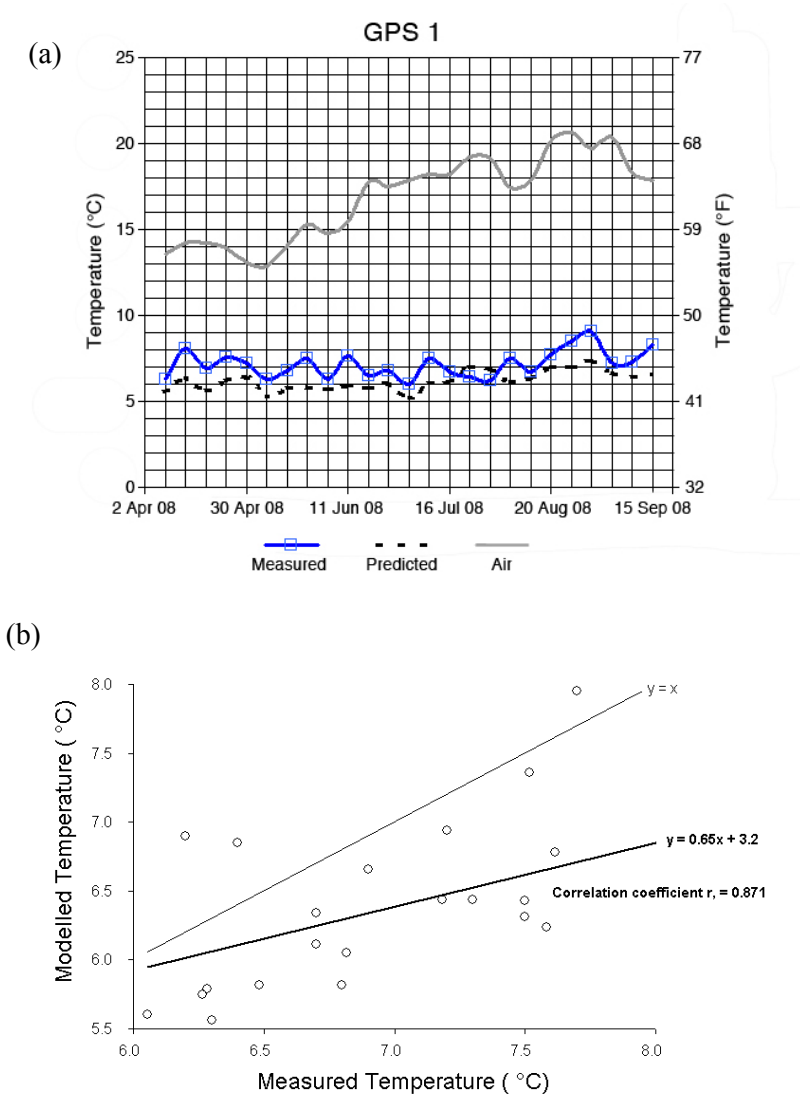

Figure 7-2: (a) The modelled, predicted and environmental temperatures for the geothermal paving system (PPS 1 outdoor rig) in a cooling cycle plotted against time. The model had a tendency of under-predicting the systems temperature (average bias of 1.9 °C); (b) The scatter plot for the best-fit line y = 0.65x+3.2, the corresponding correlation coefficient R = 0.871, and the unity line y = x for the cooling cycle measurement of the model's accuracy. For GPS 1, the model was run for the period (02/04/2009 to 11/09/2009) with n = 40 sample points.

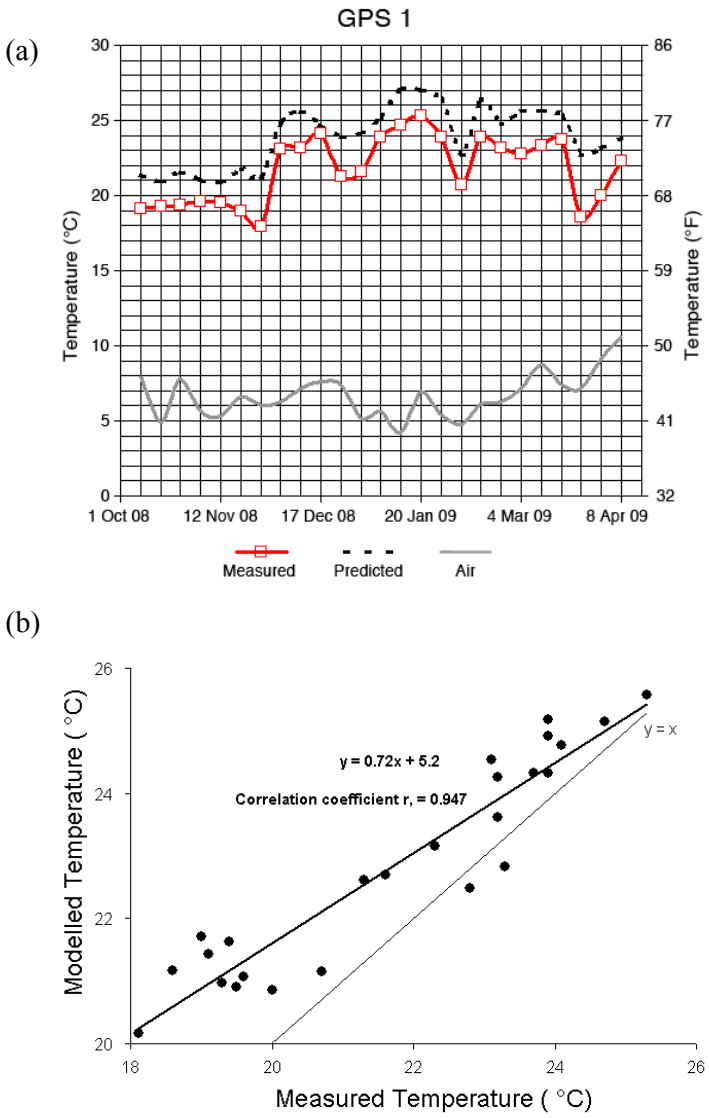

Figure 7-3: (a) The modelled, predicted and environmental temperatures for the geothermal paving system (PPS 1 outdoor rig) in a heating cycle plotted against time. The model had a tendency of over-predicting the systems temperature (average bias of 0.64 °C); (b) The scatter plot for the best-fit line y = 0.72x + 5.2, the corresponding correlation coefficient, R = 0.947 and the unity line y = x for the heating cycle measurement of the model's accuracy. For GPS 1, the model was run for the period (01/10/2008 to 08/04/2009) with n = 40 sample points.

(a)

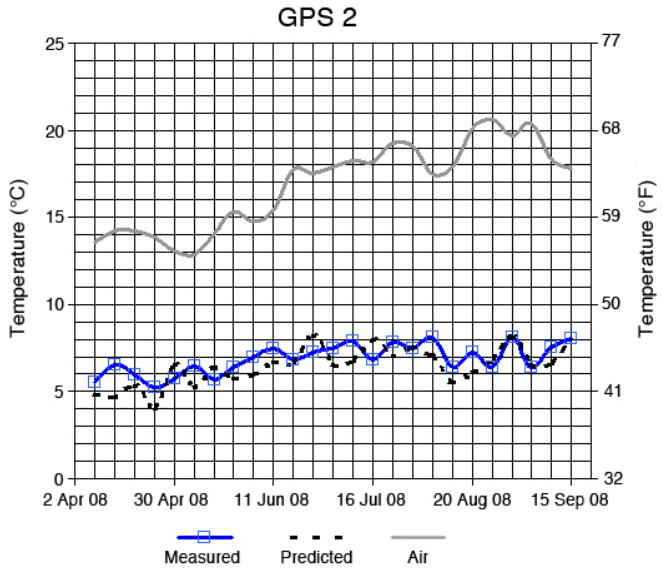

(b)

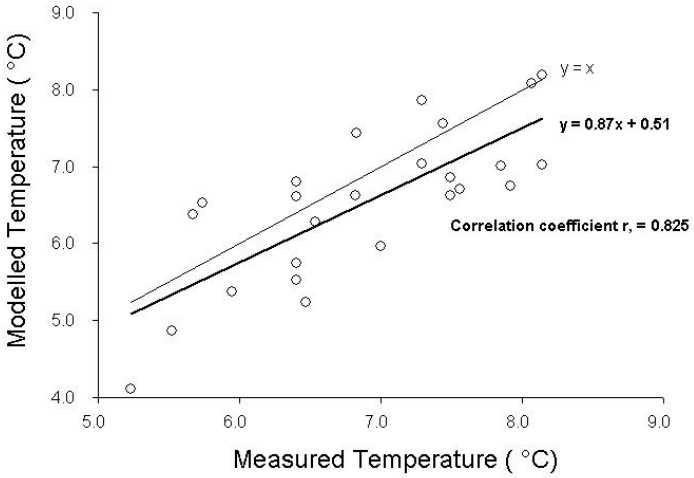

Figure 7-4: (a) The modelled, predicted and environmental temperatures for the geothermal paving system (PPS 4 outdoor rig) in a cooling cycle plotted against time. The model had a tendency of under-predicting the systems temperature (average bias of -0.75°C); (b) The scatter plot for the best-fit line y=0.87x +0.51, the corresponding correlation coefficient, R= 0.825 and the unity line y=x for the cooling cycle for measurement of the model's accuracy. For GPS 2, the model was run for the period (02/04/2008 to 11/09/2009) with n=40 sample points.

(a)

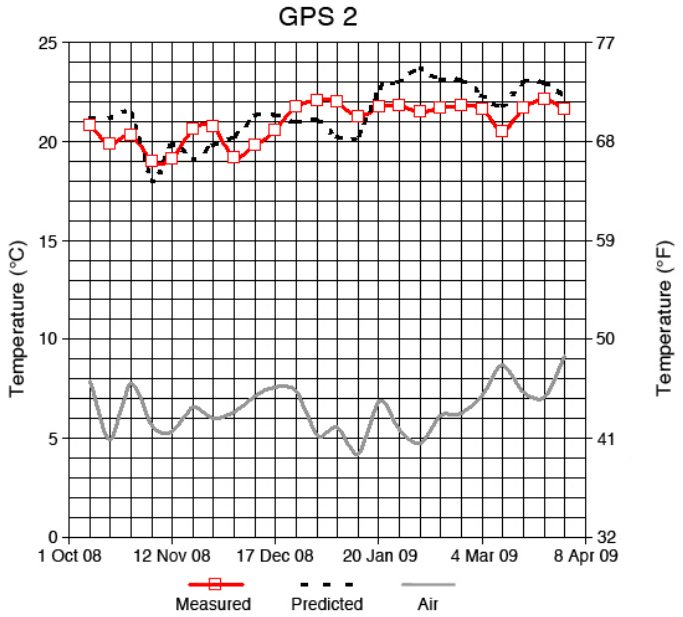

(b)

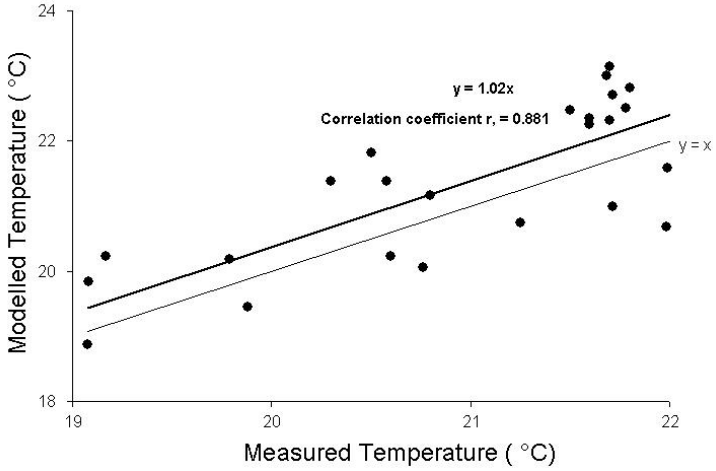

Figure 7-5: (a) The modelled, predicted and environmental temperatures for the geothermal paving system (PPS 4 outdoor rig) in a heating cycle plotted against time. The model had a tendency of over-predicting the systems temperature (average bias of 1.46° C; (b) The scatter plot for the best-fit line y=1.02x, the corresponding correlation coefficient, R = 0.881 and the unity line y = x for the cooling cycle for measuring the model's accuracy. For GPS 2, the model was run for the period (01/10/2008 to 08/04/2009) with n=40 sample points.

Table 7-2: The use of different empirical statistical equations to measure the accuracy of the 4th Order Runge-Kutta Method in predicting the temperatures.

		Statistical Validation			
Paving system (Outdoor rig)	**Thermodynamic Cycle**	**Bias μ (°C)**	**(S.D.)[a] (°C)**	**R[b]**	**(R^2)[c]**
PPS 1	Cooling	-1.91	1.2	0.871 ($p < 0.05$)	0.758
	Heating	0.64	1.9	0.947 ($p < 0.05$)	0.896
PPS 4	Cooling	-0.75	1.5	0.825 ($p < 0.05$)	0.681
	Heating	1.26	1.3	0.881 ($p < 0.01$)	0.776

[a]S.D (standard deviation), [b]R (correlation coefficient) and [c](R^2) (correlation of determination)

Table 7-2 presents the statistical results for the model's accuracy. The numerical method from the 4th Order Runge-Kutta method gave a good accuracy and showed stability in the prediction of temperatures. All correlation coefficients showed significantly ($p<0.05$) strong linear relationships with the measured and simulated data. The standard deviation was the least for the cooling cycle regarding PPS 1 (outdoor rig) and correlation coefficient (0.887) and coefficient of determination (0.758) showed a statistically significant index.

Nevertheless, PPS 1 (outdoor rig) resulted in both a high correlation coefficient and coefficient of determination for both heating and cooling cycles, showing high linkage to the measured temperatures. However, the model has a tendency to under-estimate the temperatures of PPS 1 for the heating cycle. A high standard deviation and Pearson's correlation coefficient for PPS 1 in a heating and cooling cycle were all statistically positive. The model has a tendency to under-estimate the temperatures of PPS 1 for the cooling cycle by 1.9°C (S.D. = 1.3 °C), regardless the model over-estimated the pavement's temperature for the heating cycle from October 11th, 2008 to April 24th, 2009 (bias μ = 0.64°C, S.D. = 1.8°C).

The average bias for PPS 4 was somewhat less than that for PPS 1 in the cooling cycle, whereas the average bias was very close to that of the heating cycle as seen in Table 7-2. The variations and discrepancies in the results can be a result of weather fluctuations between the summer and winter period for 2008-2009. Underestimations

and overestimations of energy vectors to the paving system would include solar radiation, longwave sky radiation and the rates of evaporation. For practical paving systems the importance of air convection and conduction through the pavement medium would account for variations in the thermal inertia of the system.

7.7 Summary

The study presented in this chapter modelled and experimentally validated thermogeological energy balances. An energy and temperature balance model for two geothermal paving rigs was designed, developed, tested and validated based on the temperature in two constructed lab-based geothermal paving systems (PPS 1 and PPS 4 outdoor). The model estimated the energy surpluses and deficits which were required to balance for temperature control within the system. The model developed can be coupled to practical geothermal paving systems for modelling short-time steps (hourly or minutely) systems analyses. The models were validated by comparing simulation results to experimental data. Major vectors of energy transfer for unheated ponds were found to be radiation heat transfer mechanisms. For heated ponds, bulk energy flow rates were also important. The model accounts for several environmental heat transfer mechanisms. The heat transfer processes which were simulated by the Runge-Kutta numerical method included solar radiation heat gain, heat and mass transfer as a result of evaporation, convective heat transfer to the atmosphere, thermal and long wave solar radiation heat transfer, conduction heat transfer to the surroundings from the pavement medium and the pavement's aquifer's zone.

The model's output is variable and can be influenced by several environmental conditions including solar radiation, convection and flow of water into and out of the system. Model runs showed that for the cooling cycle, the transport of energy through radiation dominated all energy transfer mechanisms. The energy balance on the GPS initially developed a system whereby temperatures can be assessed or controlled at the aquifer zones of permeable pavements. It is hoped that this data and the model presented can be developed and applied appropriately when monitoring built-in geothermal paving systems and for future sizing and design systems.

The potential for this model can be applied in the optimization and design for this hybrid pavement system in terms of reduction in the size of the slinky coils heat exchangers, the sizing of the aquifer zone as well as the energy efficiency of the system. The additional support offered by the numerical performance of the methods confirms that it is quite promising and deserves further research. In concluding the monitoring and assessing of potential of microbiological contamination (*Legionella)*, health and safety aspects for concurrently reusing and treating urban runoff as well as space conditioning is essential for geothermal pavements. Assessing temperatures and long term research would result in economic costs benefits with regards to further water treatment options in addition to less mechanical work for a sufficient energy output.

Chapter 8 Application of Backpropagation Artificial Neural Network Models

Artificial intelligence techniques such as neural networks are modeling tools that can be applied to analyze urban runoff water quality issues. Artificial neural networks are frequently used to model various highly variable and non-linear physical phenomena in the water and environmental engineering fields. The application of neural networks for analysing the performance of combined permeable pavement and geothermal heat pump systems is timely and novel. This chapter presents the application of back-propagation neural networks and the testing of the Levenberg-Marquardt, Quasi-Newton and Bayesian Regularization algorithms. The neural networks were statistically assessed for their goodness of prediction with respect to the biochemical oxygen demand, ammonia-nitrogen, nitrate-nitrogen, and ortho-phosphate-phosphorus by numerical computation of the mean absolute error, root square mean error, mean absolute relative error and the coefficient of correlation for the prediction versus measured dataset. The three neural network models were assessed for their efficiency in accurately simulating the effluent water quality parameters from various experimental pavement systems. The artificial neural network models predicted all key parameters with high correlation coefficients and low minimum statistical errors. The back-propagation and feed-forward neural network models performed optimally as pollutant removal predictors with regard to these two sustainable technologies. Segments of this chapter are under review for publication in the Journal of Environmental Engineering (American Society of Civil Engineers).

8.1 Introduction

Artificial neural networks are a promising tool for environmental process assessment and modelling (Maier and Dandy, 1996). Feed-forward neural networks are the most widely adopted methodology for the prediction and forecasting of water resource variables (Maier and Dandy, 1996; Zhang and Stanley, 1997; ASCE, 2000; Lingireddy and Brion, 2005).

Brion and Lingireddy, (1999) applied back-propagation neural networks to distinguish between urban and agricultural faecal contamination present in inflows to a drinking water reservoir. The neural networks helped in the identification of the sources of microbial contamination responsible for the deterioration of water quality. Zhang and Stanley, (1997) adopted artificial neural networks for water demand forecasting of the raw water quality parameters for the North Saskatchewan River in Canada. Furthermore, Zhang and Stanley, (1999) applied artificial neural networks for the assessment of water treatment and water quality issues.

Mat Isa *et al.,* (2006) predicted water quality concentrations based on algal species abundance as a function of sampled water quality parameters. Yabunaka *et al.,* (1997) developed an input-output model where measured water quality

parameters were used to estimate algal bloom. Yu *et al.,* (2000) researched the application of neural networks for coagulant dosing used in water treatment. Chaves and Kojir, (2007) modelled the biochemical oxygen demand and dissolved oxygen using fuzzy neural networks for the Barra Bonita reservoir system located in the southeast region of Brazil. Strugholtz *et al.,* (2008) developed a neural network model for a membrane microfiltration water plant used for drinking water. Najah *et al.,* (2009) predicted the water quality of the Malaysian Johor River and its tributary water quality; they focused on conductivity, dissolved solids and turbidity using feed-forward neural networks. Furthermore, Neelakantan *et al.,* (2002) identified training algorithms that would maximize the accuracy of risk ranking for *Cryptosporidium* and *Giardia*. They assessed relatively small data sets and tested various training algorithms with first and second order derivatives. Esen *et al.,* (2008) applied artificial neural networks for modeling the thermodynamic efficiency of a ground-source heat pump in terms of its coefficient of performance.

Results of all of the above-cited studies achieved satisfactory levels of precision. Previous research shows that neural network-based models that are adequately trained with several environmental factors are a better approach with more precise predictions when compared to multiple regression methods (Brion and Lingireddy, 1999). However, there is insufficient information to assess the effectiveness of neural network approaches with sustainable urban drainage systems such as permeable pavements.

Artificial neural networks are often created to mimic the structure and functioning of biological neural networks (Haykin, 1999). The use of artificial neural networks in solving complex problems is becoming popular in disciplines such as environmental engineering due to their capability to 'learn' non-linear relations (Hsu *et al.,* 1995). The method of artificial neural network has been inspired by biological nervous system. One of the most significant advantages of artificial neural networks is their ability to learn from a limited set of data.

Neural networks capture the embedded spatial and unsteady behaviour of the permeable pavement system using its architecture and non-linearity nature (Lek and Guégan, 1999). Artificial neural networks such as back-propagation feed-forward models can be applied to complex, inter-related parameters and provide efficient

simulation for non-linear relationships such as those associated with microbial water contamination (Lek and Guégan, 1999; Maier and Dandy, 2000).

A properly trained and verified artificial neural network for a specific problem of interest recognizes data patterns and makes predictions with desirable accuracy (Pigram and MacDonald, 2001; Dutot *et al.,* 2007). The problem of interest can be non-linear in nature and it can be at any degree of complexity. Neural networks are composed of simple neuron-like operating elements (neurons) and weighted connections between these elements. The network function is determined largely by the connections between neurons. A neural network can be trained to perform a particular job by adjusting the values of the connections (weights) between neurons. Various algorithmic approaches for developing artificial neural network models for specific problems exist in literature (Demuth and Beale, 2001).

8.2 Aim and objectives

The aim of this chapter was to determine whether artificial neural networks can be an effective modeling tool for predicting the efficiency of combined PPS and GHPs. The first objective of this study was to assess back-propagation feed-forward neural network models for the prediction of treatment of heavily polluted storm water. The second objective was to compare the performance of the neural network models with varying algorithms for the most optimal simulation.

8.3 Back propagation feed-forward artificial neural network models

Laboratory measurements of biochemical oxygen demand, ammonia-nitrogen, nitrate-nitrogen, and ortho-phosphate-phosphorus are labour-intensive, time-consuming and expensive. Artificial neural networks can be applied to reduce sampling costs by predicting these variables with others that are easier and less costly to determine. Neural networks can be trained in identifying patterns and extracting trends for complicated nonlinear water quality measurements. The neural network toolbox of MatLab 7.0 by Mathworks Co. (Demuth and Beale, 2001) was used

during the study. Most practical applications of back-propagation artificial neural networks employ a supervised learning environment (Lingireddy and Brion, 2005).

The back-propagation feed-forward artificial neural network model is expressed in terms of layers, which are sets of nodes. The network usually consists of three or more layers (input layer, hidden layers, and an output layer) according to Wang and Lu, (2006). Each layer consists of one or more nodes (neurons). The nodes in each layer are linked together by weights. Figure 8-1 is a schematic showing the structure of the back-propagation feed-forward neural network model used in this study. It consists of an input, hidden and output layer. In most back-propagation applications of neural networks, there are no fixed rules when determining how many input and hidden layers (including the corresponding neurons) should be applied.

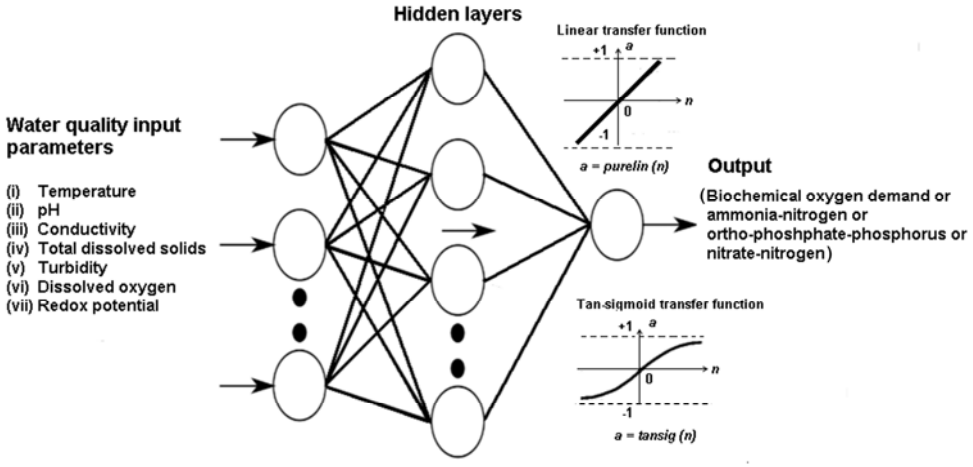

Figure 8-1: Architecture and structure of the feed-forward back propagation neural network model

The optimal architecture for the networks was found by trial and error. Initially 14 back-propagation algorithms were tested; the three most efficient ones for an optimal three-layered network included the Levenberg-Marquardt algorithm, Quasi-Newton algorithm and the Bayesian regularization algorithm resulting in the highest correlation values with the predicted and measured variables and the lowest corresponding errors.

8.4 Algorithms

Quasi-Newton back-propagation, which uses the 'Trainbfg' function in Matlab, is a network training function that updates the weight and bias values according to the Broyden-Fletcher-Goldfard-Shanno numerical method for solving nonlinear optimization. The function is based on Newton's method but does not require calculation of second derivatives. At each iteration of the algorithm, the Hessian matrix update is computed as a function of the gradient (Battiti, 1992). The line search function is used to locate the minimum. The first search direction is the negative of the gradient of performance. In succeeding iterations, the search direction is computed according to the gradient. Newton's method often converges faster than conjugate gradient methods (Battiti, 1992). The basic step of Newton's method is shown in equation (8-1).

$$x_{k+1} = x_k - A_k^{-1} g_k \tag{8-1}$$

Where x_k is a vector of current weights and biases, k is the number of iterations of the algorithm, A_k is the Hessian matrix (second derivatives) of the performance index at the current values of the weights and biases, and g_k is the current gradient.

It is complex, time-consuming and costly to compute the Hessian matrix for feed forward neural networks. Therefore, the Quasi-Newton approach can be taken as an approximation of the Hessian matrix at each iteration of the algorithm. The update is computed as a function of the gradient by using the equation (8-2) after Battiti, (1992).

$$A_{k+1} = A_k + (1 + \frac{\Delta g_k^T A_k \Delta g_k}{\Delta g_k^T}) \frac{\Delta x_k \Delta x_k^T}{\Delta x_k^T \Delta g_k} - [\frac{A_k \Delta g_k \Delta x_k^T + (A_k \Delta g_k \Delta x_k^T)^T}{\Delta g_k^T \Delta x_k}] \tag{8-2}$$

Where A_k is the Hessian matrix (second derivatives) of the performance index at the current values of the weights and biases, g_k is the current gradient, g^T_k is the initial gradient, x_k is a vector of current weights and biases, x^T_k is the initial vector of weights and biases, *k* is the number of iterations of the algorithm, and Δ being a very small change.

The Levenberg-Marquardt algorithm is a gradient-based deterministic local optimization algorithm (Mat Isa *et al.,* 2006). This algorithm, once employed to train the back-propagation model, produces a faster second-order convergence rate and keeps relative stability. The Levenberg–Marquardt algorithm converges faster than other back-propagation algorithms and usually works well when there are up to a few hundred neurons. This back-propagation method utilizes the 'Trainlm' function in Matlab as a network training function that updates weight and bias values according to the Levenberg-Marquardt optimization. The Levenberg-Marquardt algorithm is a least-squares estimation method based on the maximum neighborhood idea (Mat Isa *et al.,* 2006). It does not suffer from the problem of slow convergence. The Levenberg-Marquardt method combines the best features of the Gauss-Newton and Steepest-descent method and avoids many of their limitations (Mat Isa *et al.,* 2006). This algorithm is very efficient when training small networks. The Levenberg-Marquardt training algorithm is designed to achieve second-order training speed without computing the Hessian matrix. When the performance function is of the form of a sum of squares, then the Hessian matrix can be approximated by equation (8-3). The gradient can be computed by equation (8-4). The Levenberg-Marquardt algorithm uses an approximation to the Hessian matrix in the Newton-like equation (8-5) as discussed by Mat Isa *et al.,* (2006).

$$H = J^T J \tag{8-3}$$

Where *H* is is the Hessian matrix, and *J* is the Jacobian matrix that contains first derivatives of the network errors with respect of the weights and biases.

$$g = J^T e \tag{8-4}$$

Where *g* is the gradient, *J* is the Jacobian matrix that contains first derivatives of the network errors with respect of the weights and biases, and e is a vector of network errors.

$$x_{k+1} = x_k - [J^T J + \mu I]^{-1} J^T e \tag{8-5}$$

Where x_k is a vector of current weights and biases, k is the number of iterations of the algorithm, J is the Jacobian matrix that contains first derivatives of the network

errors with respect of the weights and biases, μ is a control parameter, and e is a vector of network errors.

When the scalar μ is zero, equation (8-5) can be interpreted as the Newton's method using the approximate Hessian matrix. When μ is large, equation (8-5) becomes gradient descent with a small step size. Newton's method is a faster and more accurate (near an error minimum); therefore, μ is decreased after each successful iteration, and only increased when a tentative step increases the performance function (Mat Isa *et al.,* 2006). Following this method, the performance function will always be reduced at each step of the algorithm.

Bayesian Regularization back-propagation, which uses the 'Trainbr' function in Matlab, is a network training function that minimizes a combination of squared errors and weights, and subsequently determines the correct combination to produce a network that generalizes well. The Bayesian regularization method is based on the Baye's Rule (Mackay, 1992), which is shown in equations (8-6) to (8-8).

$$p(\theta / D) = \frac{p(D / \theta)}{p(D)} \tag{8-6}$$

Where p is the prior probability of a parameter θ, before having seen the data, reflecting one's prior knowledge, and p(θ/D) is the likelihood function, which assesses the probability of the observed data D.

Bayes' rule is used to determine the posterior probability of θ, given the data D. This generally provides an entire distribution over possible values of θ. This process was applied to the neural networks and resulted with the probability distribution over the network weights, w, given the training data p(w/D) (Mackay 1992). Equation (8-7), and after transformation, equation (8-8) were applied to find a posterior distribution over weights. For the Bayesian Regularization method, learning the network weights w means changing the weights from the prior p(w) to the posterior p(w/D) as a consequence of seeing the data.

$$p(w / D) = \frac{p(D / w)p(w)}{p(D)} \tag{8-7}$$

Where p(w) is the prior probability of the network weights w, D is the data set, p(w/D) is the training data (parameter behave as having seen the data), and p(D/w) is the likelihood function.

$$p(w/D) = \frac{p(D/w)}{\int p(D/w)p(w)dw} \tag{8-8}$$

Where p(w) is the prior probability of the network weights w, D is the data set, p(w/D) is the training data (parameter behave as having seen the data), p(D/w) is the likelihood function, and dw is a small differential change in the network weights w.

8.5 Data Normalization

The contribution of input variables depends heavily on its variability relative to the other corresponding inputs. For example, if one input has an extremely wide range of between 0 and 1,000,000 and the other has a much smaller range of between 0 and 10, then the contribution of the second input is dwarfed by the first. Therefore, it is essential to rescale the inputs so that their variability reflects their importance (Tay and Zhang, 1999). Data normalization is necessary and common practice for back-propagation neural network algorithms and is required for effective simulation (Zhang and Stanley, 1999; Neelakantan *et al.,* 2001).

In the rescaling or data normalization process, there is often the requirement to add or subtract a constant, and then to multiply or divide by a constant (Kriger and Tzoneva, 2007). The data set was normalized using linear scaling in the range between 0 and 1. The input and output data were converted to values between zero and one.

8.6 Neural Network Training and Testing

Artificial neural network modeling of a process demands two operations: training and thereafter testing. Training involves optimization of the connected

weights through minimization of a certain function (Affandi and Wantanabe, 2007). The training step is a significant period of a neural network, in which an input is introduced to the network together with the desired target (Lingireddy and Brion, 2005). The weights and biases are adjusted iteratively in order for the network attempts to produce the desired output. The data were divided into a training set of 71 data points and a testing set of 43 points. Training was halted as soon as the mean square error was unchanged and significantly small (in the order of 0.001) for the number of epochs (iterations) to prevent over-fitting (Yang *et al.,* 2009). Trials were made with the feed-forward back-propagation neural network with different combinations of water quality parameters as inputs. The following water quality parameters were evaluated as inputs to the neural network models: pH, temperature (°C), electroconductivity (μS/cm), turbidity (NTU), total dissolved solids (mg/l), dissolved oxygen (mg/l) and redox potential (mV). These parameters were applied to the model in the input layer based on strong correlations with the effluent parameters biochemical oxygen demand (mg/l), ammonia-nitrogen (mg/l), nitrate-nitrogen (mg/l), and ortho-phosphate-phosphorus (mg/l).

The three-layered feed-forward neural network model adopted the input parameters of the network's topology for the estimation of output parameters for the combined PPS and GHP as seen in Figure 8-1. Models were generated using networks containing a single hidden layer of between 10 and 17 nodes inclusive. The tan-sigmoid and linear transfer functions were applied at the hidden and output nodes, respectively. A tangent-sigmoid transfer function was selected as an activation function between the input layer and the hidden layer, in addition to the linear transfer function that was selected between the hidden layer and the output layer for computation (Yeon *et al.,* 2009). Models were trained for a maximum of 2500 epochs (iterations) or until terminated by the algorithm (figure 8-2). The validation data set was then submitted to the trained models and the models' predictions recorded. There are many variations of the back-propogation algorithm and the simplest implementation of it updates the network weight and bias values in the direction in which the performance function decreases most rapidly; i.e. the negative of the gradient (Schlink *et al.,* 2003; Lingireddy and Brion ,2005).

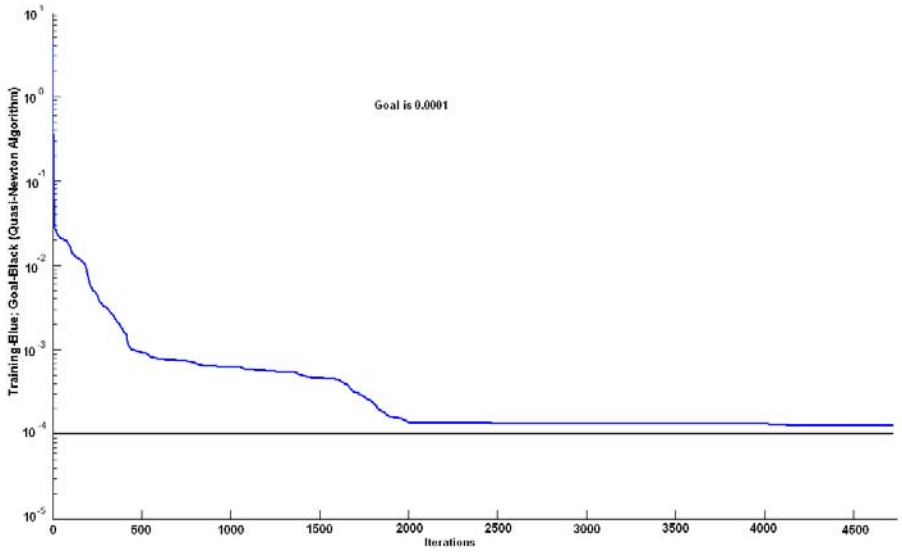

Figure 8-2: Matlab output for training period with Quasi-Newton Algorithm for BOD.

8.7 Optimization and Model Performance Evaluation

Both the neuron numbers of the three algorithms and the model performances varied greatly. In order to optimize the neuron numbers, between 4 and 25 neurons were tested and subsequently assessed using the mean-squared error and the correlation coefficient. An increase of the hidden layers by more than 20 caused an unrealistic result with significant fluctuations between the predicted and measured variables. The optimal neural network structure occurred with a tan-sigmoid transfer function with a hidden layer consisting of between 12 and 15 neurons, and a linear transfer function at the output layer as shown in Table 8-1.

Table 8-1: Results for the optimum structure of the back-propagation feed-forward network trained using various algorithms

Training algorithm	**Optimum number of hidden nodes**	**Best possible architecture and structure of network**
Levenberg-Marquardt	13	7-13-1
Quasi-Newton	12	7-12-1
Bayesian Regularization	15	7-15-1

Verification statistics are useful in evaluating neural network modellingresults. The performances of the different back-propagation neural network models were

evaluated based on the mean absolute error, root square mean error, mean absolute relative error and coefficient of correlation which represent standard statistical evaluations for artificial neural networks (US EPA, 1999 b).

The mean absolute error is the average closeness between the predicted and observed (measured) values. Its values are used to summarize the overall quality of the model. A low accuracy-related value indicates better performance (US EPA, 1999b). The computation equation for accuracy is shown in equation (8-9).

$$MAE = \frac{1}{N}\left(\sum_{i=1}^{N}|y_i - o_i|\right) \tag{8-9}$$

Where *MAE* is the mean absolute error also referred to as the accuracy (A), *N* is the total number of data records, *y* is the predicted value, and *o* is the observed or measured value. The root square mean error is the measure of the prediction error. Its values are used to summarize the overall quality of the model. Lower numbers of the root square mean error indicate good performance of the model (US EPA, 1999b). This error can be calculated by applying equation (8-10).

$$RSME = \sqrt{\frac{1}{N}\sum_{i=1}^{N}(y_i - o_i)^2} \tag{8-10}$$

Where *RSME* is the root square mean error, *N* is the total number of data records, *y* is the predicted value, and *o* is the observed or measured value. The mean absolute relative error provides an unbiased error estimate, because it gives appropriate weight to all magnitudes of the predicted variable (Wang and Lu, 2006). This error indicator is computed by equation (8-11).

$$MARE = \frac{1}{N}\sum_{i=1}^{N}\left|\frac{o_i - y_i}{o_i}\right| \tag{8-11}$$

Where *MARE* is the mean absolute relative error, *N* is the total number of data records, *o* is the observed or measured value, and *y* is the predicted value. The coefficient of correlation statistic from (equation 7-51) was applied to evaluate the linear correlation between the measured and computed values.

8.8 Results and Discussion

The performance of the neural network model is assessed by comparing the measured and estimated values with each other. The models analysed were functions of the readily available water quality parameters. The statistics of the entire data set used for training and testing are given in Table 8-2. Figure 8-3 shows the forecasted (predicted) effluent concentrations of the biochemical oxygen demand for the Bayesian Regularization, Quasi-Newton and Levenberg-Marquardt algorithms. Outflow concentrations for both measured and modelled BOD ranged from 0mg/l-13.8mg/l (Figure 8-3). The back-propagation neural network models were applied to simulate and predict the effluent biochemical oxygen demand of the combined permeable pavement and GHP. The biochemical oxygen demand is a major water quality parameter, and is used as an indicator for the purity of the water. However, the determination of this parameter is resource-intensive, and exchange with an inexpensive surrogate parameter would be an advantage.

Table 8-2. Statistical performance parameters of algorithms for back-propagation feed-forward neural networks

Parameter	Algorithm	Training dataset				Validation dataset			
		MAE[a]	RSME[b]	MARE[c]	R[d]	MAE[a]	RSME[b]	MARE[c]	R[d]
BOD	QN[e]	0.69	0.88	0.18	0.96	0.70	0.89	0.18	0.98
	LM[f]	0.69	0.93	0.17	0.94	0.71	0.94	0.18	0.96
	BR[g]	0.68	0.89	0.15	0.96	0.69	0.90	0.1551	0.98
NH_3-N	QN[e]	0.02	0.04	0.63	0.98	0.02	0.04	0.65	1.00
	LM[f]	0.02	0.05	0.49	0.954	0.03	0.05	0.50	0.97
	BR[g]	0.03	0.05	0.68	0.96	0.03	0.05	0.69	0.98
NO_3-N	QN[e]	0.10	0.14	0.63	0.97	0.11	0.14	0.65	0.98
	LM[f]	0.13	0.19	0.49	0.94	0.13	0.20	0.50	0.96
	BR[g]	0.10	0.13	0.68	0.97	0.10	0.13	0.69	0.99
PO_4-P	QN[e]	0.05	0.07	0.06	0.99	0.06	0.07	0.07	0.99
	LM[f]	0.06	0.08	0.07	0.98	0.06	0.08	0.07	0.92
	BR[g]	0.06	0.09	0.08	0.99	0.07	0.09	0.08	0.99

[a][Mean Absolute Error]; [b][Root Square Mean Error]; [c][Mean Absolute Relative Error] [d][Correlation Coefficient]; [e][Quasi-Newton]; [f][Levenberg-Marquardt]; [g][Bayesian Regularization].

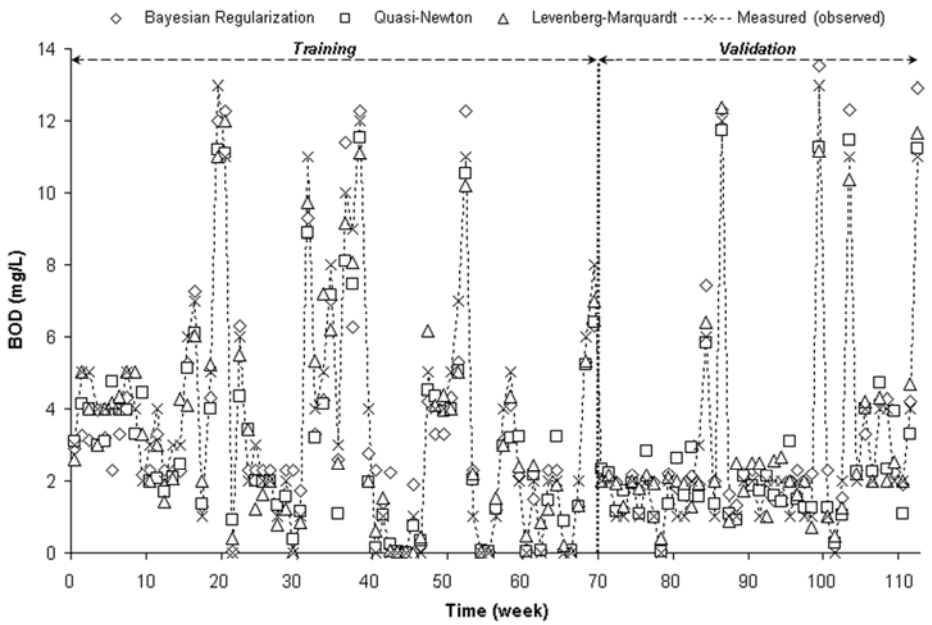

Figure 8-3: Comparison of the measured (observed) and predicted biochemical oxygen demand (BOD) concentrations.

The computed findings match the measured biochemical oxygen demand for all three back-propagation neural network models (Figure 8-3). Table 8-2 shows the performance results obtained for the training and testing periods of the tested algorithms. The mean absolute errors for training and testing were in the range of 0.69 to 0.71. The Quasi-Newton algorithm resulted in the lowest accuracy of 0.69 for the training period, whilst the Levenberg-Marquardt algorithm was associated with the highest accuracy. These findings provide an indication of the goodness of prediction with respect to the biochemical oxygen demand during the training period. The Quasi-Newton algorithm was optimal, and resulted in a good estimation of the modelled concentrations. With regards to the validation or verification period, the Bayesian Regularization algorithm produced the lowest mean absolute error values, implying that this was the best possible simulation.

The root square mean error statistic measures the residual variances that indicate global goodness of fit between the predicted and observed variables. The root square mean error associated with the Quasi-Newton algorithm (0.88) was the smallest during the training period (Table 8-2). The largest root square mean error of 0.93 was computed with the Levenberg-Marquardt algorithm during the same period.

Nevertheless, for the validation period, the Quasi-Newton algorithm performed most optimal, having a root square mean error of 0.89, followed by Bayesian Regularization (0.90), and finally by the Levenberg-Marquardt algorithm (0.94).

An unambiguous measure of the average error is the mean absolute relative error, which can be used to assess the predictive ability of a model. The largest mean absolute relative error occurred with the Quasi-Newton algorithm (0.18), whilst the Bayesian Regularization produced the least mean absolute relative error (0.15) during the training phase. Similarly, throughout the validation phase, the Bayesian Regularization had the smallest and the Quasi-Newton algorithm the largest mean absolute relative error.

The correlation coefficient and the coefficient of determination were relatively high during the training and testing period for all algorithms studied (with $R>0.90$ and $R^2>0.88$). This was also verified by the linear graphs shown in Figures 8-4(a) to 8-4(c) with R^2 values >0.9 for all neural networks, showing highly linear relationships between the measured and modelled effluent concentrations. Linear regression equations were (i) $BOD_{estimated}=0.88\ BOD_{observed}+ 0.33$, (ii) $BOD_{estimated}=0.87\ BOD_{observed} +0.21$ and (iii) $BOD_{estimated}=0.94\ BOD_{observed} +0.24$ for the Quasi-Newton, Levenberg-Marquardt and Bayesian Regularization algorithms respectively (Figures 8-4(a) –(c)). Thus, the application of back-propagation neural networks is an effective methodology for the estimation of the biochemical oxygen demand for combined PPS and GHP.

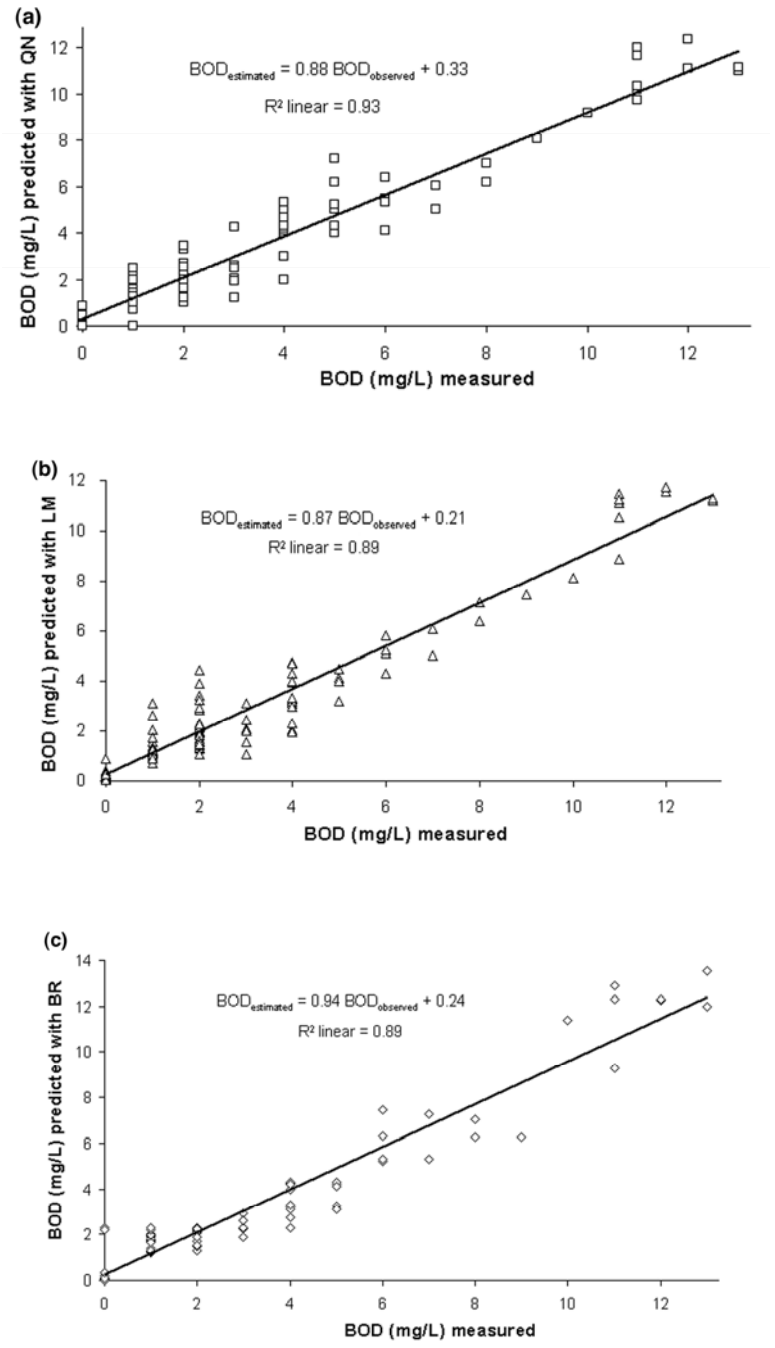

Figure 8-4: Linear regression between the network outputs and corresponding targets for the biochemical oxygen demand (BOD) using the (a) Levenberg-Marquardt, (b) Quasi-Newton, and (c) Bayesian Regularization algorithms

The data size was suitable for accurate predictions of the biochemical oxygen demand. The statistical performance analysis indicated that the neural networks using

network structures of 7-13-1 for the Levenberg-Marquardt, 7-12-1 for the Quasi-Newton and 7-15-1 for the Bayesian Regularization algorithms produced relatively good biochemical oxygen demand performance predictions during the training and testing phases. There was no statistically significant difference in the performance of all three algorithms for the prediction of the effluent biochemical oxygen demand. The back-propagation neural network models incorporating these algorithms performed classification and regression tasks without knowledge of the underlying physical process occurring throughout the pavement system. The neural network methodology is suitable for estimating the biochemical oxygen demand concentrations using an input layer consisting of pH, temperature, electroconductivity, turbidity, total dissolved solids, dissolved oxygen, and redox potential. The results show that for varied effluent concentrations of BOD, applications of artificial neural networks compute a convincing outcome.

Ammonia-nitrogen can be modelled well as shown in Figure 8-5. Ammonia-nitrogen concentrations varied from 0-0.85mg/l when measured, and similarly for all three algorithms. Figure 8-5 shows the pre-eminence for all three algorithms performance for such low concentrations.

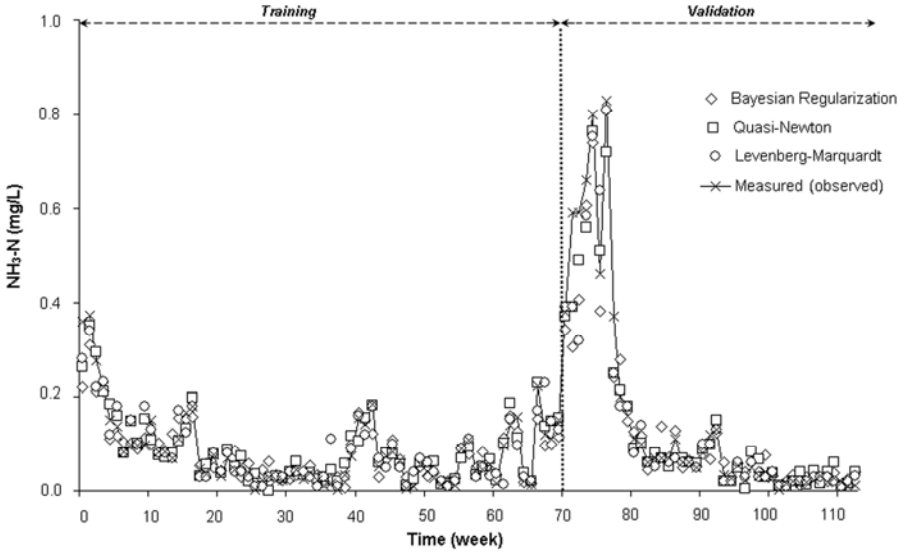

Figure 8-5: Comparison of the measured (observed) and predicted ammonia-nitrogen (NH_4-N) concentrations

A lower accuracy (Mean Absolute Error) was computed for ammonia-nitrogen when compared to the biochemical oxygen demand, which led to a more precise prediction of this variable (Table 8-2). This was a result due to the larger range of BOD effluent concentrations when compared to all other nutrients. The Quasi-Newton algorithm resulted in the lowest mean absolute error (0.022) for ammonia-nitrogen prediction, representing a very high-quality simulation during the training period, with the highest accuracy being the Bayesian Regularization as seen in Table 8-2. Accuracies were computed throughout the validation period. The Quasi-Newton algorithm had the lowest and the Bayesian Regularization technique had the largest accuracy values. The Quasi-Newton algorithm also consisted of the smallest root square mean error for training (0.035) and testing (0.036). The Bayesian Regularization and the Levenberg–Marquardt techniques were less accurate. Nevertheless, the Levenberg-Marquardt algorithm had the smallest mean absolute errors for both training (0.491) and testing (0.499).

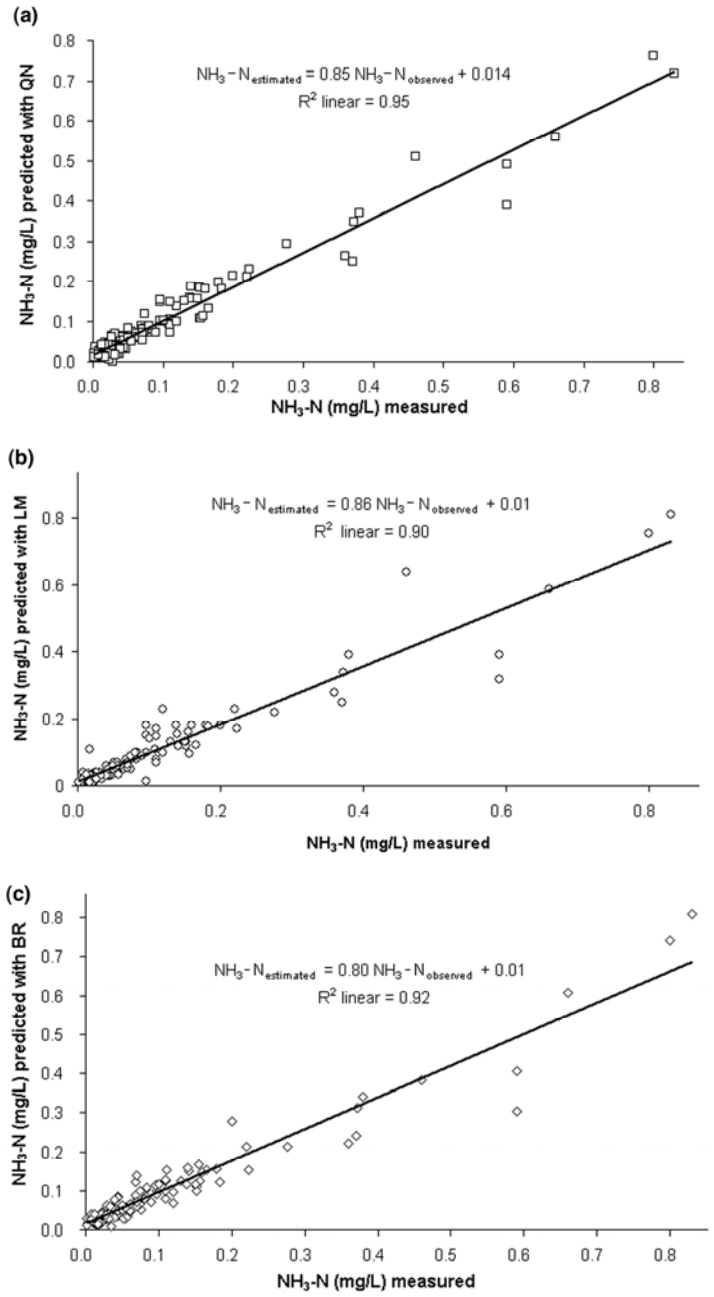

Figure 8-6: Linear regression between the network outputs and corresponding targets for the ammonia-nitrogen (NH_4-N) using the (a) Levenberg-Marquardt, (b) Quasi-Newton, and (c) Bayesian Regularization algorithms

The correlation coefficient was greater than 0.95 for all algorithms with the Quasi-Newton algorithm performing the best with a correlation coefficient of 0.9782 and 0.996 for both phases, respectively. As shown in Figures 8-6(a) to 8-6(c), a near linear relationship occurred for all three models with the coefficient of determination

>0.90. Linear regression analysis shows the relation between simulated ammonia-nitrogen and measured are represented by (i) $NH_3\text{-}N_{estimated} = 0.85\ NH_3\text{-}N_{measured} + 0.01$, (ii) $NH_3\text{-}N_{estimated} = 0.86\ NH_3\text{-}N_{measured} + 0.01$ and (iii) $NH_3\text{-}N_{estimated} = 0.80\ NH_3\text{-}N_{measured} + 0.01$ for the Quasi-Newton, Levenberg-Marquardt and Bayesian Regularization algorithms respectfully (Figures 8-6(a) – 8-6(c)). The Quasi-Newton algorithm was most suitable for ammonia-nitrogen simulation. The selected input variables pH, temperature, electroconductivity, turbidity, total dissolved solids, dissolved oxygen and redox potential can successfully be applied as a modellingtool for monitoring purposes. Although ANN's belong to the class of data driven approaches keeping the number of inputs and therefore the size of the networks to a minimum produces higher reliability of forecasted results. No significant statistical variation was noted between all three selected algorithms, when simulating ammonia-nitrogen.

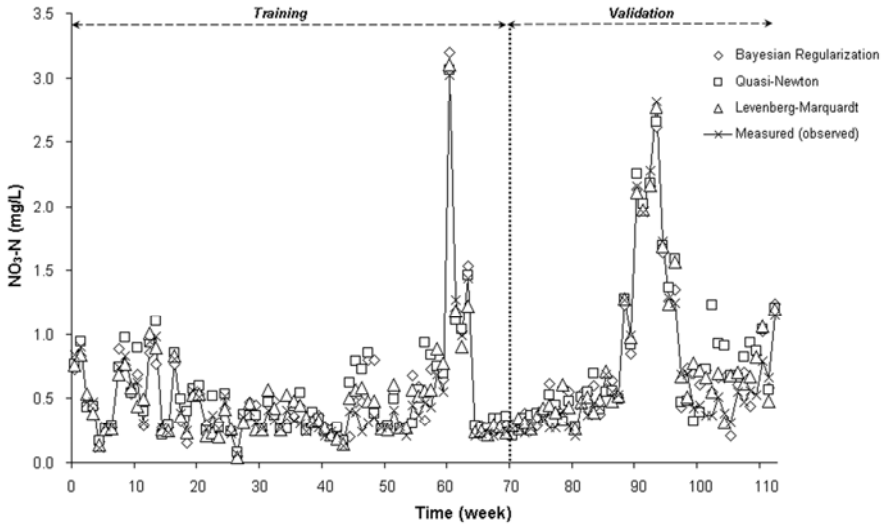

Figure 8-7: Comparison of the measured (observed) and predicted nitrate-nitrogen (NO_3-N) concentrations

It is clear from Figure 8-7 that effluent nitrate-nitrogen concentrations are significantly related to the input parameters, although the relationships are uncertain and dynamic. Observed concentrations ranged from 0.0-3.4mg/l.The back-propagation neural network mimics the effluent nitrate concentrations very well (Figure 8-7) and show the effectiveness of neural network modellingfor such low concentrations and a relatively moderate dataset. The validation phase followed suit to the training segment for all algorithms. From the statistical analysis, the mean absolute error was high for all three algorithms concerning nitrate-nitrogen simulation. The Bayesian Regularization technique resulted with the smallest mean absolute error for both training (0.127) and validation (0.129). The Levenberg-Marquardt algorithm computed the least mean absolute relative errors of 0.491 and 0.500 for testing and validation, respectively.

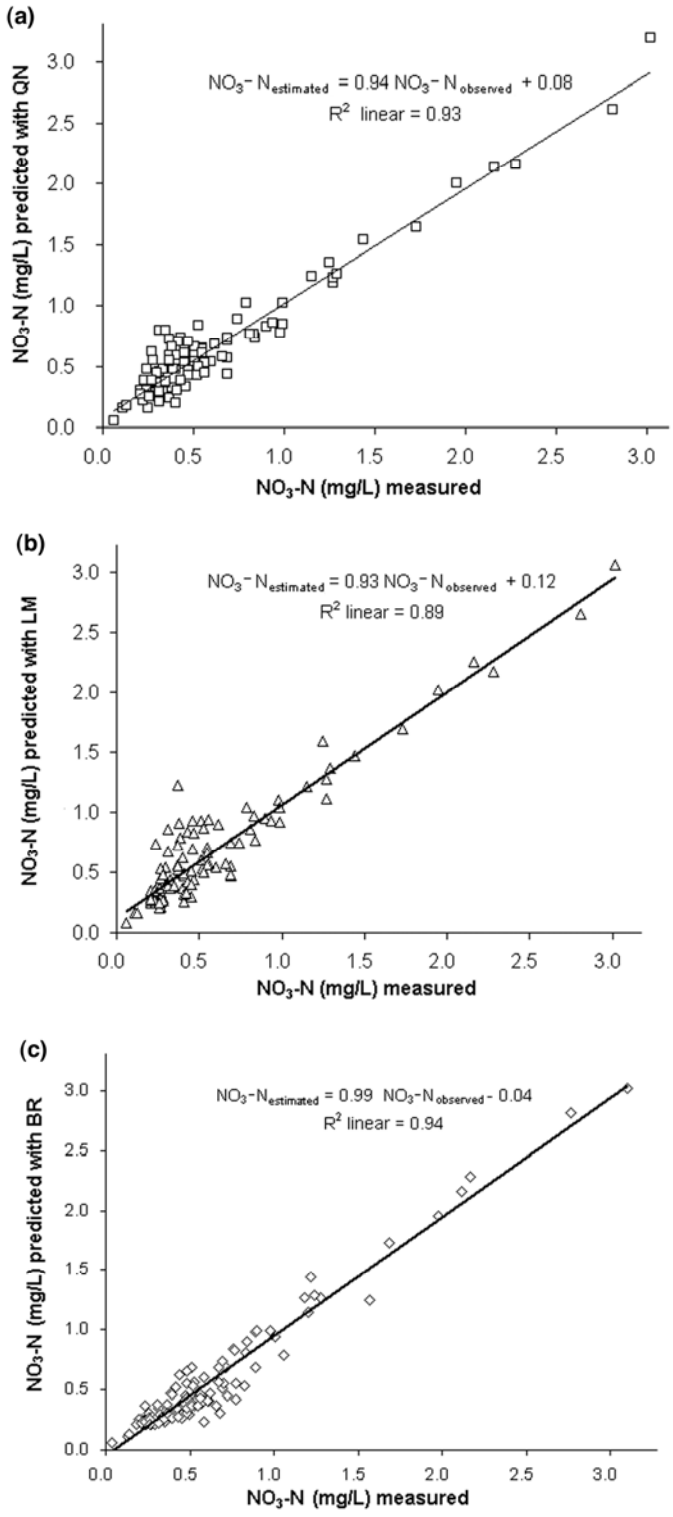

Figure 8-8: Linear regression between the network outputs and corresponding targets for the nitrate-nitrogen (NO_3-N) using the (a) Levenberg-Marquardt, (b) Quasi-Newton, and (c) Bayesian Regularization algorithms

The correlation coefficient was >0.94 indicating very good predictions for all algorithms. Very strong linear relationships between the measured and predicted effluent nitrate-nitrogen concentrations were computed as shown in Figures 8-8(a) to 8-8(c). From the linear regression analysis shown in Figures 8-8(a) to 8-8(c), the relation between modelled ammonia-nitrogen and observed are expressed by (i) $NO_3\text{-}N_{estimated} = 0.94\ NO_3\text{-}N_{measured} + 0.08$, (ii) $NO_3\text{-}N_{estimated} = 0.93\ NO_3\text{-}N_{measured} + 0.12$ and (iii) $NO_3\text{-}N_{estimated} = 0.99\ NO_3\text{-}N_{measured} + 0.04$ for the Quasi-Newton, Levenberg-Marquardt and Bayesian Regularization algorithms respectfully. The Bayesian Regularization algorithm had the highest correlation coefficient (0.95) and subsequently the highest coefficient of determination with a neural network structure of 7-15-1. Once more, all three algorithms showed very good regression performances with the lowest coefficient of determination recorded for the Levenberg-Marquardt algorithm (0.89). There was no statistically significant difference between the Levenberg-Marquardt algorithm, Quasi-Newton algorithm and Bayesian Regularization algorithm. The superiority of ANN in the learning and generalizing complex relationships shows its successful applications to nutrient control and monitoring within permeable pavements.

For surface runoff, ortho-phosphates are applied to agricultural, residential and commercial land as a fertilizer and present in pesticides. It can reach a stream via overland runoff, if the corresponding phosphorus species do not bind to soil particles. Therefore, analysis of orthophosphates is critical for assessing the heath of recycled water.

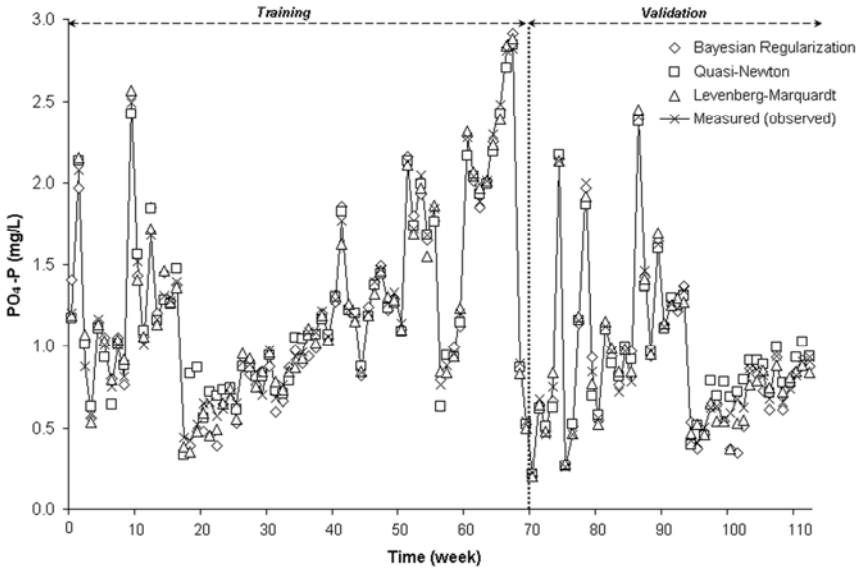

Figure 8-9: Comparison of the measured (observed) and predicted ortho-phosphate-phosphorus (PO_4-N) concentrations

The estimation of ortho-phosphate-phosphorus for both the training and validation period is shown in Figure 8-9. The observed orthophosphates nutrient concentrations ranged from 0.2mg/l to 2.8mg/l and were well-matched by the models. The simulated ortho-phosphate-phosphorus models contained minor prediction errors for all three algorithms and showed no statistical difference. The performance statistics for the modelled data used for training and validation showed high efficiencies for simulation as well as stability throughout both phases. The best model with the smallest mean absolute relative error and overall dispersion was the Quasi-Newton algorithm. The Quasi-Newton algorithm for both the training and validation phases resulted in the smallest accuracy and root mean square error values of 0.064 and 0.065, respectively. This was also the case for the mean absolute relative error.

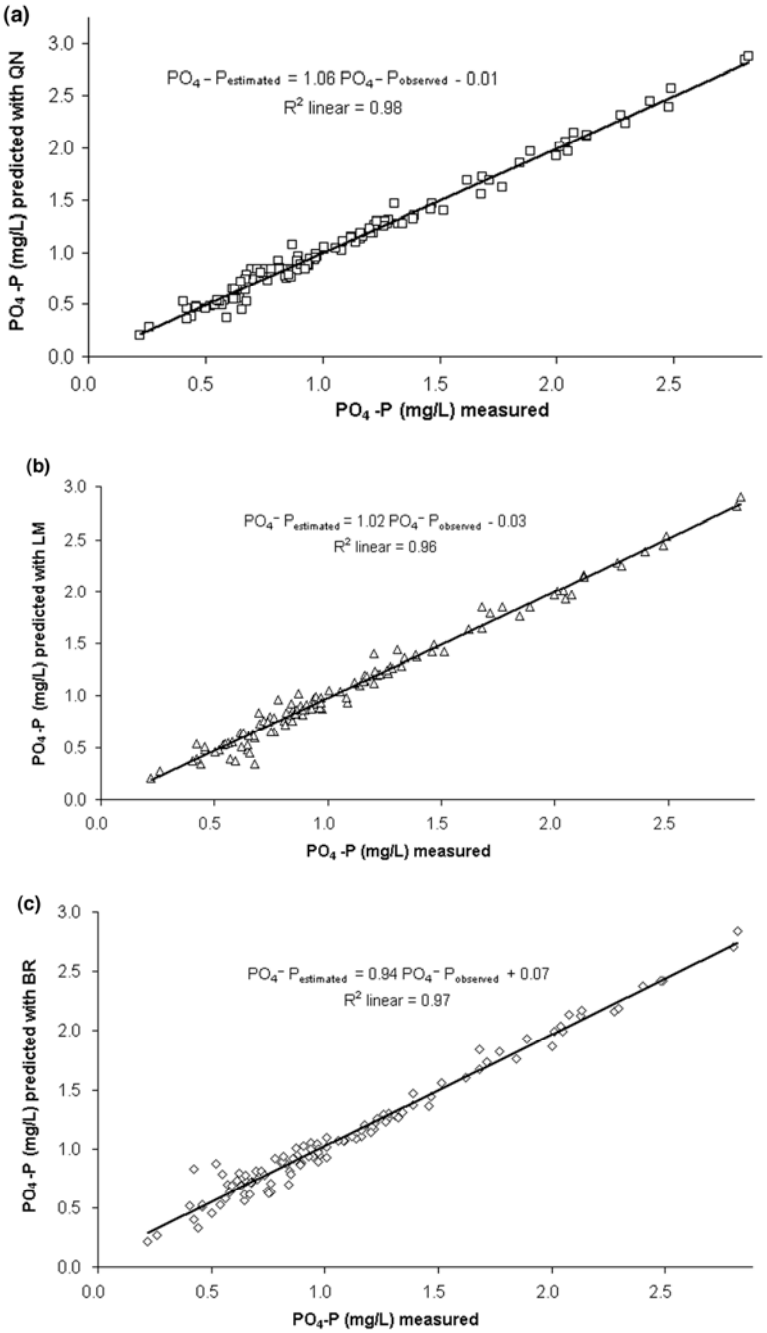

Figure 8- 10: Linear regression between the network outputs and corresponding targets for the ortho-phosphate-phosphorus (PO_4-N) using the (a) Levenberg-Marquardt, (b) Quasi-Newton, and (c) Bayesian Regularization algorithms

From the linear best fit graphs represented in Figures 8-10(a) to 8-10(c), the linkage between predicted ammonia-nitrogen and observed are expressed by (i) PO_4-P $_{estimated}$ = 1.06 PO_4-P $_{measured}$ - 0.01, (ii) PO_4-P $_{estimated}$ = 1.02 PO_4-P $_{measured}$ -0.03 and

(iii) PO_4-P $_{estimated}$ = 0.94 PO_4-P $_{measured}$ + 0.07 for the Quasi-Newton, Levenberg-Marquardt and Bayesian Regularization algorithms respectfully. The correlation coefficients were >0.98 for all algorithms, with the Quasi-Newton having the best linear fit graphs as seen in Figures 8-10(a) to 8-10(c). Consequently, the coefficient of determination was very high for ortho-phosphate-phosphorus predictions. There was again no statistically significant difference between all algorithms when predicting ortho-phosphate-phosphorus. The application of the back-propagation method for the simulation of the effluent concentrations of ortho-phosphate-phosphorus was successful. Post-learning and validation results showed high correlations with the observations, and indicate effective and reliable prediction of ortho-phosphate-phosphorus. The relevance of ANN for ortho-phosphate-phosphorus monitoring and forecasting with permeable pavements demonstrated successful utilization for the data observations from the water quality consisting of commonly measured parameters.

8.9 Summary

The research shows that artificial neural networks are an effective modelling tool for combined permeable pavement and heat transfer systems. The findings show that a simple feed-forward back-propagation artificial neural network model with only one hidden layer provided good predictions of effluent biochemical oxygen demand, ammonia-nitrogen, nitrate-nitrogen and ortho-phosphate-phosphorus concentrations. The presence of the GHP did not alter the removal efficiencies for the contaminants nor did it affect the modellingoutcomes and results. The average errors between the measured and modelled parameters were relatively small. Suitable input parameters were pH, temperature, electroconductivity, turbidity, total dissolved solids, dissolved oxygen and redox potential.

Data normalization techniques were applied to improve network performances. The applications of neural networks for the combined hybrid sustainable system has been shown to provide prediction results that have statistical parameters significantly superior to those obtained using these techniques separately. This work also shows the benefit of neural networks in their ability to represent highly nonlinear

relationships, even for a system that has operational data limitations such as imprecision associated with measured variables, a limited range of variables, and a large number of missing values, as long as the input data have been orthogonalized. Compared to statistical methods, neural networks provide a general framework for determining relationships between water quality data and do not require the specification of any functional form.

All three ANN algorithms were capable of generating competitive models. No algorithm can be considered inherently superior to another. However, it is essential to optimize both the network architecture and training algorithm.

Chapter 9 Application of Kohonen Self-Organising Map Model

Kohonen self-organising map (KSOM) modelling has been applied increasingly for analysis, estimation and prediction of several hydrological processes such as water quality that are embedded with high complexity, dynamism and non-linearity. KSOM or unsupervised neural networks was applied to microbial data (*Escherichia coli*, *Enterococci sp.*, and total coliforms) from the effluent of the two year data set (2008-2010) on 2 outdoor PPS (PPS 1 and PPS 4) which both treated stormwater runoff contaminated with gully pot liquor and faecal matter from dogs. KSOM models can reduce time-consuming and expensive microbial water quality analysis, by the use of alternative parameters, which are faster and easier for measurement. The results suggest that the selected microbial pathogens can be efficiently estimated by applications of machine learning tools such as KSOM with input variables including temperature, pH, electroconductivity, total dissolved solids, suspended solids, turbidity, and chemical oxygen demand (COD) which can be monitored in real time. The application of KSOM is simple, computationally efficient and highly accurate for predicting the effluent concentrations for these microbial pollutants. The methodology based on KSOM is proposed, as a tool in aiding decision makers for sustainable storm water management and its impact on surface water, were trends could be examined, compared and identified in optimizing permeable pavement systems.

9.1 Modelling microbial pathogenic organisms for stormwater reuse.

Bacterial pathogenic parameters are important in monitoring the microbiological pollution load for urban runoff reuse and the assessment and biotreatability can be represented by artificial neural networks (Kashefipour *et al.,* 2005). Determining the numerous types of bacterial pathogenic organism present in urban stormwater is time-consuming, expensive and prone to errors. Modelling of a permeable pavement system and one integrated with GHPs performance for the removal of microbiological pollutants is significant for improving this hybrid paving technology whilst assessing its removal efficiency and optimizing its design, operation and maintenance.

9.2. Kohonen Self Organising Maps (KSOM)

Over the last decade, Kohonen self organising maps (KSOMs) have increasingly been used for analysis, estimation and prediction for various hydrological and environmental processes. Another fascinating ability of KSOMs is the way they can be used in automatically grouping and or typifying data according to different

properties. Kohonen self-organising maps (KSOM) is an unsupervised neural network as is also referred to as the Kohonen neural network (KNN), approximates the probability density function of the input variables and performs a non-linear projection of the multivariate data set into a hyper-dimensional space (Kohonen, 2001). Mukherjee, (1997) referred to the term 'self-organising' as the ability to learn and organize information without being given the corresponding dependent output values for the input patter. It is based on unsupervised neural network applications with competitive learning technique (Kohonen *et al.,* 1996). The goal of KSOM is mapping the spatial relationships between clusters of data points in hyper-dimensional space, normally two-dimensional. Once the KSOM is trained, it can be used in identifying unknown data patterns such as microbiological pollutant concentrations in water quality. KSOM potentially outperforms multi-linear regressions because of its ability and efficiency in dealing with non-linearity systems, and handling noisy or irregular data with an ease of updating (Hong and Rosen 2001). The KSOM model was developed for assessment of water quality of reservoirs and its ability to predict trophic status of coastal waters showing a strong ability in identifying diversity between the data (Aguilera *et al.,* 2001, Gevrey *et al.,* 2004). KSOM has been used extensively in modeling various types of water and environmental data set (Lee and Scholz, 2006a; Kalteh *et al.,* 2008; Scholz, 2008). The advantage of the KSOM algorithm is its visualization and classifications are taken into account (Gevrey *et al.,* 2004; Lee and Scholz, 2006a; Scholz, 2008). These studies showed that KSOM has the potential for analyzing multidimensional data and can simplify complex data sets into a visual form for ease of analysis.

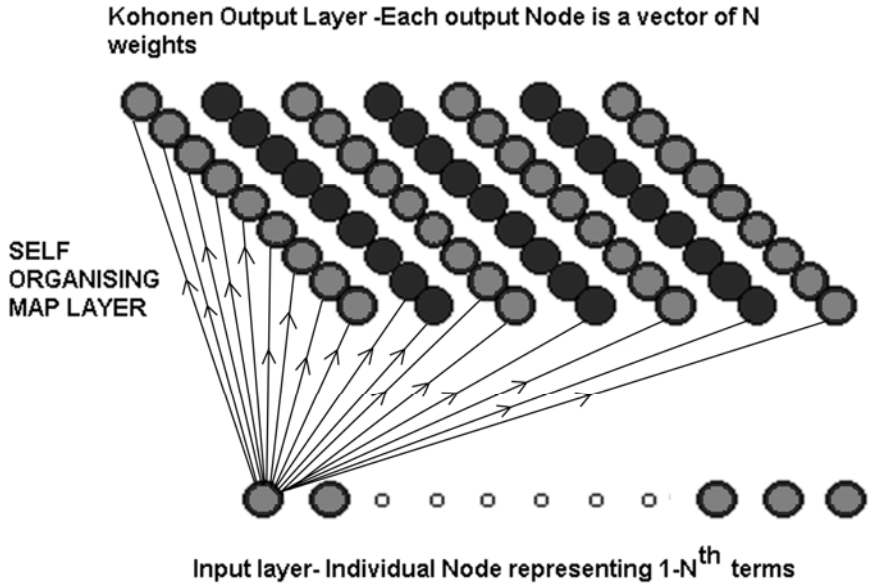

Figure 9-1: Illustrating the Kohonen Self-Organising Map and its neighborhood network.

KSOM consists of the input data layer and the output map layer. Each neuron of the input layer represents an input variable and has a weighted connection to each of the output layer as shown in Figure 9-1. The connection weights are adaptively changing at each iteration for the unsupervised training algorithm. The algorithm implements a nonlinear projection from the high-dimensional input space onto a low-dimensional network of neurons normally a 2-dimensional grid. This is achieved by unsupervised training, which means there is no teaching for the output. KSOM is used at the first abstraction level for a cluster and allows efficient use of the clustering process from the algorithms to divide the prototypes into grounds, and the 2-D grid allows visual presentation and additional for interpretation of the clusters outlined. This mapping roughly preserves the most important topological and metric relationships of the original data elements and implies that negligible information is lost during the mapping (Rustum and Adeloye, 2007). In training the network, the unsupervised Kohonen learning rule is applied. For the training step, one vector x from the input set is chosen and all the weight vectors of the SOM are calculated using a distanced measure, known as the Euclidian distance, (Kohonen, 2001; Lee and Scholz, 2006 b). The KSOM model has not often been implemented for water and wastewater treatment process control strategies when compared to traditional

neural networks. However, Lee and Scholz, (2006 a) applied KSOM as a prediction tool for heavy metal removal within constructed wetlands. Rustum and Adeloye, (2007) modelled the activated sludge wastewater treatment plant with KSOM, back-propagation artificial neural networks and multiple regression analysis and showed that KSOM is superior to the two latter modelling techniques.

Within KSOM algorithms, the topological relations and the number of neurons or nodes are fixed initially (Kohonen *et al.,* 1996). Each neuron i is represented by an n-dimensional weight or model vector $m_i = [m_{i1}, m_{i2}\ldots,m_{in}]$ (n, dimension of the input vectors). Each neuron contains a weight vector (Zhang *et al.,* 2008, 2009). At the beginning of the model, the weight vectors are initializes using random values. For the period of training, the weight vectors are calculated using some distance measure such as the Euclidian distance as is defined as

$$D_i = \sqrt{\sum_{j=1}^{n}(x_{ij} - m_{ij})^2} \quad , i = `,2,\ldots.,M \tag{9-1}$$

Where D_i =Euclidian distance between the input vector and the weight vector i; x_{ij} = jth element of the current input vector; m_{ij}=jth element of the weight vector i; M= number of the neurons within the Kohonen self-organising maps; and n = dimension of the input vectors (Zhang *et al.,* 2008, 2009).

Node c (Equation 9-2) whose weight vector is closest to the input vector is selected as the best matching unit (BMU). This neuron is chosen as the winning node or the BMU. When the BMU is found, the weight vectors mi are updated. The BMU and its topological neighbours are moved closer to the input vector. The update rule of the weight vector is based on equation (9-3).

$$\|x - m_c\| = \min\{\|x - m_i\|\} \tag{9-2}$$

Where x= input vector; m=weight vector; and $\| \|$=a distance measure.

$$m_i(t+1) = m_i(t) + \alpha(t)h_{ci}(t)[x(t) - m_t(t)] \tag{9-3}$$

Where m(t) = weight vector indicating the output unit's location in the data space at time t; $\alpha(t)$ = learning rate at time t; $h_{ci}(t)$ = neighbourhood function centreed in the 'winner unit' c at time t; and x(t) = input vector drawn from the input data set at time t. In this manner each node in the map internally develops the ability to recognize the input vectors similar to itself. As a result of no external information being supplied in leading to a classification, this characteristic is referred to be self-organising (Penn, 2005; Rustum and Adeloye, 2007).

The neighbourhood functions and the learning rates affect the learning effectiveness of the KSOM and must be selected carefully (Penn, 2005). In particular, the learning rate decreases monotonically with an increased number of iterations described in equation (9-4)

$$\alpha(t) = \alpha_0 \left(\frac{0.005}{\alpha_0} \right)^{t/T} \tag{9-4}$$

Where α_0 = initial learning rate and T= training length (Vesanto *et al.,* 2000), thus forcing the weight vector to converge. The neighbourhood function is normally chosen to be Gaussian centred in the winner unit c, and follows equation (9-5):

$$h_{ci}(t) = \exp\left(- \left\| r_c - r_i \right\|^2 / [2\sigma^2(t)] \right) \tag{9-5}$$

Where r_c and r_i = position of nodes c and I on the KSOM grid and $\sigma(t)$ = neighbourhood radius. Similarly the learning rate $\alpha(t)$, like $\sigma(t)$ decreases monotonically as the number of iterations increases. After this competitive learning process, the clusters corresponding to characteristics features can be illustrated on the map. The learning rate and neighbourhood radius were set with default values. The default number of neurons is determined by the heuristic equation (9-6). The ratio between side lengths of the map grid was set to the square root of the ratio of the two highest *eigenvalues* of the data sample (Vesanto *et al.,* 2000; García and González, 2004)

$$M \approx 5\sqrt{n}\,, \tag{9-6}$$

Where M= number of neurons and n= total number of data samples. A guideline by García and González, (2004) which also works well, is

$$\frac{l_1}{l_2} = \sqrt{\frac{e_1}{e_2}} \tag{9-7}$$

Where l_1 and l_2=number of rows and columns respectively; e_1=biggest eigenvalue of the training data set; and e_2= second largest eigenvalue.

9.3 Aims and Objectives

The aim of this chapter is to propose a simple and robust Kohonen neural network model appropriate for providing real time control of the treatment performances of a standalone permeable pavements systems (PPS 6, outdoor rig) and permeable pavement integrated with geothermal heat pumps (PPS 4, outdoor rig), which can be applied for developments of sustainable urban drainage techniques. The corresponding objectives are as follows:

(i). To identify relationships between key outflow variables from the pavement systems by self-organising maps visualization

(ii). To predict the expensive and time consuming microbiological parameters including *Escherichia coli*, *Enterococci sp.* and total coliforms using a KSOM model based on a more rapidly, easier and economical measurable water quality parameters.

(iii). To assess the differences for KSOM simulation between a permeable pavement systems combined with ground-source heating and cooling for prediction of these parameters to typical permeable pavement systems.

9.4 KSOM Numerical Analysis and Modelling

The SOM toolbox for Matlab 7.0 (The MathWorks, Inc. UK, Cambridge, United Kingdom) was used in this study. The KNN toolbox was developed by the Laboratory of Information and Computer Science at Helsinki University of Technology, Finland (Vesanto *et al.,* 2000). For modelling purposes, the dataset was mixed in a random order and subsequently sub-divided into the training segment and verification segment. The two year data set from 2008-2010 was split into a first set of 64 observations to train the model (training phase) and the second set of 51 observations to test the model (validation and verification period). The amount of data points used was comparable and greater than those used in previous neural network prediction models (Lee and Scholz, 2006 a, 2006 b). The Kolmogorov–Smirnov tests ($p>0.01$) were used to check that the distribution of the data approximated normality, prior to neural network applications. The raw data set was pre-processed by utilizing a log transformation method, if it did not follow a normal distribution.

The KSOM model was applied using the data obtained from both pavement systems to identify the relationship between the influent stormwater quality variables and the microorganism removal efficiency. The prediction was implemented by finding the BMU within the map for each data set. The performance of the models during training and validation were statistically evaluated using equation (7-51) for the correlation coefficient, and equations (8-9) to (8-11) for the mean absolute error (MAE), the root square mean error (RSME) and the mean absolute relative error (MARE). The performances of the KSOM neural network models were evaluated based on these statistical numerical evaluations and are useful in evaluation of KSOM modeling results.

9.5 Results and Discussion

The use of advanced modelling techniques such as KNN or KSOM for predicting the effluent of microbial diversity for these key aquatic communities is an important step in defining the reference conditions for water quality from treated urban runoff. The advantages of KNN are that the techniques are tolerant to noisy data and are capable of handling outliers. The component planes for each variable for the KSOM are shown in Figures 3, 5 and 7 illustrating the associations between variables. A (7 × 6) KSOM map is used and the hexagonal grid displayed. Each component plane can be viewed as a portion of the KSOM, because it consists of the values of single vector variables in all map units (Tran *et al.,* 2003).These planes are filled with grey shades to show the individual values of the given feature of the SOM unit in the two dimensional grid (Tran *et al.,* 2003). The darker grey areas are associated with a low relative component value whilst the lighter grey shades are linked to a high relative component value of the corresponding weight vector. As a result, the component planes assist in visualization for the illustrated map, showing the relationships between the microbiological parameters (*Escherichia coli*, *Enterococci sp.* and Total Coliforms) and the selected water quality variables used for analysis.

The unified distance matrix (U matrix) representation of the KSOM map indicates the distances between the map neurons (Vesanto *et al.,* 2000; Lee and Scholz, 2006 a; Hedmark *et al.,* 2009). The distances between the neighbouring map neurons were visualized by the grey shading scales between each neuron. The component plane represents the value of the variable presented in each map unit (Lee and Scholz, 2006 a, 2006 b). Visualization of KSOM aids in identification and subsequent illustration of the clusters within the input data set. The inter-unit values are the Euclidean distances between adjacent map units. The levels of grey shown inside a specific unit are found by taking the median of the surrounding grey level values. A dark (light) shade between the neurons corresponds to a large (small) Euclidean distance and this large (small) gap between the values in the input space. The U-matrix visually suggests the presence neuron clusters.

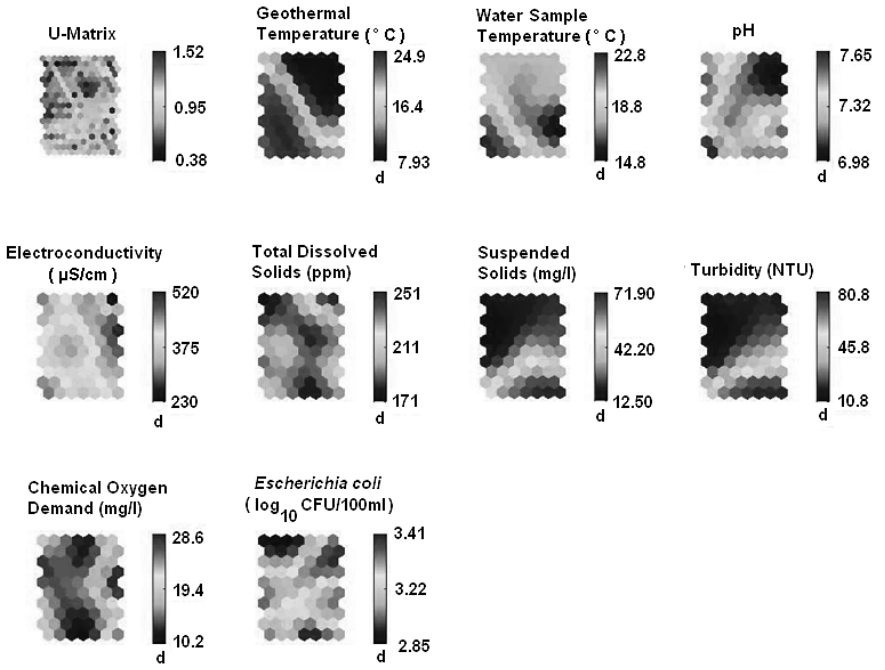

Figure 9-2: Component planes and U-matrix visualizations of the relationships between *Escherichia Coli* (CFU/100ml) and Geothermal Heating/Cooling Temperature (°C), Water sample Temperature (°C), pH, Electroconductivity (µS/cm), Total Dissolved Solids (mg/l), Suspended Solids (mg/l), Turbidity (NTU), and Chemical Oxygen Demand (mg/l) in stormwater for PPS 4 (outdoor rig) the combined permeable pavement and geothermal heat pump system.

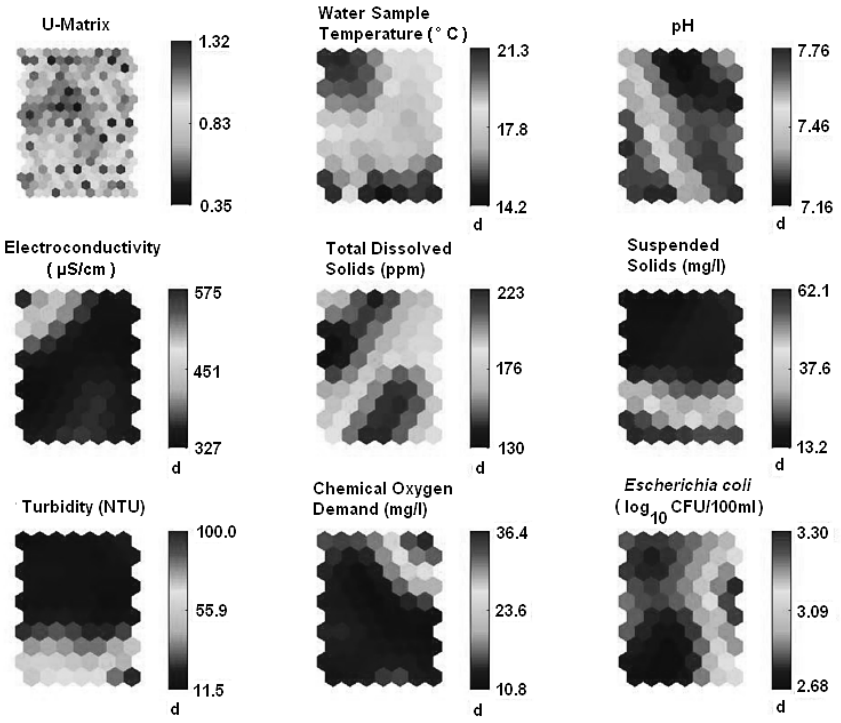

Figure 9-3: Component planes and U-matrix visualizations of the relationships between *Escherichia Coli* (CFU/100ml) and Water Sample Temperature (°C), pH, Electroconductivity (µS/cm), Total Dissolved Solids (mg/l), Suspended Solids (mg/l), Turbidity (NTU), and Chemical Oxygen Demand (mg/l) in stormwater for PPS 6 (outdoor rig) the standalone permeable pavement system.

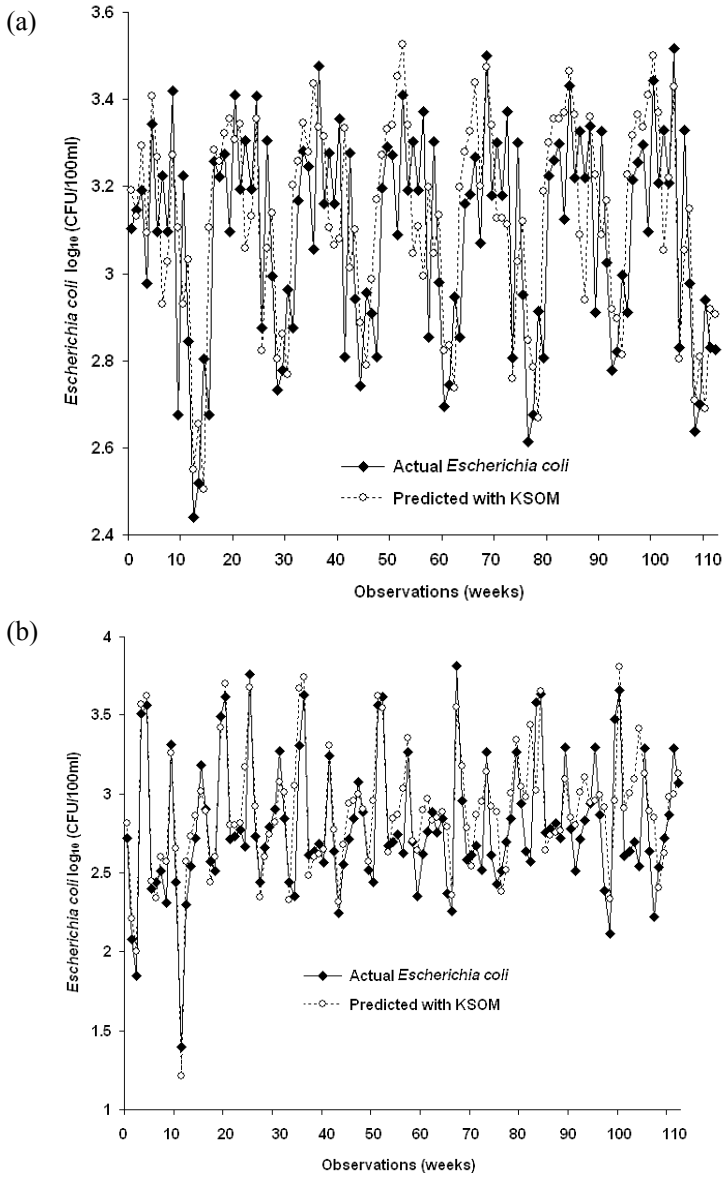

Figure 9-4: Comparison of the Actual and predicted effluent concentrations of *Escherichia coli* by self-organising map (SOM) for (a) PPS 4(outdoor rig) permeable pavement combined with geothermal heat pump system and (b) PPS 6 (outdoor rig) standalone permeable pavement system. Sample number n= 112 weeks for a 2 year period from 4 March 2008 to 5 March 2010).

Figure 9-2 shows the U-matrix and the component planes for the combine GHP and PPS for *Escherichia coli* effluent simulations. The U-matrix shows the distances between the neighbouring prototype vectors of the neighbouring map units. Thus, a group of map units (neurons) which is too concentrated implies a cluster which occurred for suspended solids, turbidity and geothermal temperatures and its relation to *Escherichia coli*. The highest values correspond to the dark regions and the lowest

ones to the lighter grey zones. *Escherichia coli* concentrations from 719 to approximately 2000 CFU/100ml are linked to lower suspended solids concentrations (< 42 mg/l) and Turbidity (< 45 NTU). There is also a higher association of geothermal temperatures between 16 and 25 °C for *Escherichia coli* concentrations. No apparent link can be associated to the chemical oxygen demand and the *Escherichia coli* concentrations.

The component planes for the standalone PPS are shown in Figure 9-3 for *Escherichia coli* illustrating the associations between variables. Each component plan can be viewed as a portion of the KSOM because it consists of the values of single vector variables in all map units presented. The planes filled with lighter grey shades shows the individual value for the given feature of the KSOM unit in a two dimensional lattice. Temperature and total dissolved solids shows a higher relative component value of the corresponding weight vector in relation to the *Escherichia coli* concentrations. Concentrations of *Escherichia coli* ranging from 487 to 600 CFU/100ml are linked to turbidity levels from 50 to 100 NTU, COD concentrations (< 23 mg/l), suspended solids from 37 to 63 mg/l, electroconductivity values from 327 to approximately 460 (µS/cm) and a pH (< 7.6) respectively. Figures 4 (a) and (b) presents the KSOM model prediction illustrating the trends for simulating *Escherichia coli* effluent concentrations for both systems. The outflow pathogenic organism is in conformity between the actual (measured) and predicted concentrations. This indicates the KSOM model performed very well in predicting *Escherichia coli* for both systems within a very low range of 2.4 to 3.6 $\log_{10}$(CFU/100ml) for the combined PPS and GHP system (PPS 4) and 1.1 to 4.0 $\log_{10}$(CFU/100ml) for the standalone PPS (PPS 6).

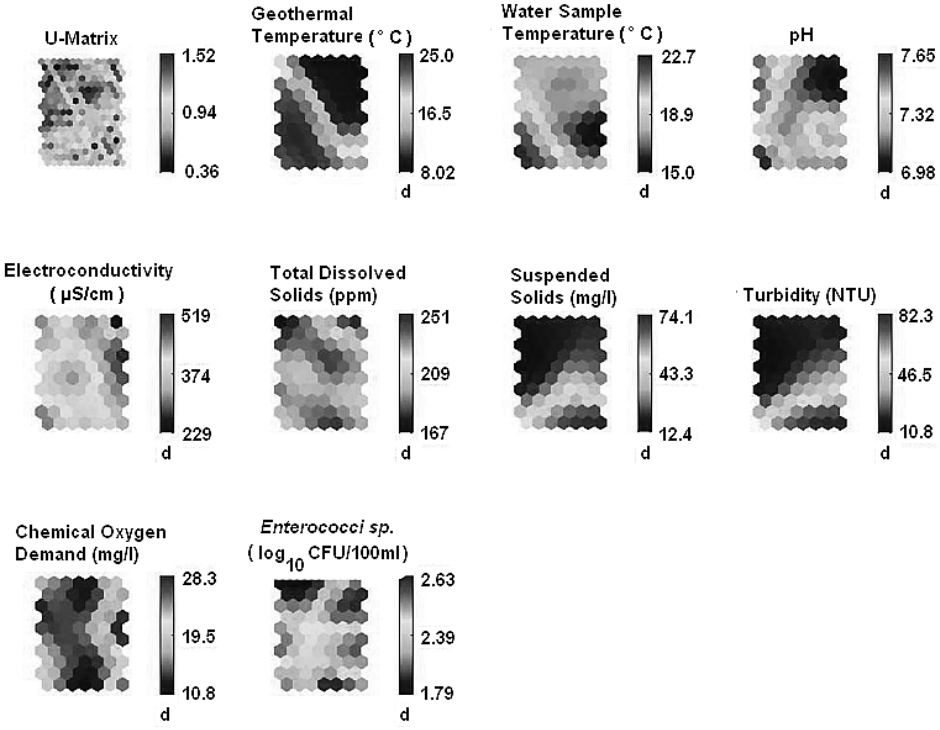

Figure 9-5: Component planes and U-matrix visualizations of the relationships between *Enterococci sp.* (CFU/100ml) and Geothermal Heating/Cooling Temperatures (°C), Water Sample Temperature (°C), pH, Electroconductivity (µS/cm), Total Dissolved Solids (mg/l), Suspended Solids (mg/l), Turbidity (NTU), and Chemical Oxygen Demand (mg/l) in stormwater for PPS 4 (outdoor rig) combined permeable pavement and geothermal heat pump systems.

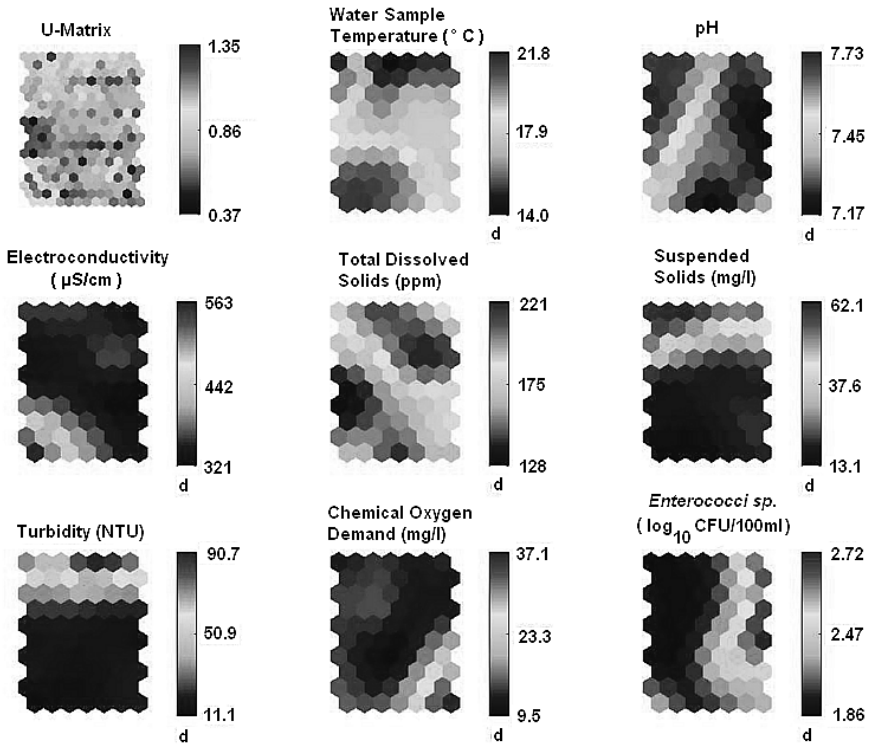

Figure 9-6: Component planes and U-matrix visualizations of the relationships between *Enterococci sp.* (CFU/100ml) and Water Sample Temperature (°C), pH, Electroconductivity (µS/cm), Total Dissolved Solids (mg/l), Suspended Solids (mg/l), Turbidity (NTU), and Chemical Oxygen Demand (mg/l) in stormwater for PPS 6 (outdoor rig) the standalone permeable pavement system.

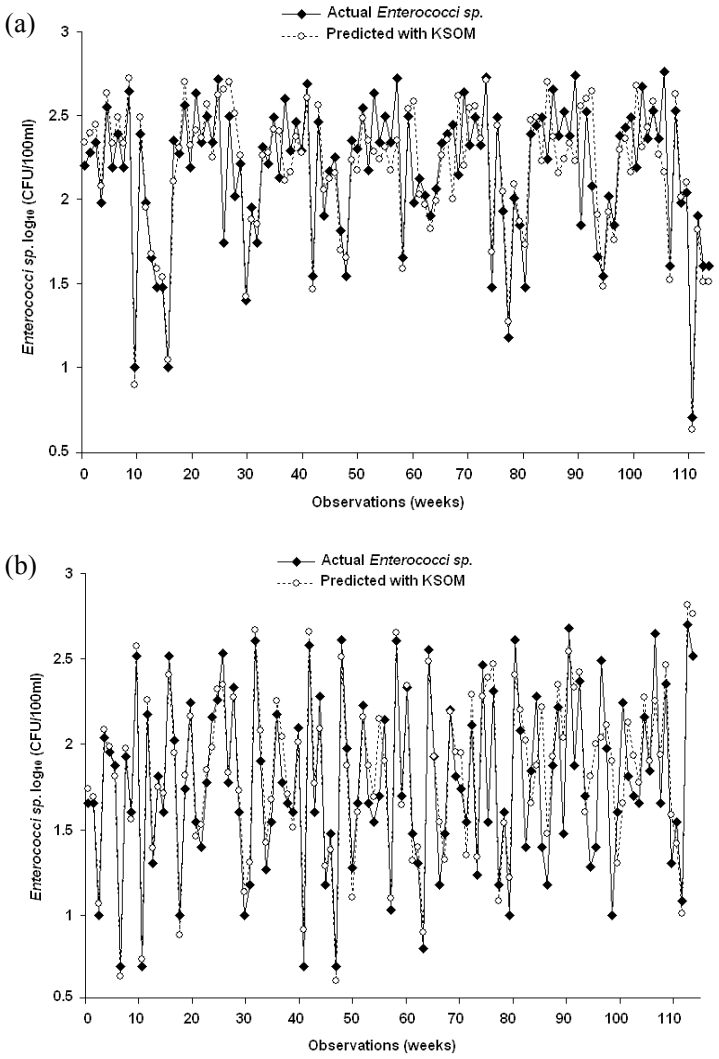

Figure 9-7: Comparison of the Actual and predicted effluent concentrations of *Enterococci sp.* by self-organising map (SOM) for (a) PPS 4 (outdoor rig) permeable pavement combined with geothermal heat pump system and (b) PPS 6 (outdoor rig) standalone permeable pavement system. Sample number n= 112 weeks for a 2 year period from 4 March 2008 to 5 March 2010).

For the prediction of *Enterococci sp.*, the KSOM U-matrix and component planes are represented in Figures 9-5 and 9-6 respectively. The outflow concentrations of the *Enterococci sp.* bacteria are classified according to the gradient of water quality parameters composition within the KSOM map shown in Figures 9-5 and 9-6. For the combined PPS and GHP system (PPS 4) (Figure 9-5), *Enterococci sp.* effluent concentrations in the range of 62 to 400 CFU/100ml are linked to geothermal temperatures of around 8 to 15 (°C), sample water temperatures of 18 to

22 (°C), ph of 7 to 7.3, electroconductivity ranging from 230 to 500 (μS/cm), total dissolved solids of 170 to 240 (mg/l), suspended solids from 12 to 40 (mg/l) and a turbidity of 10 to 35 NTU. The turbidity and suspended solids component plans have similar patterns to each other and shows a relationship to higher concentrations of *Enterococci sp.* Figure 9-6 represents the standalone PPS (PPS 6) and the cluster structure of the KSOM maps for the component planes. The density of the KSOM vectors including electroconductivity, suspended solids, turbidity, and chemical oxygen demand reflects the density of the data points and the distances along the KSOM vectors replicates the distribution of the dataset. These parameters correspond to higher concentrations of *Enterococci sp.* in the range of 299 to 525 CFU/100ml. The corresponding predictions for both systems are shown in Figures 9-7 (a) and (b) respectively. A similar time-series sequence was observed for both predictions (Figure 9-7(a, b)). The KSOM model simulation mimicked that of the *Enterococci sp.* effluents for very low concentrations ranging from 0.5 to 3.0 $\log_{10}$ (CFU/100ml) respectively. This shows the efficiency for KSOM neural networks and its capabilities in dealing with an extremely limited dataset and low concentrations using the input variables. Both systems performed similarly indicating that the presence of geothermal heat pumps does not affect the outcome of the KSOM modelling technique.

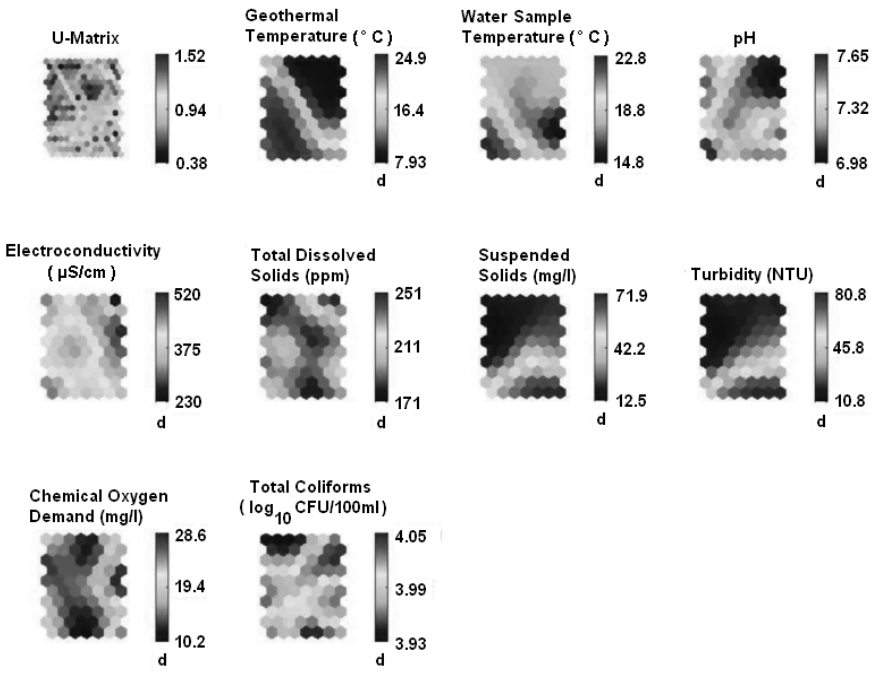

Figure 9-8: Component planes and U-matrix visualizations of the relationships between Total Coliforms (CFU/100ml) and Geothermal Heating/Cooling Temperatures (°C), Water Sample Temperatures (°C), pH, Electroconductivity (µS/cm), Total Dissolved Solids (mg/l), Suspended Solids (mg/l), Turbidity (NTU), and Chemical Oxygen Demand (mg/l) in stormwater for PPS 4 (outdoor rig) combined geothermal heat pumps and permeable pavement system.

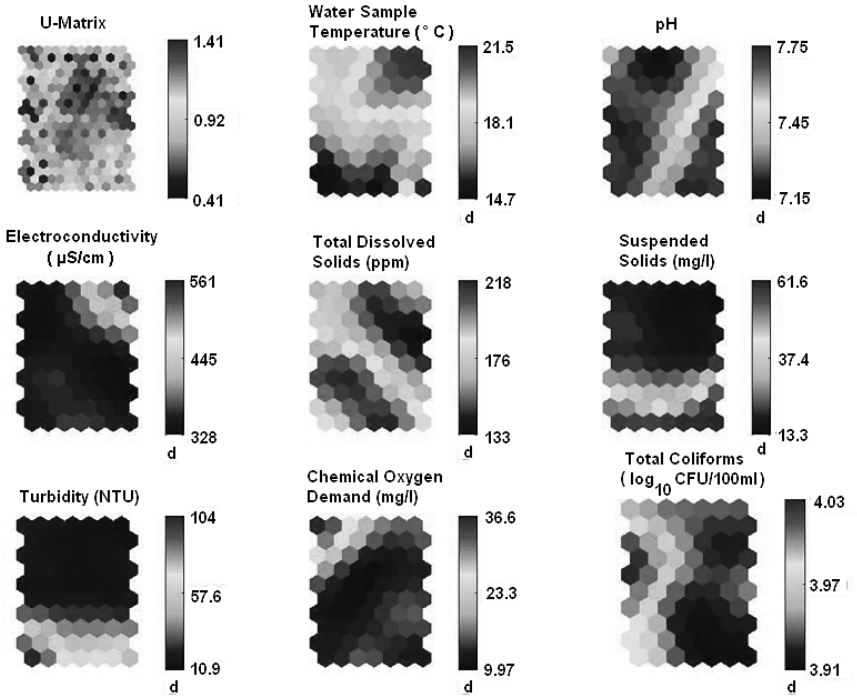

Figure 9-9: Component planes and U-matrix visualizations of the relationships between Total Coliforms (CFU/100ml) and Water Sample Temperature (°C), pH, Electroconductivity (µS/cm), Total Dissolved Solids (mg/l), Suspended Solids (mg/l), Turbidity (NTU), and Chemical Oxygen Demand (mg/l) in stormwater for PPS 6 (outdoor rig) standalone permeable pavement system.

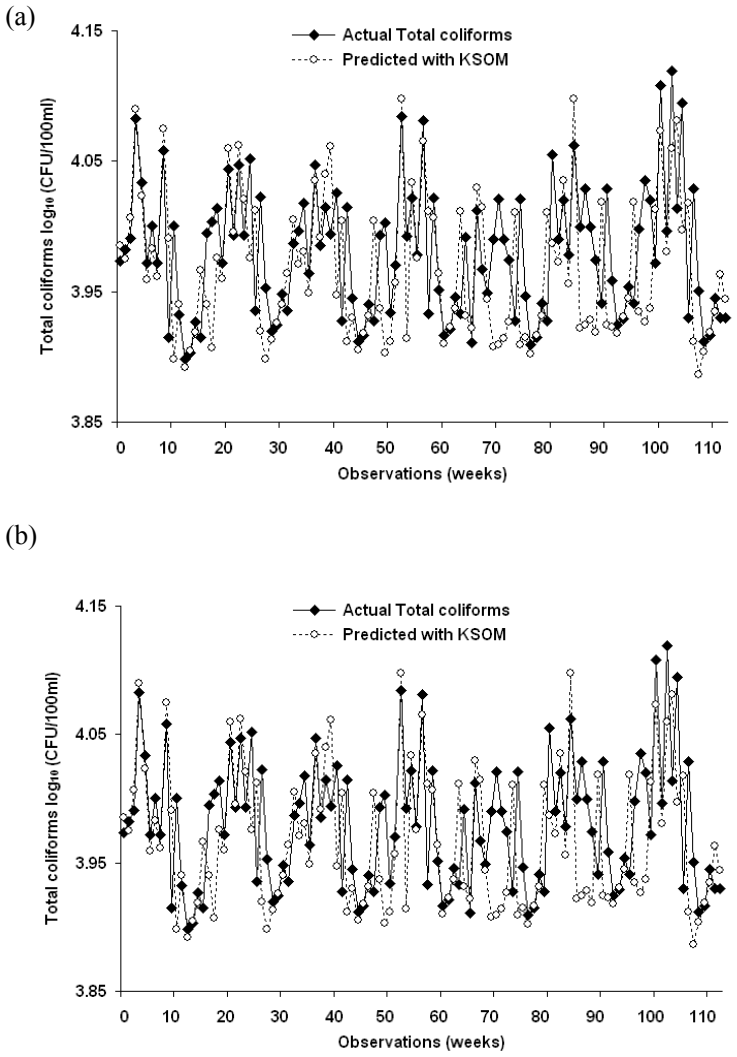

Figure 9-10: Comparison of the Actual and predicted effluent concentrations of Total coliforms by self-organising map (SOM) for (a) PPS 4 (outdoor rig) permeable pavement combined with geothermal heat pump system and (b) PPS 6 (outdoor rig) standalone permeable pavement system. Sample number n= 112 weeks for a 2 year period from 4 March 2008 to 5 March 2010).

With regards to the total coliforms clusters, relationships can be identified in the lower part of each component plane within the U-matrix as shown in Figures 9-8 and 9-9. Once more, the suspended solids and turbidity are high for the equivalent are of the component plane, linking to higher effluent concentrations of the bacteria (11,400 CFU/100ml) as seen in Figure 9-8 for the combined PPS and GHP system (PPS 4). Geothermal temperatures between 16 and 25 (°C) are associated to higher concentrations of total coliforms. For temperature, pH, electroconductivity, and total

dissolved solids, the lighter grey shades shows the higher relative component value of the corresponding weight vectors for these water parameters. Thus, the component planes assist in visually illustrating the relationship between total coliforms effluent and the water variables considered in the analysis. For the standalone PPS (PPS 6) illustrated in figure 9-9, the component plans and U-matrix shows the clusters of darker grey areas for electroconductivity, suspended solids, turbidity and chemical oxygen demand in relation to the outflow total coliforms concentrations. Bacterial concentrations for total coliforms in the range of 8000 to 9200 CFU/100ml appear to be associated to turbidity of 10 to 55 NTU, COD between 26 and 35 mg/l, electroconductivity (>445 μS/cm) and suspended solids range of 36 to 62 mg/l respectively.

Figure 9-10 proves the predictive capacity of the KNN model once more. The KSOM simulation for total coliforms was optimal and resulted in a good estimation for the modelled concentrations. The time-series progression outflow concentrations ranged from 3.85 to 4.20 $\log_{10}$(CFU/100ml). Again, the presence of geothermal heat pumps did not alter the prediction capabilities of KSOM for the combined PPS and GHP and seen in figure 9-10(a) and there was likewise prediction performance for the standalone PPS as shown in figure 9-10(b) respectively.

To ensure the statistical significance of the findings in Table 9-1, the prediction results were compared with each other and analysed by using an analysis of variance (Anova). The Anova threshold for statistically significant findings ($p < 0.05$). It follows that pairs of MAE, RMAE, RMSE and R for both systems can be regarded as similar with $p \geq 0.05$. The outcome of Anova showed that the measured statistical variables were not statistically different for the combined PPS and GHP (PPS 4) with the standalone PPS system (PPS 6). From the findings, it can also be concluded that there is no statistical variations from the computed values during the training and validation period. The summary of the statistical simulation results for both the training and validation periods as presented in Table 9-1 shows very similar performances for the mean absolute error (MAE), the relative mean absolute error (RMAE), the root mean square error (RMSE), and the coefficient of correlation (R). When predicting microbial pathogenic parameters the smaller the MAE, RMAE and RMSE the more effective the modeling system. With respect to MAE, total coliforms

resulted with the lowest values of 0.040, and 0.044 for the combined PPS and GHP in the training and validation period and performed similarly with a MAE of 0.042 and 0.046 for the standalone PPS for the training and verification phases respectively. Such low MAE shows the closeness between the measured and predicted variables. Both *Enterococci sp.* and *Escherichia coli* resulted in the lowest RMAE, however the standalone PPS effluent *Escherichia coli* simulation had the lowest RMAE of 0.078 and 0.085 for the training and validation phases respectively. The RMAE calculating the unbiased error estimations shows how well the models performed during both phases for all three selected microbial organisms. Once more, the total coliforms prediction resulted in the lowest RMSE for both the dual PPS/GHP (PPS 4) and the standalone PPS (PPS 6) of 0.053, 0.058 and 0.057 and 0.062 for the training and verification stages, respectively. Total coliforms bacteria resulted in the least prediction error because of the higher concentration values and show an overall better modeling performance. The correlation coefficient (R) ranged from 0.751 to 0.891 for all waterborne microbial organisms assessed. This indicates the strong linear relationship existing between the predicted and actual bacteria. Moreover, the difference between the correlation coefficients for the training and verification periods were marginal ($p>0.05$).

Table 9-1: Summary of statistical measurements of KSOM models for *Escherichia coli*, *Enterococci sp*. and Total Coliforms predictions during training and (verification) with PPS 4 (permeable pavement combined with geothermal heat pump) and PPS 6 (standalone permeable pavement system)

Statistical Measurement	***Escherichia coli***		***Enterococci sp.***		**Total Coliforms**	
	PPS 4	PPS 6	PPS 4	PPS 6	PPS 4	PPS 6
MAE[a]	0.166 (0.181)	0.188 (0.206)	0.163 (0.179)	0.176 (0.193)	0.040 (0.044)	0.042 (0.046)
RMAE[b]	0.240 (0.263)	0.078 (0.085)	0.079 (0.087)	0.088 (0.096)	0.182 (0.199)	0.169 (0.185)
RMSE[c]	0.198 (0.217)	0.254 (0.278)	0.232 (0.254)	0.247 (0.270)	0.053 (0.058)	0.057 (0.062)
Correlation Coefficient (R)	0.751 (0.763)	0.832 (0.844)	0.846 (0.857)	0.877 (0.881)	0.868 (0.879)	0.858 (0.891)

[a] Mean Absolute Error ; [b] Relative Mean Absolute Error [c] Root Mean Square Error

In considering the uncertainties in the dataset used for training the KSOM model, primarily owing to the high variability in coliform concentrations there is no statistical difference for the combined GHP and PPS (PPS 4) and the standalone PPS (PPS 6). All statistical measurements as presented in table 9-1 are fractionally different throughout the training and verification periods. Furthermore, the number of data points used (n=112) to develop the KSOM model limits the overall performance. As a general rule of thumb, with KSOM applications, the more data points available for modelling developments, the performance is likely to increase as a result of greater pattern extractions from a larger data set (Rustum *et al.,* 2008).

9.6. Summary

KSOM's have increasingly been applied for analysis, estimation and prediction in the field of water quality and environmental engineering. This research addressed the use of raw stormwater quality data from the effluent of two permeable pavement systems at The University of Edinburgh, U.K, during a two year period. It has been demonstrated that KSOM a type of unsupervised neural network is an efficient tool for diagnosing the effect of stormwater treatment for with several water quality variables, extracting the dependencies between variables and the microbiological data set. The Kohonen self-organising map was successfully applied for modelling

the effluent concentrations of *Escherichia coli*, *Enterococci sp.* and total coliforms. These microbial pathogenic organisms can be most-effectively monitored by application of KSOM models by other outflow parameters, which can be measured more rapidly, reducing laboratory procedures, time and cost. The relationships for the permeable pavement systems, with and without ground-source heat pumps, effluent water quality characteristics was well predicted by application of the self-organising map model (KSOM). It has been shown that KSOM is capable of capturing the complex relationships between water quality variables from sustainable urban drainage systems such as permeable pavements with no prior knowledge about the removal efficacy and mechanism involved. Finally, the KSOM model principally provides a useful tool in monitoring and controlling water quality from PPS on a daily basis.

Chapter 10 Conclusions and Recommendations

10.1 Conclusions

Stormwater reuse is attractive particularly where available water supplies are overcommitted and cannot meet increasing water demands to supply growing populations. PPS are key sustainable urban drainage systems that allow large quantities of stormwater to infiltrate, thus reducing peak runoff volumes and flows. It was shown experimentally how effective PPS are for improving urban runoff water quality by various physical and biological processes. PPS introduces an appropriate urban drainage system which can effectively minimise the risk of flooding and provide improved water quality by reducing and eliminating contaminants, mitigating the risk of downstream pollution to watercourses. GHPs recognised worldwide as an energy-saving tool using the Earth's energy can be utilised within PPS structures as a heat source when operating in a heating mode and a heat sink when functioning in a cooling mode. One of the many advantages of the combined PPS-GHPs is that they can offer both heating and cooling at virtually any location, with great flexibility to meet any demands providing stormwater reuse.

Findings from combined a PPS and GHP system and standalone PPS were able to significantly lower levels for all physical, chemical and microbiological water quality parameters, with extremely high removal efficiencies. Results also indicated that the permeable pavement rigs successfully removed microbial pollutants. Extremely high degradation rates for total coliforms, *E.coli*, *Enterococci sp* *Salmonella sp* and *Shingella sp* occurred (> 85 %) throughout the analysis. Despite the relatively high temperatures in the indirectly heated sub-base of the pavement, the potential pathogenic organism *Legionella* was not detected for the two-year study period. Outflow concentrations for all pavement systems met the European Commission Environment Urban Wastewater Treatment Directive (91/271/EEC). These water quality results can be transferred for real case applications on permeable pavement sites to give indications of the performance and ability of PPS to remove and degrade organic urban runoff pollutants.

The effluent concentrations for indoor bins with regards to NH_4-N, PO_4-P, *E.coli*, *Enterococci sp*, total coliforms, *Salmonella sp*, *Shigella sp* and BOD statistically varied to the outdoor bins outflow concentrations ($p < 0.05$). There were no significant differences for PPS integrated with GHP during the heating and cooling cycles for PO_4-P, NO_3-N, TDS, BOD and THB. The presence of the geotextile layer showed significant differences ($p < 0.05$) in outflow concentrations for most water quality parameters with the exceptions of PO_4-P and NH_4-N. Considerable production of carbon dioxide (CO_2) occurred with PPS containing a geotextile layer ($p < 0.05$) when compared to PPS without. Results based on the computed COP and EER for both indoor and outdoor rigs were in the range of 200 to 500 %. This provided evidence of the geothermal heating and cooling applications are well suited within the permeable pavement structure. However, a domestic GHP should be integrated within a PPS car park for assessment and comparison to the water quality and energy and performance obtained in the research.

Furthermore, disinfection was assessed by the application of photocatalytic oxidation with titanium dioxide (TiO_2) to the effluent from the permeable pavements. For supplementary removal and treatment with photocatalytic disinfection, three microbial groups including total coliforms, *E.coli*, and *Enterococci sp.* were used as indices to test the disinfection efficacies. The disinfection results showed the treated stormwater from permeable pavements and photocatalytic oxidation for short irradiation times (<1.5hrs) met the requirements for the United States of America Environmental Protection Agency (US EPA) water recycling guidelines and the World Health Organisation (WHO) guidelines for potable water consumption with regards to microbial contamination and had negligible re-growth of bacteria after 24 hours.

An energy and temperature balance was developed for two experimental geothermal paving systems (combined permeable pavements and ground-source heat pumps). The heat fluxes were analysed for a heating and cooling cycle to determine the thermogeological relationship for the systems. The Runge-Kutta numerical method was developed to model the heat fluxes and energy balance using measured temperature data employing environmental factors such as solar radiation, convection and evaporation heat fluxes for the pavement system. The model showed

its validity and concluded that the Runge-Kutta technique proved to be an effective and reliable predictive tool for the energy and temperature fluxes for combined PPS and GHP systems.

Machine learning techniques such as Artificial Neural Networks (backpropagation feed-forward neural networks and self-organising map (SOM)), successfully predicted NH_4-N, NO_3-N, PO_4-P and BOD (backpropagation), *E.coli*, *Enterococci sp.*, and total coliforms (SOM) and demonstrated an alternative method of analysing water quality performance indicators. The results suggest that cost-effective and easily measurable variables such as dissolved oxygen, total dissolved solids, turbidity, suspended solids, electroconductivity, redox potential, temperature and pH can efficiently predicted nutrient and microbial pollutant concentrations by applying artificial neural network models. The performances of these models are encouraging and support their potential for future use as promising tools for real time optimisation, monitoring and prediction of urban stormwater quality removal within PPS.

The overall outcome of this research is a significant contribution to the development of a novel pavement technology. The research project proves that PPS is one of the most appropriate systems for GHP installation, and does not affect its efficiency in water pollutant removal. The design and construction of PPS integrated with GHP from a laboratory-scaled system has convincingly demonstrated to be a viable solution for meeting the demands for sustainable clean water supply and renewable energy. The sustainable approach with the concept of combined permeable pavements and geothermal heat pumps accomplishes the objectives of reducing runoff which can lead to flooding by overloading stormwater conveyances, providing allowances for the storage of treated stormwater which can be used for irrigation and non-potable purposes (toilet flushing, car washing and garden watering) and applications of domestic hot water with further disinfection and space cooling to nearby buildings. The pollutant retention in the systems was especially investigated with respect to nutrients, sediments and waterborne bacteria. The hybrid paving system (integrated PPS and GHP) and standalone PPS showed their effectiveness for treating highly concentrated urban runoff. The climate in Edinburgh, where the outdoor experiments took place, has highly variable seasons;

nevertheless the water quality performances were not affected. The overall results shows that the combined PPS-GHP and standalone PPS operated well both in environmentally controlled conditions and outdoors, with extremely high removal efficiencies for all water pollutant parameters.

The key conclusions resulting from this study summaries as follows:

(i) The combined systems provided comparable data which can be applied for practical sites for combined GHP and PPS when measuring the energy efficiency regarding the coefficient of performance (COP), energy efficiency ratio (EER).

(ii) PPS and GHPs provide economic and environmental benefits, and combined is an attractive sustainable technology for domestic, commercial and industrial usage. In 2007, legislation in UK requires the use of SUDS from all discharged surface water runoff to the environment (controlled Activity Regulations GBR 10). The Department of Trade and Industry, UK provides grants to assist with the costs of installing GHPs with many other countries (USA, Canada and Japan) supporting GHP installation through rebates, tax incentives and other grants.

(iii) All experimental bins successfully removed nutrients (NO_3-N, NH_3-N, PO_4-P), sediments (turbidity, total dissolved solids and suspended solids), and waterborne bacterial pathogens (*E.coli*, Enterococci sp. *Salmonella sp*. *Shigella sp.,* total coliforms, total heterotrophic bacteria) despite temperature fluctuations caused by the presence of GHP. Water quality parameters for the removal of BOD, COD, sediments, and nutrients met the US EPA guidelines for non-potable water reuse and EU urban wastewater treatment directive. The effluent from the pavement systems can be discharged directly to soils and water sources and do not pose an ecological or environmental health risk to humans or the environment.

(iv) *Legionella* was not detected throughout the period of study; however due to health risks and concerns it is still a critical parameter which must be assessed regarding water heating systems.

(v) CO_2 levels measured for bins with and without geotextiles membranes provide indicators of the high microbiological activities surrounding the geotextile layer and the increased rates of biodegradation; therefore reducing organic pollutant loads in addition to bacterial organisms.

(vi) The decrease in dissolved oxygen levels confirms that the pavement systems role as in-situ aerobic bioreactors significantly reduces high organic levels for BOD, COD and microbes.

(vii) Molecular microbiological analysis by Gram stain showed the high reductions of both Gram-negative and Gram-positive bacteria within the system. However PCR-DNA techniques proved that other microbial pathogenic organisms exists from the effluent of the pavements and the need for further disinfection and treatment of the effluent.

(viii) Statistical analysis (Anova) showed that the presence of geotextiles significantly aids in the removal of all the water pollutants. The integration of GHP showed inconsistencies with the effluent concentrations for certain parameters but its presences did not seem to affect or alter the water treatment processes. Analysis between the indoor and outdoor rigs showed no real significant differences when treating both gully pot liquor and gully pot liquor mixed with dog faeces with removal efficiencies ranging from 70 to 99 % for microbial pollutants.

(ix) Photocatalytic disinfection with titanium dioxide (TiO_2) compared to UV radiation was used as a polishing and further treatment of the effluent from the pavement systems. Photocatalytic oxidation in the presence of TiO_2 proved to be an economic and viable option when further

disinfection of the outflow from PPS is required. The removal and degradation of waterborne bacterial pathogens met the World Health Organisation (WHO) standards for potable water consumption. With this further treatment the recycled water can be used for grey water purposes such as toilet flushing, garden watering, irrigation, streets, pavement and vehicular washing (aesthetic applications).

(x) The 4^{th} order Runge-Kutta method was used to model the energy and temperature balances between two PPS from the outdoor rig. The model was statistically proven for its validity and can be applied as a management tool for monitoring energy transfers, energy consumption and temperatures at the bottom of the pavement system, especially when monitoring pathogenic organisms such as *Legionealla* which is often present within water heating systems.

(xi) Artificial neural networks (Back propagation feed-forward) and self-organising maps (SOM) was applied for the modeling and prediction of water quality parameters. The neural networks demonstrated that these tools can be used for real life applications of permeable pavements for it operations, optimizations and stormwater management. Both backpropagation and SOM uses a 'black box' system whereby more cost-effective, rapid and easier to measure water quality parameters such as temperature, pH, electroconductivity, turbidity, dissolved oxygen and suspended solids can be used to accurately predict nutrients (ammonia-nitrogen, nitrate-nitrogen, phosphates), BOD and waterborne bacterial pathogens. The neural networks is encouraging and has tremendous potential and can be effectively used to support management decisions in real-time.

10.2 Recommendations for future research

Permeable pavements use physical, biological and chemical processes, which receives and treat highly variable inflows of urban stormwater. The findings indicate the great potential and significant implications for future pavement designs regarding stormwater treatment and renewable energy applications for combined PPS and GHPs. The study demonstrated the positive role of permeable pavements and integrated GHPs with permeable pavements. Nevertheless there is need to carry out further investigations. Some essential futuristic research frontiers are as follows:

- A more comprehensive laboratory scale research for permeable pavements involving different aggregates (permavoid boxes of recycled tyres, recycled bricks), two-layered geotextiles PPS structures and alternative porous materials such as asphalt should be conducted to identify permeable paving materials that are suitable for varying geological and applicability conditions and that can retain high concentrations of pollutants.

- Further investigations at laboratory and field scales for pesticides and fertilizers retention and degradation within permeable pavements are required.

- Comprehensive field scale microbiological examinations such as the microbial population dynamics is recommended to quantify bacterial and viral contaminants when compared to laboratory-scaled pavement systems.

- Combination of permeable pavements with photocatalyst titanium dioxide (TiO_2) for further stormwater purification. TiO_2 can be added to the cement mortar of permeable pavement blocks in order to create blocks for diminishing the air polluting effects of nitrous and sulphur oxides by vehicular exhaust. In a more global approach, the application of TiO_2 as an air purifying material can be studied for implementation on urban and sub-urban streets and roads where its antiseptical action oxidises and reduces air

pollutants. The application of TiO_2 within permeable pavements can have a dual decontamination effect on both water and air pollutants.

- Microfluidics and biosensors for microbial pollutants and viruses detection within the permeable pavement systems can be addressed. Microfluidics and biosensors using chips placed within the layers of the pavement structure can analyse the purification stages by measuring automatic changes in patterns of proteins or protein gradients onto a surface whereby bacterial or viral cells can subsequently be cultured to investigate or control their behaviour. This technique can be used as a precise measurement for the rates of aerobic treatment and biodegradation occurring within the pavement.

- A life cycle analysis should be assessed for the combined permeable pavements and geothermal heat pump technology to assess the impacts associated with all stages of raw materials, maintenance, repairs and life expectancy. The life cycle assessment can aid on the environmental social and economic benefits of this novel paving technology.

- Development of appropriate standards and guidelines regarding stormwater treatment and water reuse from best management practices such as SUDS should be implemented. These would aid in the assessment and efficiency for various drainage systems for designers, contractors and public awareness.

References

Abbott, C.L. and Comino-Mateos, L. (2001). In situ performance monitoring of an infiltration drainage system and field testing of current design procedures. *Water and Environment Journal;* 15, 198-202.

Abbott, C.L., and Comino-Mateos, L. (2003). In-situ Hydraulic Performance of a Permeable Pavement Sustainable Urban Drainage System. *Water and Environment Journal;* 17, 187-190.

Abbott, C.L., Weisgerber, A. and Ballard, W.B. (2003). Observed hydraulic benefits of two UK permeable pavement systems. *Proceedings of the Second National Conference on Sustainable Drainage*. (23-24 June 2003) Coventry University, UK.

Acea, M.J. and Alexander, M. (1988). Growth and survival of bacteria introduced into carbon-amended soil. *Soil, Biology and Biochemisty;* 20,703-709.

Affandi, A., and Wantanabe, K. (2007). Daily groundwater level fluctuation forecasting using soft computing technique. *Nature and Science;* 5, 1-9.

Aguilera, P.A., Garrido Frenich, A., Torres, J.A., Castro, H., Martinez Vidal, J.L., and Canton, M. (2001). Application of the kohonen neural network in coastal water management: methodological development for the assessment and prediction of water quality. *Water Research;* 35, 4053-4062.

Ahsan, T. and Alaert, G.J. (1997). Modeling separation of flocculant particles in horizontal-flow gravel bed. *Journal of Environmental Engineering*, 123, 1254-1260.

Alderiso, K., Wait, D. and Sobsey, M. (1996). Detection and characterization of make-specific RNA coliphages in a New York City Reservoir to distinguish between human and nonhuman sources of contamination. *Proceedings of a Symposium on New York City Water Supply Studies*, Herndon-American Water Resources Association.

Alexandri, E., and Jone, P. (2007). Developing a one-dimensional heat and mass transfer algorithm for describing the effect of green roofs on the built environment: Comparison with experimental results. *Building and Environment;* 42, 2835-2849.

Andersen, C.T., Foster, I.D.L. and Pratt, C.J. (1999). The role of urban surfaces (permeable pavements) in regulating drainage and evaporation: development of a laboratory simulation experiment. *Hydrological Processes;* 13, 597-609.

Angelakis, A.N., and Bontoux, L. (2001). Wastewater reclamation and reuse in Eureau countries. *Water Policy;* 3, 47-59.

Argue, J. R. (2004). Water sensitive urban design: Basic procedures for 'Source Control' of stormwater-A handbook for Australian practice, (1st Edn.) Urban Water Resources Centre, University of South Australia, Adelaide, Australia.

Armour, C. L. (1991). *Guidance for Evaluating and Recommending Temperature Regimes to Protect Fish*. US Fish and Wildlife Service, Biological Report, 90(22). Washington DC, USA.

Asaeda, T., Ca, V.T. and Wake, A. (1996). Heat storage of pavement and its effect on the lower atmosphere. *Atmospheric Environment*; 30, 413-427.

Asaeda, T. and Ca, V.T. (2000). Characteristics of permeable pavement during hot summer weather and impact on the thermal environment. *Building and Environment*; 35, 363-375.

ASCE, (2000). American Society of Civil Engineers Task Committee on Application of Artificial Neural Networks in Hydrology-Artificial neural networks in hydrology I: Preliminary Concepts. *Journal of Hydrologic Engineering;* 5, 115–123

ASCE and WEF, (1998). *Urban runoff quality management*. American Society of Civil Engineers (ASCE) Manuals and Report of Engineering Practice No. 87, Reston, VA and Water Environment Federation (WEF), Manual of Practice No. 23, Alexandria, VA, USA.

Ashbolt, N.J., Grabow, W.O.K. and Snozzi, M. (2001). Indicators of microbial water quality [in:] *Guidelines, Standards and Health: Assessment of risk and risk management for water-related infectious disease*; World Health Organisation (WHO); IWA Publishing, London.

ASHRAE, (1993). *Handbook of Fundamentals, American Society of Heating, Refrigeration and Air-Conditioning Engineers*; American Society of Heating, Refrigerating, and Air-Conditioning Engineers, Atlanta, Georgia.

ASHRAE, (1997). *Ground source heat pumps-Design of geothermal systems for commercial and institutional buildings*; American Society of Heating, Refrigerating, and Air-Conditioning Engineers, Atlanta, Georgia.

Astebol, S.O., Hvitved-Jacobson, T. and Simonsen, O. (2004). Sustainable stormwater management at Fornebu, from an airport to an industrial and residential area of the city of Oslo, Norway. *Science of the Total Environment;* 334-335, 239-249.

Atlas, R. M. (1993). *Handbook of Microbiological Media*. CRC Press, Boca Raton, Florida, USA.

Ausland, G., Stevik, T.K., Hanssen, J.F., Kohler, J.C. and Jenssen, P.D. (2002). Intermittent filtration of wastewater-removal of fecal coliforms and fecal streptococci; *Water Research*; 36, 3507–3516.

Balades, J.D., Legret, M., and Madiec, H. (1995). Permeable pavements-pollution management tools. *Water Science and Technology;* 32, 49-56.

Banks, D. (2008). *An Introduction to Thermogeology: Ground Source Heating and Cooling*, Blackwell Publishing Ltd, Oxford, UK.

Bannerman, R.T., Owens, D.W., Dodds, R.B. and Hornewer, N.J. (1993). Sources of Pollution in Wisconsis Stormwater. *Water Science and Technology;* 28, 241-259.

Barrett, M., Kearfott, P. and Malina, J. (2006). Stormwater Quality Benefits of a Porous Friction Course and its Effect on Pollutant Removal by Roadside Shoulders. *Water Environment Research*; 78, 2177-2185.

Bartram, J. and Helmer, R. (1996). *Water quality monitoring-A practical guide to design and implementation of freshwater quality studies and monitoring programmes*. E & RFN Spon, London.

Battiti, R. (1992). First and second-order method for learning between steepest descent and Newton's method. *Neural Computation;* 4, 141-166.

Bean, E.Z., Hunt, W.F., Bidelspach, D.A. (2007). Evaluation of four permeable pavement sites in eastern North Carolina for runoff reduction and water quality impacts. *Journal of Irrigation and Drainage Engineering;* 133, 583-592.

Berbee, R., Rijs, G., de Brouwer, R. and van Velzen, L. (1999). Characterization and treatment of runoff from highways in the Netherlands paved with impervious and pervious asphalt. *Water Environment Research;* 71, 183-190.

Berry, C.T. (1995). *Control of urban runoff through the use of permeable pavements*, PhD thesis, Coventry University.

Bilotta, G.S. and Brazier, R. E. (2008). Understanding the influence of suspended solids on water quality and aquatic biota. *Water Research;* 42, 2849-2861.

Birch, G.F., Fazeli, M.S., and Matthai, C. (2005). Efficiency of an infiltration basin in removing contaminants from urban stormwater. *Environmental Monitoring and Assessment;* 101, 23-38.

Bliss, R.W. (1961). Atmospheric radiation near the surface of the ground. *Solar Energy*; 5, 103-120.

Booth, D.B. and Leavitt, J. (1999). Field evaluation of permeable pavement systems for improved stormwater management. *Journal of the American Planning Association;* 65, 314-325.

Booth, D.B., Leavitt, J. and Peterson, K. (1998). *The University of Washington permeable pavement demonstration project-background and first-year field results.* Seattle, WA, USA.

Boyd, M.J., Buffil, M.C. and Knee, R.M. (1993). Pervious and impervious runoff in urban catchments. *Hydrological Sciences,* 38, 463-478.

Bran and Luebbe, (1999). Bran Luebbe AA3 autoanalyser methods: *G-109-93 and 94.* Norderstedt, Germany.

Brattebo, B.O. and Booth, D.B. (2003). Long-term stormwater quantity and quality performance of permeable pavement systems. *Water Research;* 37, 4369-4376.

Brion, G. M. and Lingireddy, S. (1999). A neural network approach to identifying non-point sources of microbial contamination. *Water Research;* 33, 3099-3106.

British Standards Institution, (1992). *BS 882 Specification for aggregates from natural sources for concrete*. British Standards Institution, London.

Burkhard, R., Deletic, A. and Craig, A. (2000). Techniques for water and wastewater management: a review of techniques and their integration in planning. *Urban Water;* 2, 197-221.

Butler, D., and Davies, J.W. (2004). *Urban drainage* (2nd Edn). Spon Press Taylor and Francis Group, London.

Ca, V.T., and Asaeda, T. (1997). Evaporation at the surface of permeable pavement and its impacts on the urban thermal environment. *Proceedings, Congress of the International Association of Hydraulic Research, IAHR, v A,* Managing Water: Coping with Scarcity and Abundance.

Carr, G. M. and Neary, J.P. (2008).*Water quality for ecosystem and human health*, (2nd Edn.) United Nations Environment Programme Global Environment Monitoring System (GEMS)/Water Programme. Burlington, Ontario, Canada.

Campbell, N., D'Arcy, B., Frost, A., Novotny, V. and Sansom, A. (2004). *Diffuse pollution-an introduction to the problems and solutions*. International Water Association Publishing, London U.K.

Cappuccino, J.G. and N. Sherman, (1996). *Microbiology, a laboratory manual*, (4th Edn.) Rockland Community College, Suffern, New York, USA.

Cengel, Y. A. and Boles, M. A. (2007). *Thermodynamics: An engineering approach* (6th Edn.) McGraw-Hill, New York, USA.

Chapra, S.C. (2005). *Applied Numerical Methods with MATLAB for Engineers and Scientists*, McGraw-Hill, New York, USA.

Charbeneau, R.J. (2000). *Groundwater hydraulics and pollutant transport*. Prentice-Hall, Inc, New Jersey, USA.

CIWEM, (2000). *Diffuse pollution impacts, The environmental and economic impacts of diffuse pollution in the UK*. Chartered Institution of Water and Environmental Management. D'Arcy, B.J., Ellis, J.B., Ferrier, R.C., Jenkins, A. and Dils, R. (ed.).

Chaves, P., and Kojiri, T. (2007). Conceptual fuzzy neural network model for water quality simulation. *Hydrological Processes;* 21, 634-646.

Chiasson, A.D. (1999). *Advances in Modeling of Ground-Source Heat Pump Systems*, MSc thesis, Oklahoma State University, Oklahoma, USA.

Chin, D. (2006). *Water-quality engineering in natural systems*. John Wiley and Sons, Hoboken, New Jersey, USA.

Cho, M., Chung, H., Choi, W. and Yoon, J. (2004). Linear correlation between inactivation of *E. coli* and OH radical concentration in TiO_2 photocatalytic disinfection. *Water Research;* 38, 1069-1077.

CIRIA. (2007). *The SUDS Manual* (C697). CIRIA, London.

CIRIA (2002) *Source control using constructed pervious surfaces* (C582). CIRIA, London.

Clesceri, L.S., Eaton, A.D., Greenberg, A.E. and Franson, M.A.H. (1998). *Standard methods for the examination of water and wastewater*, (20th ed). American Public Health Association, American Water Works Association and Water Environment, Washington, District Council, USA.

Collins, K.A., Lawrence, T.J., Stander, E.K., Jontos, R.J., Kaushal, S.S., Newcomer, A.T., Grimm, N.B. and Cole Ekberg, M.L.C. (2010). Opportunities and challenges for managing nitrogen in urban stormwater: A review and synthesis. *Ecological Engineering;* 36, 1507-1519.

Collins, K.A., Hunt, W.F., and Hathaway, J.M. (2008). Hydrologic comparison of four types of permeable pavement and standard asphalt in Eastern North Carolina. *Journal of Hydrologic Engineering;* 13, 1146-1157.

Cool planet/Mitsubishi Electric (2009) Ground-source renewable energy solutions-Technically advanced highly efficient ground source renewable energy solutions with assured expert installation. Available online at: http://www.cool-planet.co.uk/about/downloads/ [Accessed October 2009].

Coupe, S.J. (2004). *Oil biodegradation and microbial ecology within Permeable Pavement Systems*. PhD thesis. Coventry University.

Coupe, S.J., Charlesworth, S. and Faraj, A.S. (2009). Combining permeable paving with renewable energy devices: Installation, Performance and Future Prospects. *Proceedings of 9th International Conference on Concrete Block Paving (ICCBP)*, Argentinean Concrete Block Association (AABH), Small Element Paving Technologists (SEPT), Buenos Aires, Argentina, 18-21 October, 2009, p. 1-10.

Coupe, S.J., Smith, H.G., Newman, A.P., and Puehmeier, T. (2003). Biodegradation and microbial diversity within permeable pavements. *European Journal of Protistology*; 39, 495-498.

Curtis, R., Lund, J., Sanne, B., Rybac, L. and Hellströ, G. (2005). Ground source heat pumps-geothermal energy for anyone, anywhere: current worldwide activity. *World Geothermal Congress* Antalya, Turkey, 24-29 April 2005.

Datta, A.K. (2002). *Biological and bioenvironmental heat and mass transfer*, Marcel Dekker, Inc, New York, USA.

DayWater, (2003). *Review of the use of stormwater BMPs in Europe*. Adaptive Decision Support System for the Integration of Stormwater Source Control into Sustainable Urban Water Management Strategies, Report 5.1 Project under EU RTD, 5th Framework Programme. (18th August 2003) Middlesex University. Available online at: daywater.enpc.fr/www.daywater.org/REPORT/D5-1.pdf. [Accessed August 2008].

DEFRA, (2007). Funding and charging arrangements for sustainable urban drainage systems. Department for Environment, Food and Rural Affairs (DEFRA), London. Available online at: http://www.defra.gov.uk/environment/quality/water/waterquality/diffuse/non-agri/documents/suds-report.pdf. [Accessed March 2009]

Delatte, N. (2008). Concrete pavement design, construction and performance. Taylor and Francis, Abingdon, Oxon, U.K.

Dempsey, B.A., Tai, Y.L. and Harrison, S.G. (1993). Mobilization and removal of contaminants associated with urban dust and dirt. *Water Science and Technology;* 28, 225-230.

Demuth, H., and Beale, M. (2001). *Neural network toolbox learning for use with MATLAB*, The Math Work Inc, Natick, MA, USA.

Department of National Health and Welfare, (1977). *Microbiological quality of drinking water*. 77-EHD-2, Environmental Health Directorate, Department of National Health and Welfare, Ottawa, Ontario, Canada.

Diefenderfer, B.K., Al-Qadi, I.L. and Diefenderfer, S.D. (2006). Model to predict pavement temperature profile: development and validation. *Journal of Transportation Engineering*; 132, 162-167.

Dierkes, C., Kuhlman, L., Kandasamy, J. and Angelis, G. (2002). Pollution retention capability and maintenance of permeable pavements. In: Strecker, E.W. (ed.) *Proceedings of the 9th International Conference on Urban Drainage* (8-13 September 2002), Portland, USA.

Dieter, H., and Stephan, B.K. (2006), *Heat and mass transfer,* (2nd Edn.) Springer-Verlag Berlin, Heidelberg, Germany.

Duffie, J.A. and Beckman, W.A. (2006). *Solar engineering of thermal processes* (3rd Edn.), John Wiley and Sons, New York, USA.

Dutot, A., Rynkiewicz, J., Steiner, F. E., and Rude, J. (2007). A 24-h forecast of ozone peaks and exceedance levels using neural classifiers and weather predictions. *Environmental Modelling and Software*; 22, 1261-1269.

Edberg, S. C., Rice, E. W., Karlin, R. J., Allen, M. J., (2000). *Escherichia coli*: the best biological drinking water indicator for public health protection. *Journal of Applied Microbiology;* 88, 106S-116S.

Elvidge, C.B. and Raymond, G.P. (1999). Survivability of nonwoven geotextiles on open-graded crushed aggregate. *Geosynthetics International;* 6, 93-117.

Environment Agency, (2007). *A review of the cost benefit of undertaking SUDS retrofit in urban areas*. Environment Agency Science Report-SC060024, Environment Agency, Bristol, U.K.

Environmental Campaigns, (2003). *Dog and animal fouling policy statement*. EnCams, UK. Available from: http://www.encams.org/home/ [Accessed November 2008].

Esen, H., Inalli, M. and Esen, M. (2006). Technoeconomic appraisal of a ground source heat pump system for a heating season in eastern Turkey. *Energy Conversion and Management;* 47, 1281-1297.

Esen, H., Inalli, M., Sengur, A. and Esen, M. (2008). Forecasting of a ground-coupled heat pump performance using neural networks with statistical data weighting pre-processing. *International Journal of Thermal Sciences;* 47, 431-441.

European Commission Environment, (1991). *EU urban wastewater treatment directive 91/271/EEC*. European Communities, Brussels, Belgium. Available online at: http://ec.europa.eu/environment/water/water-urbanwaste/index_en.html.

European Commission Environment, (2006). *EU bathing water directive (2006/7/EC)*. European Communities, Brussels, Belgium. Available online at: http://ec.europa.eu/environment/water/water-bathing/#2006.

Fach, S. and Geiger, W.F. (2005). Effective pollutant retention capacity of permeable pavements for infiltrated road runoffs determined by laboratory tests. *Water Science and Technology;* 51, 37-45.

Ferguson, B.K. (2005). *Porous pavements, integrative studies in water management and land development*. CRC Press, Boca Raton, Florida, USA.

Fernández-Ibáñez, P., Sichel, C., Polo-López, M. I., de Cara-García, M. and Tello, J. C. (2009). Photocatalytic disinfection of natural well water contaminated by

fusarium solani using TiO_2 slurry in solar CPC photo-reactors. *Catalysis Today;* 144, 62–68.

Fletcher, M. (1977). Effects of culture concentration and age, time, and temperature on bacterial attachment to polystyrene. *Canadian Journal of Microbiology;* 23, 1–6.

Freeze, R.A. and Cherry, J.A. (1979). *Groundwater*. Prentice Hall, Inc. Englewood Cliffs, New Jersey, USA.

Fujishima, A., Rao, T. N. and Tryk, A. D. (2000). Titanium dioxide photocatalysis. *Journal of Photochemistry and Photobiology C: Photochemistry;* 1, 1-21.

García, H.L. and González, I.M. (2004). Self-organizing map and clustering for wastewater treatment monitoring. *Engineering applications of artificial intelligence*; 17(3), 215-225.

Geothermal International, (2010). *Ground Source Heat Pumps*. Available online at: http://www.geothermalint.co.uk/ground-source-heat-pumps/. [Accessed on June 2010]

Gerardi, M.H. and Zimmerman, M.C. (2005). *Wastewater pathogens*. Hoboken Wiley-Interscience, New Jersey, USA.

Gerrits, C. and James, W. (2002). Restoration of infiltration capacity of permeable pavers. *Proceedings of the 9th International Conference on Urban Drainage* (8-13 September 2002), Portland, USA.

Gevrey, M., Rimet, F., Park, Y.S., Giraudel, J.L., Ector, L. and Lek, S. (2004). Water quality assessment using diatom assemblages and advanced modelling techniques. *Freshwater Biology*; 49, 208-220.

Gromaire-Mertz, M.C., Garnaud, S., Gonzalez, A., and Chebbo, G. (1999). Characterisation of urban runoff pollution in Paris. *Water Science and Technology;* 39, 1-8.

Grzechulska, J., Hamerski, M. and Morawski, A. W. (2000). Photocatalytic decomposition of oil in water. *Water Research;* 34, 1638-1644.

Hanova, J and H Dowlatabadi, H. (2007). Strategic GHG reduction through the use of ground source heat pump technology. *Environmental Research Letters;* 2, 044001.

Hanson Formpave, (2009). Stormwater source control system. Aquaflow permeable paving leaflet. Available online at: http://www.formpave.co.uk [Accessed May 2009]

Haykin, S. S. (1999). *Neural networks: a comprehensive foundation*, Prentice Hall, Upper Saddle River, New Jersey, USA.

Healy, P.F. and Ugursal, V.I. (1997). Performance and economic feasibility of ground source heat pumps in cold climate. *International Journal of Energy Research;* 21, 857-870.

Hedmark, Å., Zhang, L., Scholz, M., Aronsson, P. and Elowson, T. (2009). Self-organizing map analysis of planted soil infiltration systems for treatment of log yard runoff. *Forest Science*; 55, 183-188.

Hepbasli, A., 2005. Thermodynamic analysis of a ground-source heat pump system for district heating. *International Journal of Energy Research;* 29, 671-687.

Hepbasli, A. and Akdemir, O., 2004. Energy and exergy analysis of a ground source (geothermal) heat pump system. *Energy Conversion and Management;* 45, 737-753.

Hepbasli, A., Akdemir, O. and Hancioglu, E., 2003. Experimental study of a closed loop vertical ground source heat pump system. *Energy Conversion and Management;* 44, 527-548.

Herb, W.R., Janke, B., Mohseni, O., Stefan, H.G. (2008). Ground surface temperature simulation for different land covers. *Journal of Hydrology;* 356, 327-343.

Hermansson, Å. (2001). Mathematical model for calculation of pavement temperatures: comparison of calculated and measured temperatures. *Journal of the Transportation Research Board*; 1764, 180-188.

Hermansson Å. (2004). Mathematical model for paved surface summer and winter temperature: comparison of calculated and measured temperatures. *Cold Regions Science and Technology;* 40, 1-17.

Herrera Melián, J. A., Doña Rodríguez, J. M., Viera Suárez, A., Tello Rendón, E., Valdés do Campo, C., Arana, J. and Pérez Peña, J. (2000). The photocatalytic disinfection of urban wastewaters. *Chemosphere*; 41, 323–327.

Herrmann, J.M. (2005) Heterogeneous photocatalysis: state of the art and present applications. *Topics in Catalysis;* 34, 49–65.

Highways Agency, (2009). *Road Pavements, Unbound Cement and Other Hydraulically Bound Mixtures*. Manual of Contract Documents for Highway Works Series 800, Volume 1. Specification for Highway works. Available online: http://www.standardsforhighways.co.uk/mchw, [Accessed July 2009].

Hsu, K. L., Gupta, H. V. and Sorroshian, S. (1995). Artificial neural network modeling of the rainfall-runoff process. *Water Resources Research;* 31(10), 2517–2530.

Huang, Y.H. (2004). *Pavement analysis and design*, (2nd Edn). Upper Saddle River, Prentice Hall, New Jersey, USA.

Hunt, B., Stevens, S. and Mayes, D. (2002). Permeable pavement use and research at two sites in
Eastern North Carolina, *Proceedings of the 9th International Conference on Urban Drainage*, Global Solutions for Urban Drainage, ASCE, Portland, Oregon, USA.

Hunter, P.R. (1997). *Waterborne diseases.* Wiley, Chester, UK.

Incropera, F.P., DeWitt, D.P., Bergman, T.L. and Lavine, A.S. (2007). *Fundamentals of heat and mass transfer*, John Wiley and Sons Inc. Hoboken, New Jersey, USA.

Inalli, M. and Esen, H. (2004). Experimental thermal performance evaluation of a horizontal ground-source heat pump system. *Applied Thermal Engineering;* 24, 2219-2232.

International Energy Agency, (2006). *World Energy Outlook*. The International Energy Agency (IEA). Available online at http://www.iea.org. [Accessed September 2009].

Interpave, (2010). *Guide to the design, construction and maintenance of concrete block permeable pavements* (6th Edn.) Interpave, Leicester, U.K. Available online at: www.paving.org.uk. [Accessed April 2010].

Interpave/Scott Wilson, (2006). *The costs of paving-comparative initial and whole of life costs for pavements*. Interpave, London, UK.

Ioannides, A.M., Thompson, M.R., and Barenberg, E.J. (1985). The Westergaard solutions reconsidered. *Journal of the Transportation Research Board*; 1043, 13-23.

James, W. and Shahin, R. (1998). Pollutants leached from pavements by acid rain. In: James, W.(ed.), *Advances in Modeling the Management of Stormwater Impacts.* 6, 321-349. Computational Hydraulics International, Guelph, Canada.

James, W. and von Langsdorff, H. (2003). The use of permeable concrete block pavement in controlling environmental stressors in urban areas. In*: Proceedings of the 7th International Conference on Concrete Block Paving PAVE AFRICA*, 12–15 October, 2003. Sun City, South Africa.

Kadurupokune, N. and Jayasuriya, N. (2009). Pollutant load removal efficiency of pervious pavements: is clogging an issue? *Water Science and Technology;* 60, 1787-1794.

Kalteh, A.M., Hjorth, P., and Berndtsson, R. (2008). Review of the self-organizing map (SOM) approach in water resources: analysis, modelling and application. *Environmental Modelling and Software;* 23, 835-845.

Karasawa, A., Toriiminami, K., Ezumi, N. and Kamaya, K. (2006). Evaluation of performance of water retentive concrete block pavements. *Proceedings of the 8th International Conference on Concrete Block Paving*, *Sustainable Paving for Our Future.* ICPI, San Francisco, CA, USA.

Kashefipour, S.M., Lin, B., and Falconer, R.A. (2005). Neural networks for predicting seawater bacterial levels. *Water Management*, 158, 111-118.

Kazemi Yazdi, S. and Scholz, M. (2008). Combined bio-filtration, water detention and infiltration system treating road runoff. *Proceedings of the 10th British Hydrological Society Symposium*, (15-18 September 2008), Sustainable Hydrology for the 21st Century. Exeter, UK.

Kiely, G. (1997). *Environmental Engineering*. McGraw Hill London.

Kim, R.H., Jinwoo, J., Lee., S. and Gee, C.S. (2006). Estimation of environment-friendly permeable pavement at laboratory test. *Materials Science Forum;* 510-511, 914-917.

Koerner, G.R., Koerner, R.M., and Martin, J.P. (1994). Geotextile filters used for leachate collection systems. *Journal of Geotechnical Engineering;* 120, 1792–1803.

Kohonen, T. (2001). *Self-Organizing Maps*, (3rd Edn). Springer-Verlag Inc, New Jersey, USA.

Kohonen, T., Oja, E., Simula, O., Visa, A. and Kangas, J. (1996). Engineering applications of the self-organizing map. *Proceedings of the IEEE;* 84, 1358-1384.

Koizumi, H., Nakadai, T., Usami, Y., Satoh, M., Shiyomi, M. and Oikawa, T. (1991). Effect of carbon dioxide concentration on microbial respiration in soil. *Ecological Research;* 6, 227-232.

Korkut, E.N. (2003). *Geotextiles as biofilm attachment baffles for wastewater treatment*. Ph.D. Thesis, Drexel University.

Kriger, C. and Tzoneva, R. (2007). Neural networks for prediction of wastewater treatment plant influent disturbances. *Proceedings of the 8th Institute of Electrical and Electronics Engineers, IEEE AFRICON Conference*, 26 -28 September *2007,* Windhoek, Namibia.

Lamoureux , J., Tiersch , T.R. and Hall, S.G. (2006). Pond heat and temperature regulation (PHATR): Modeling temperature and energy balances in earthen outdoor aquaculture ponds. *Aquacultural Engineering;* 34, 103-116.

Lebcir, L. (1992). *Factors controlling the performance of horizontal flow roughing filters*. PhD thesis, Newcastle University.

Leclerc, H., Mossel, D.A.A., Edberg, S.C. and Struijk, C.B. (2001). Advances in the bacteriology of the coliform group: their suitability as markers of microbial water safety. *Annual Review of Microbiology;* 55, 201-234.

Lee, B.H. and Scholz, M. (2006a). Application of the self-organizing map (SOM) to assess the heavy metal removal performance in experimental constructed wetlands. *Water Research*, 40, 3367-3374.

Lee, B.H. and Scholz, M. (2006b). A comparative study: prediction of constructed treatment wetland performance with k-nearest neighbors and neural networks. *Water, Air and Soil Pollution;* 174, 279-301.

Lee, H., Swamikannu, X., Radulescu, D., Kim, S., and Stenstrom, M.K. (2007). Design of stormwater monitoring programs. *Water Research;* 41, 4186-4196.

Legret, M., Colandini, V. and Lemarc, C. (1996). Effects of a porous pavement with reservoir structure on the quality of runoff water and soil. *Science of the Total Environment;* 190, 335-340.

Legret, M. and Colandini,V. (1999). Effects of a porous pavement with reservoir structure on runoff water: water quality and fate of heavy metals, *Water Science and Technology;* 39, 111-117.

Lek, S. and Guégan, J. F. (1999). Artificial neural networks as a tool in ecological modelling, an introduction. *Ecological Modelling;* 120, 65-73.

Line, D.E., White, N.M., Osmond, D.L., Jennings, G.D. and Mojonnier, C.B. (2002). Pollutant export from various land uses in the upper Neuse river basin. *Water Environment Research;* 74, 100-108.

Ling, H.I., Tatsuoka, F. and Wu, J.T.H. (1993). Hydraulic conductivity of geotextiles under typical operational conditions. *Geotextiles and Geomembranes*; 12, 509-542.

Lingireddy, S. and Brion, G. M. (2005). *Artificial neural networks in water supply engineering*, American Society of Civil Engineers, Reston, VA, USA.

Lonnen, J., Kilvington, S., Kehoe, S. C., Al-Touati, F. and McGuigan, K. G. (2005) Solar and Photocatalytic Disinfection of Protozoan, Fungal, and Bacterial Microbes in Drinking Water. *Water Research;* 39, 877–883.

Lund, J.W., Sanner, B., Rybach, R., Curtis, R. and Hellström, G. (2004). Geothermal (ground-source) heat pumps -A world overview. *Geo-Heat Center (GHC) Quarterly Bulletin,* 25.

Lund, J.W., Freeston, D.H. and Boyd, T.L. (2005). Direct application of geothermal energy: 2005 Worldwide review. *Geothermics;* 34, 691-727.

Mac Berthouex, P. and Brown, L.C. (2002). *Statistics for environmental engineers*, Lewis Publishers, Boca Raton, Florida, USA.

Macdonald, K. and Jefferies, C. (2001). Performance of sustainable urban drainage systems for urban runoff. *Proceedings of the 1st National Conference on Sustainable Drainage*, Coventry University, U.K.

Mackay, D. J. C. (1992). Bayesian interpolation. *Neural Computation;* 4, 415-447.

Madge, B., Selvakumar, A., Field, R. and Sullivan, D. (2004). *The use of best management practices (BMPs) in urban watersheds*. EPA/600/R-04/184. United States Environmental Protection Agency, Cincinnati, Ohio, USA.

Maier, H. R. and Dandy, G. C. (1996). The use of artificial neural networks for the prediction of water quality parameters. *Water Resources Research;* 32, 1013-1022.

Maier, H. R. and Dandy, G. C. (2000). Neural networks for the prediction and forecasting of water resources variables: a review of modeling issues and applications. *Environmental Modelling Software;* 15, 101-124.

Maier, R. M., Pepper, I. L. and Gerba, C.P. (2000). *Environmental Microbiology*. Academic Press, San Diego, California, USA.

Mallick, R. B. and El-Korchi, T. (2009). *Pavement Engineering: Principles and Practice.* CRC Press, Boca Raton, Florida, USA.

Marre, R., Kwaik, Y.A., Bartlett, C., Cianciott, N. P., Fields, B. S., Frosch, M., Hacker, J. and Lück, P.C. (2002). *Legionella*. American Society for Microbiology (ASM) Press. Washington DC, USA.

Mat Isa, N. A., Hashim, F. R., Mei, F. W., Ramli, D. A., Wan Omar, W. M. and Zamli, K. Z. (2006). Predicting quality of river's water based on algae composition using artificial neural network. *Proceedings of the 4th Institute of Electrical and Electronics Engineers IEEE International Conference on Industrial Informatics*, Singapore.

Mays, L.W. (2004). *Urban stormwater management*. McGraw-Hill, New York, USA.

McCaig, A.E., Ann Glover, L., and Prosser, J. I. (2001). Numerical analysis of grassland bacterial community structure under different land management regimens by using 16S ribosomal DNA sequence data and denaturing gradient gel electrophoresis banding patterns. *Applied and Environmental Microbiology;* 67, 4554-4559.

Mengelkamp, H.T., Warrach, K. and Rascke, E. (1999). SEWAB - a parameterization of the surface energy and water balance for atmospheric and hydrologic models. *Advances in Water Resources;* 23, 165-175.

Memon, F.A. and Butler, D. (2002). Assessment of gully pot management strategies for runoff quality control using a dynamic model. *Science of the Total Environment;* 295, 115-129.

Metcalf and Eddy, (2007). *Water Reuse, issues, technologies and applications In:* Aecom., Asano, T., Burton, F.L., Leverenz, H.L., Tsuchihashi, R., and G. Tchobanoglous, G. McGraw Hill, New York, USA.

Milkovič M., Carbajo, A. E. and Rubel, D. (2009). Spatial distribution of canine faeces in Buenos Aires suburbs: implications for public health. *Area* 41, 310-318.

Mukherjee, A., (1997). Self-organizing neural network for identification of natural models. *Journal of Computing in Civil Engineering*, 11, 74-77.

Muyzer, G., Waal, E.C.D. and Uitterlinden, A.G. (1993). Profiling of complex microbial populations by denaturing gradient gel electrophoresis analysis of polymerase chain reaction-amplified genes coding for 16S rRNA. *Applied and Environmental Microbiology;* 59, 695-700.

Myers, B.R., Beecham, S., van Leeuwen, J.A., and Keegan, A. (2009). Depeletion of E.coli in permeable pavement mineral aggregate storage and reuse systems. *Water Science and Technology;* 60, 3091-3099.

Najah, A., Elshafie, A., Karim, O. A. and Jaffar, O. (2009). Prediction of Johor River water quality parameters using artificial neural networks. *European Journal of Scientific Research;* 28, 422-435.

National Research Council, (2004). *Indicators for waterborne pathogens*. National Academic Press, Washington DC. USA.

NCBI, (2008). National Centre for Biotechnology Information. Available online at: http://www.ncbi.nlm.nih.gov [Accessed on September 2008].

Neelakantan, T. R., Brion, G. M. and Lingireddy, S. (2001). Neural network modelling of Cryptosporidium and Giardia concentrations in the Delaware River, USA. *Water Science and Technology;* 43, 125-132.

Neelakantan, T. R., Brion, G. M. and Lingireddy, S. (2002). Effectiveness of different artificial neural network training algorithms in predicting protozoa risks in surface waters. *Journal of Environmental Engineering;* 128, 533-542.

Newman, A.P. (2003). Geotextile bags for the containment, filtering and decontamination of slurries. *In*: Dixon, N., Smith, D.M., Greenwood, J.R. and Jones, D.R.V. (ed.) *Geosynthetics: Protecting the environment*, 65-72, Thomas Telford Publishers, Coventry, U.K.

Newman, A.P., Pratt, C.J., Coupe, S.J. and Cresswell, N. (2002). Oil bio-degradation in permeable pavements by microbial communities. *Water Science Technology*; 45, 51-56.

Newton, D.B. (2005). *The effectiveness of modular porous pavement as a stormwater treatment device*. PhD thesis. Griffith University.

Nicol, G.W., Tscherko, D., Martin Embley, T. and Prosser, J.I. (2005). Primary succession of soil *Crenarchaeota* across a receding glacier foreland. *Environmental Microbiology;* 7, 337–347.

Niemczynowicz, J. (1990). Swedish way to stormwater enhancement by source control. *In:* Torno, H.C. (ed.), *Urban stormwater quality enhancement: source control, retrofitting and combined sewer technology, Proceedings of an Engineering Foundation Conference*, American Society of Civil Engineers, New York, USA.

Nkwonta, O.I. and Ochieng, G.M. (2010). Total dissolved solids removal in wastewater using roughing filters. *Chemical Sciences Journal;* CSJ-6, 1-6.

Ochsner, K. (2007). *Geothermal heat pumps: A guide to planning and installing*. Earthscan, London, U.K.

Olivieri, V.P., Kruse, C. W. and Kawata K. (1977). *Microorganisms in urban stormwater*. US Environmental Protection Agency, Washington DC, USA.

Omer, A.M. (2008). Ground-source heat pumps systems and applications. *Renewable and Sustainable Energy Reviews;* 12, 344-371.

Omoto, S., Yoshida, T. and Hata S. (2003). Full-scale durability evaluation testing of interlocking block pavement with geotextileed. *Proceedings of the 7th International Conference on Concrete Block Paving (PAVE AFRICA, 12-15/10/2003)*, Sun City, South Africa.

Pagotto, C., Legret, M. and Le Cloirec, P. (2000). Comparison of the hydraulic behaviour and the quality of highway runoff water according to the type of pavement. *Water Research;* 34, 4446-4454.

Parliamentary Office of Science and Technology U.K. (2010) *Postnote Renewable Heating*, No. 353. Available online: http://www.parliament.uk/documents/documents/upload/postpn353.pdf. [Accessed July 2010].

Pearlstine, S. (2010). *Water: catch it if you can: A simple guide to saving, storing and reusing water*. Author-House, Bloomington, Indiana, USA.

Peavy, H.S., Rowe, D.R. and Tchobanoglous, G. (1985). *Environmental Engineering.* McGraw-Hill Publishing Company, New York, USA.

Penn, B.S. (2005).Using self-organizing maps to visualize high-dimensional data. *Computers and Geosciences;* 31, 531-544.

Perez, F.L. (2000). The influence of surface volcaniclastic layers from Haleakale (Maui, Hawaii) on soil water conservation. *Catena;* 38, 301-332.

Phetteplace, G. (2007). Geothermal heat pumps. *Journal of Energy Engineering*; *133*, 32-38.

Pigram, G. M. and MacDonald, T. R. (2001). Use of neural network models to predict industrial bioreactor effluent. *Environmental Science and Technology;* 35, 157–162.

Pond, K. (2005). *Water recreation and disease: plausibility of associated infections: acute effects, sequelae and mortality*. IWA publishing, London, UK.

Pratt, C.J. (1999). Use of permeable, reservoir pavement constructions for storm water treatment and storage for reuse. *Water Science and Technology;* 39, 145–151.

Pratt, C.J., Mantle, J.D.G. and Schofield, P.A. (1989). Urban stormwater reduction and quality improvement through the use of permeable pavements. *Water Science and Technology;* 21, 769-778.

Pratt, C.J., Mantle, J.D.G. and Schofield, P.A. (1995). UK research into the performance of permeable pavement, reservoir structures in controlling stormwater discharge quantity and quality. *Water Science and Technology;* 32, 63-69.

Pratt, C.J., Newman, A.P. and Bond, P.C., 1999. Mineral oil biodegradation within a permeable pavement: Long term observations. *Water Science and Technology,* 39, 103-109.

Raimbault, G. (1997). French developments in reservoir structures, *In:* Rowney, A.C., Stahre, P. and Roesner, L.A. (ed.), *Sustaining urban water resources in the 21st century: proceedings of the American Society of Civil Engineers,* September 7-12, 1997, Malmo, Sweden.

Rawlings, R.H.D and Sykulski, J.R. (1999).Ground source heat pumps: A technology review. *Building Service Engineering Research and Technology;* 20(3), 119-129.

Reeves, R.L., Grant, S.B., Mrse, R.D., Copil Oancea, C.M., Sanders, B.F. and Boehm, A.B. (2004). Scaling and management of fecal indicator bacteria in runoff from a coastal urban watershed in Southern California*. Environmental Science and Technology;* 38, 2637-2648.

Rincón, A. G. and Pulgarin, C. (2003) Photocatalytical inactivation of *E. coli*: Effect of (continuous-intermittent) light intensity and of (suspended-fixed) TiO_2 concentration. *Applied Catalysis B: Environmental;* 44, 263–284.

Rushton, B.T. (2001). Low-impact parking lot design reduces runoff and pollutant loads. *Journal of Water Resources Planning and Management;* 127, 172-179.

Rustum, R. and Adeloye, A.J. (2007). Replacing outliers and missing values from activated sludge data using kohonen self-organizing map. *Journal of Environmental Engineering;* 133, 909-916.

Rustum, R., Adeloye, A.J. and Scholz, M. (2008). Applying kohonen self-organizing map as a software sensor to predict biochemical oxygen demand. *Water Environment Research;* 80, 32-40.

Salih, F. M. (2002). Enhancement of solar inactivation of *Escherichia coli* by titanium dioxide photocatalytic oxidation. *Journal of Applied Microbiology;* 92, 920–926.

Sambrook, J., Fritsch, E.F. and Maniatis, T. (2000). *Molecular Cloning: A Laboratory Manual*. Cold Spring Harbor Laboratory Press, Cold Spring Harbor, New York, USA.

Sanner, B., Karytsas, C., Mendrinos, D. and Rybach, L. (2003). Current status of ground source heat pumps and underground thermal energy storage. *Geothermics;* 32, 579-588.

Sansalone, J.J. (1999). Adsorptive infiltration of metals in urban drainage-media characteristics. *Science of the Total Environment;* 235, 179-188.

Schlink, U., Dorling, S., Pelikan, E., Nunnari, G., Cawley, G., Junninen, H., Greig, A., Foxall, R., Ebeb, K., Chatterton, T., Vondracek, J., Richter, M., Dostal, M., Bertucco, L., Kolehmainen, M. and Doyle, M. (2003). A rigorous inter-comparison of ground-level ozone predictions. *Atmospheric Environment;* 37, 3237–3253.

Scholz, M. (2006 a) *Wetland systems to control urban runoff.* Elsevier, Amsterdam, Holland.

Scholz, M., (2006 b). Practical sustainable urban drainage system decision support tools. *Engineering Sustainability;* 159, 117-125.

Scholz, M. (2008). Classification of flood retention basins: the Kaiserstuhl case study. *Environmental and Engineering Geoscience*; 14, 61-80.

Scholz, M. and Grabowiecki, P. (2007). Review of permeable pavement systems. *Building and Environment;* 42, 3830-3836.

Scholz, M. and Grabowiecki, P. (2009). Combined permeable pavement and ground source heat pump system to treat urban runoff. *Journal of Chemical Technology and Biotechnology;* 84, 405-413.

Schueler, T.R. (1987). *Controlling urban runoff: A practical manual for planning and designing urban BMPs*. Washington Metropolitan Water Resources Planning Board, Washington DC, USA.

SEPA, (1997). *Urban best management practice database*. Technical Report EQI, 17 December 1997, Scottish Environment Protection Agency, East Region, Edinburgh, Scotland.

SEPA, (2005). *Drainage assessment. A guide for Scotland.* Scottish Environment Protection Agency,Corporate Office, Stirling, Scotland.

Shannon, M. A., Bohn, P. W., Elimelech, M., Georgiadis, J. D., Marinãs, B. J. and Mayes, A. M. (2008). Science and technology for water purification in the coming decades. *Nature;* 452, 301–310.

Sigee, D.C. (2005). *Freshwater microbiology-biodiversity and dynamic interactions of microorganism in the aquatic environment*. John Wiley and Sons, Chichester, West Sussex, England.

Singhal, N., Elefsiniotis, T., Weeraratne, N. and Johnson, A. (2008). Sediment retention by alternative filtration media configurations in stormwater treatment. *Water, Air and Soil Pollution;* 187, 173–180.

Smith, M.S., Thomas, G.W., White, R.E., Ritonga, D. (1985). Transport of *E. coli* through intact and disturbed columns. *Journal of Environmental Quality;* 14, 87–91.

Soares, E. T., Lansarin, M. A. and Moro, C. C. (2007). A study of process variables for the photocatalytic degradation of Rhodamine B. *Brazilian Journal of Chemical Engineering;* 24, 29–36.

Spicer, W.J. (2008). *Clinical microbiology and infectious diseases* (2nd Edn). Elsevier, Philadelphia, PA USA.

Spicer, G.E., Lynch, D.E., Newman, A.P. and Coupe, S.J. (2006). The development of geotextiles incorporating slow-release phosphate beads for the maintenance of oil degrading bacteria in permeable pavements. *Water Science and Technology;* 54, 273-280.

Stevik, T.K., Aa, K., Ausland, G. and Hanssen, J.F. (2004). Retention and removal of pathogenic bacteria in wastewater percolating through porous media: a review. *Water Research;* 38, 1355-1367.

Strugholtz, S., Panglisch, S., Gebhardt, J. and Gimbel, R. (2008). Neural networks and genetic algorithms in membrane technology modeling. *Journal of Water Supply: Research and Technology-AQUA;* 57, 23–34.

Taebi, A. and Droste, R.L. (2004). Pollution loads in urban runoff and sanitary wastewater. *Science of the Total Environment;* 327, 175–184.

Tamura, K., Dudley, J., Nei, M. and Kumar, S. (2007). MEGA4: Molecular evolutionary genetics analysis (MEGA) software version 4.0. *Molecular Biology and Evolution;* 24, 1596-1599.

Taghizadeh, M. M., Torabian, A., Borghei, M. and Hassani, A.H. (2007). Feasibility study of water purification using vertical porous concrete filter. *International Journal of Environmental Science and Technology;* 4, 505-512.

Tate, R. L. (1978). Cultural and environmental factors affecting the longevity of *E. coli* in histosoils. *Applied and Environmental Microbiology;* 35, 925-929.

Tay, J. H. and Zhang, X. (1999). Neural fuzzy modeling of anaerobic biological wastewater treatment systems. *Journal of Environmental Engineering;* 125, 1149–1159.

TecEco, (2009). Sustainable drainage technologies with permecocrete pervious concrete. Available online at: http://www.tececo.com.au/products.permecocrete.php. [Accessed on August 2009].

Tejedor, J. M. T., Gonzalez, M. M., Pita, M. L., Lupiola, G. P. and Martin B. J. L. (2001). Identification and antibiotic resistance of faecal enterococci isolated from water samples. *International Journal of Hygiene and Environmental Health;* 203, 363-368.

Tosun, İ.(2007). *Modeling in transport phenomena: a conceptual approach*. Elsevier, Amsterdam, The Netherlands.

Tota-Maharaj, K. and Scholz, M. (2010). Efficiency of permeable pavement systems for the removal of urban runoff pollutants under varying environmental conditions. *Environmental Progress and Sustainable Energy;* 29, 358-369.

Tran, L. T., Knight, C.G., O'Neill, R. V., Smith, E. R. and O'Connell, M. (2003). Self-organizing maps for integrated environmental assessment of the mid-atlantic region. *Environmental Management;* 31, 822-835.

Tyler, D. (2007). *Fecal Coliform TMDL for Eau Gallie River* (WBID 3082). Florida Department of Environmental Protection-Division of Water Resource Management, Bureau of Watershed Management, Tallahassee, Florida, USA.

US DOE, (1999). *Geothermal Heat Pumps Make Sense for Homeowners* Office of Geothermal Technologies, National Renewable Energy Laboratory DOE/GO-10098-651, United States Department of Energy, Washington DC, USA.

US DOE, (2001). *Ground-Source Heat Pumps applied to Federal Facilities.* United States Department of Energy, Washington DC, USA.

US EPA, (1993). *Handbook-urban runoff pollution prevention and control planning*. United States Environmental Protection Agency, EPA/625/R-93/004, Washington DC, USA.

US EPA, (1999 a). *Stormwater technology fact sheet - porous pavement*. EPA 832-F-99-023, Office of Water, United States Environmental Protection Agency, Washington D.C. U.S.

US EPA, (1999 b). *Guideline for developing an ozone forecasting program*, Office of Air Quality Planning and Standards, United States Environmental Protection Agency, Research Triangle Park, Durham, NC, USA.

US EPA, (2002). *Urban stormwater BMP performance monitoring: A guidance manual for meeting the national stormwater BMP database requirements*. EPA-821-b-01-001. United Stated Environment Protection Agency, Washington DC, USA.

US EPA, (2003). *Protecting water quality from urban runoff*. EPA 841-F-03-003. United Stated Environmental Protection Agency, Washington DC, USA.Available online: http://www.epa.gov/npdes/pubs/nps_urban-facts_final.pdf [Accessed October 2008].

US EPA, (2004 a) *Primer for municipal wastewater treatment systems*. 832-R-04-001. EPA/832/R-04/001, United States Environmental Protection Agency, Washington, DC, USA.

US EPA. (2004 b). *Guidelines for water reuse*, EPA/625/R-04/108. United States Environmental Protection Agency, Washington, DC, USA.

Valavala, S., Montes, F., and Haselbach, L. M. (2006). Area-rated rational coefficients for Portland cement pervious concrete pavement. *Journal of Hydrologic Engineering,* 11, 257-260.

Van Buren, M.A., Watt, W.E., Marsalek, J., Anderson, B.C. (2000). Thermal enhancement of stormwater runoff by paved surfaces. *Water Resources;* 34, 1359–1371.

van Der Wel, B. (1995). Dog pollution. *The Magazine of the Hydrological Society of South Australia.* 2, 1.

Vesanto, J., Himberge, J., Alhoniemi, E. and Parhankangas, J. (2000). Self-organizing map (SOM) toolbox for Matlab 5, report no. A57, Helsinki University of Technology, Laboratory of Computer and Information Sciences, Helsinki, Finland. Available online at: http://www.cis.hut.fi/projects/somtoolbox/ [Accessed: January 10, 2010].

Wang, Y. and Hong, C. (1999) Effect of Hydrogen Peroxide, Periodate and Persulfate on Photocatalysis of 2-Chlorobiphenyl in Aqueous TiO_2 Suspensions. *Water Research;* 33, 2031-2036.

Wang, D. and Lu, W. Z. (2006). Forecasting of ozone level in the time series using MLP model with a novel hybrid training algorithm. *Atmospheric Environment;* 40, 913-924.

Wark, K., 1999. *Advanced Thermodynamics for Engineers*: McGraw-Hill Education, Maidenhead, Berkshire, UK.

Water Furnace. (2008). *Earth loop designs*. Available from:http://www.waterfurnace.com/content [Accessed March 2008].

Watts, R. J., Kong, S., Orr, M. P., Miller, G. C. and Henry, B. E. (1995) Photocatalytic Inactivation of Coliform Bacteria and Viruses in Secondary Wastewater Effluent. *Water Research;* 29, 95–100.

Weiner, E.R. (2008). *Applications of environmental aquatic chemistry: A practical guide.* (2nd edn). CRC Press, Boca Raton, Florida, USA.

Weisburgh, W.G., Brans, S.M., Pelletier,D.A. and Lane, D.J. (1991). 16S Ribosomal DNA amplification for phylogenetic study. *Journal of Bacteriology;* 73, 697-703.

Westergaard, H.M.S. (1926). Computation of stresses in concrete roads. *Journal of the Transportation Research Board;* 5, 90-112.

Wong, N.H. and Chen, Y. (2009). *Tropical urban heat islands: climate, buildings and greenery*. Taylor and Francis, Abingdon, Oxon, U.K.

World Bank, (2010). *World bank development report, development and climate change*. Washington DC, USA.

Wilson, M. (2002). *Laboratory study of entrapment and transport of particulates through permeable pavers*. MEng report, University of Guelph.

Wilson, S., Newman, A.P., Puehmeier, T. and Shuttleworth, A. (2003). Performance of an oil interceptor incorporated into a pervious pavement. *Engineering Sustainability;* 156, 51-58.

Wist, J., Sanabria, J., Dierolf, C., Torres, W. and Pulgarin, C. (2002) Evaluation of photocatalytic disinfection of crude water for drinking-water production. *Journal of Photochemistry and Photobiology A: Chemistry;* 147, 241–246.

WHO, (2010). *World Health Organisation Initiative for Vaccine Research-Bacterial Infections.* Available online at:
http://www.who.int/vaccine_research/diseases/soa_bacterial/en/index.html. [Accessed March, 2010].

WHO, (2004). *World Health Organisation Guidelines for Drinking-water Quality: Recommendations*, (3rd Edn.), Volume 1, Geneva, Switzerland.

Yabunaka, K., Hosomi, M., and Murakami, A. (1997). Novel application of a back-propagation neural network model formulated to predict algal bloom. *Water Science and Technology;* 36, 89–97.

Yang, Z. P., Lu, W. X., Long, Y. Q. and Li, P. (2009). Application and comparison of two prediction models for groundwater levels: a case study in Western Jilin Province, China. *Journal of Arid Environments;* 73, 487-497.

Yeon, I. S, Jun, K. W. and Lee, H. J. (2009). The improvement of total organic carbon forecasting using neural network discharge model. *Environmental Technology;* 30, 45–55.

Yu, R. F., Kang, S. F., Liaw, S. L. and Chen, M. C. (2000). Application of artificial neural network to control the coagulant dosing in water treatment plant. *Water Science and Technology;* 42, 403-408.

Zahraa, O., Maire, S., Evenou, F., Hachem, C., Pons, M. N., Alinsafi, A. and Bouchy, M. (2006) Treatment of wastewater dyeing agent by photocatalytic process in solar reactor. *International Journal of Photoenergy;* 46961, 1–9.

Zhang, Q. and Stanley, S. J. (1997). Forecasting raw-water quality parameters for the North Saskatchewan River by neural network modeling. *Water Research;* 31, 2340–2350.

Zhang, L., Scholz, M., Mustafa, A., and Harrington, R. (2008). Assessment of the nutrient removal performance in integrated constructed wetlands with the self-organizing map. *Water Research;* 42, 3519-3527.

Zhang, L., Scholz, M., Mustafa, A., and Harrington, R. (2009). Application of the self-organizing map as a prediction tool for an integrated constructed wetland argoecosystem treating agricultural runoff. *Bioresource Technology;* 100, 559-565.